# Durham E-Theses

## *Cosmic rays*

Abbas, Tariq Abdul Hameed

COSMIC RAYS

by

Tariq Abdul Hameed Abbas, B.Sc. (Mosul)

A thesis submitted to the University of Durham
for the degree of Master of Science

Department of Physics,                    January, 1984
Durham University,U.K.

13. APR. 1984

TO TANIA AND CHIA

CONTENTS

# ABSTRACT

The design and implementation of an automatic data collection system, using an eight channel microcomputer data acquisition unit, is described in the early part of this thesis. The calibration of the system and the methods of data collection and analysis are discussed. The system is used to measure the response of geiger counters and scintillation counters on the passage of cosmic ray muons and electrons.

An experiment is described to measure the flux of cosmic ray muons at different zenith angles and to note whether there is any difference between the flux of particles from the east and the flux from the west. This work used a Geiger-Müller cosmic ray telescope consist of two layers of Geiger-Müller counters each containing six identical counters. The rate of coincidence events using a coincidence unit has been measured by using a microcomputer data acquisition system to record both the occurrence time of an event and the geiger counter pulse height in each layer of counters. The distribution in time separation of the occurrence times of the events has also been studied.

A second experiment is described which used two scintillation counters to measure the density spectrum of electrons at sea level over the range 1 - 335 electrons $m^{-2}$. Discriminators and a two fold coincidence are used and a microcomputer data acquisition system is employed to record the scintillator pulse heights. The experiment used two scintillation counters each of 0.4 $m^2$ area and 5 cm thick.

# PREFACE

This thesis describes the work performed by the author in the Physics Department of the University of Durham, while he was a research student under the supervision of Dr. F. Ashton, during the period 1981 to 1983.

During this time, the author has carried out an experiment to study the zenith angle distribution of muons at sea level and also an experiment to measure the electron density spectrum over the range 1 - 335 electrons $m^{-2}$. Both experiments were mainly undertaken to operationally test an 8 channel microcomputer data acquisition system. The author is solely responsible for calculations, analysis and interpretation of experimental data described in this thesis.

## ACKNOWLEDGEMENTS

CHAPTER ONE

COSMIC RADIATION - ITS NATURE AND IMPORTANCE

## 1.1 INTRODUCTION

Particles with variable combinations of energy, charge and mass, that move through space at nearly the speed of light and that continuously bombard the earth's atmosphere from all directions were first detected in 1912. Most of them consist of high energy protons but other types of particle are also represented. The discovery of these particles, the cosmic rays, activated man's resources to obtain an understanding of what they are, their physical properties and where they come from. The energy spectrum of the cosmic rays extends to $10^{20}$ eV. In comparison the highest available energies from man-made accelerators are currently limited to less than about $10^{14}$ eV. This is achieved at the CERN $p\bar{p}$ collider where 250 GeV protons collide with 250 GeV antiprotons in head on collisions. For antiprotons incident on protons at rest the collisions are equivalent to an incident antiproton beam of energy $10^{14}$ eV.

## 1.2 THE DISCOVERY OF THE RADIATION

The discovery of the existence of a naturally occurring penetrating radiation of unknown origin was demonstrated at the turn of the century by certain experiments on the conductivity of gases. The most likely explanation of the observed phenomena seemed to be that the radiation was due to radioactive materials in the earth. However, the balloon flights of Hess (1912) led him to conclude that the radiation was of extraterrestrial origin and the absence of significant changes in the ionization between day and night indicated that it did not emanate from the sun. At first it

was assumed that the radiation was γ-rays due to its penetrating power. This doubtful idea was clarified after the discovery of the latitude effect. A number of workers realised that charged primaries would have their trajectories affected in the magnetic field whereas uncharged particles would be unaffected. For particles that enter earth's atmosphere vertically and parallel to the magnetic lines of force at the poles there is little interaction. At the equator the magnetic field is perpendicular to the direction of the cosmic rays, where the horizontal component of the earth's geomagnetic field is stronger, and the interaction is greater resulting in the effect that the energetic cosmic rays are deflected away from the earth more than at the magnetic poles, and hence Clay (1927), concluded that the primary of cosmic rays must be charged particles. The east-west effect (see Chapter three) which shows that more particles arrive from the west than the east led Johnson and Street (1933) to the conclusion that the majority of primary cosmic rays were positively charged. The mathematical theory of the effect of the earth's magnetic field on incoming charged particles had been worked out in considerable detail by Störmer to try to account for the aurora borealis. The theory was suitable for its application to cosmic rays and Lemaître and Vallarta (1933) calculated the allowed orbits and trajectories of all cosmic particles in the vicinity of the earth.

With the advent of high altitude balloon flights the presence of a significant proportion of protons were observed in the primary flux (about 90%) in 1948. It was found later that heavy nuclei were also present. The development in particles detectors led to the discovery of many new particles such as the positron, Anderson (1932), which had been predicted by Dirac and the pion by Powell and his

co-workers in 1947, which proved to be the particle proposed by Yukawa. Further search disclosed the existence of both charged and neutral kaons and various hyperons. Primary electrons were discovered in 1961 in balloon experiments. Their existence in the galaxy and radio sources had already been inferred from the synchrotron nature of radio-emission.

Cosmic x-rays and discrete x-ray sources were discovered in 1962, first in rocket experiments and later with balloons. Investigation of the deep underground muon intensity at a depth of 3 km below ground led to the setting up of high energy cosmic ray neutrino experiments. The first neutrino interactions were observed in 1945. A great many possible source and acceleration processes of cosmic rays have been identified. Their relative importance for generating different cosmic ray components is still not clear. It also appears now that the highest energy cosmic ray particles may be of extragalactic origin.

## 1.3 THE NATURE OF THE COSMIC RADIATION

In order to learn and obtain information on what and where the cosmic ray sources are, we must know the composition of these particles. Hitherto only direct measurements of the composition have been made in the energy range $10^{10} - 10^{13}$ eV by using balloon and satellites carrying emulsion stocks and ionization calorimeters. The composition of the primary flux for Ep $\leqslant 10^3$ GeV is given in table 1.1 after Julliusson (1975), normalized to a percentage of the total. These figures depart from those of Ginzburg and Syrovatskii (1964) in the respect that the abundances clearly depend on energy. The rise in abundance of iron with energy is perhaps due partly to interaction and spallation in the interstellar medium, energy losses

| Z Elements | Kinetic energy per nucleus (eV) | | | |
|---|---|---|---|---|
| | $10^{10}$ | $10^{11}$ | $10^{12}$ | $10^{13}$ |
| 1 Hydrogen | 58 ± 5 | 47 ± 4 | 42 ± 6 | 24 ± 6 |
| 2 Helium | 28 ± 3 | 25 ± 3 | 20 ± 3 | 15 ± 5 |
| 3-5 Light nuclei | 1.2 ± 0.1 | 1.1 ± 0.1 | 0.6 ± 0.2 | - |
| 6-8 Medium nuclei | 7.1 ± 0.4 | 12.2± 0.8 | 14 ± 2 | - |
| 10-14 Heavy nuclei | 2.6 ± 0.2 | 6.7± 0.5 | 10 ± 1 | - |
| 16-24 Very heavy nuclei | 1.2 ± 0.2 | 3.6± 0.4 | 4 ± 1 | - |
| 26-28 Iron group nuclei | 1.2 ± 0.2 | 4.5± 0.5 | 10 ± 2 | 24 ± 7 |
| ≥30 Very very heavy nuclei | | 0.007 ± 0.004 | | |

TABLE 1.1 : Composition of cosmic rays at high energies
(after Julliusson, E. , 1975).

caused by solar modulation and, most likely, as a consequence of the production mechanism at the source. For higher energies the chemical composition is not certain due to the low flux of cosmic rays rendering direct methods of detection inefficient.

Figure 1.1 shows the abundance of elements in cosmic rays in the range of a few hundred MeV per nucleon to about one GeV per nucleon for hydrogen up to iron as given by Meyer et al (1974). For comparison the solar system abundances are also shown in figure 1.1. A comparison between abundances in cosmic rays and the universe shows that there is an excess of the elements (lithium, beryllium and boron), in cosmic rays which are believed to come from the fragmentation of heavy cosmic ray nuclei, (mainly from C, N and O), during their passage from the source through the interstellar medium. The observed relative abundance of light nuclei suggests that cosmic rays at least in the energy range where relative abundances have been measured, have traversed $\simeq 2.5$ gcm$^{-2}$ of interstellar hydrogen which corresponds to an average age for the cosmic rays of a few million years. The ratio of He$^3$ to all helium nuclei may also be used to estimate the amount of interstellar material traversed by cosmic rays.

## 1.4 THE PRIMARY ENERGY SPECTRA

The spectra of the primary particles can be expressed in a variety of ways, the choice being usually determined by the method of measurement. Studies of different latitude, which essentially use the earth's field as a magnetic analyser, determine the number of particles above a given threshold rigidity (pc/Ze) (where p is the momentum, c the velocity and Ze the charge of the particle).
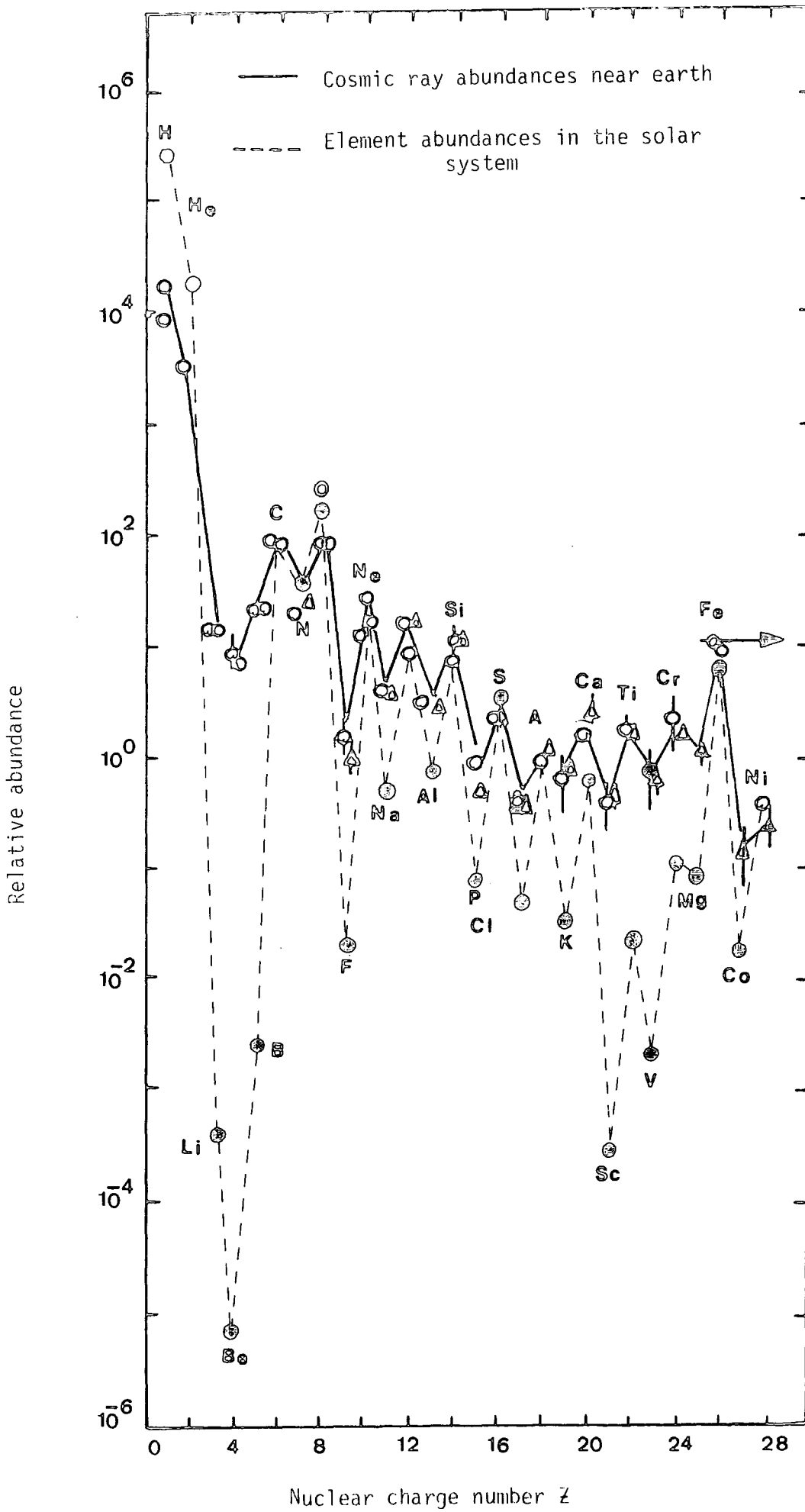
Figure 1.1 : Relative abundance of the elements from hydrogen to the iron group normalized to that of carbon (c = 100) (After Meyer et al. 1974).

A survey of the data that are at present available is presented in Figure 1.2 from the summary of Wolfendale (1973). There are four different regions of the spectra to be considered. At energies below about $10^9$ eV satellite measurements are possible and precise measurements can be made. In this region the interplanetary magnetic field reduces the primary intensity below its value far from the sun (the 'galactic intensity'). The lowest intensities are observed at times of high solar activity and this may impose an asymmetry in the arrival direction of these particles.

The primary spectrum of all nuclei summed together can be written in the form $j(E) \alpha E^{-\gamma(E)}$, Greisen (1965), Wolfendale (1973), where $\gamma(E)$ is approximately constant (at $\simeq 2.6$) for $10^{10} < E < 3.10^{15}$ eV and has a different value ($\simeq 3.2$) for $E > 3.10^{15}$ eV.

Direct measurements have been carried only to $10^{14}$ eV but have not met with universal acceptance. The spectrum measured beyond $10^{14}$ is investigated by means of the extensive air shower technique in which the atmosphere amplifies the effect of a single high energy primary to such an extent that particle detectors need to be used at large separations in installations covering several square kilometers in area. These respond to primary cosmic rays of the highest energies : $10^{14}$ eV to $10^{20}$ eV.

A change in the slope of the spectrum at about $10^{15}$ eV where the position of what is called the knee, is clearly shown in figure 1.3 as summarised by Kempa et al (1974) from available EAS studies, and the most plausible interpretation associates it with the onset of escape of particles from some local trapping region, probably the galaxy. Peters (1960) pointed out that if it were indeed the curvature of trajectories in magnetic fields that determine the local retention of particles, the spectra might fall sharply
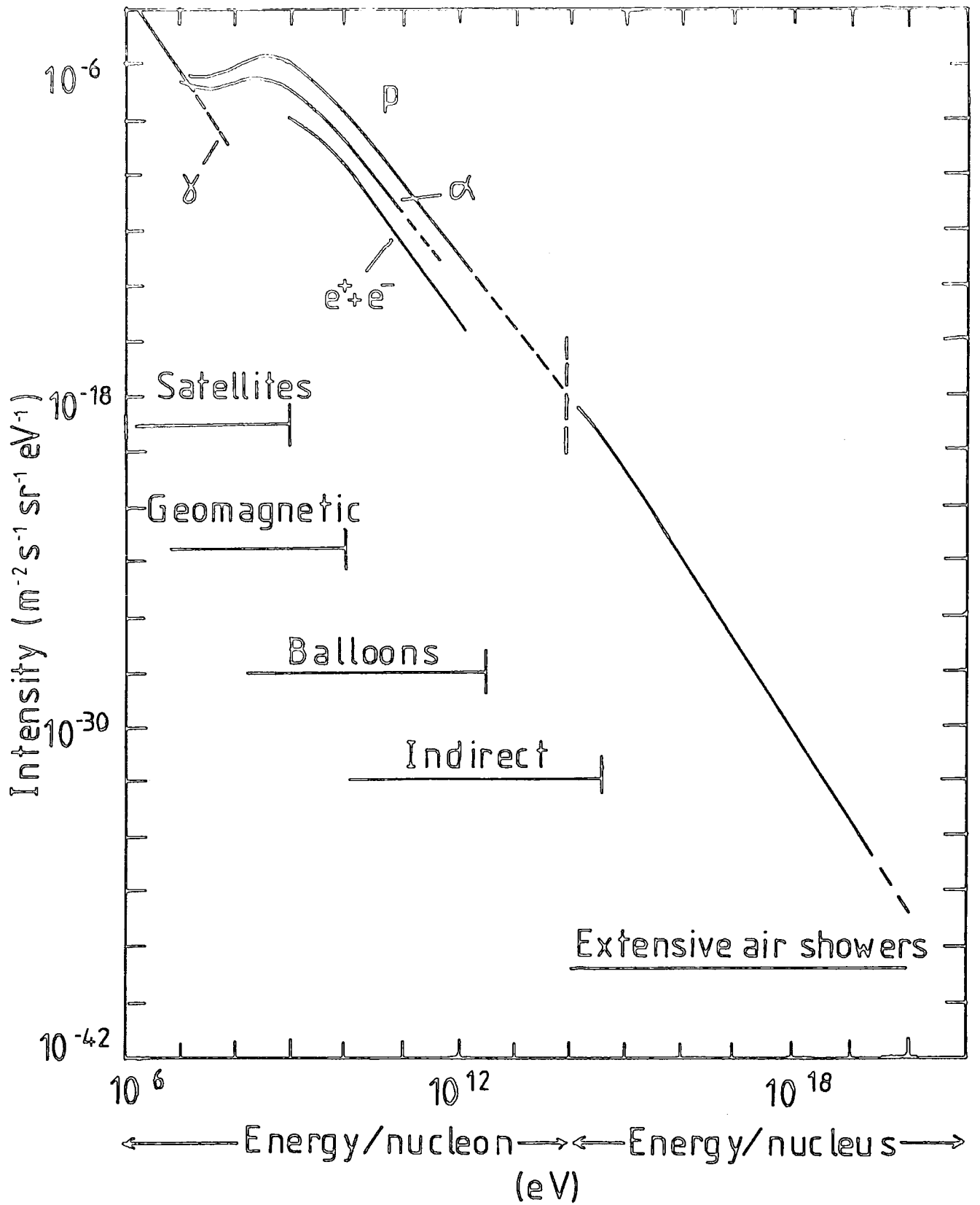
FIGURE 1.2 : Primary Cosmic Ray Spectra (after Wolfendale 1973)

H ⇒ Haverah Park (1975)

S ⇒ Sydney (1974)

Energy per nucleus E(eV)
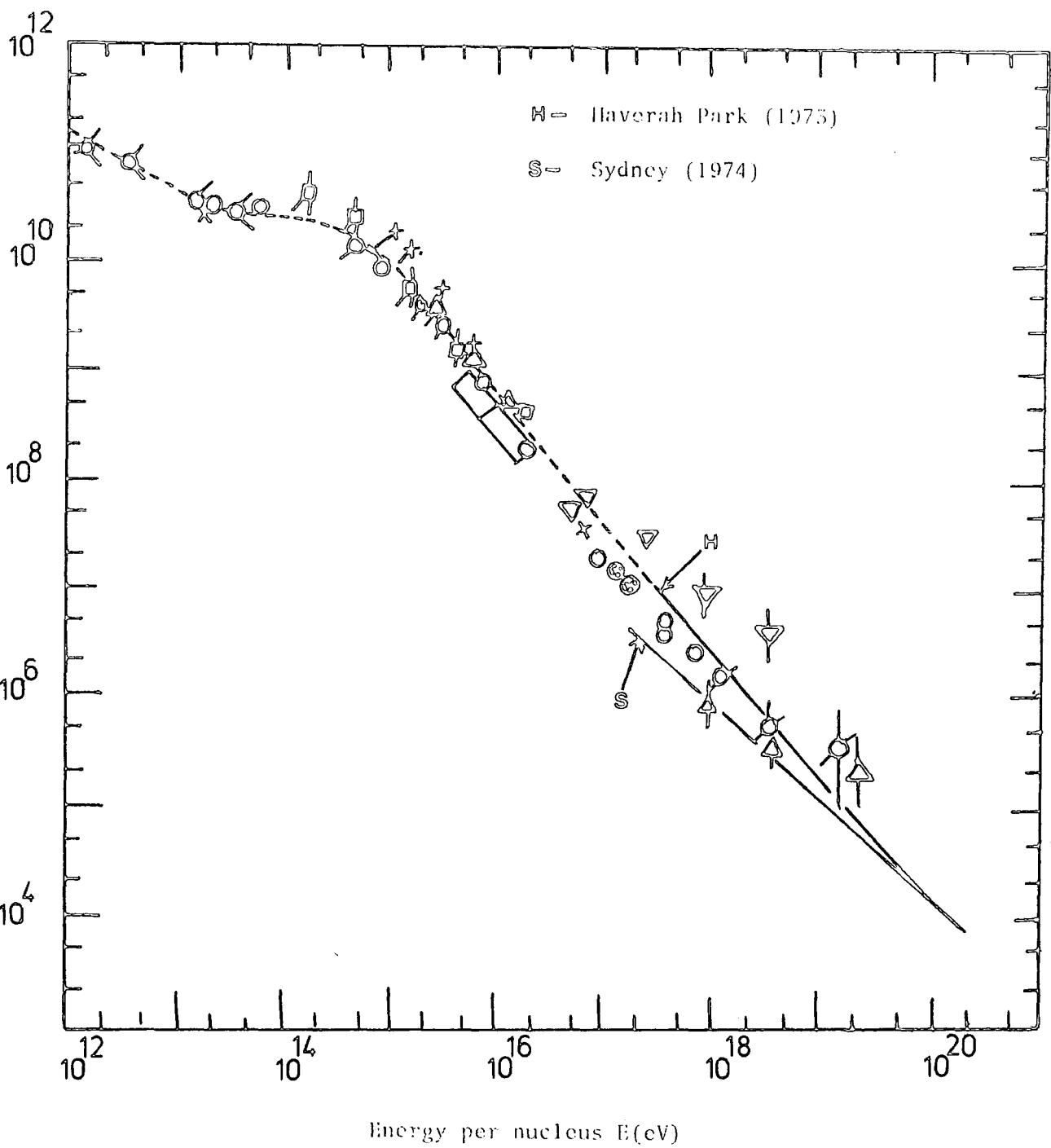
Figure 1.5 : The integral primary cosmic ray spectrum. Combination of data from Figure 2 and Figure 4 of Kempa et al (1974).

beyond a certain magnetic rigidity; for heavy nuclei of charge Z this would correspond to an energy Z times higher than for protons; so just beyond the "knee" of the energy spectrum the primary radiation should be much rich in heavy nuclei, assuming the composition at the source is not energy dependent. Alternatively, the start of some energy loss process in the accelerating region may perhaps be the cause for the change in slope.

It has been thought for a long time that the cosmic rays of the highest energy were all extragalactic since the galactic magnetic field would be unable to contain them and because there is no observable anisotropy in this region. Proposals made by Greisen (1966) that there should be a cut-off at about $10^{20}$ eV in the primary energy spectrum have recently been investigated by Strong et al (1974) in some detail. This cut-off arises from photonuclear reactions with the 2.7 K black body radiation. Figure 1.4 shows the differential energy spectrum of primary cosmic rays obtained from the results of various workers. The line marked Kempa et al (1974) is the best fit line of Figure 1.3. The figure shows the onset of electron pair production (c.$10^{18}$ eV) and pion production (c. $5.10^{19}$ eV) which are clearly visible. However, Hillas in his summary (1975), pointed out that there is no such discontinuity in the spectrum up to approximately $10^{20}$ eV.

## 1.5 PROPAGATION OF COSMIC RAYS THROUGH THE ATMOSPHERE - EAS

The extensive air shower (EAS) has been the subject of detailed study for approximately 40 years. The early experiments (Auger et al 1939) Kolhörster (1938) were concerned with establishing the main characteristics of the EAS and linking the effect to the already well known electromagnetic cascades produced by the passage of high energy electrons and photons through matter. The early ground level
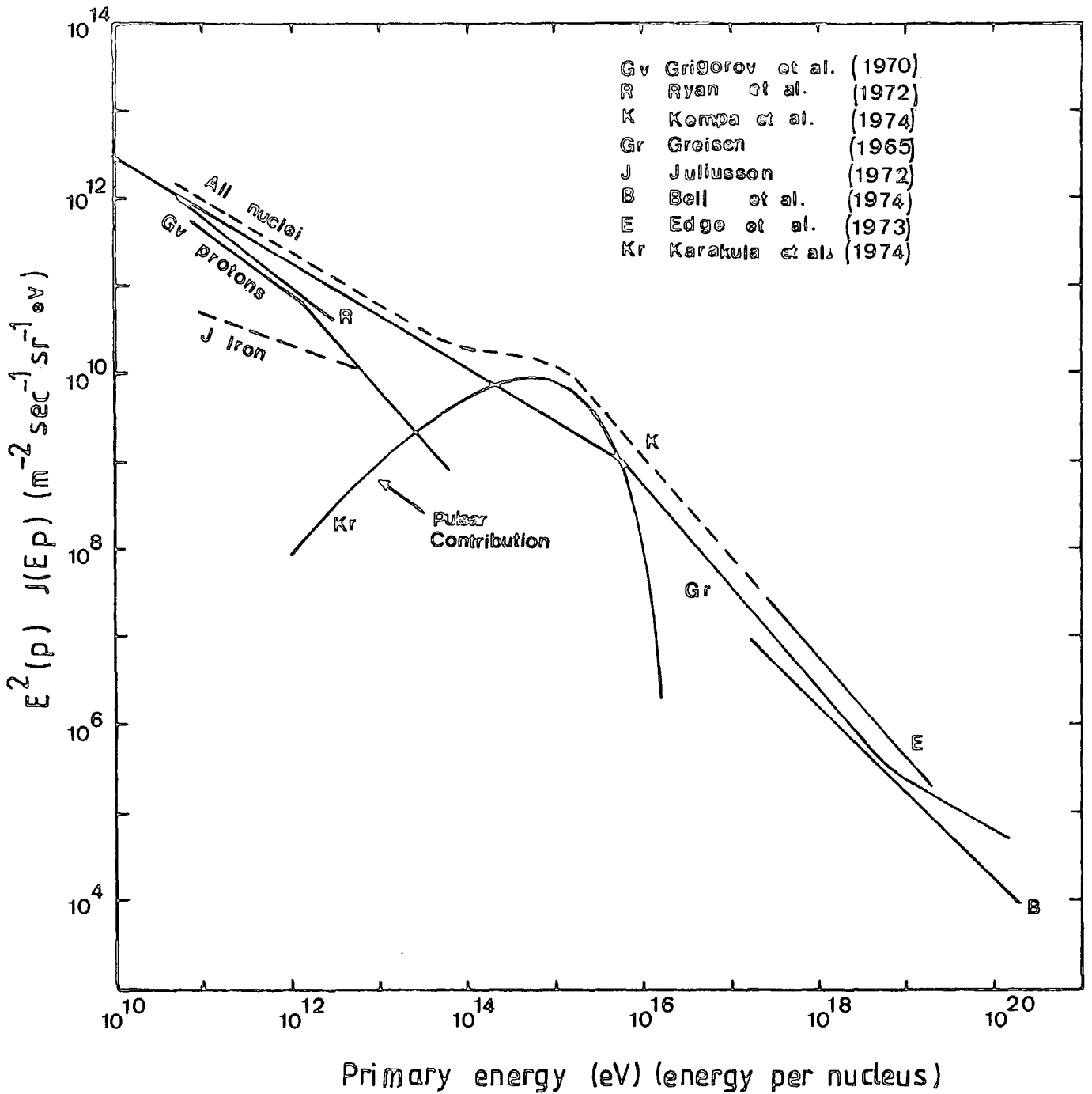
**Figure 1.4** : The differential energy spectrum of primary cosmic rays obtained from the results of various workers.

experiments studying the electromagnetic components used widely spaced counters to detect the simultaneous arrival of charged particles over hundreds of square metres, a sampling technique similar to that used by the majority of modern particle arrays.

Other experiments at this time (Froman and Stearn 1938) indicated the presence of a 'head' component capable of passing through 15 cm of lead without interaction, proving that the electromagnetic cascade theory alone was not the full explanation of the development of EAS. Later balloon work using nuclear emulsions discovered the presence of protons and heavier nuclei in the primary radiation. Spurred by the fact that EAS were the results of the interactions of the highest energy cosmic ray primaries, interest in EAS increased and gradually, during the last three decades, a standard model of the generation of EAS in the atmosphere has been developed.

Extensive air showers are initiated by the interactions of primary cosmic rays with the nuclei of air atoms. When a primary cosmic ray (mainly protons and $\alpha$-particles) enters the atmosphere, on average it travels 70-80 gcm$^{-2}$ of air before it interacts with an air nucleus and then loses about 50% of its energy at each interaction. This means that the first interaction takes place on average 10-30 km above sea level. In these high energy interactions secondary particles are produced most of which are pions. On average equal numbers of positive, negative and neutral pions are produced. Other particles such as kaons, hyperons, nucleons and antinucleons may also be produced. The neutral pions immediately decay (mean life time $\simeq 10^{-15}$ sec) into pairs of photons and these photons produce electron-positron pairs by means of pair production. The relativistic electrons produce further photons by bremsstrahlung. These photons then produce more electrons and the shower of particles

resulting is known as an electromagnetic cascade. These cascades form the electromagnetic component of EAS.

The charged pions (life time $\approx 2 \times 10^{-8}$ sec) together with nucleons and other secondary particles which are produced by the interaction of the primary cosmic rays form the cascade of nuclear-active particles. This cascade is the skeleton of the shower, ~~continue to travel on in direction very close to the original~~ ~~direction of the primary, and~~ regenerating the electromagnetic component by continuously feeding energy into that component by way of ^the^ production of neutral pions. The cascade of nuclear-active particles is also a source of the second most numerous component, the muon component, which is formed via decay of the charged pions.

$$\pi^{\pm} \to \mu^{\pm} + \nu_{\mu}$$
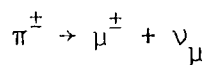
The decay probabilities of pions are a function of their energy and zenith angle. For a given zenith angle these particles have a greater chance of interacting rather than of decaying as their energy increases. As the zenith angle increases, the air density per unit path length decreases and hence the interaction probability decreases and more numbers of pions decay into muons. The produced muons have ~~an even long life time (2 x 10⁻⁶ sec),~~ ~~means that the muons have~~ a high chance of reaching sea level without decay or interaction. Their greater mass than that of an electron (207 times) means that they are not scattered to such a large extent. Figure 1.5 shows the major processes taking place in the atmosphere when an EAS is observed at sea level.

Finally, in addition to these three components (electromagnetic, nuclear active and muon) which are the main ones recorded at the various observation levels, one can quote some others produced as a result

Primary proton
$(E \geqslant 10^{13} ev)$

air nucleus

$\pi^+, \pi^-$   $\pi^+$   $\pi^-$      $\pi^0$      $\pi^+$   $\pi^-$

n,p

$\mu^+$          $e^+$  $e^-$  $\gamma$  $e^-$       $\mu^-$

$\mu^\pm$

nucleon cascade       e-$\gamma$ cascade

$e^+$                                         $e^-$
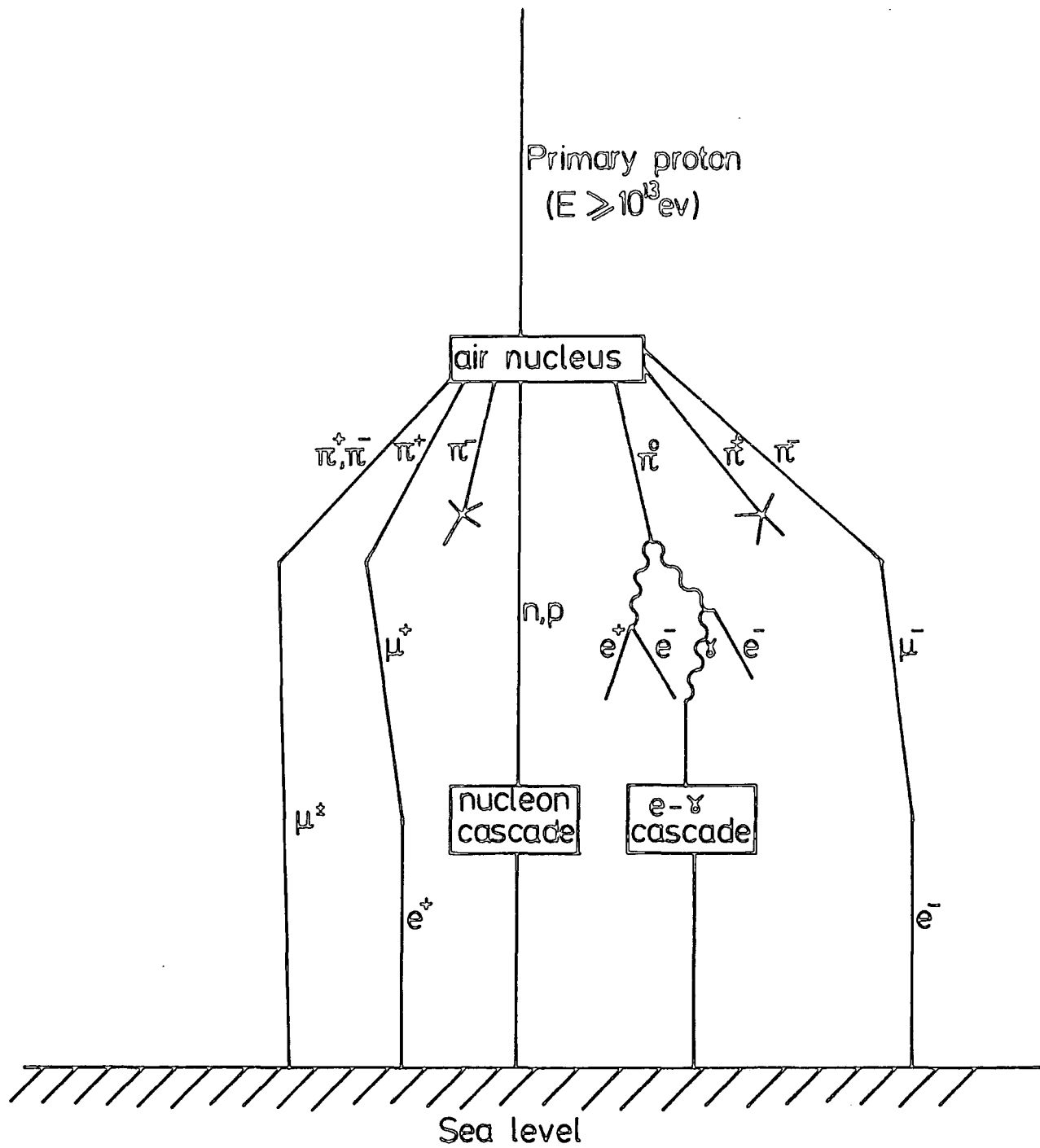
Sea level

Figure 1.5 :   Diagram showing the major processes taking
place in the atmosphere when an extensive
air shower is observed at sea level.

of the passage of the shower through the atmosphere, notably the Cerenkov component and the radio waves emitted by EAS.

## 1.6  THE ORIGIN OF COSMIC RAYS

The search for the origin and acceleration mechanism of the cosmic radiation has been proceeding ever  since the radiation was discovered, but for many years only very general considerations were possible since little was known of the detailed properties of the primary radiation.  Experimental evidence indicates that neglecting short term fluctuations the cosmic ray intensity has not varied systematically by more than a factor of two over the past $10^9$ years. This constancy in time argues strongly against cosmic ray creation in a single event.  Energy requirements, mass composition, energy spectrum, gamma ray astronomy and arrival direction studies, all provide pointers to the source regions.  There are basically three major regions in which the cosmic rays could be contained and be presumed to originate:-

(a)   -   Solar Origin

(b)   -   Galactic Origin

(c)   -   Universal or extra-Galactic Origin

(a)  Solar Origin : At first it was believed that the sun is the main source of cosmic rays and that the isotropy of the radiation arises from the trapping of the particles within the solar system by an extended magnetic field.  The observation of increases in cosmic ray intensity at the time of solar flares shows that there is an acceleration mechanism available on the sun that is capable of generating particles with energies up to 10 GeV.  Later, it was suggested that particles of higher energies also originate from the sun where their energies are acquired from the interplanetary magnetic

field (H) in storage times of $10^3$ - $10^8$ years before reaching the earth.

Now one can give several obvious arguments against such a possibility. First the energies of the primaries extend up to at least $10^{19}$ eV so that a very much more powerful mechanism is required, and the weak magnetic field of the solar system ( $\simeq 10^{-5}$ gauss) cannot contain the highest energy particles. Second, solar particle events are associated mostly with visible flares and the chemical composition of the solar particles is different from that of galactic cosmic rays. Therefore, the sun cannot be the only cosmic ray source. The necessity of other cosmic ray sources and a more powerful mechanism of particle acceleration is required.

(b)     Galactic Origin : The assumption is that other stars like the sun in the galaxy (containing $10^{11}$ stars) generate cosmic rays. The required total observed flux would not be produced in this way. Therefore, we have to look for additional sources in other types of star. Several suggestions have been made. For example, stars such as magnetic variable stars as well as novae and supernovae are considered. Current theories seem to favour supernovae because they seem to be capable of supplying the necessary energy. Supernovae are also believed to be rich in heavy elements and this is consistent with the measured cosmic ray composition. However, the energies reached by particles accelerated at their source of origin is likely to be less than the highest energy particles observed. A possible explanation for the highest energy particles observed is that an additional acceleration process is operative. This probably comes from the collision of cosmic ray particles with randomly moving magnetised gas clouds as they stream through the arm of the galaxy.

(c)    Universe or extra-Galactic Origin : Studies of cosmic ray

EAS have established the change in slope of the primary cosmic

ray spectrum at an energy of around $3 \times 10^{15}$ eV.  This change in

the slope has been explained by a mixed origin of the primary cosmic

rays, galactic and extra-galactic (e.g. pulsar origin and universal

production).  Unfortunately, a significant amount of data on arrival

directions has yet to be acquired.  However, particles have been

observed to arrive from directions almost perpendicular to the

galactic plane and this evidence would be strongly suggestive of

extragalactic origin.  It has also been suggested that very high

energy cosmic ray particles producing EAS of size $> 10^6$ have an

extragalactic origin, because their energies are too high to be

confined within the galaxy by the galactic magnetic field.  The

galactic component may be limited at high energy by the size of

the accelerating region and/or containment volume, to about

$10^{15}$ eV.  Therefore, they leak out from one galaxy into space and

then enter other galaxies to contribute an extragalactic

component to the cosmic ray flux.

## 1.7  THE SIGNIFICANCE OF COSMIC RAY STUDIES

There are two main reasons for investigating the primary

radiation.  The first is that information is gained of astrophysical

and geophysical interest, such as for example, electromagnetic

conditions in the galaxy and solar system.  Second, primary radiation

constitutes a source of high energy particles, mainly protons, which

can be used to perform experiments in nuclear physics.  For both

aspects of the subject we need to know the composition, flux and

energy spectrum of the particles and, in studies of astrophysical

and geophysical significance, measurements of time-variations and

directional effect are also useful.

For several decades cosmic ray research concentrated on the nuclear physics aspects of the particle beam and many important discoveries were made. Notably, the identification of the positron, the muon, the pion and the strange particles. More recently, cosmic ray studies have expanded so as to cover both elementary particle physics and astrophysics. Current fundamental problems in particle physics are whether quarks, magnetic monopoles or tachyons exist as real entities. If they do exist then it is likely that any of these objects would be either incident on the earth in the primary cosmic ray flux or be produced in the atmosphere in very high energy primary cosmic ray interactions. Astrophysicists are concerned with the origin of primary cosmic rays, the processes required in possible sources and the interstellar medium to explain the energy spectrum, mass composition and the variation of primary cosmic ray flux incident on the earth. Perhaps the most interesting problem is the study of mechanisms by which primary particles can be generated and accelerated to such energies as seen in cosmic rays.

## 1.8 SUMMARY

Although many elaborate and well designed accelerator experiments are in operation or under construction, which enable controlled experiments with energies up to about $10^{14}$ eV to be carried out, cosmic rays will be in use for many years to come simply because they are a cheap high energy beam of particles.

The role of extensive air showers in an effort to understand the nature of nuclear processes at the highest energies cannot be denied. As yet they provide the only means of investigating the properties of what occurs at energies in excess of $10^{14}$ eV and it appears as though they will be the main contributor to this sector

for a long while. The study of extensive air showers also provides a valuable tool for investigating the condition of the galaxy and beyond and it is to these two ends that the extensive air shower needs to be pursued.

As mentioned earlier, there are two aspects of cosmic ray studies which physicists are interested in; nuclear physics and astrophysics. The study of the primary and secondary radiations provides a good opportunity for nuclear physicists to investigate the characteristics of particles and the nature of high energy interactions. For astrophysicists, undoubtedly the most fascinating problem is the origin of cosmic rays and the mechanism in which these particles are accelerated to such high energies as seen in air showers.

CHAPTER TWO

## DESCRIPTION AND CALIBRATION OF PET DATA ACQUISITION UNIT (D.A.U)

## 2.1 HARDWARE DESCRIPTION OF THE PET DATA ACQUISITION UNIT

The Data Acquisition Unit consists of four major parts. They are:

      (a)  Analogue part

      (b)  Trigger control circuitry

      (c)  PET interface

      (d)  Microprocessor subsystem

The PET Data Acquisition Unit - block diagram is shown in Figure 2.1.

### (a) Analogue part

The analogue part buffers and then converts analogue input signals. The analogue inputs are connected to the inputs of eight buffer amplifiers. The diode input protection is provided to prevent accidental damage to the buffer amplifiers. The buffer amplifiers are connected as unity gain inverting amplifiers.

The output of the buffer amplifiers is connected directly to eight inputs of the sample/hold circuits, whose function is to hold the analogue information during the analogue to digital conversion. The sample/hold circuits are operating in the track-and-hold mode, thus reducing the acquisition time. The outputs of the sample/hold circuits follow the input signal until switched into the hold mode by the trigger control circuitry.

After the sample/hold circuits have been switched to hold mode their outputs are individually connected into the input of the analogue to digital converter via the analogue multiplexer. The routing of the analogue multiplexer is under the control of the microprocessor.

BUFFERS  SAMPLE & HOLD CIRCUITS  ANALOG MULTIPLEXER  ANALOG TO DIGITAL CONVERTER

ANALOG INPUTS

8x

8x

8x

S/H

A/D

TRIGGER OUT

EXT TRIG IN

EXTERNAL TRIGGER

TEST OUT

THRESHOLD ADJUST

4

TRIGGER CONTROL

TMR 1
TMR 2
INTERNAL
TRIG MODE
ARM 3
Trigger

HOLDING TRACK/HOLD

ANAL. CHANNEL SELECT

3

START CONVERSION/ READ DATA

CONVERSION COMPLETE

ADC DATA

8

MICROPROCESSOR SUBSYSTEM

RESET P.B

PET (IEEE) INTERFACE

IEEE ADDRESS SWITCH

PET BUS

16

IEEE

PET

FIG. 2·1     PET DATA ACQUISITION UNIT — BLOCK DIAGRAM

The microprocessor controls also the start of actual data conversion
and data storage. The analogue to digital converter is a 12 bit
converter connected via the bipolar mode with input voltage range
of ±10 V.

The sequence of data acquisition is as follows:-
While waiting for a trigger the sample/hold circuits are in the track
mode and follow the input signals. The trigger controlling circuitry
is armed and waiting. When the trigger signal is received, the
sample/hold circuits are switched into the hold mode. The holding
flag flip-flop is set, signalling to the microprocessor that the
trigger has occurred and the conversion can start. The microprocessor
then issues a start conversion signal to the A/D converter and waits
for a conversion complete return signal from the A/D converter. When
the conversion is done, the microprocessor switches the A/D to
"READ DATA" mode and reads the converted value.

After this the processor switches the analogue multiplexer
to the next channel and starts conversion again. This is repeated
until all the required analogue channels are read. After this the
trigger control circuits are again armed to receive the next trigger.

(b) Trigger control circuitry

The data conversion cycle can be started from one of several
possible sources of the trigger signal. The source of the trigger
can be derived from:-

(i)    External source,

(ii)   Internal signal under program control, or

(iii)  One of two real times of the data acquisition unit

The selection of the particular source of the trigger signal is under microprocessor control, and the selection and setting of timing of the real time timers must be done prior to data conversion itself. The selection will route the outputs of various trigger sources via digital multiplexers to the clock input of the holding flip-flop, which is the master signal controlling the sample/hold amplifiers. A fast digital multiplexer (MA25LS253) is used in order to minimise the delay between the trigger and switching of the sample/hold circuit to hold mode.

## (i)  External trigger

The external trigger is derived from the signal applied to the "EXTERNAL TRIGGER" input of the data acquisition unit.  The signal through the potential divider is applied to the input of a fast comparator (LM361).  The 10 turn potentiometer located next to the "EXTERNAL TRIGGER" input sets the threshold level.  This level can be set between ±7 V.  The comparator output is taken into the "EXTERNAL TRIGGER OUT" socket; this 2mm socket outlet is provided to check the setting of the threshold level.

The comparator has two complimentary outputs.  The outputs are connected to two inputs of the trigger multiplexer, providing high-to-low or low-to-high transition triggering capability.  The outputs are also connected to the inputs of two monostable multivibrators providing external delay capability.  In this mode a delay of 6 μs is introduced between the trigger transition and actual switching of the sample/hold mode, allowing the buffer amplifiers and sample/hold circuits to acquire the step input signal to the desired accuracy.

(ii)   Internal trigger

The internal trigger is a microprocessor generated pulse. This pulse is issued by the program at the beginning of every data acquisition cycle and if the internal triggering is not required, this pulse is filtered out by the trigger multiplexer.

(iii)   Real time timers trigger

The data acquisition unit has two internal timers for generation of a real time clock.  These two timers are part of the VIA interface adapter (6522) of the microprocessor system.  The interface adapter is capable of generating trigger periods from a few μs to 6500 seconds.  There are two timers TMR1 and TMR2.  The TMR1 timer is used for the generation of a shorter time period, up to 131 ms.  For longer periods TMR2 must be used to count the number of time-out periods of the TMR1.  TMR2 can be used to count up to 65535 time-out periods of the TMR1.

(c)   PET interface

The controlling microprocessor of the data acquisition unit communicates with the PET via the IEEE bus interface.  The GPIB interface adapter (MC68488) is used to interface the microprocessor to the PET bus.  The GPIB interface adapter in an integrated circuit of the 6800 family designed to interface the 6800 family microprocessor to the IEEE 488 bus.  The major portion of the IEEE 488 bus communication protocol is handled by this interface. The GPIB is buffered by special IEEE 488 buffers (MC 3778).  The outputs and inputs of these buffers are directly connected with the PET bus.

The physical connection is done by a multicore cable terminated by a socket suitable to be plugged into the bus outlet of the PET. To allow daisy chaining of other devices with the data acquisition unit a PCB outlet similar to the PET IEEE bus outlet is provided on the back of the data acquisition unit. The unit itself does not affect adversely the correct functioning of the bus even when it is switched off and can be left connected to the PET permanently.

(d)  Microprocessor subsystem

The microprocessor subsystem controls the function of the data acquisition unit, including data capture and communication with the PET. The heart of the microprocessor system is a 6802 microprocessor running at 1 MHz. it is supplemented by 2K of static RAM (used for storage of data), 4K of ROM for the controlling program and two peripheral adaptors providing connection of the microprocessor to the rest of the system. They are PIA (MC 6821) and VIA (MC 6522) integrated circuits. A separate special integrated circuit controls communication with PET.

2.2  SOFTWARE CONTROL FROM PET

The data acquisition unit is controlled from the PET via the IEEE bus by a series of commands. The command line consisting of a command (or a series of commands separated by semi-colons) is sent to the data acquisition unit where it is analysed and executed. The data acquisition unit sends back the return code and the accumulated data where appropriate.

The command consists of one or two words. The first word generally indicates the action required. There are two groups of commands:-

        (a)  Control commands
        (b)  Data acquisition commands

(a)  Control commands

This group of commands set the data acquisition unit to readiness for the data acquisition command.  The available commands in this group are:-

(i)   INIT - Initialise command

(ii)  TRG  - Trigger commands

(iii) TMR  -  Timer command

(i)  Initialise command

This command initialises all internal states of the data acquisition unit resets and reconfigurates the components to the data acquisition mode.  It should be used only after manual reset of the data acquisition unit or after synchronisation between the data acquisition unit and the PET has been lost or when the way of triggering the data acquisition is to be changed.

(ii) Trigger commands

The data acquisition unit, as described before, is designed in such a way that it is possible to trigger data acquisition from one of several sources.  They are real time internal timers, external sources or under program control from the PET.  The TRG command will set up the trigger multiplexer so that the trigger is taken from the required source.  Available trigger commands are:-

TRG INTR-Internal

The conversion is started as soon as the data conversion command from PET is received and analysed.

TRG TMR1 - Timer 1

The real timer 1 is used to trigger conversion.  Once routing to this timer and the timing period is specified (by TMR command),

it will trigger the data acquisition repeatedly until disabled by the INIT command. This timer can generate time periods between 2μs - 131000μs. The minimum practical period of the timer depends on the data acquisition command.

## TRG TMR2 - Timer 2

This mode is for the generation of longer periods between triggers. The timer period of the TMR2 timer is generated by counting n time-out periods of the TMR1 timer. When the count of TMR1 time-outs is reached the TMR2 timer itself will time out and trigger the conversion.

## TRG EXTL - External trigger low to high

The data capture is triggered by a change of the state of the external trigger source. The low to high transition of the external trigger signal will start the conversion.

## TRG EXTH - External trigger high to low

The high to low transition of the external trigger signal starts conversion.

## TRG EXTDL - External trigger delayed low to high

The data capture is delayed for approximately 6.5 μs from the time of the external trigger changing state from low to high. This mode is included to accommodate a 6 μs data acquisition time for the internal sample/hold circuits.

## TRG EXTDH - External trigger delayed high to low

The data capture is delayed for approximately 6.5 μs from the time of the external trigger changing state from high to low.

(iii)  Timer command

The timer command will set up the timer period of the internal real time timers TMR1 and TMR2.  Both timers are set by one common command.  In the TMR1 mode only part of the command is used, but both parts must be supplied by the PET.  The second word of the TMR command consists of three parts.  The first part is numbered between 1 - 65535 which specifies the number of TMR1 time-outs to be counted by TMR2 before itself time outs.  The second part is a single letter identifying the way the third part of the word is to be interpreted.

(b)  Data acquisition commands

The data capture commands trigger the data acquisition in the data acquisition unit and when the requested command is performed, the data are returned from the data acquisition unit.  The available commands are:-

(i)     READ - Read command

(ii)    CAPT - Capture commands

(iii)   FCAPT1 - Fast capture channel 1 command

(i)  Read command

The read command waits for the trigger, reads the specified channels and sends the channel numbers followed by the appropriate values back to the PET.

(ii)  Capture commands

The capture commands consist of two words.  The first word specifies the type of capture and the number of channels to be read.  The second word specifies how many times the capture should be repeated before terminating the command.  The command repeatedly

captures data and stores them in the internal memory. The process
is repeated until the number of data captures is completed and then
all reading is transferred to the PET.

The capture and read commands check if trigger overrun has
occurred. The trigger overrun is indicated when a second trigger
pulse arrives before the data conversion has started. When this
occurs the overrun LED indicator will be set on and the overrun
marker is superimposed onto the last data of the current readings.

Another kind of trigger overrun is marked onto the data,
but not indicated on the LEDs. This happens when the start of
the data capture arrives after the arrival of the trigger. As there
is no way of knowing when this trigger arrived there is no way of
estimating the amount of sample and hold droop. For this reason
the data are also marked as overrun and must be treated as incorrect.

(iii)  Fast capture channel 1 command

Captures first channel repeatedly in the fast mode. In this
mode minimal periods between successive triggers must be 74 µs.
If trigger occurs faster, it is lost and no indication is given.


2.3  LOADING AND RUNNING THE PET DATA ACQUISITION PROGRAM

The "PET DATA ACQUISITION PROGRAM" given in appendix (A)
is the program subsequently used to operate the system when input
pulse heights are required to be recorded. Loading and running
the program is as follows.

The data acquisition unit must be connected to the PET
microcomputer, via the IEEE 488 outlet of the PET. When the
printer is used for hard copy output, the printer connector must
be connected to the PET interface outlet of the data acquisition unit.

When all required parts of the system are connected together the mains power and individual units can be switched on. After a short time, the PET microcomputer will display a power on message and then prompt for a command. At this point everything is ready for loading the program.

Tape with the controlling program can be placed in the cassette drive of the PET and it must be rewound to the start position. To load the program on the PET, one must type (LOAD "PET DACQ") on the PET keyboard. The PET prompts to start the cassette and the program will be loaded from the tape. When the program is loaded, the cassette drive will stop and a (READY) message appears on the screen of the PET. The program tape must be rewound to the start position and it must be removed from the drive. The program is now loaded and ready to be run.

To run the program, one must type (RUN) on the PET keyboard, then the program will enter initial dialogue. The user is asked what action must be performed and can then be selectively activated. The first question asked is whether a hard copy of the session is required. The hard copy facilitates identifying information and then data are gathered during the session onto the PET printer. The next question asked is whether the session should be recorded onto the cassette. If the cassette copy is required, the user is asked for an 8 character file name. This file name must uniquely identify the file and can be different from the session identifier. The file created and recorded onto the tape is marked using this file name and can only be recorded using that name. The user is then prompted to rewind the data tape to the start position. It is important to check that no cassette key is pressed down before any key is pressed on the PET which will start recording of the file

header onto the tape.  When the file header is recorded, the program
will resume its main flow of the initial question session.  The user
is asked for a session identification, which is an 80 character
long string which can be printed onto the printer and recorded on
the cassette if the cassette option is selected.  The session
identifier is there purely for the convenience of the user to help
him to record additional information about this session.  Some rules
are related to the date, which again can be 80 characters long.
The date is specified just to remind the user to enter the data
(for future use).  After the session identifier and the date the
user is asked about the time.  The time entered must be in 24.00
notation.

Another question asked is whether to calibrate the zero of
the recording channels.  The user is asked to connect all inputs to
ground and to press.D.(done) to save the reading as a new zero
correction.  The last question asked is whether the user wishes to
calibrate the gain.  To do that, the user is asked to connect all
inputs to a positive voltage (in the region of 9.5 V) and to press
.D. when done, then he must enter the exact input voltage to
5 millivolt precision.  However, he is also asked to connect all
inputs to a negative voltage and to do the same as he did with the
positive voltage.  Now the program is ready to collect data and
record them on the cassette.

The "FILES READER PROGRAM" which is also given in Appendix (A)
is used to read the recorded data from the cassette and prints them
on the printer by using the file name which identifies that file.

## 2.4 CALIBRATION OF THE DATA ACQUISITION SYSTEM

The calibration of the microcomputer data acquisition system which was described before used constant DC level inputs to each channel from a voltage power supply. In practice negative voltage pulses with decay time ≃10 µs are required to be recorded and the method for calibration is as follows. A precision exponential and square pulse generator, attenuator, emitter follower, stretcher amplifier, and oscilloscope were used with the data acquisition unit in the calibration. The aim of the calibration is to adjust the data acquisition unit to have a standard response to the passage of a cosmic ray particles through it to give us the real value of the pulse heights at the cosmic ray detector outputs. The system was calibrated as below:

### (i)    Measurements with no stretcher amplifier

The data acquisition unit (D.A.U.) was calibrated with no stretcher amplifier, and the block diagram of the system used is shown in Figure 2.2. The output pulses from the pulse generator were passed through the attenuator, then the pulse heights of the output pulses were displayed on the oscilloscope and on the PET through the D.A.U.

The threshold readable pulse width in µs at the input to the D.A.U. was determined by using a pulse generator to generate square pulses of different width at the input to the D.A.U. As shown in Figure 2.3a it was found that the threshold readable pulse width at the input to the D.A.U. is approximately 6.5 µs.

Using a pulse generator to generate negative square pulses of different width at the input to the D.A.U., a good relation was found between the pulse height at the input to the D.A.U.
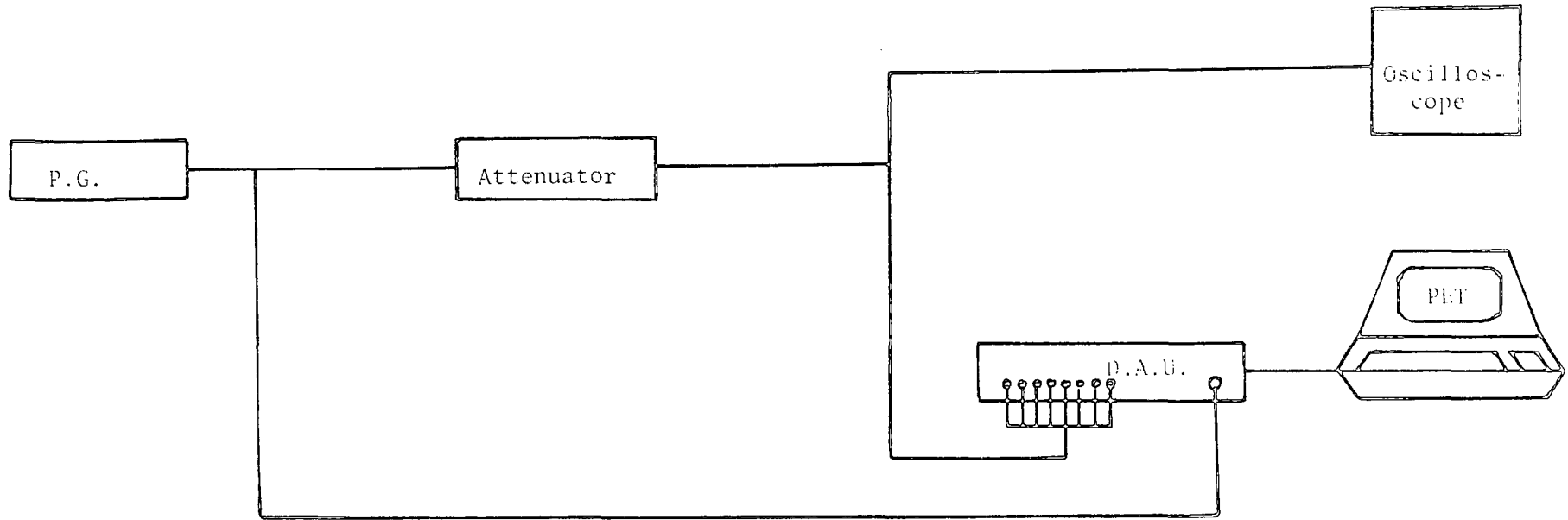
Figure 2.2 : Block diagram of the system used to calibrate the data acquisition unit
(D.A.U.) with no stretcher amplifier.
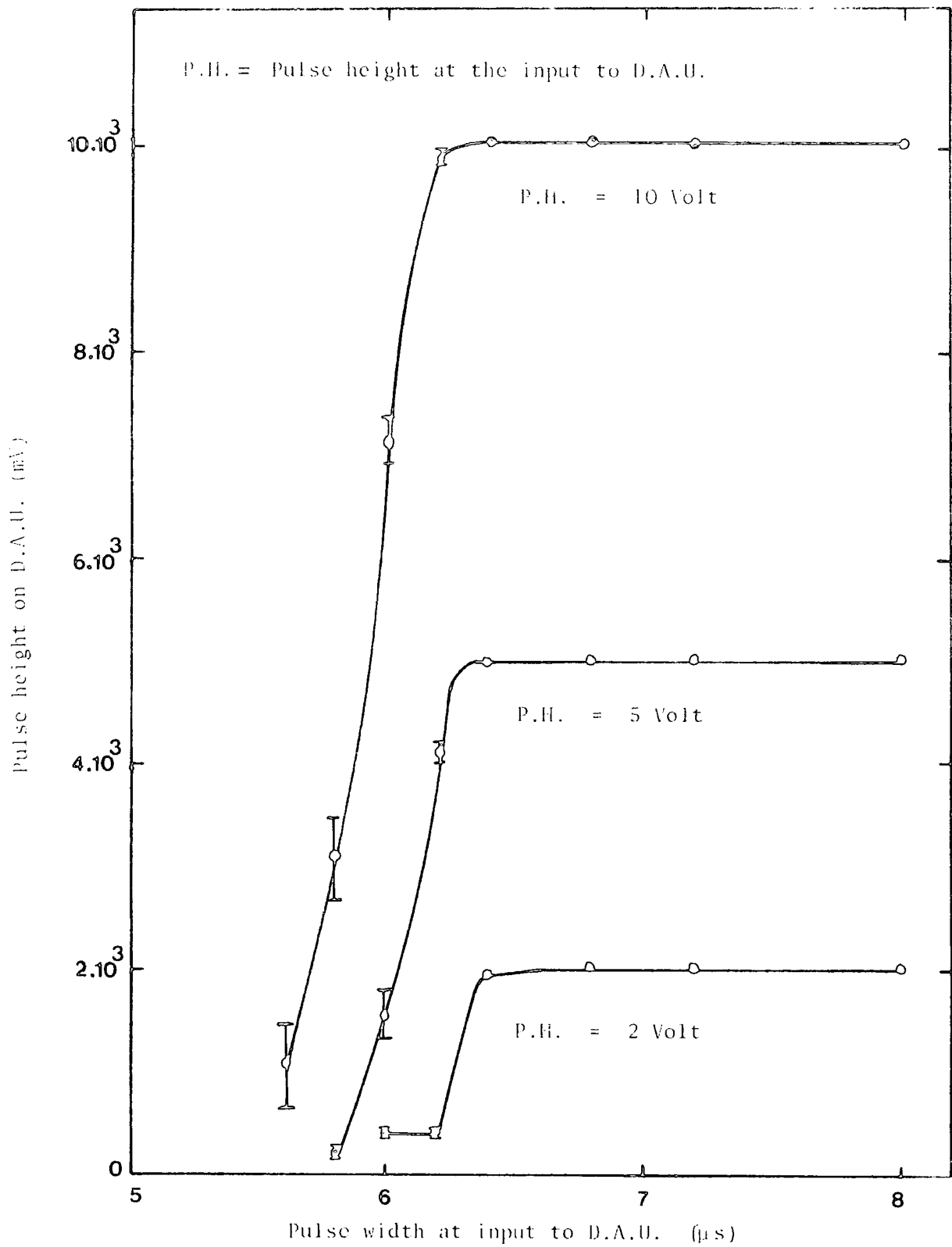
Figure 2.3a : Determination of threshold readable pulse height at the input to the data acquisition unit.

(pulse height on the oscilloscope) and the pulse height at the output of the D.A.U. (pulse height on the PET) for pulse widths down to 7 µs. Figure 2.3b shows a relation between the pulse height at the input to the D.A.U. and the pulse height at the output of the D.A.U. for pulses of width 50 µs at the input to the D.A.U.

The D.A.U. was calibrated by using a pulse generator to generate negative exponential pulses of different decay time at the input to the D.A.U. It was found that using pulses of long decay time there is a good relation between the pulse height at the input to the D.A.U. and the pulse height at the output of the D.A.U., and the slope of the best line through the measurements was found to be approximately 1 (see Figure 2.3c). But not the same agreement was found using pulses of short decay time. That is clear because the data captured by the D.A.U. was delayed for approximately 6.5 µs from the time of the external trigger, where as shown before the external trigger delay command was used.

(ii)    Measurements using the stretcher amplifier to generate pulses of different decay time at the input to the D.A.U.

The block diagram of the system used in that case is shown in Figure 2.4. The D.A.U. was calibrated here by using a stretcher amplifier to generate pulses of different decay time at the input to the D.A.U. Exponential pulses of decay time 1 µs and 10 µs at the input to the stretcher amplifier were used (see Figures 2.5a,b).

(iii) Calibration of the final workable system

To enable the D.A.U. to be capable of measuring the real value of cosmic ray pulses with short decay time at the output of the head unit of scintillators A and B in the electron density spectrum experiment (see Chapter four), a stretcher amplifier was
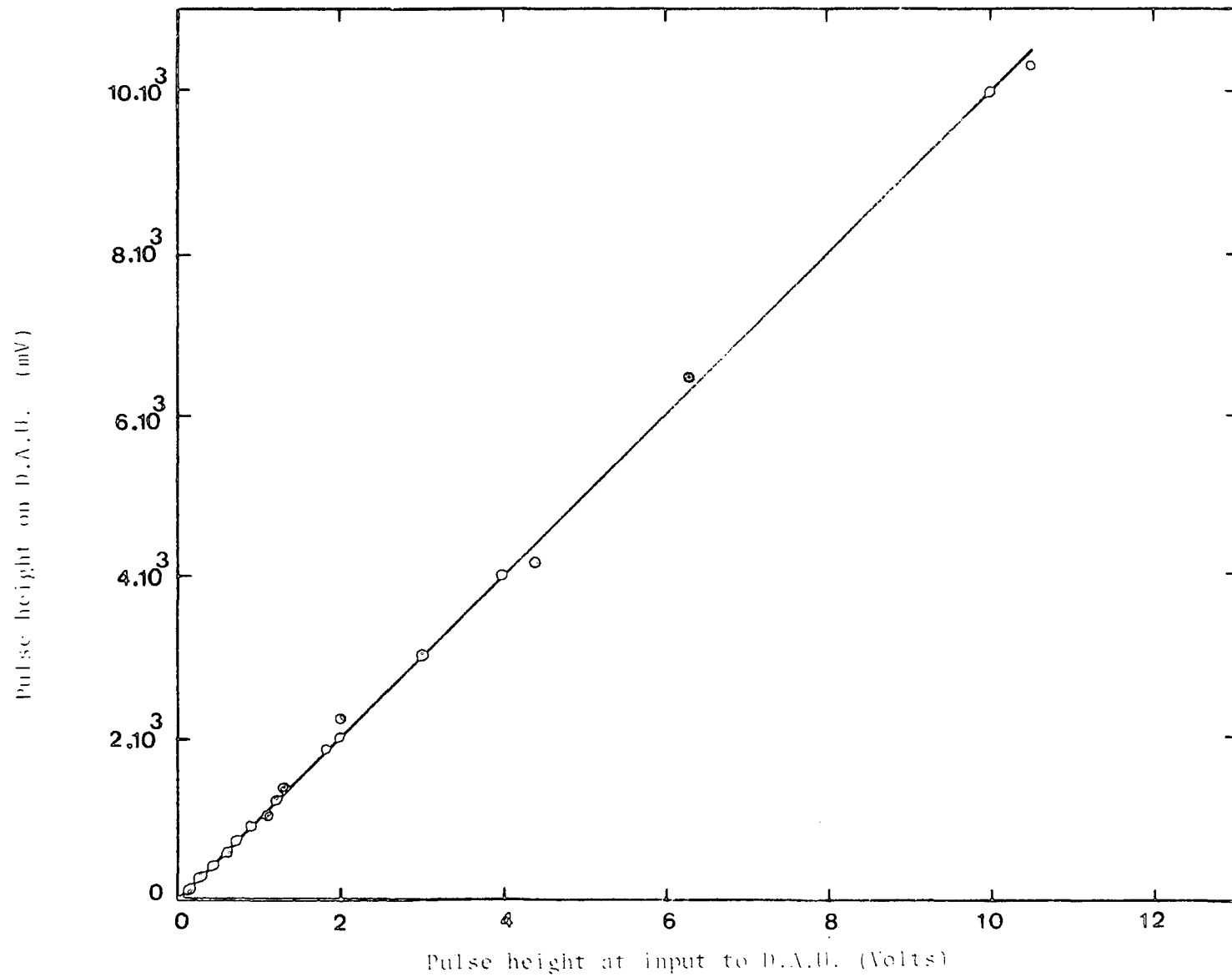
Figure 2.5b : Calibration of the data acquisition unit using 50 μs width input
square pulses. Similar results obtained for pulse widths down
to 7 μs (see figure 2.3a).
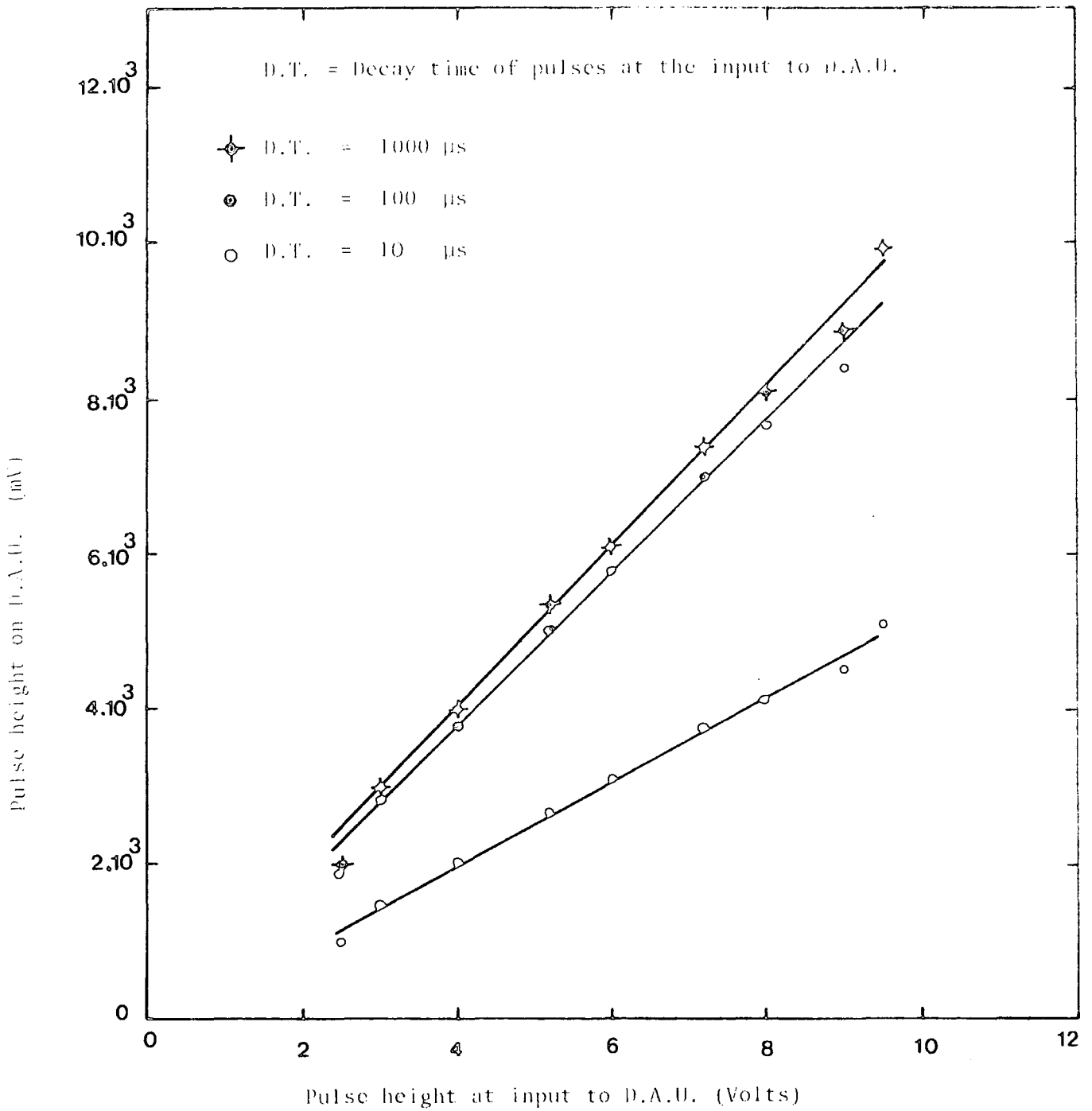
Figure 2.3c : Calibration of the data acquisition unit using negative exponential pulses.
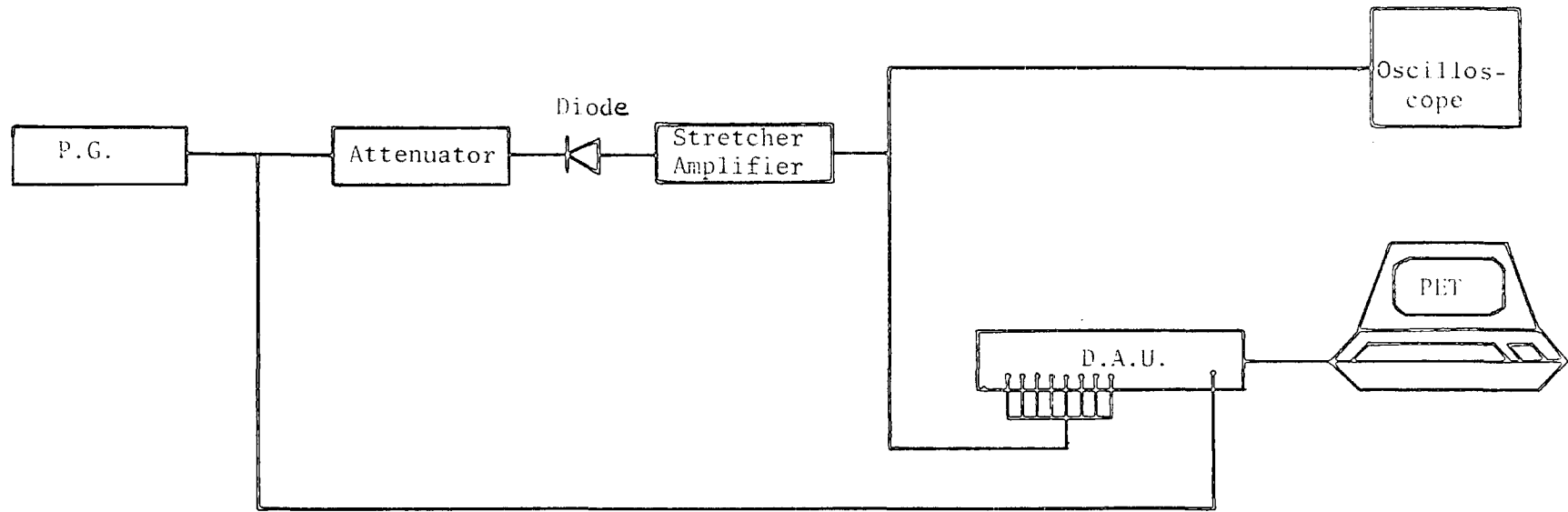
Figure 2.4 : Block diagram of the system used to calibrate the data acquisition
unit (D.A.U.) using a stretcher amplifier to generate pulses of
different decay time at the input to the D.A.U.
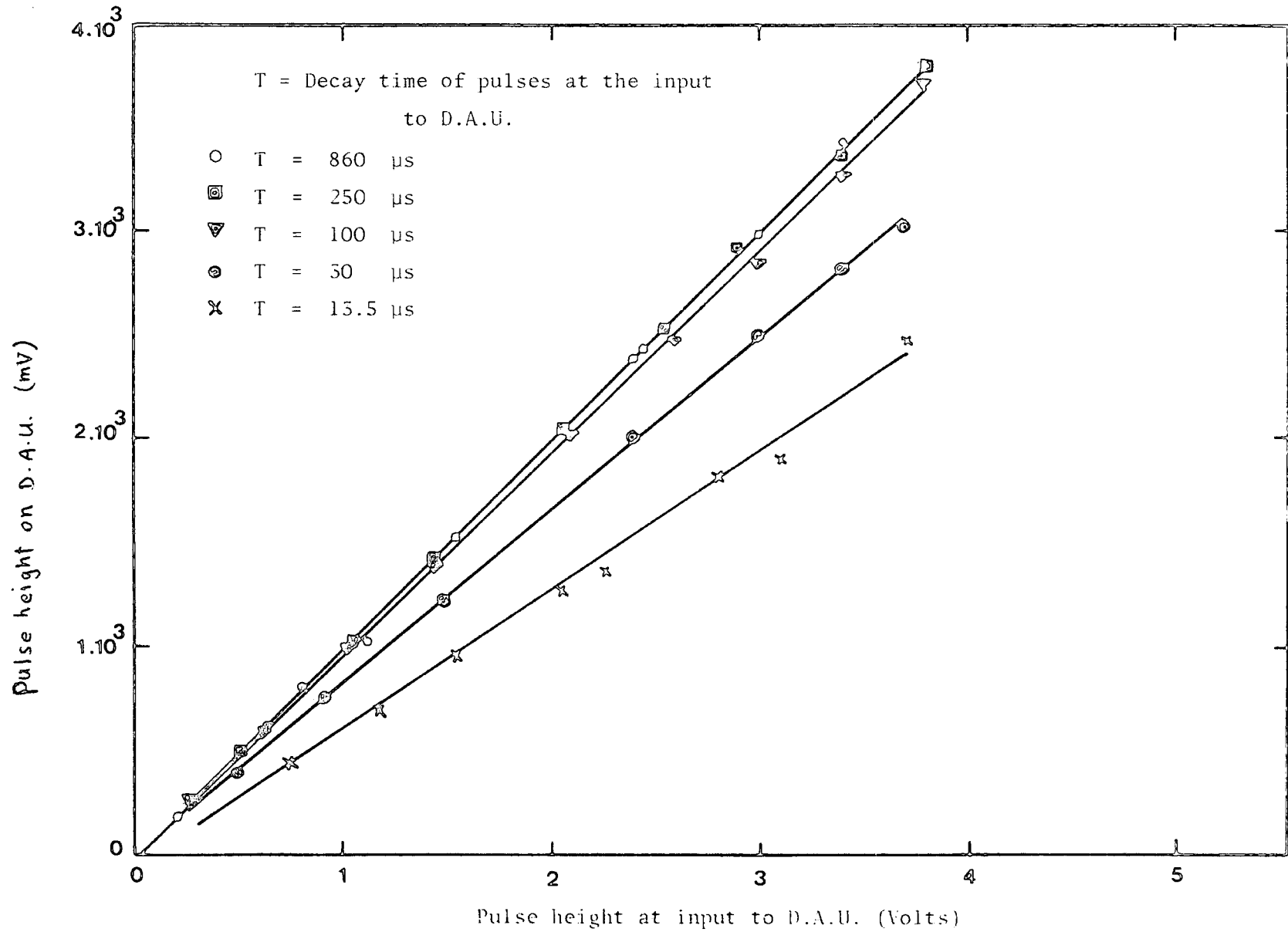
Figure 2.5a : Calibration of the data acquisition unit using a stretcher amplifier to generate pulses of different decay time at the input to the D.A.U. Pulses of decay time 10 μs at the input to the stretcher amplifier were used.
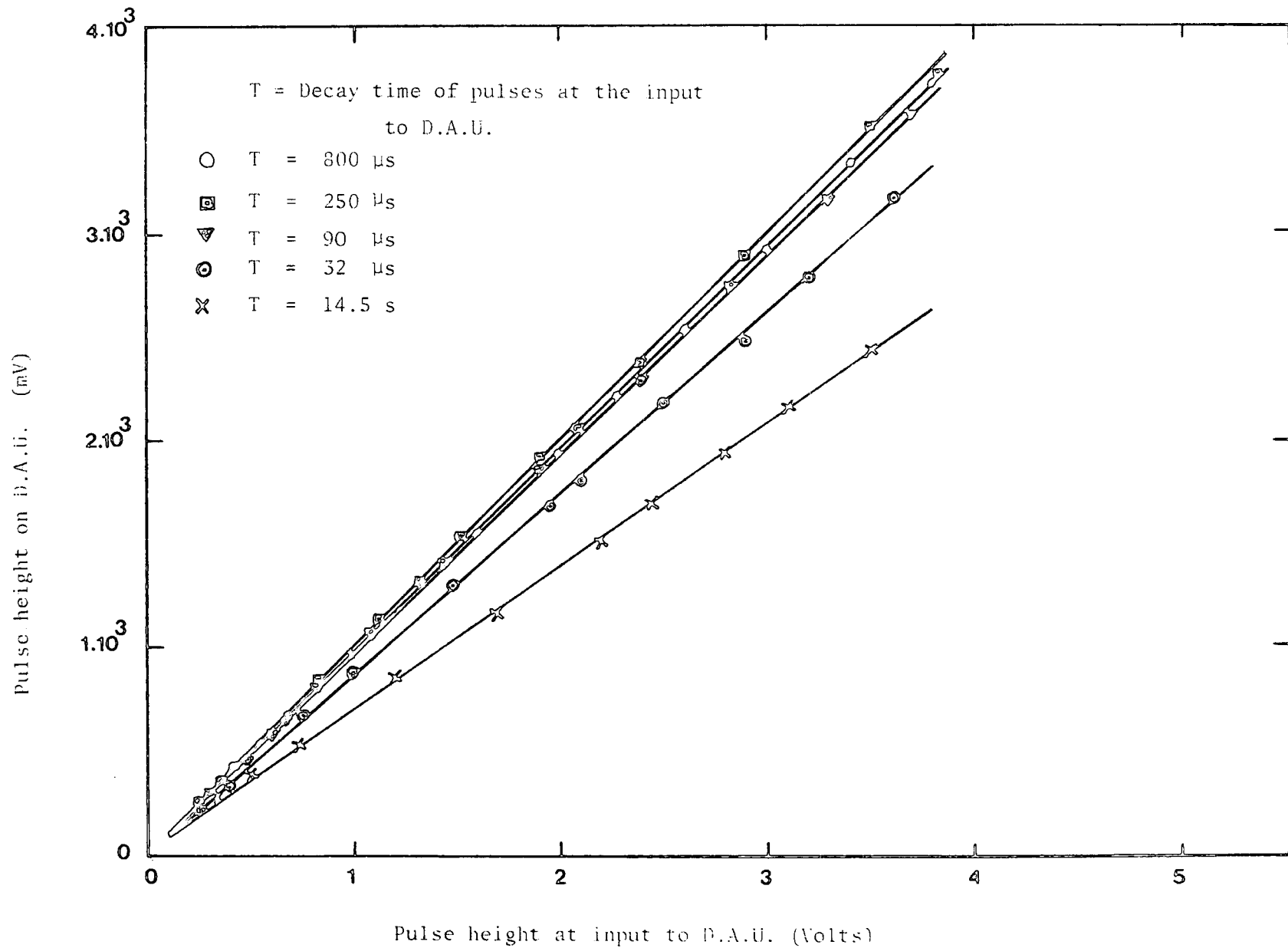
Figure 2.5b : Calibration of the data acquisition unit using a stretcher amplifier to generate
pulses of different decay time at the input to the D.A.U. Pulses of decay time
1 μs at the input to the stretcher amplifier were used.

used for each scintillator to generate pulses of long decay time at the input to the D.A.U. The decay time of cosmic ray pulses captured in that experiment was found to be approximately 8.5 µs.

A block diagram of the final workable system used for calibration of the combination of the stretcher amplifier and the D.A.U. is shown in Figure 2.6. The system was calibrated by using exponential pulses of decay time 1 µs and 10 µs at the input to the stretcher amplifier, see Figures 2.7a,b. Square pulses of decay time 1 µs and 0.1 µs at the input to the stretcher amplifier were also used to calibrate the system as shown in Figures 2.7c, d.
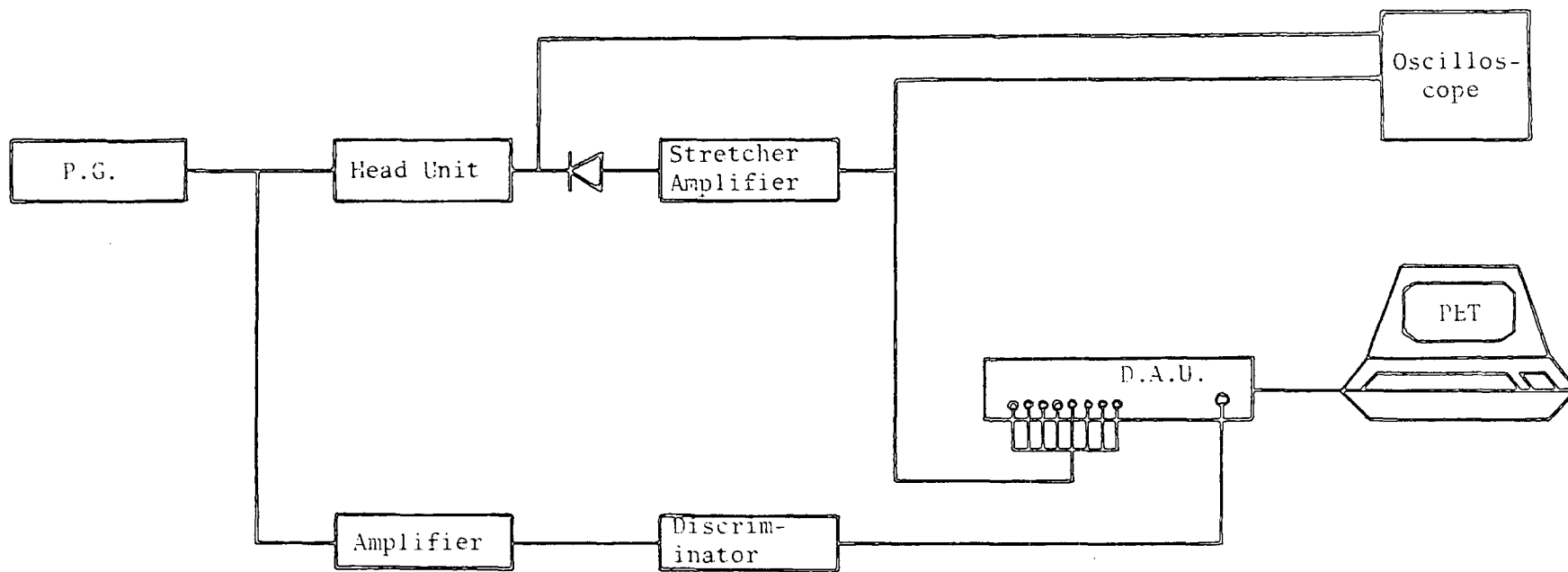
Figure 2.6 : Block diagram of the final workable system used for calibration of the combination
of the stretcher amplifier and the data acquisition unit (D.A.U.)
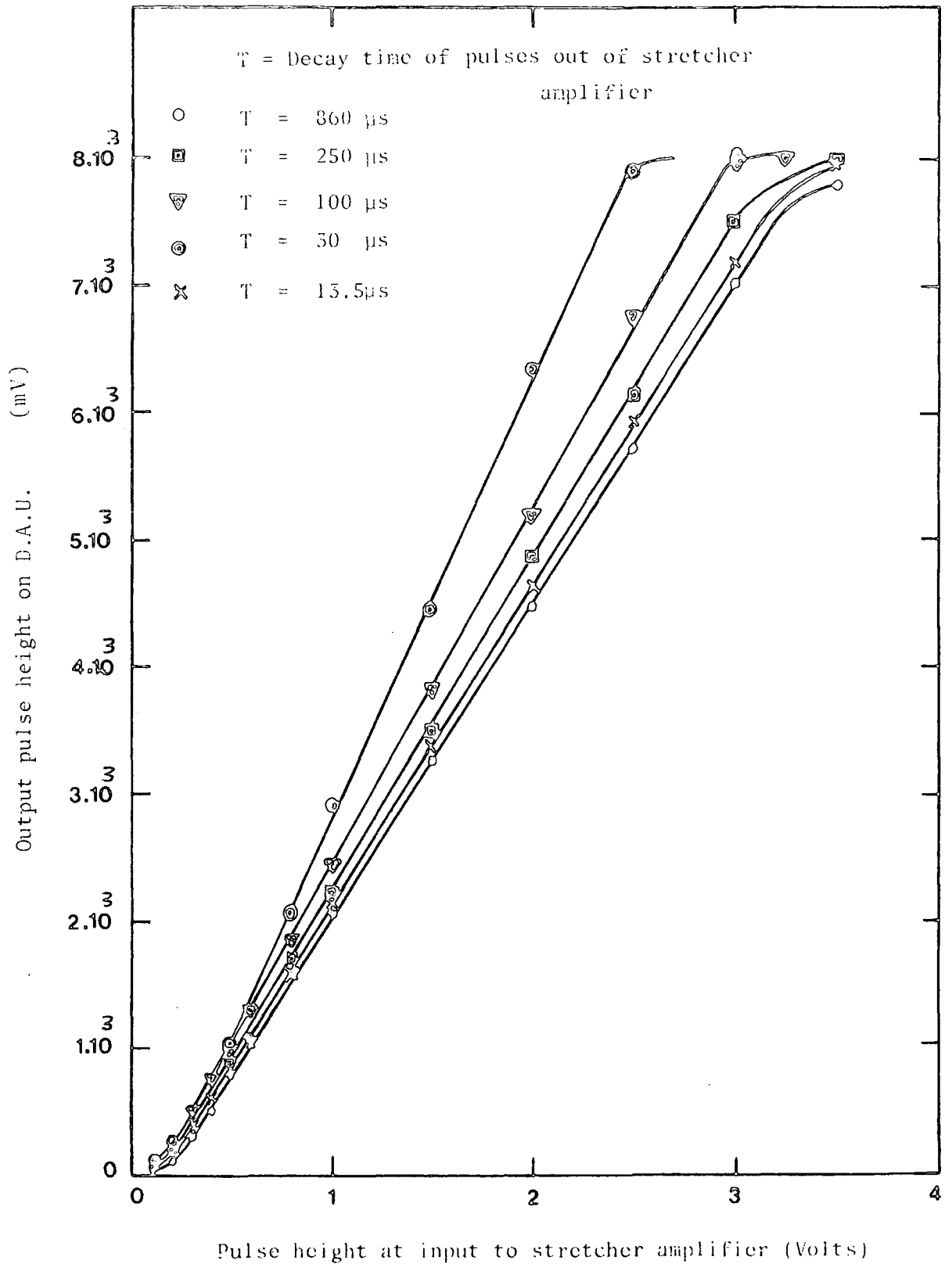
Figure 2.7a : Calibration of the combination of stretcher amplifier and the data acquisition unit using 10 μs decay time input exponential pulses.
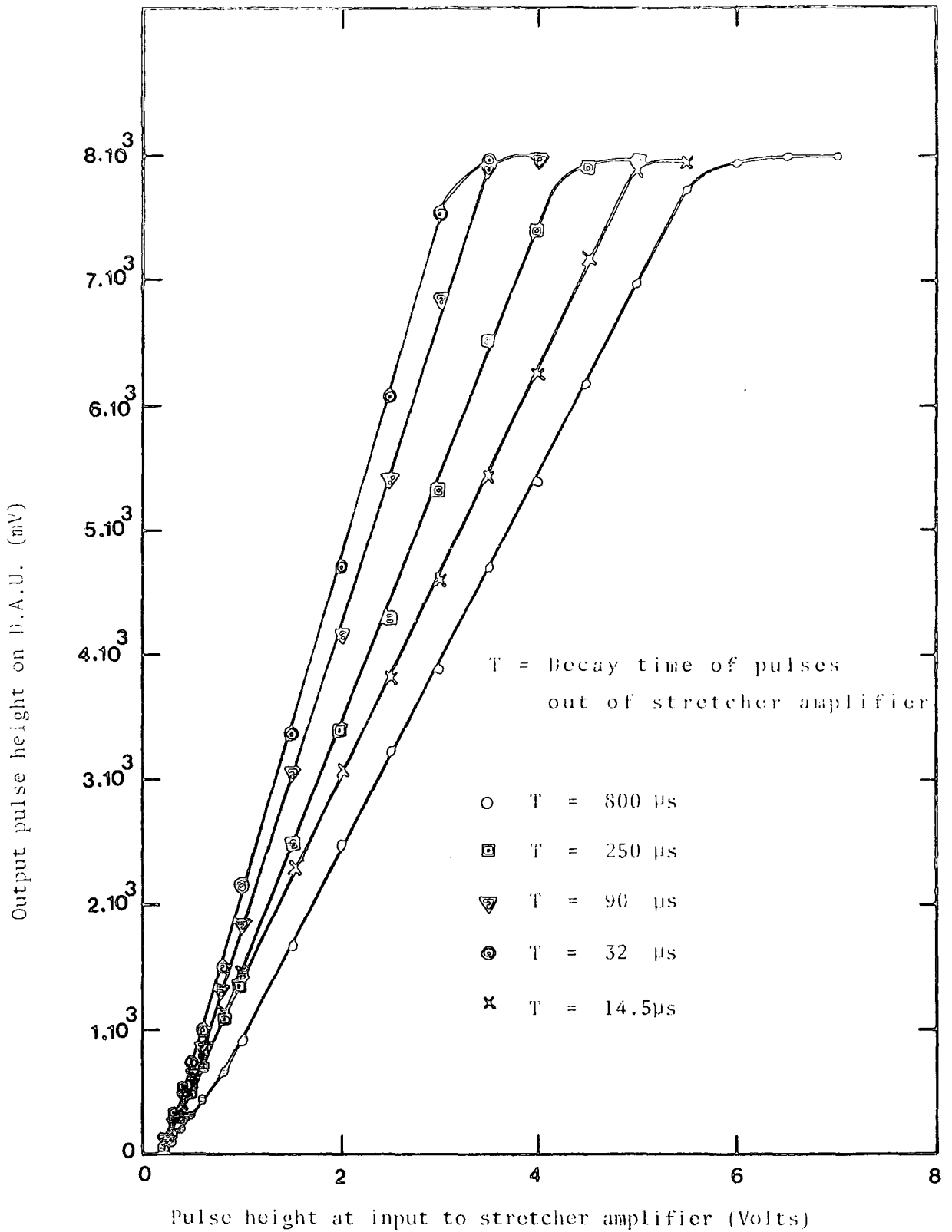
Figure 2.7b : Calibration of the combination of stretcher
amplifier and the data acquisition unit using
1 µs decay time input exponential pulses.
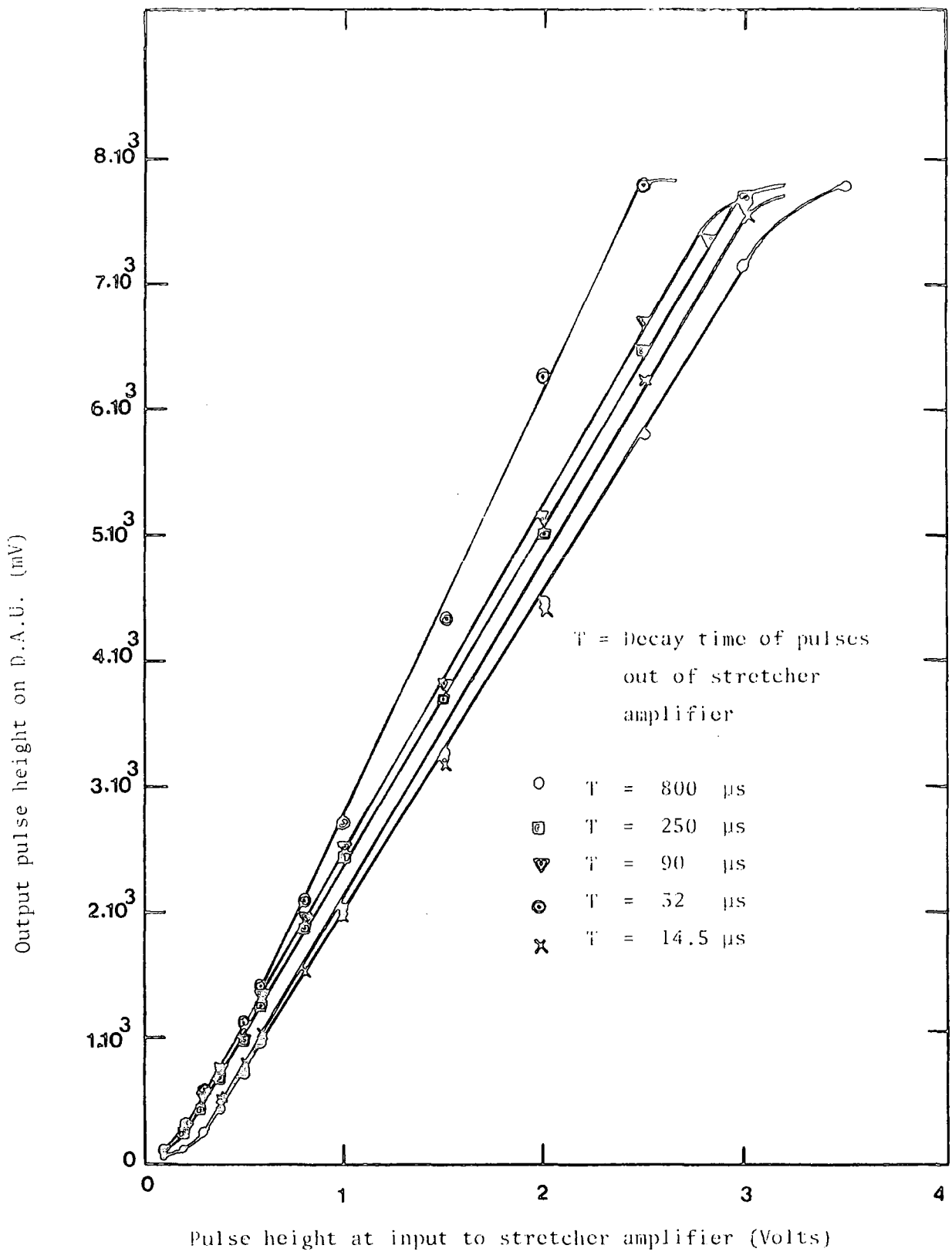
Figure 2.7c : Calibration of the combination of stretcher
amplifier and the data acquisition unit using
1 μs decay time input square pulses.
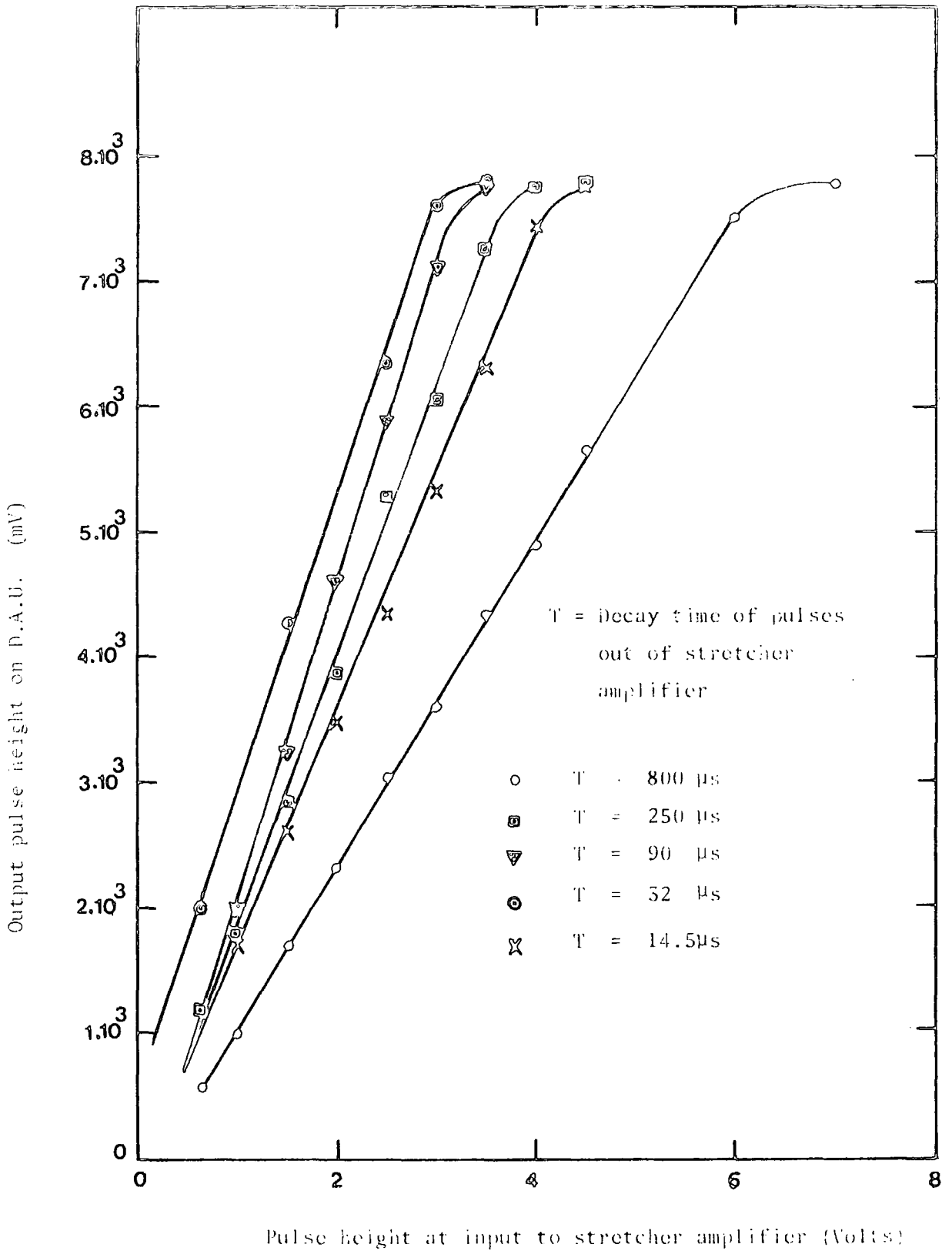
Figure 2.7d : Calibration of the combination of stretcher
amplifier and the data acquisition unit using
10 ns decay time input square pulses.

# CHAPTER THREE

## GEIGER MÜLLER COSMIC RAY TELESCOPE

### 3.1 INTRODUCTION

The great majority of the particles of cosmic radiation which are incident on the earth's surface are not primary particles but are secondaries which owe their origin to high energy, nucleon-nucleus interactions in the atmosphere. The approximate composition of the primary radiation is 87% protons and 13% neutrons, the latter being bound in nuclei. Such nucleons have an interaction length of approximately 80 gcm$^{-2}$ and the probability of their arriving at the earth's surface without interacting is less than 10$^{-5}$. In the interactions of the primary particles in the atmosphere, both charged and uncharged particles, mainly pions and kaons, are produced (see Chapter one). The charged pions, if they do not interact, decay to muons as do also some of the kaons. The majority of the muons so generated, being weakly interacting particles and having a lifetime of 2 x 10$^{-6}$sec, tend to traverse the remaining atmosphere without interacting or suffering decay. The main mechanism by which muons lose energy is that of ionization and the typical loss for a muon travelling in the near vertical direction is 2 GeV (for E$\mu$ < 100 GeV).

The purpose of the present experiment is to measure the flux of cosmic rays at different zenith angles, to note whether there is any difference between the flux from the east and the flux from the west and to find the rate of coincidence events through the coincidence unit using the data acquisition unit (D.A.U) and scaler.

## 3.2 EXPERIMENTAL ARRANGEMENT

The block diagram of the cosmic ray telescope is shown in Figure 3.1. The apparatus used consisted of two layers of Geiger-Müller counters each containing six identical counters, which could be tipped at any desired zenith angle. The distance between those two layers was selected to give a suitable count rate at the same time as giving a fair resolution, and it was 56.8 cm (see Figure 3.2).

The length of each counter was 73 cm, the sensitive length was 67 cm, the internal diameter was 3.5 cm, and the diameter of the central anode wire which was made of tungsten was 0.01 cm. Figure 3.3 shows the construction of the counter used.

The apparatus was housed in a laboratory on the first floor in the building of the physics department in Durham University, the roof and the wall of which is composed mostly of concrete. This means that cosmic ray electrons from the atmosphere would be absorbed before reaching the telescope so that only muons were detected.

At first, each of the Geiger counters was checked to ensure that it was working correctly and that the voltage on that particular counter was neither too high nor too low. Hence, by using the switches attached to the tray, one and only one counter could be selected and the number of particles passing through that counter was counted by switching in only the one input into the coincidence unit. The starting potentials of the counters were checked daily and all counters were operated at exactly the same voltage above the starting potential. Each counter was operated at 50 volts above its starting potential, the starting potentials were approximately 1300 volts (see Figure 3.4).
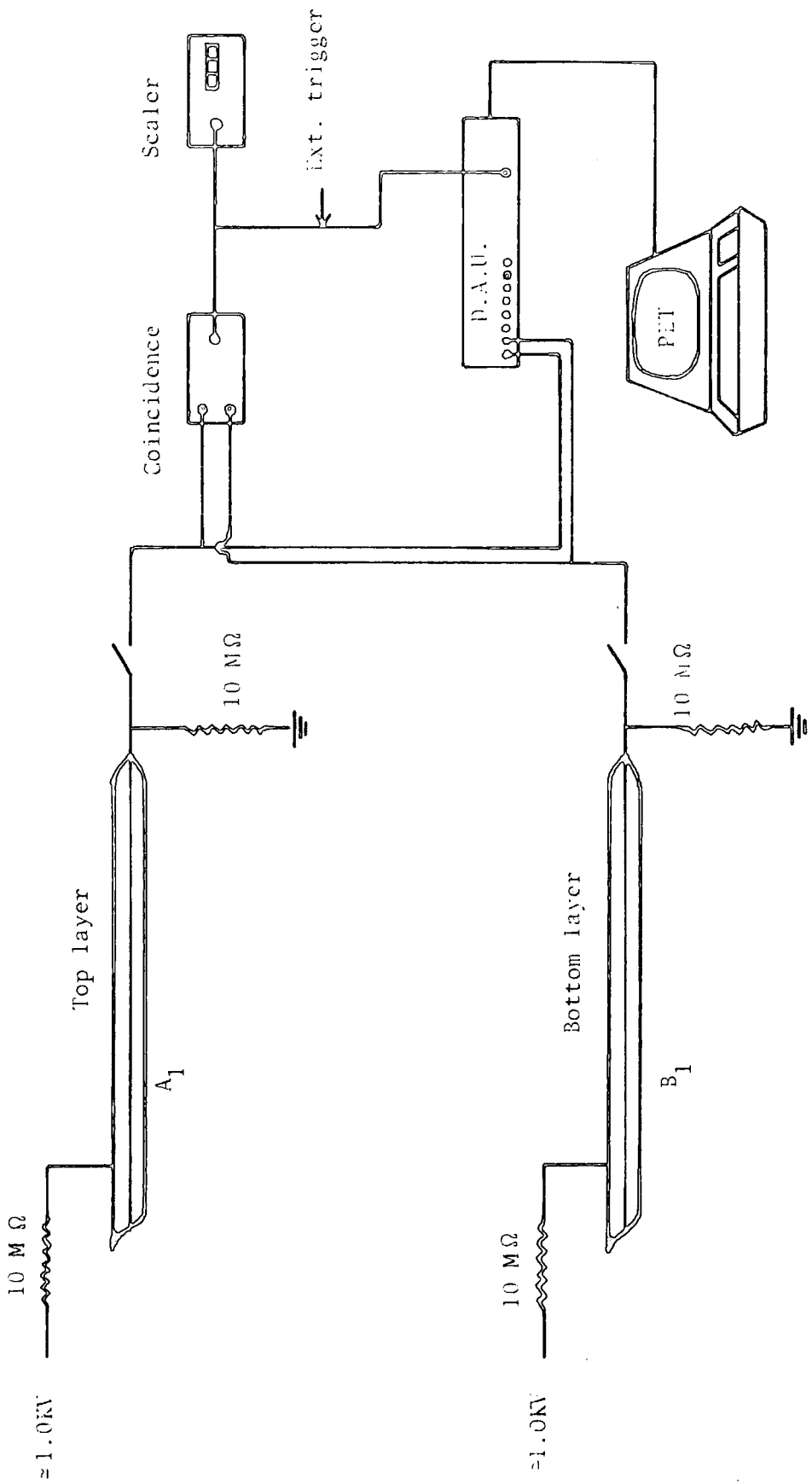
Figure 5.1 : Block diagram of Geiger-Müller cosmic ray telescope

A

Top layer

1 2 3 4 5 6

B

Bottom layer

1 2 3 4 5 6

Front view
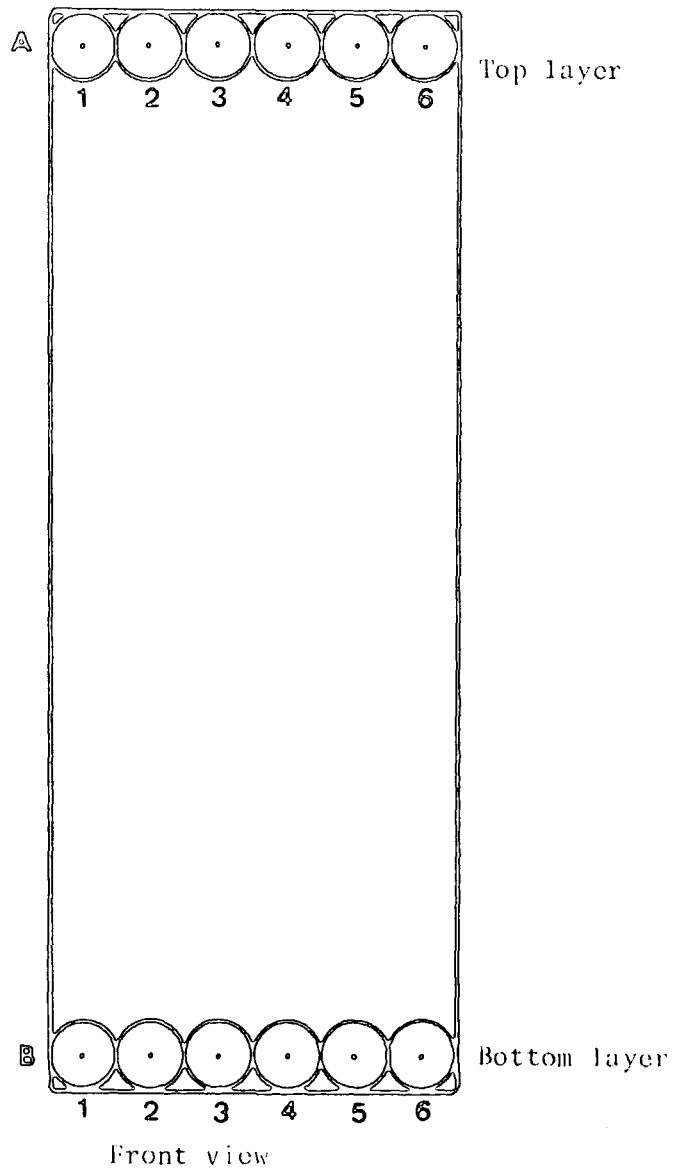
Scale : 
0     4 cm

Figure 3.2a : Front view of the Geiger-Muller cosmic
ray telescope.

Top layer

$A_1$

Bottom layer

$B_1$
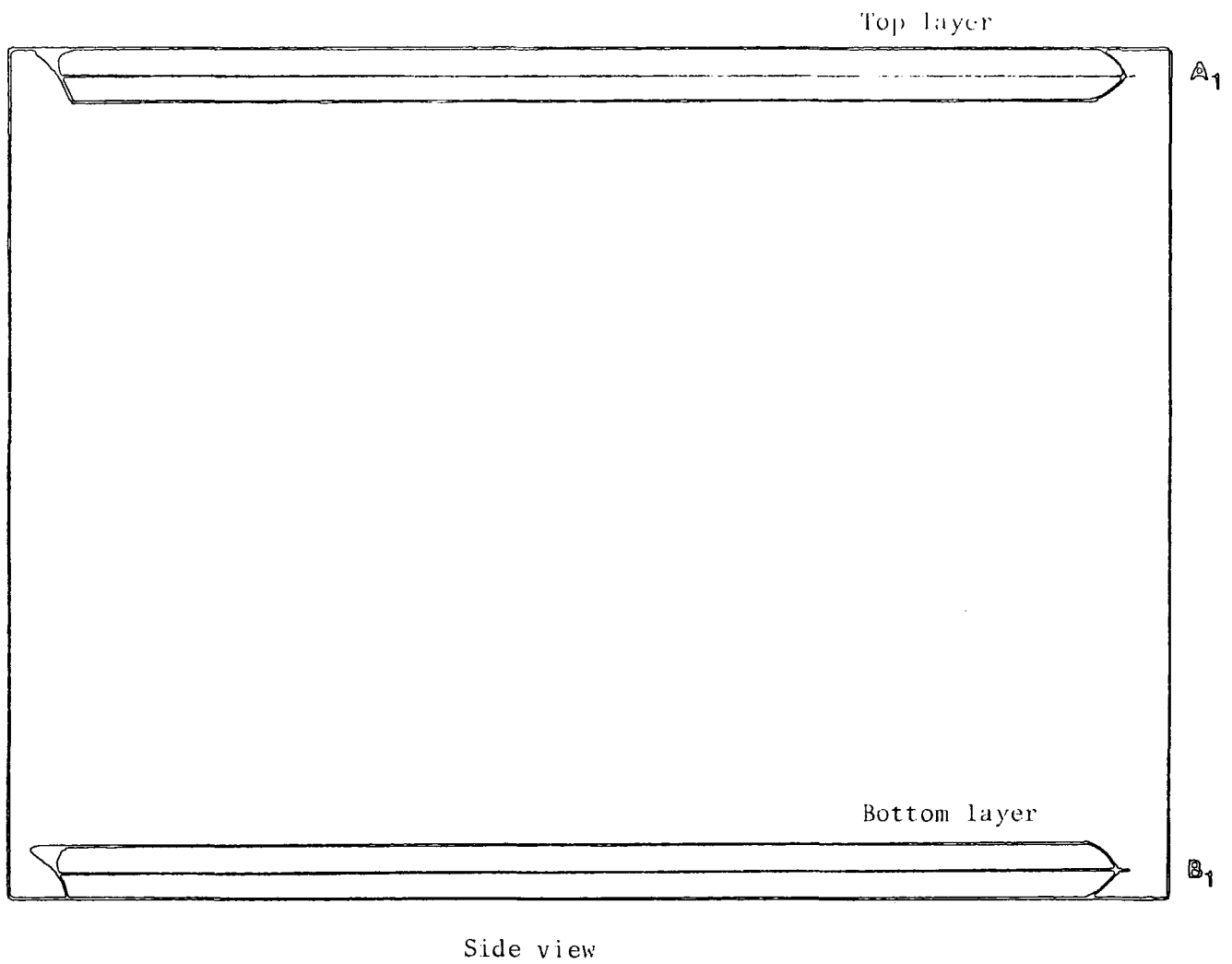
Side view

Scale: 
|----|
0     4 cm

Figure 3.2b : Side view of the Geiger-Muller cosmic ray telescope.
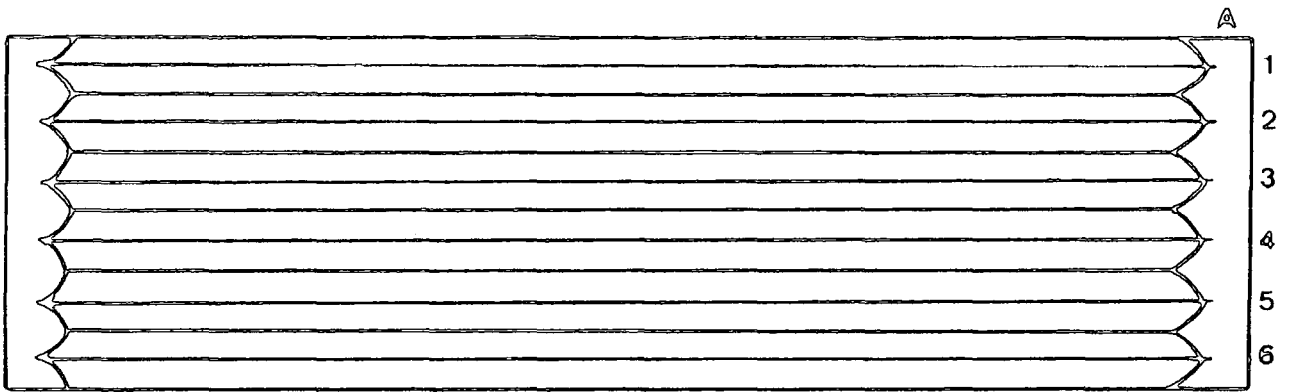
Top view

Scale: ⊢━━━┤
0    4 cm

Figure 3.2c : Top view of the Geiger-Müller cosmic ray telescope.

Tungsten wire of diameter 0.1 mm.

Thin graphite conducting layer

3.5

73

Sensitive length of central
wire = 66.5

Scale:   0      5 cm
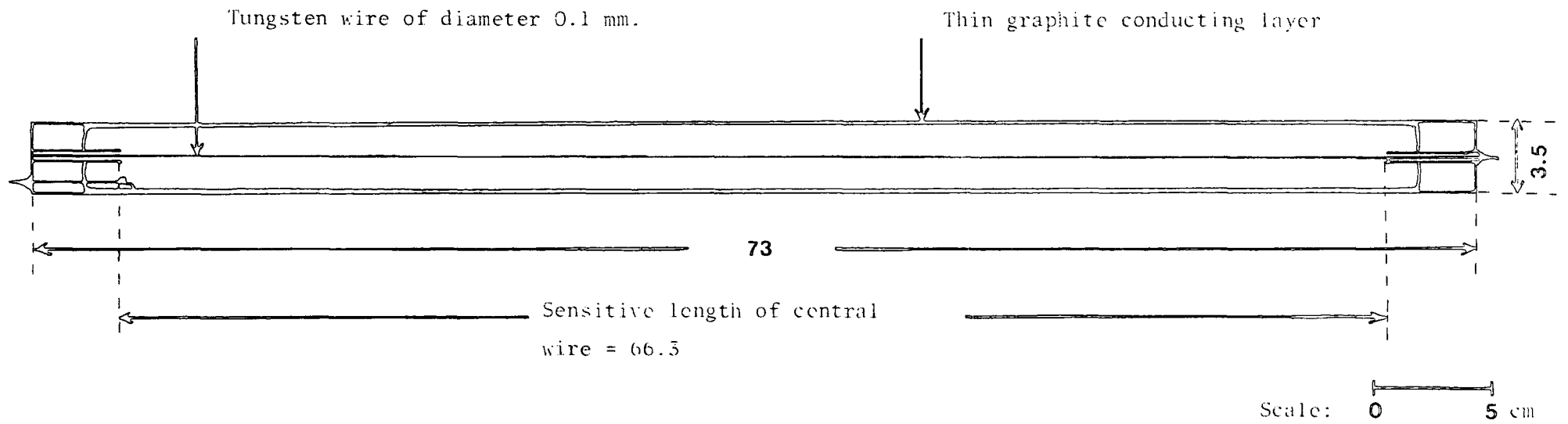
Figure 5.5 : Diagram showing Geiger-Müller counter construction. All dimensions are in centimetres.

Counting rate (min.$^{-1}$)

Applied Voltage (Volts)
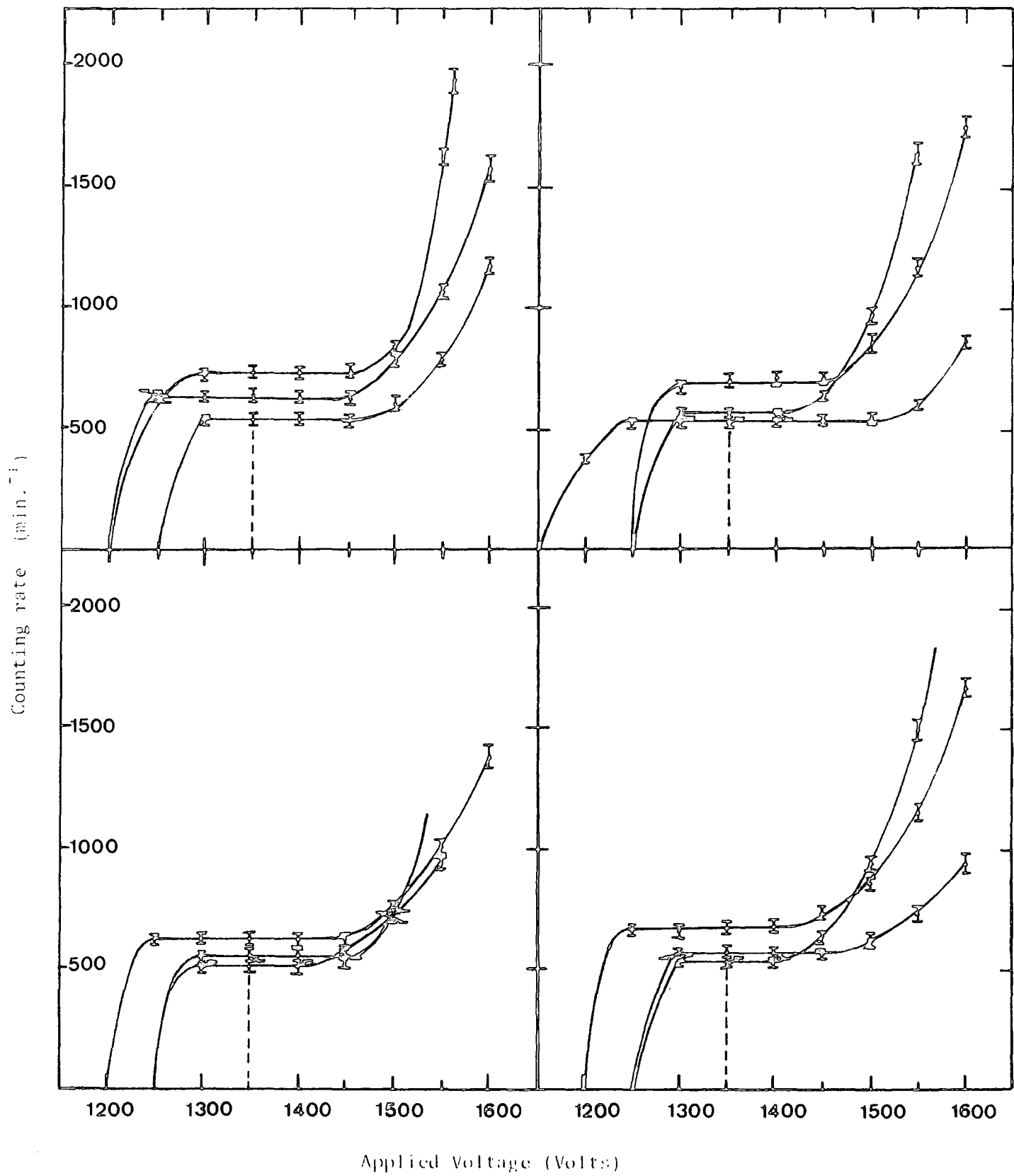
Figure 3.4 : Determination of operating voltage of the counters used in the Geiger-Müller cosmic ray telescope.

The principal measurements were of the coincidence rate between the counters in the top layer and the counters in the bottom layer. The particles passing any one of the six counters produces a pulse which is fed along coaxial cable to the coincidence unit. Similarly for the other array of counters a pulse on any of the counters gives a signal at the coincidence unit. If there is a signal on both inputs to the coincidence unit then there is an output to the PET (through the D.A.U) and to the scaler at the same time.

The zenith angles at which measurements were made were between 0° to 90° to the east and to the west, the axes of the counters being always in the south-north direction. The rate of events at those different angles have been measured and the graph was obtained of count rate versus angle, which will be described later.

## 3.3   ZENITH ANGLE DISTRIBUTION

The zenith angle distribution of the muon component at sea level has previously been measured by Greisen (1942). Representing the angular distribution by $R(\theta) = R_0 Cos^n\theta$ Greisen found n = 2.1. For particles in extensive air showers (corresponding to events produced by much higher primary energies than the low energy muon component) several studies have been made and this work is now summarised.

The size dependence of the zenith angle distribution of extensive air showers at sea level is a fundamental constant of the cosmic radiation. Also the exact form of the zenith angle distribution is sensitive to the characteristics of high energy interactions (Kalmykov et al 1973).

The angular distribution of showers about the zenith can be found from the observed altitude dependence of the rate of air showers by making use of the Gross transformation. At a given altitude, apparatus detecting showers will record not only those with axes at the zenith, but also those at large angles. The response of the apparatus depends not only on the angular distribution of showers axes about the vertical, but also on its own lateral dimension and disposition on the horizontal plane. Assume that the primary particles are falling isotropically on the atmosphere, and that the development of the shower depends only on the amount of air shower, and is independent of decay processes of mesons produced in the nuclear interaction.

At the horizontal plane through P, let the vertical intensity of showers per unit solid angle at a depth t be $I(t,o)$. This intensity at P from the direction $\theta$, $I(t,\theta)$ would be then equal to $I(t \sec \theta, 0)$, but in practice this is not so because of the geometry of the detecting apparatus and the variation in the lateral structure of the shower with height. The equivalent height, $t \sec \theta$, for the inclined shower is lower in the atmosphere, and the lateral spread of the shower is inversely proportional to air density $\rho$.

The zenith angle dependence of the showers for a detector which is isotropic in response can be represented by using the equation below (Galbraith, 1958).

$$I(t,\theta) = \frac{R(t \sec \theta)}{2\pi} \left[ n+1-t \sec\theta \frac{\partial\log R(t \sec \theta)}{\partial t} \right] \cos^n \theta$$

where $R(t)$ is a counting rate at depth t, and n is a constant.

Kraybill (1949) used the above method to determine the zenith angle distribution of air shower axes, to find values of $R(t)$ and its

derivative $\partial \log R(t)/\partial t$. He also computed the differences which arise in the determination of the zenith angle distribution using detectors of different angular sensitivity. The cases he considered were (i) isotropic detector, (ii) cylindrical detectors, (iii)tray of G-M counters, and the results showed that the angular distribution was essentially independent of the angular response of the detectors. Kraybill's (1949) calculations were compared with the results of experiments by Daudin (1945), and those of Deutshmann (1948) at sea-level. It was found that there was reasonably good agreement with the theory.

Previous measurements Galbraith (1958), Hayakawa (1969), Ashton et al (1975) related to a wide range of shower size and no systematic studies using a single EAS array have been made. Ashton et al (1979) used fast timing to determine the zenith angle of individual EAS and the zenith angle distribution as a function of shower size was studied over the size range $10^4 - 1.4.10^6$ particles at sea level. Representing the zenith angle distribution by $I(\theta) = I(o)\cos^n(\theta)$ the measurements are consistent with $n = 8.4 \pm 0.3$ over the size range $5.10^4 - 1.4.10^6$. At the smallest sizes studied $10^4 < N < 5.10^4$ the measurements suggest n decreases to $5.1 \pm 1.3$.

In the present experiment the cosmic ray angular distribution was found in the range $\theta = 0° - 90°$. We have described the zenith angle distribution by $R(\theta) = R_o \cos^n \theta$ where the telescope is not pointing in the vertical direction but at some angle, $\theta$, where $R(\theta)$ represent the rate of showers at zenith angle $\theta$. $R_o$ is vertical rate, and the index n is a constant which may be a function of shower size, where usually the zenith angle dependence of EAS,

caused primarily by the absorption effect by the atmosphere is represented by the equation above. To find the best value of n that describes the zenith angle distribution of showers in $R(\theta) = R_0 \cos^n \theta$/unit area/unit time/unit solid angle, $LogR(\theta) - Log \cos \theta$ plot method has been used. If $R(\theta) = R_0 \cos^n \theta$ then a plot of $\log R(\theta)$ versus $\log \cos \theta$ will be a straight line of slope n. We found that the value of $n = (1.54 \pm 0.01)$ in the range of zenith angle $\theta = 0° - 70°$, and $n = (1.82 \pm 0.01)$ in the range of zenith angle $\theta = 0° - 40°$, see figure 3.5 . The latter value is consistent with previous work. The reason for the decrease of n with increasing range of zenith angle is believed to be due to the soft component (knock on electron showers etc.) which accompanies the muon component under absorbers. Small vertical electron photon showers accompaning vertical muons will be registered by the telescope as two fold coincidences at large zenith angles. This will give a smaller value of n than the true value. However this effect should become decreasingly important as the zenith angle decreases as is found in the present measurements.

## 3.4   GEOMAGNETIC EFFECTS

The effect of the earth's magnetic field on cosmic rays has been known for a long time and a great deal of experimental data has been accumulated on the consequent variations of the flux with respect to inclination to the vertical, latitude and longitude. The basic problem to be considered is the interaction of a primary cosmic ray with the earth's magnetic field as it approaches the earth. Only comparatively high energy primaries ($\geq 10$ GeV) produce charged secondaries which are able to arrive at sea level before being absorbed. This means that the geomagnetic effects will be much less at sea level than at high altitudes because it is the low energy

n = 1.54 ± 0.01

n = 1.82 ± 0.01
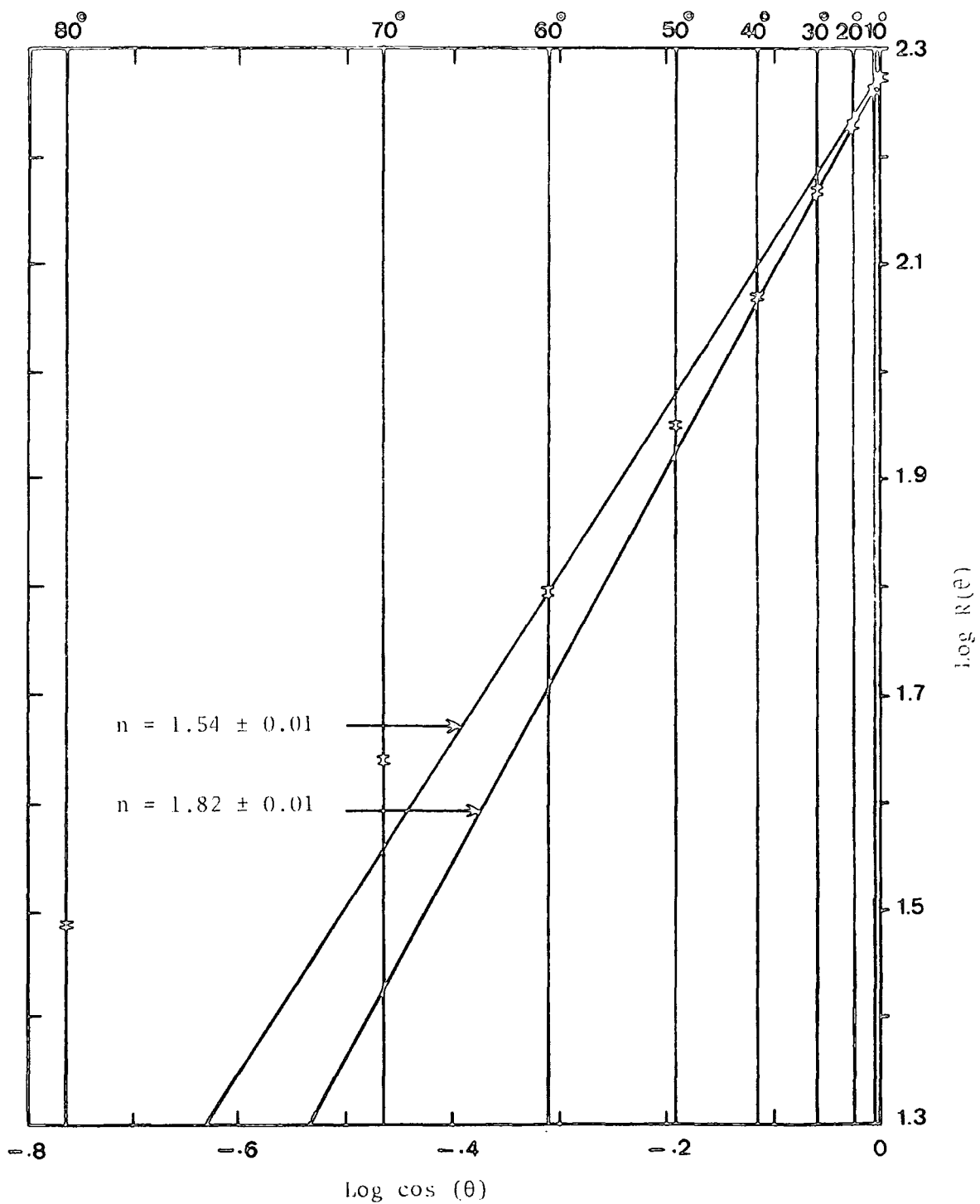
Figure 3.5 : Log R(θ) - log cos (θ) plot   (R = counting rate
per minute)

primaries that are most affected by the earth's field. The fund-
amental relation concerning the motion of a particle in a magnetic
field is : $\rho = \dfrac{1}{300} \dfrac{pc}{Ze} \dfrac{1}{H}$ , where $\rho(cm)$ is the radius of gyration
of a particle of charge $Ze$ and momentum $p$ $^{eV}/c$ in a magnetic field
of strength H gauss. $^{pc}/Ze$ is called the magnetic rigidity of the
particle. Solutions have been given by Störmer$^{(1932)}$ and later by Le Maitre,
~~Lemaitre~~ Vallarata and others. It has been shown that, at a partic-
ular point on the earth's surface, there are allowed and forbidden
directions of incidence for each magnetic field rigidity considered.
If we neglect the effect of the atmosphere and using the equation
above and if we know the value of earth's magnetic field and radius
we can find the rigidity of a particle trapped by the earth's field
and made to travel round the magnetic equator just above the earth's
surface. Particles of rigidity above this limit can always reach
the earth and particles of lower rigidity can only reach certain
regions and the extreme, particles of very low rigidity can only get
through to the earth by travelling along the axis of the dipole
and arriving at one of the poles. Usually the positively charged
particles arriving from the west have rigidities less than the
particles arriving from the vertical direction and the rigidities
from the vertical less than the rigidities of particles arriving
from the east.

In the present experiment measurements were made on the
variation of counting rate with angle to the vertical (zenith angle),
and it has been found that there is a difference between the rates
when measured with eastward and westward inclination. This
phenomenon is called the east-west effect and has been known for
many years. The variation is represented in Figure 3.6. It is usual
to define the east-west effect as $\epsilon = \dfrac{R_W(0)-R_E(0)}{\frac{1}{2}[R_W(0)+R_E(0)]}$ , where $R_W(0)$
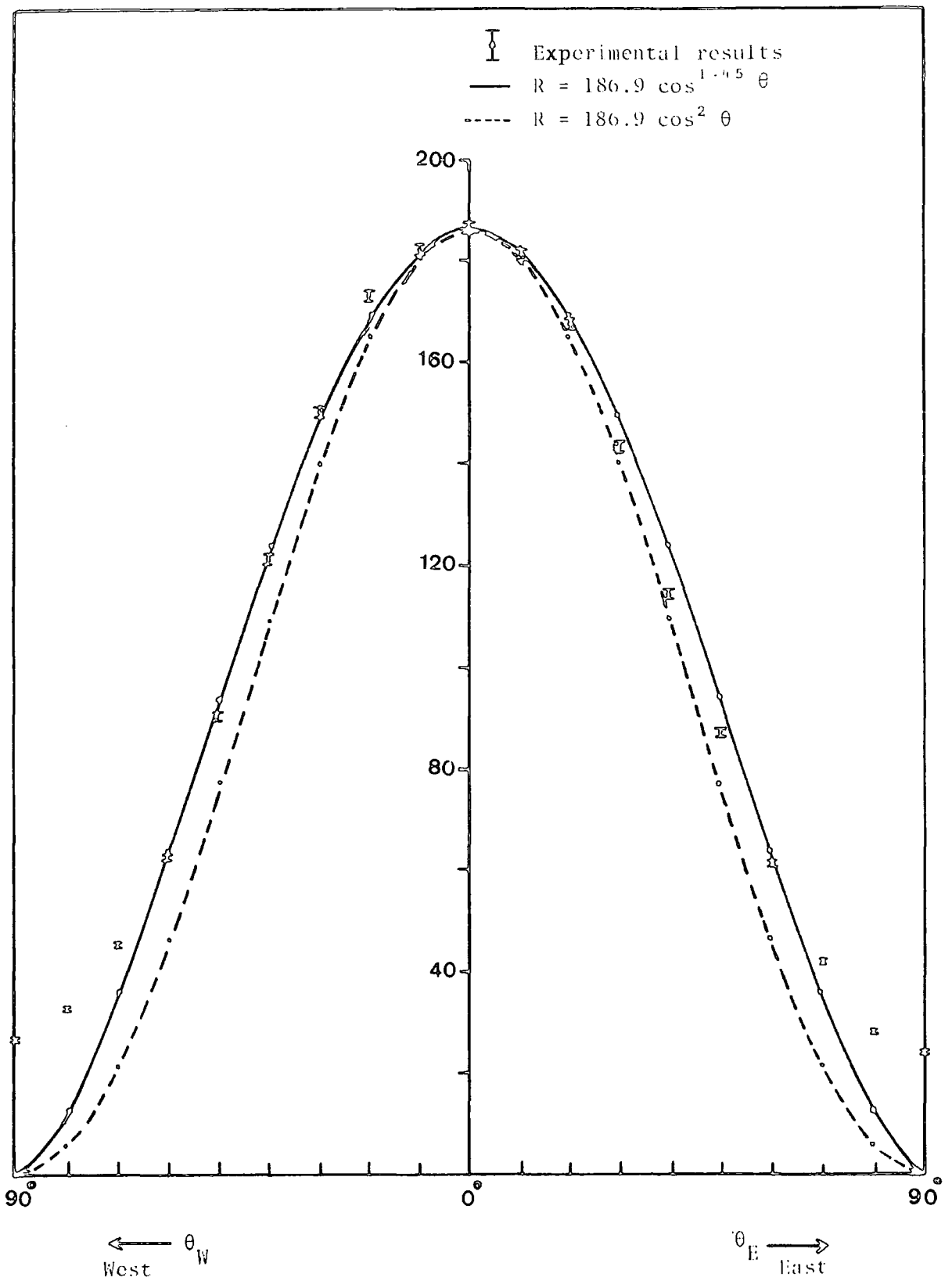
Figure 3.6  :  East-west effect.  The variation of counting rate
with zenith angle.

and $R_E(\theta)$ are the rate of zenith angle $\theta$ toward the west and east, respectively. It can be seen from Table 3.1 that the main results found are that $\varepsilon$ increases with zenith angle up to about 40°, above which it falls off. Typical value for the maximum value of $\varepsilon(\theta \approx 40°)$ is : $\varepsilon \simeq 0.06 \pm 0.01$.

The explanation of the effect in physical terms is quite simple. Briefly, since the primary radiation is entirely positively charged, there is a higher cut-off rigidity towards the east than toward the west and both rigidities increase with decreasing latitude. At any given latitude the energy lost by the secondaries in getting through the atmosphere increases with increasing $\theta$, i.e. increasing path length in the atmosphere (tsec $\theta$) where t is depth of atmosphere. This means that the energy of the primaries responsible for generating the particles arriving at sea level increases with increasing $\theta$. Now the difference in the rigidities between east and west increases with $\theta$ so that there are two competing effects occurring, the increasing difference in rigidities causing an increase in $\varepsilon$ and the increasing mean energy trying to produce a decrease in $\varepsilon$. The result is that $\varepsilon$ goes through a maximum value in the region of $\theta = 40°$ as we found in our results.

In addition to the latitude effect at sea level, there is a small longitude effect. Thus the rate is not quite constant along a line of constant geomagnetic latitude; the variation arises from two causes : local magnetic anomalies, and the fact that the earth's field is best represented not by a centre dipole but by an eccentric dipole whose axis cuts the earth at 80.9° N, 83.3° W. The result is a variation of about 4 per cent along the geomagnetic equator and smaller variations at higher latitudes.

| Zenith angle ($\theta°$) | Geographic west rate ($R_W$) (min.$^{-1}$) | $\sigma_{R_W}$ | Geographic east rate ($R_E$) (min.$^{-1}$) | $\sigma_{R_E}$ | $\dfrac{R_W}{R_E}$ | $\dfrac{R_E}{R_W}$ | $\dfrac{R_W - R_E}{\frac{1}{2}(R_W + R_E)}$ ($\varepsilon$) |
|---|---|---|---|---|---|---|---|
| 0 | 186.9 | 1.25 | 186.9 | 1.25 | 1.000 ± 0.009 | 1.000 ± 0.009 | 0 |
| 10 | 182.8 | 1.23 | 181.4 | 1.23 | 1.008 ± 0.010 | 0.992 ± 0.009 | 0.008 ± 0.009 |
| 20 | 173.8 | 1.20 | 167.7 | 1.18 | 1.036 ± 0.010 | 0.965 ± 0.010 | 0.036 ± 0.010 |
| 30 | 150.6 | 1.12 | 143.4 | 1.10 | 1.050 ± 0.011 | 0.952 ± 0.010 | 0.049 ± 0.011 |
| 40 | 121.4 | 1.00 | 114.5 | 0.98 | 1.060 ± 0.013 | 0.943 ± 0.011 | 0.058 ± 0.012 |
| 50 | 90.4 | 0.87 | 87.6 | 0.85 | 1.032 ± 0.014 | 0.969 ± 0.013 | 0.031 ± 0.014 |
| 60 | 63.1 | 0.73 | 61.7 | 0.72 | 1.023 ± 0.017 | 0.978 ± 0.016 | 0.022 ± 0.016 |
| 70 | 45.3 | 0.61 | 42.1 | 0.59 | 1.076 ± 0.021 | 0.929 ± 0.018 | 0.073 ± 0.019 |
| 80 | 32.9 | 0.52 | 28.4 | 0.49 | 1.158 ± 0.027 | 0.863 ± 0.020 | 0.147 ± 0.023 |
| 90 | 27.2 | 0.48 | 24.4 | 0.45 | 1.115 ± 0.028 | 0.897 ± 0.023 | 0.109 ± 0.026 |

Table 3.1 : East-west effect. The variation of counting rate when measured with eastward and westward inclinations

## 3.5   BAROMETRIC EFFECT

For extensive air showers the variation in the rate of showers of a given size with change of barometric pressure is of interest because it affords a measurement of the attenuation of the shower, once past its maximum of development in the atmosphere. An increase in pressure effectively corresponds to the apparatus being situated at a greater depth, and hence the rate of showers of a given total number of particles will decrease.

For pure photon-electron cascades the barometer coefficient is expected to become progressively smaller as the shower energy increases. In practice, experiments showed that the barometric coefficient of extensive showers in the lower atmosphere (below 650 $gcm^{-2}$) is approximately constant and equal to about 10 per cent$\left(cm \ Hg\right)^{-1}$ pressure over quite a wide range of shower sizes. This behaviour is certainly incompatible with the theoretical predictions for a photon electron cascade, but the accuracy of measurements does not permit definite conclusions to be made about possible variations in the barometer coefficient with shower size. Most recent work suggest that the barometer coefficient of showers is increasing with shower size and for showers containing more than $10^7$ particles is significantly greater than 10 per cent$\left(cm \ Hg\right)^{-1}$.

The present measurements refer to the low energy muon component. The variation of the rate of any secondary cosmic ray component with atmospheric pressure at the level of observation can be expressed as follows : $R = R_0 exp- \ \beta(p-p_0)m^{-2}sec^{-1}sr^{-1}$ where R is the cosmic ray rate at pressure p, $R_0$ is the rate at the standard atmospheric pressure $p_0$ (76 cm of Hg). The barometric pressure at Durham during the time this experiment was running

varied over the range 75.5 - 77.15 cm.Hg. The measurements of the

counting rate variation of cosmic rays due to the pressure was

found to be very small during the period dated 8/7/1982 to 19/7/1982.

In the present work, $\beta$, is the barometric coefficient defined as

the percentage change in the counting rate with atmospheric pressure

calculated from the above formula as follows:

$$\beta = \frac{dR}{Rdp} = (3.40 \pm 0.55)\% \left(cm . Hg\right)^{-1}$$

The results are shown in Figure 3.7. It is seen that the effect of

atmospheric pressure changes on the flux of the low energy muon

component is considerably less than on the flux of high energy

extensive air showers.


## 3.6   COSMIC RAYS RATE AT SEA LEVEL

Near the base of the atmosphere or under any very heavy absorber,

almost the entire electron component of cosmic rays does not have its

origin from decay and collision processes of muons, chiefly from

decay. Thus the relative intensity of mesons and electrons at low

altitude (or under a heavy absorber) may be used to furnish information

regarding meson decay. This has been pointed out by Euler and

Heisenberg (1938). Rossi (1942) measured the intensities of the

hard and of the soft component of comic rays as a function of altitude

and zenith angle. The directional intensities were calculated on the

assumption that all of the multiple coincidences obtained were due to

the passage of single particles through the counters. No attempt

was made to distinguish sharply between mesons and electrons, but

rather the distinction was between particles capable of penetrating

only the counter walls and those capable of penetrating also certain

thicknesses of lead.
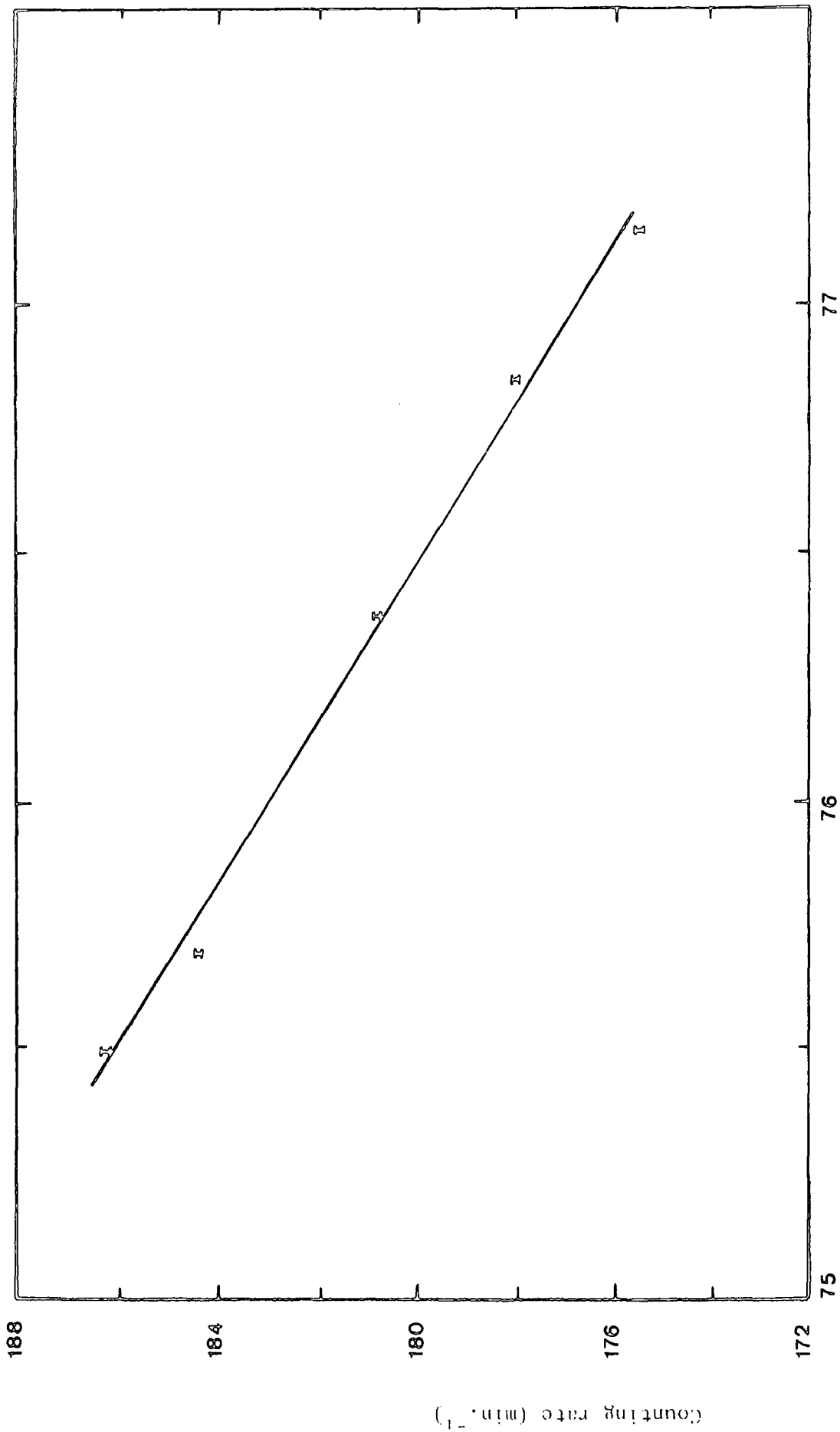
Figure 5.1 : Variation of counting rate with atmospheric pressure.

Due to difficulties concerning uncertain detector edge effects and in estimating the overall efficiencies of counter systems many experiments have normalized their results to a standard intensity point. Until recently this point was that deduced by Rossi (1948) from the data of Greisen (1942). Rossi applied a correction amounting to 4% to the Greisen value to account for the combined effect of showers and scattering in the Greisen apparatus. Allkofer et al (1970b), using a scintillation counter telescope which included lead absorber, measured the differential intensity at 1 GeV to be $(3.09 \pm 0.21) \times 10^{-6}$ cm$^{-2}$ sr$^{-1}$ s$^{-1}$(MeV/c)$^{-1}$, which is approximately 26% higher than the 1 GeV/c Rossi point. This result is supported by Crookes and Rastin (1971a) who measured the intensity at 0.35 GeV/c using a Geiger counter telescope and flash-tube stack. Quantitively Crookes and Rastin measured an intensity 9% higher than that measured by Greisen.

Measurement of the absolute intensity of muons of higher momenta (above 3.48 GeV/c and 7.12 GeV/c) have been made by Ayre et al (1971a) using the Durham stectrograph MARS. Ayre et al conclude that at the lower momenta the intensities are $(7.7 \pm 1.3)$% greater than those previously given by Aurela and Wolfendale (1967) which were based on the Rossi normalization. Further measurements by C.A.Ayre et al (1972 private communication) indicate an intensity somewhat greater than that initially reported, being $(10.9 \pm 1.3)$% and $(9.5 \pm 1.4)$% greater than the values of Aurela and Wolfendale (1967) at momenta of 3.48 GeV/c and 7.12 GeV/c respectively. Ashton et al (1972) have measured the integral muon intensity above 0.88 GeV/c as $(8.22 \pm 0.04) \times 10^{-3}$ cm$^{-2}$ sr$^{-1}$ s$^{-1}$, which is also higher than expected on the basis of the Rossi point.

The differential response curves of meson detectors (Dorman 1959) at two different depths in the atmosphere are related approximately in the following way:

$$\frac{dN}{dP}(P,x_1) = \frac{E(x_2)}{E(x_1)} \cdot \frac{dN}{dP}\left(P. \frac{E(x_2)}{E(x_1)}, x_2\right)$$

If $\int_{Pmin}^{\infty} \frac{dN}{dP}(P,x_1) = 100$, then $\frac{E(x_2)}{E(x_1)} \int_{Pmin}^{\infty} \frac{dN}{dP}\left(P. \frac{E(x_2)}{E(x_1)}, x_2\right) = 100$

$\frac{dN}{dP}(P,x_1)$ is the differential response at rigidity P and depth $x_1$,

$\frac{E(x_2)}{E(x_1)} \frac{dN}{dP}\left(P. \frac{E(x_2)}{E(x_1)}, x_2\right)$ is the differential response at rigidity

$P. \frac{E(x_2)}{E(x_1)}$ and depth $x_2$.

If the differential response curve at a depth x is known, then the response curve at another depth can be obtained using the above relation. The differential response curve for sea level meson detectors, calculated in this way from the curve for meson detectors at 312 gcm$^{-2}$ is shown in figure 3.8. Response curves applied to meson detectors at a depth of 40 and 60 m.w.e can also be derived in this way from the response curve of a meson detector at a depth 312 gcm$^{-2}$ (Webber and Quenby 1959), taking $E(x_2)/E(x_1)$ = 12 and 19 respectively.

The cosmic rays detected by the present telescope consisted of two components : a hard component consisting predominantly of μ-mesons with a small contamination of a soft component which is primarily made up of electrons,positrons and photons. The hard
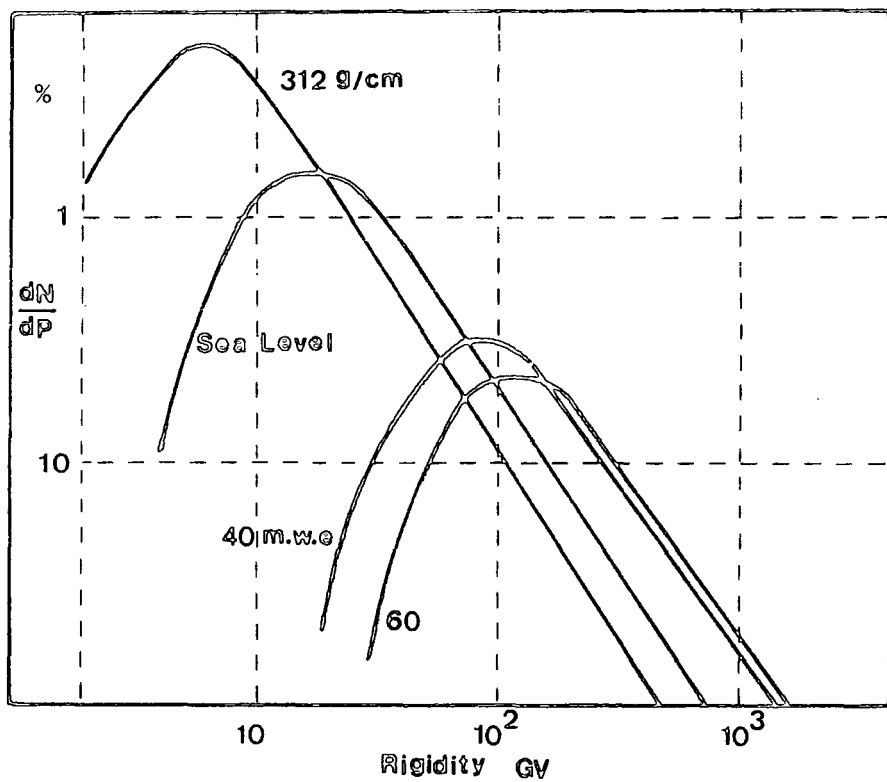
Figure 3.8  :  Differential response curves for meson
monitors (after Webber and Quenby 1959).

component has great penetrating power while the soft component is easily absorbed out by a few centimetres of lead and this difference in composition of the two types of cosmic rays can easily be shown with our telescope. A coincidence counting rate was found with and without a layer of wood of about 2 cm thickness, then one layer of lead = 5 cm, and two layers of lead = 10 cm. The result was that no big difference was found between these measurements (see table 3.2).

Using single counters ($A_1$ and $B_1$) in the top and bottom layers of the telescope and the arrangement shown in figure 3.1 the pulse heights from both counters as well as the occurrence time of events was recorded.

The mean pulse height and standard deviation ($\sigma$) of pulse height distribution about the mean for counters $A_1$ and $B_1$ have been found using the microcomputer data acquisition system as shown in Figure 3.9a. The measurements were repeated for different runs at different values of operating voltages along the plateau for each counter $A_1$ and $B_1$. The distribution in time separation of the occurrence times of the events has been measured using the micro-computer data acquisition system. By using a scaler, 240 events were observed in a running time of 41.58 minutes corresponding to an average events rate of $(0.10 \pm 0.01)\text{sec}^{-1}$ or a mean time separation of the events of 10 seconds. Figure 3.9b shows the distribution of the waiting time between 96 good successive events found from the microcomputer data acquisition system and it was found that it is consistent with a distribution of the form $n(t) = (63.9 \pm 23.6)e^{-(0.10 \pm 0.01)t}$. From this the average rate of good successive events was found to be $(0.10 \pm 0.01) \text{ sec}^{-1}$ or a

| Absorber | Counting | Time(hr) | $\sqrt{\text{Count}}$ | Counting rate (min.$^{-1}$) | $\sigma$ |
|---|---|---|---|---|---|
| Without | 135807 | 12 | 368.5 | 188.6 | 0.512 |
| Board only | 202782 | 18 | 450.3 | 187.7 | 0.417 |
| One layer of Pb 5cm | 179685 | 18 | 423.9 | 166.4 | 0.392 |
| Two layers of Pb 10cm | 114522 | 12 | 338.4 | 159.1 | 0.470 |

Table 3.2 : Table showing counting rate of cosmic ray at different thickness of absorbers using Geiger-Müller telescope.
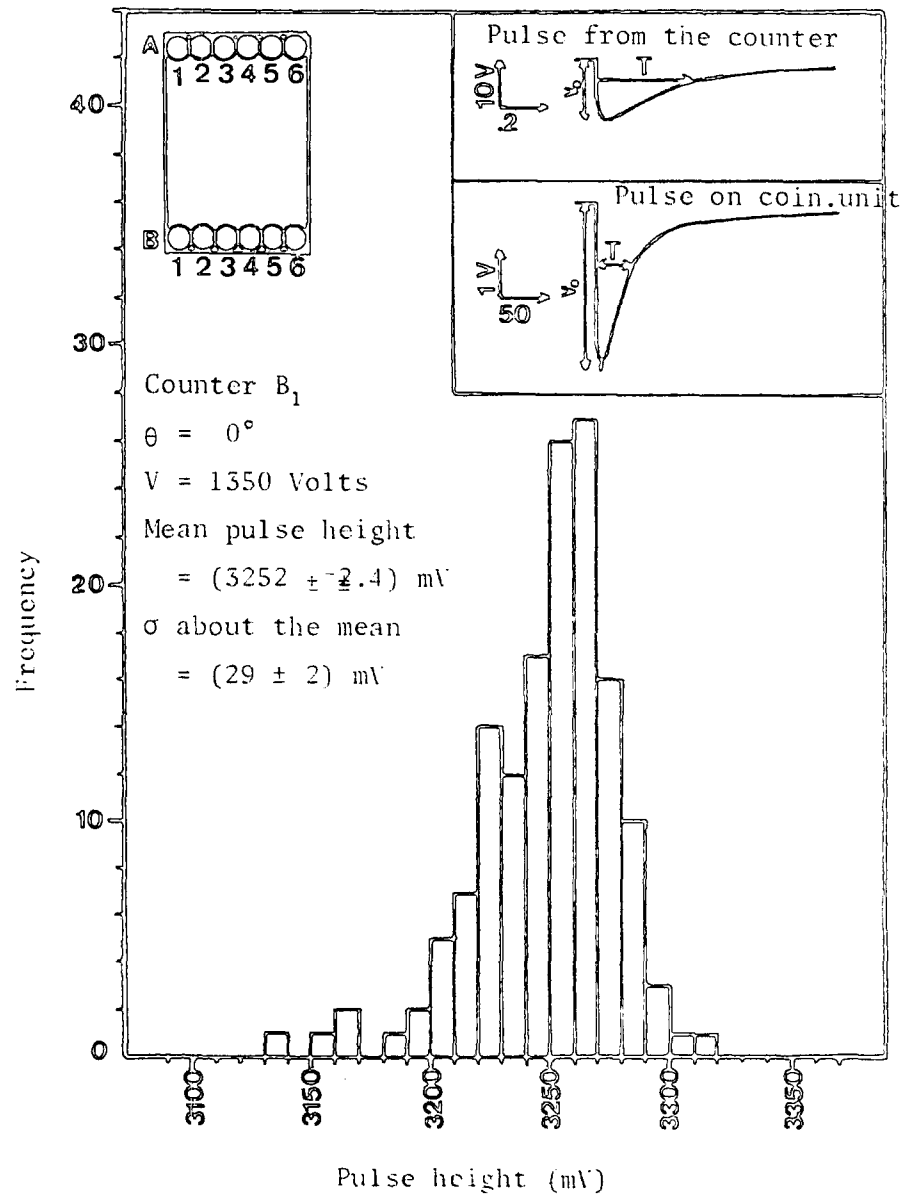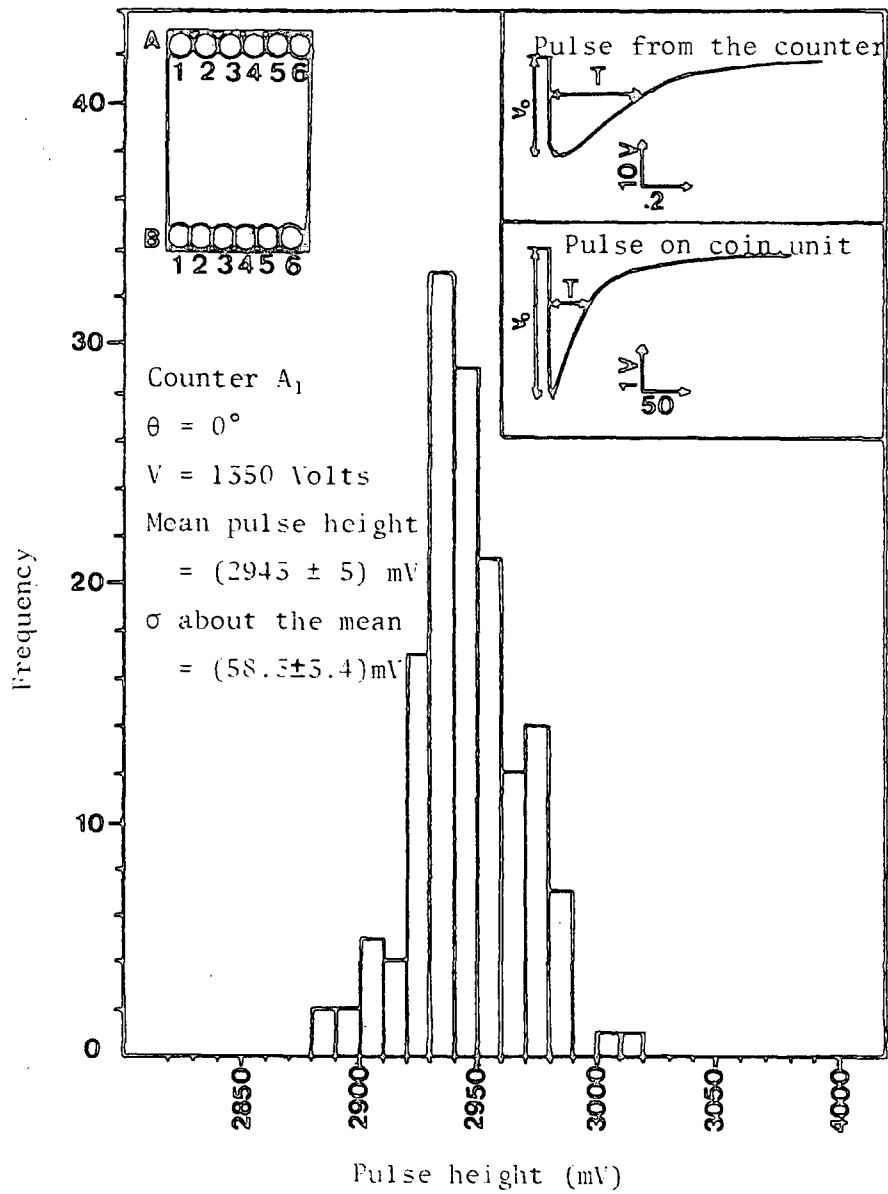
Figure 5.9a : Pulse height distribution obtained by Geiger-Muller counters $A_1$ and $B_1$.
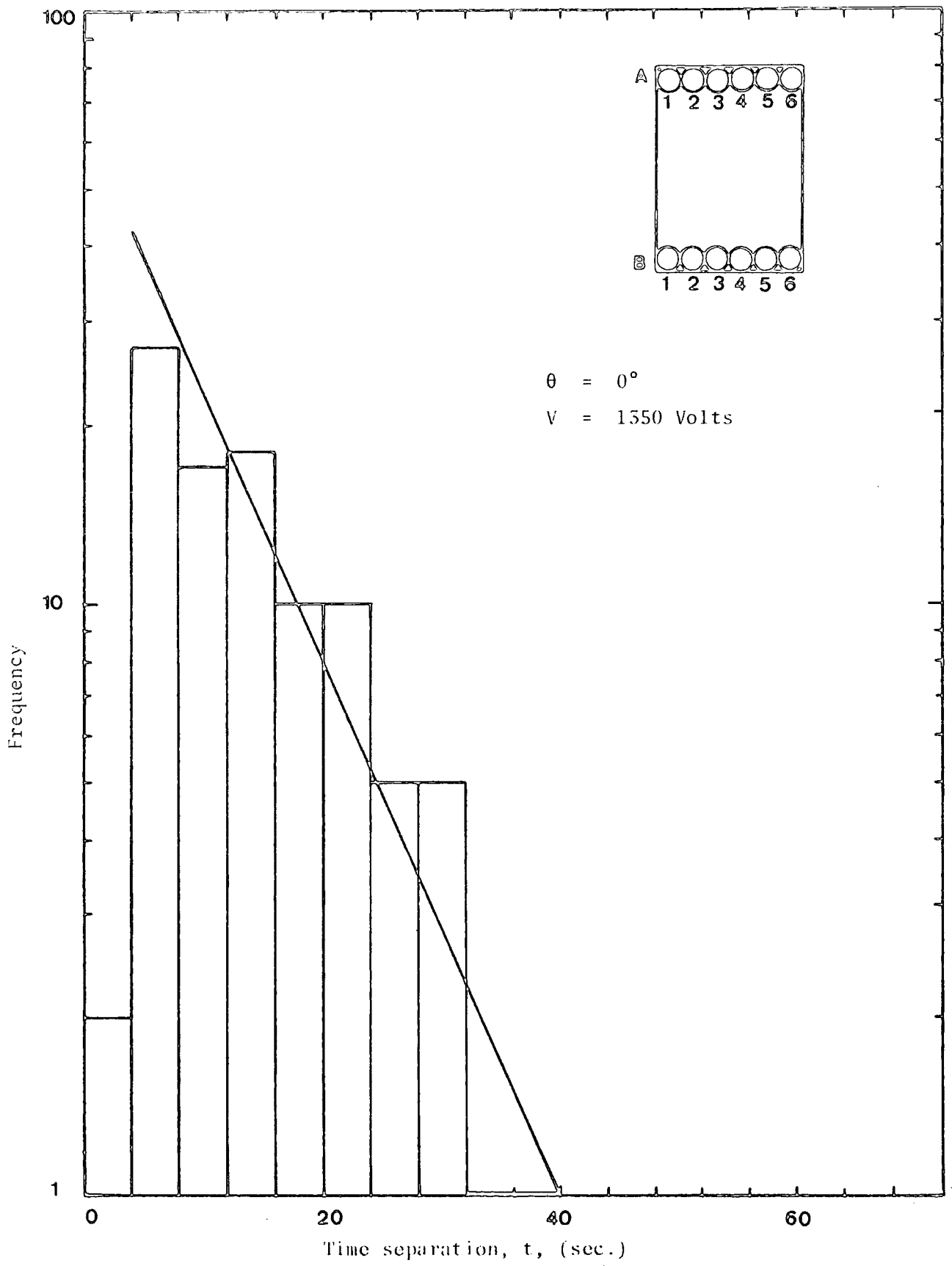
Figure 3.9b : Differential distribution of time separation of 96 good
successive events for counters A₁ and B₁ in a running time
0.69 hrs. corresponding to a mean time separation T = 10 seconds.
The fitted straight line is of the form $n(t) = n(o)e^{-t/T}$.

mean time separation of the events of 10 seconds.

The effect of applied voltage on the Geiger counter pulse height has been found from the results of mean pulse heights out of different runs at different values of operating voltage as shown in figure 3.10. Dependence of the standard deviation ($\sigma$) of the pulse height distribution about the mean value on the counter operating voltage is shown in figure 3.11. It is clear from that figure that the standard deviation reached a minimum value at operating voltages along the plateau. Finally comparison of the variation of the standard deviation ($\sigma$) of the pulse height distribution about the mean value with counter operating voltage and the variation of the background counting rate with operating voltage for counters $A_1$ and $B_1$ have also been found - Figure 3.12. The summary of all results are shown in Table 3.3.

## 3.7 SYSTEMATIC ERRORS IN THE MEASUREMENTS

Sources of error in coincidence measurements with a conventional cosmic-ray telescope are due to the following effects (1) chance coincidences, (2) inefficiency of counters, (3) scattering in absorber or in the counter walls, and (4) cosmic-ray showers. The existence of these sources of error has been recognized for many years.

An important quantity for many applications of counters is the resolving time of the counter array. The question that is often important is 'how close in time can two particles be resolved which traverse separate counters?' This time interval depends on the variability of the delay between the passage of a cosmic ray through a counter and the appearance of a pulse on the wire of sufficient height to be recorded. The variability arises from the different
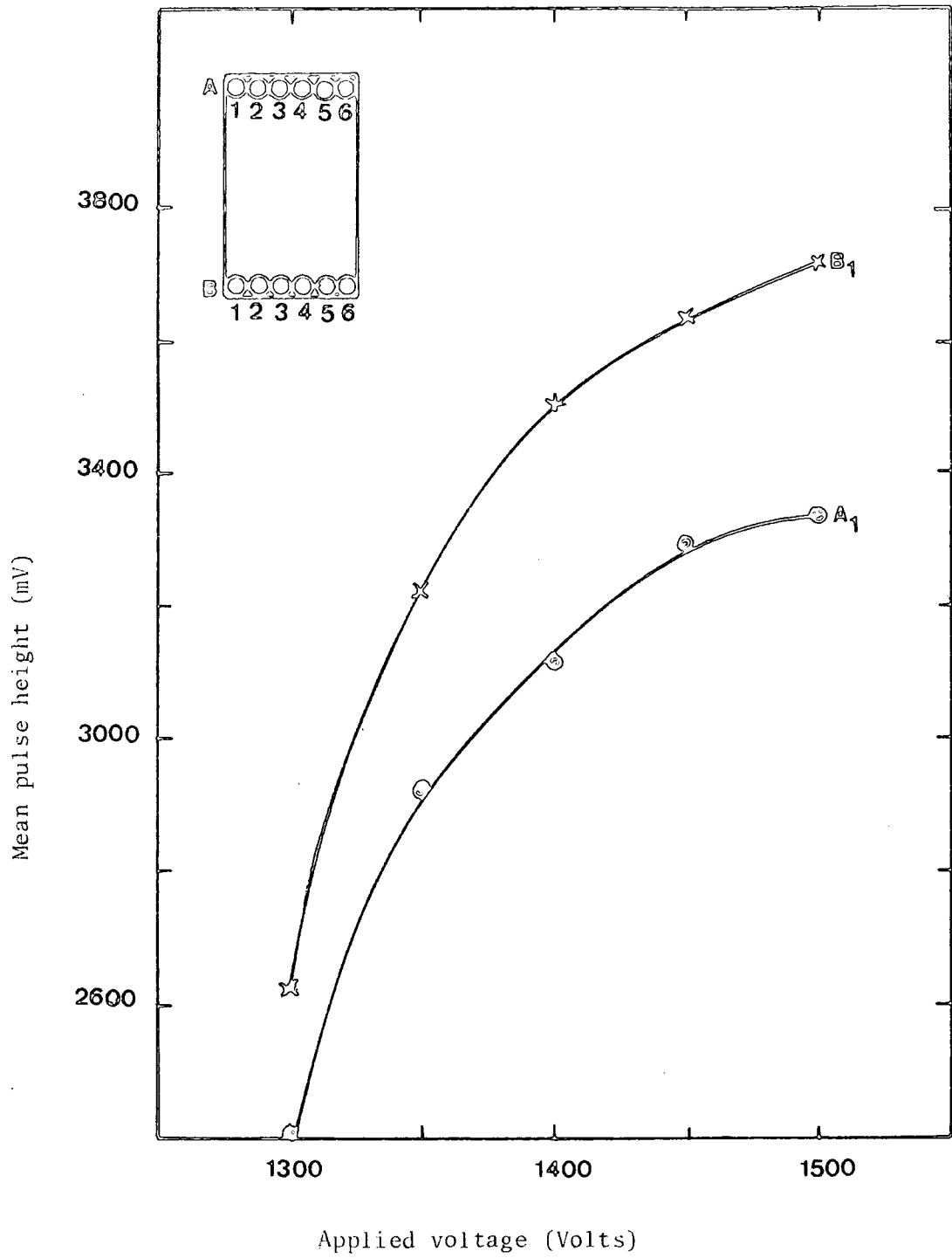
Figure 3.10 : Effect of applied voltage on the pulse
height of Geiger-Müller counters
$A_1$ and $B_1$.
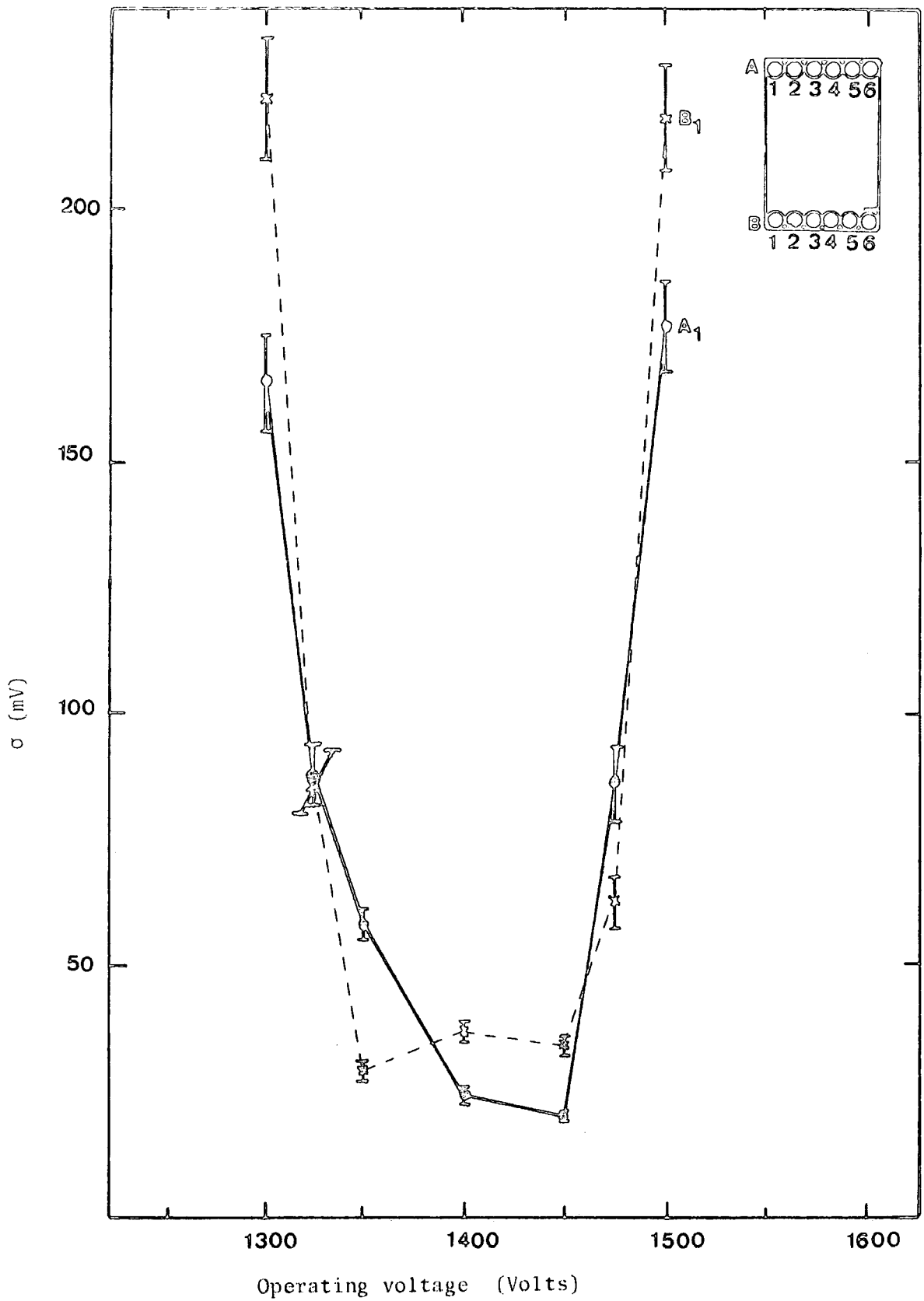
Figure 3.11 : Dependence of the standard deviation ($\sigma$) of the pulse height distribution about the mean value on the counter operating voltage for counters $A_1$ and $B_1$.
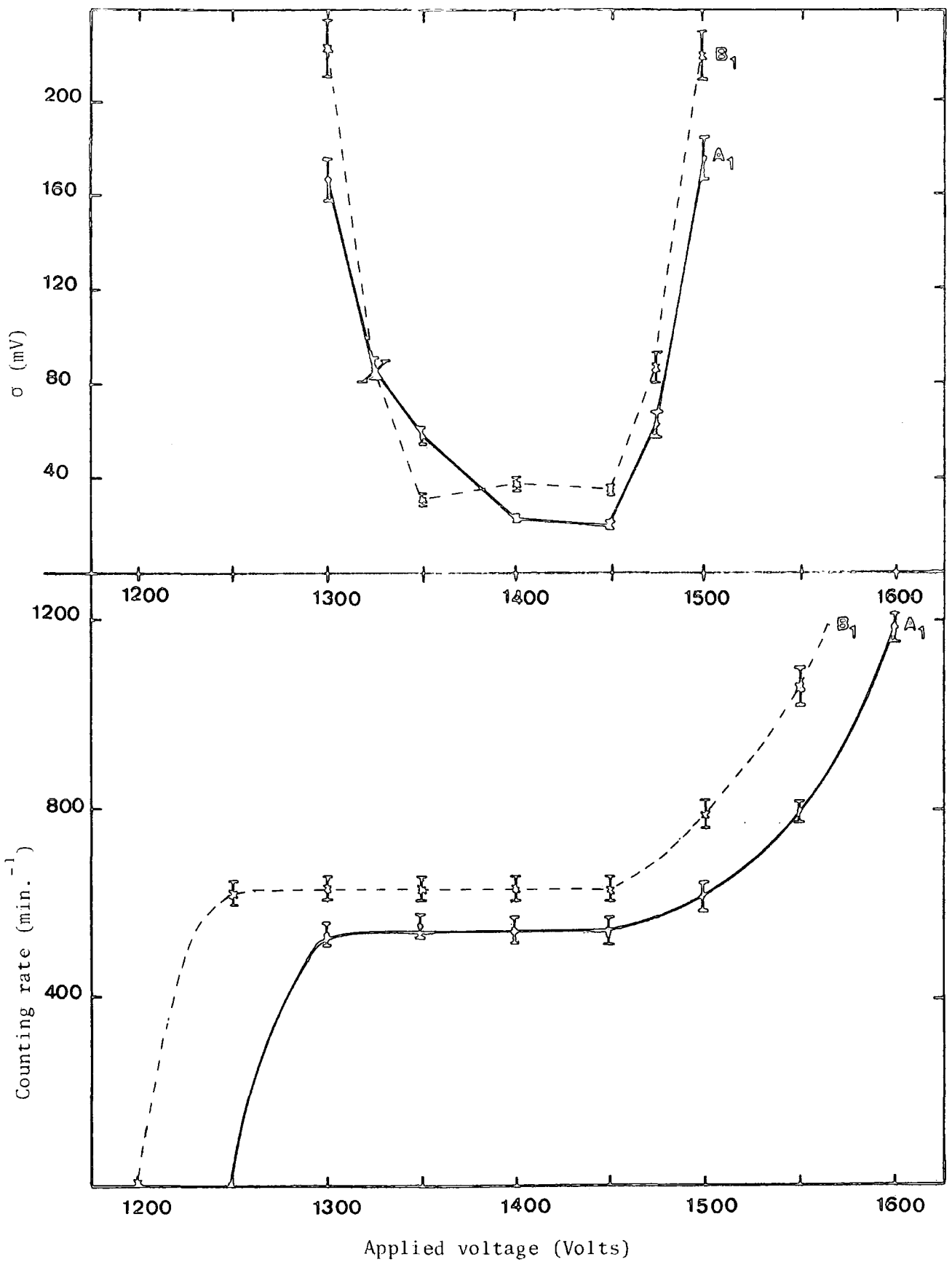
Figure 3.12 : Comparison of the variation of the standard deviation ($\sigma$)
of the pulse height distribution about the mean value with
counter operating voltage and the variation of the
background counting rate with operating voltage for
counters $A_1$ and $B_1$.

| Counter | Operating voltage (volt) | Mean pulse height (mV) | $(\sigma)$ (mV) | Coincidence rate | |
|---|---|---|---|---|---|
| | | | | Scaler $(\text{sec}^{-1})$ | Found from time separation of good successive events $(\text{sec}^{-1})$ |
| A1 | 1300 | $2401 \pm 13$ | $166 \pm 9$ | $.089 \pm .005$ | $0.115 \pm 0.012$ |
| B1 | | $2644 \pm 17$ | $222 \pm 12$ | | |
| A1 | 1350 | $2943 \pm 5$ | $58 \pm 3$ | $.096 \pm .006$ | $.104 \pm .013$ |
| B1 | | $3252 \pm 2.4$ | $29 \pm 2$ | | |
| A1 | 1400 | $3122 \pm 2.1$ | $24 \pm 1.5$ | $.092 \pm .006$ | $.113 \pm .01$ |
| B1 | | $3510 \pm 3.3$ | $37 \pm 2.4$ | | |
| A1 | 1450 | $3285 \pm 2$ | $20 \pm 1$ | $.105 \pm .006$ | $.082 \pm .017$ |
| B1 | | $3661 \pm 3$ | $34 \pm 2$ | | |
| A1 | 1500 | $3360 \pm 13$ | $177 \pm 9$ | $.090 \pm .010$ | $.114 \pm .014$ |
| B1 | | $3711 \pm 16$ | $218 \pm 11$ | | |

Table 3.3 :  Table giving the summary of mean pulse height,
Standard deviation of pulse height distribution
about the mean and two fold coincidence rate for
counters A  and B  at different values of
operating voltage.

transit times of electron from their production in different parts
of the counter to the central wire, and the delay is a maximum for
a cosmic ray passing through the counter at glancing incidence.
A typical value is 0.5 μsec and a time interval less than this
cannot be resolved.

Inefficiency is present due to the 'dead time' of the counter.
Two nearly simultaneous particles traversing the same counter will
not produce separate pulses since each pulse is followed by a dead
time. This arises from the effect of the positive ion sheath in
preventing subsequent electrons from initiating further avalanches.
This continues until the sheath has moved out sufficiently far
from the anode for a small avalanche to be formed by later electrons.
After the dead time has passed a small pulse is produced and the
further interval of time until the pulse produced by the second
particle is of full size is termed the resolving time (again a few
hundred μsec). A quenching pulse is often applied to the counter
and is of sufficient duration to cover both these characteristic
times so that the actual dead time is in the region of 1 msec.

Stever (1942) has published an analysis of the dead time
phenomenon in self-quenching counters, obtained by an oscillographic
method. Stever's photographs show that following a discharge there
is a period of complete insensitivity (during which the counter
acts as a proportional amplifier, and the pulses are too small to
be seen on the oscilloscope), which is followed by a period of
about the same length during which the pulse size gradually
recovers to its full normal value.

The period during which the counter is apparently 'dead' will
depend on the sensitivity of the recording apparatus, just as the

exact value of the 'starting potential' of a counter also depend on the sensitivity of the detecting device. For our purpose, we define the 'dead time' as the time interval following a discharge until the counter has recovered to the point where another pulse may be recorded by our circuit. If N is the discharge rate and $t_o$ is the dead time, the inefficiency due to the dead time is $(1-\exp-Nt_o)$.

Rose and Ramsey (1941) have shown the existence of other types of inefficiency which are not due to the dead time, and have investigated this inefficiency for counters filled with oxygen or with an argon-oxygen mixture. The effect which they observed is greatest when the primary particle passes through the counter near the edge. The causes for this phenomenon may be : (1) when the primary particle passes near the edge of a counter, the path length through the counter is short; therefore, it may happen occasionally that no ions are produced; or (2) when the particle passes near the edge, only a few ions are produced, and the field intensity is low : it is therefore likely that the electrons may be captured, and slowly moving negative ions may be formed. This may either delay or prevent the discharge. Because of the dependence on the number of ions produced, the probability for either of the processes (1) or (2) depends on the distance r from the wire to the path of the primary ray in the form $\exp[-(a^2- r^2)^{\frac{1}{2}}/K]$, where K is a constant and a is the radius of the counter. In addition, the probability of process (2) may have a term depending on the field strength, but this varies slowly with r except near the wire.

Other sources of error which affect the counting rate are due to showers, and the main effect is that of side showers on coincidence

measurements. The effect of showers on an array of counters is strongly dependent on the number of counters in the array, their geometrical arrangement, the physical surroundings of the apparatus, and the altitude at which measurements are made, as well as on the type of observer used and on its shape and position. The error due to the side showers, is a large error, and it becomes more serious at greater zenith angles of the counter telescope. This effect was observed in figure 3.6 of the present work for zenith angles $>80°$.

In general if two counters having separate counting rate $N_1$ and $N_2$ are connected in coincidence and the circuit has resolving time $\tau$, the rate of accidental coincidences due to separate particles passing through the two counters is $2N_1N_2\tau$. If there are n counters, or set of counters connected in coincidence, the accidental rate is $nN_1N_2....N_n\tau^{n-1}$. Since the value of $N_1\tau_1, N_2\tau_2$ etc. are always much less than unity the accidental rate falls rapidly with increasing number of sets of counters and it is always possible to reduce it to negligible proportions by using a sufficient number of layers of counters. For measurements on the cosmic ray flux at sea level two layers of counters are usually sufficient. In the present experiment if we assume the resolving time of the coincidence circuit is 5 $\mu$s, the accidental rate at the vertical position for counters $A_1$, $B_1$ when they are connected in coincidence is $2N_1N_2\tau = 2 \times 10.5 \times 8.6 \times 5 \times 10^{-6} = 0.9 \times 10^{-3}$ counts/sec, where $N_1$, $N_2$ are the counting rate per second for counters $A_1$, $B_1$ respectively. This rate is small for all counting rates between zenith angles of $0°$ and $90°$, see figure 3.6.

## 3.8 CONCLUSION

The main results obtained using the geiger telescope are -

1.  The zenith angle distribution of the low energy muon
    component of cosmic rays at sea level is of the form
    $R(\theta) = R_0 \cos^n\theta$ where $n = 1.82 \pm 0.01$ for $0° < \theta < 40°$.

2.  The barometer coefficient of the low energy muon
    flux is $(3.40 \pm 0.55)\% \, (cmHg)^{-1}$.

3.  The other studies described were carried out to
    operationally test the functioning of the computerised
    data acquisition unit (D.A.U).  It was found that the
    D.A.U functioned as expected and was suitable for
    use in other cosmic ray experiments.

CHAPTER FOUR

MEASUREMENT OF THE DENSITY SPECTRUM OF ELECTRONS AT
SEA LEVEL OVER THE RANGE 27.5-335 ELECTRONS PER SQUARE
METRE USING A MICRO COMPUTER DATA ACQUISITION SYSTEM

## 4.1  INTRODUCTION

The integral density spectrum of electrons $R(>\Delta)$ is defined
as the frequency with which the charged particle density at a fixed
point in space exceeds the value $\Delta$.  In a given shower, the
particle density varies with distance from the axis, but if we assume
that the lateral structure is the same for all showers, the particle
density at a given distance from a point is then proportional to
the total number of particles in the showers whose axes fall at
that point.  Thus, from a study of the density spectrum of showers,
information about the number spectrum of showers can be obtained,
and this in turn gives us information on the energy spectrum of
the primary particles producing the showers.  Moreover, measurements
of the density spectrum of showers at various altitudes reflect
the longitudinal development of showers.  Several experiments were
carried out by many authors to measure the density spectrum with a
variety of detectors and although all measurements are consistent
with each other up to densities of about $\Delta = 1,000$ m$^{-2}$, there are
some discrepancies for higher densities.

The simplest method of determining the density spectrum of
air showers is to use detectors whose response is proportional to
the number of particles passing through them.  Every time an air
shower strikes in the neighbourhood, there is a certain probability
that enough ionizing particles hit simultaneously the detectors
and generate a coincidence pulse.  The density spectrum can be
measured directly from the records of the pulse heights.  The

present experiment was performed using two scintillation counters,

each with 0.4 m$^2$ area. Before describing the present experiment

a number of previous measurements of the density spectrum of

extensive air showers, carried out at sea level and mountain altitudes,

using different types of detectors will be described in the

next section.

## 4.2  SOME PREVIOUS MEASUREMENTS OF THE ELECTRON DENSITY SPECTRUM

### 4.2.1   R.J. NORMAN (1956)

The integral density spectrum of EAS in the range $\Delta$ = 20-1,000 m$^{-2}$

has been measured by Norman with a proportional counter. The

experimental arrangement comprised three proportional counters of

the control grid type (Norman, 1955) each 0.05 m$^2$ in area, arranged

in a horizontal place at the three corners of a 5 metre equilateral

triangle at 60 metre elevation above sea level. A three-fold

coincidence was used as a method of EAS selection. The pulse height

distribution of observed densities recorded by a single counter

was photographed on an oscilloscope and converted to a density

spectrum, assuming the most probable pulse height of single muons

observed in a calibration run is equivalent to one particle.

Norman expressed his results by

$$R(>\Delta) = 540 \ \Delta^{-(1 \cdot 39 \pm 0 \cdot 04)} hr^{-1} \text{ for } 20 < \Delta < 500 \text{ m}^{-2}$$

with evidence of an increase of the slope to -2.2 at $\Delta$ = 1,000 m$^{-2}$

### 4.2.2  J.R. PRESCOTT (1956)

The density spectrum of EAS has been measured by Prescott

using cylindrical ionisation chambers 57.6 cm long and 8.8 cm in

diameter filled to 39 atmosphere with nitrogen. The apparatus

consisted of a complementary ionisation chamber and Geiger counter

system. The Geiger counters in coincidence were located immediately above one chamber which acted as a 'master group'. Counters were located at 3 and 5 metre from the master group which allowed bursts due to extensive showers to be identified.

The experimental data for coincidence bursts greater than a given size in both chambers at a separation of 5 metres obtained in 725.8 hr running time indicated that there is a 7% probability that a single line of slope -1.45 fits all the observed data in the range $\Delta = 400\text{-}4,500 \text{ m}^{-2}$. Prescott, however, measured the distribution of burst sizes in a single ionisation chamber situated at a distance of 5 metres from the master group. In 627.9 hr running time 115 bursts were observed.

For densities $\Delta < 1,000 \text{ m}^{-2}$ the slope of spectrum was found to be the same as it was obtained previously (Norman 1956), though its absolute rate was greater by a factor of two compared to the former one. The probability that the experimental results obtained, analysing the results of a single ionisation chamber, fit a single line in the whole range of measured densities with slope of -1.45 was found to be 4%. The observation based on the second method showed that the slope of integral density spectrum is -1.54 ± 0.14 in the region of $\Delta = 500 - 1,000 \text{ m}^{-2}$ for the integral density spectrum at sea level.

## 4.2.3  J. GEMESY et al. (1964)

Gemesy et al. employed a cloud chamber to investigate the density spectrum of EAS. A coincidence pulse of four Geiger counters (of an area of 320 cm² each) was placed at the corners of a (10 x 9)m² rectangle enclosing the chamber. The chamber was a multiplate one, where only the volume above the upper plate in the chamber was scanned when counting the number of tracks shown on the photographs. The

illuminated area of the uppermost plate of the chamber was 150 cm$^2$. The observation was carried out at 410 m elevation.

A total of 3,274 coincidences was recorded in the region of $\Delta$ = 70 - 13,000 m$^{-2}$. They found that there was no significant change in the slope of density spectrum and that the exponent of the integral density spectrum was 1.49 ± 0.08 in the range 70 - 200 m$^{-2}$ and 1.57 ± 0.03 in the range 70 - 13,000 m$^{-2}$.

## 4.2.4 F. ASHTON et al. (1975)

The density spectrum of electrons in the range 40 < $\Delta$ < 5,000 electrons m$^{-2}$ at sea level has been measured by Ashton et al. using a proportional counter of internal dimensions 13.8 x 13.8 x 98.4 cm$^3$ (area = 0.14 m$^2$) filled with a 90% argon, 10% methane gas mixture at atmospheric pressure. EAS were selected by the simultaneous passage of a predetermined number of particles through each of three liquid scintillation counters N, M and S (each of area 1.24m$^2$) placed in close proximity to one another. They expressed their results by

$$R(> \Delta) = 411 \, \Delta^{-(1.50 \pm 0.05)} \, hr^{-1} \quad \text{in the range } 40 < \Delta < 1,000 \text{ m}^{-2}$$

$$R(> \Delta) = 1.3.10^4 \Delta^{-(2.0 \pm 0.2)} \, hr^{-1} \quad \text{in the range } 1,000 < \Delta < 5,000 \text{ m}^{-2}$$

where $\Delta$ is in units of electrons m$^{-2}$.

The results indicated that the integral density spectrum of EAS at sea level has a slope of -1.50 in the density range $\Delta$ = 40 - 1,000 m$^{-2}$. This is approximately consistent with most of the experimental data obtained in this range of density. The slope of the spectrum was found to be -2.0 in the range of $\Delta$ > 1,000 m$^{-2}$. As a comparison they found that the absolute rate given by Greisen (1960), was higher compared with their experiment with a ratio

of 2.0 at $\Delta$ = 100 m$^{-2}$, but they found a better agreement compared with the result given by ~~Cocconi (1949) and~~ Cocconi and Tongiorgi (1949). They concluded that if one takes the average measured rate between their results and those of Greisen it will approximately agree with the absolute rate as given by Cocconi and Cocconi and Tongiorgi in the range of 40 < $\Delta$ < 1,000 m$^{-2}$.

## 4.2.5 MEASURED DENSITY SPECTRUM AT MOUNTAIN ALTITUDES

The density spectrum of EAS has been measured using proportional counters and cloud chambers at mountain elevations.

The experimental results of the measured integral density spectrum obtained by McCaughan et al. (1965b), Swinson and Prescott (1965,1968) showed that the slope of spectrum is about -1.4 for lower densities and increases continuously.

The transition region, i.e. the region where before it the slope of the spectrum is fairly constant (about -1.4) depends on the altitude of observation.

Swinson and Prescott (1965) have shown that at all altitudes the spectra are essentially the same shape and that, apart from absolute rates, the spectra can be superimposed by a density scale-change in the approximate proportions, 1 : 7.5 : 22 for sea level, 2,285 m and 3,260 m respectively (densities are expressed in units of particles m$^{-2}$). This was done in the first instance by a trial and error fit of the sea level spectrum to those at the higher altitudes, in which the density spectrum was displaced in steps until the ordinates of the two curves bore the same ratio to each other at six points. They applied a similar technique to the cloud chamber data of McCaughan et al. (1965b) and found a ratio

of about seven between sea level and 2,285 m, in good agreement with the proportional counter data. Swinson and Prescott (1968) also investigated the density spectrum at 1,575 m elevation using proportional counters. They however showed that the transition region increases as altitude of observation increases and found a ratio of 1 : 5 : 7.5 : 22 for sea level, 1,575 m, 2,285 m and 3,260 m elevation respectively. These values were obtained using proportional counters for the density spectrum measurements. If densities are expressed per square lateral scattering unit, the above proportions become 1 : 7 : 13.5 : 47 for sea level, 1,575 m, 2,285 m and 3,260 m respectively.

## 4.2.6 GREISEN (1960) AND THE PREVIOUS MEASURED DENSITY SPECTRUM

Based on summarised experimental results, Greisen (1960) gives the following expression for the integral density spectrum in the range $1 < \Delta < 10^4$ m$^{-2}$.

$$R( > \Delta) = 540 \, \Delta^{-(1.3 + 0.055 \, \text{Log}_{10} \Delta)} \quad \text{hr}^{-1} \quad \text{at sea level}$$

$$R( > \Delta) = 576 \, \Delta^{-(1.25 + 0.065 \, \text{Log}_{10} \Delta)} \quad \text{hr}^{-1} \quad \text{at 3,260 m (705 gcm}^{-2})$$

The previous integral density spectra measured at sea level and mountain altitude are shown in figures 4.1 and 4.2 respectively. Each measured density spectrum, shown in figure 4.1, has been normalized so that the rate at $\Delta = \Delta_0$ be identical to the rate given by Greisen at sea level ($\Delta_0$ is the minimum density measured in each experiment). Gemesy et al. (1964) have reported their measured spectrum in the form of $R( > N)$ as a function of $N$ where $N$ is the number of tracks observed in their cloud chamber. It is obvious that the absolute rate of the density spectrum is a function of the level of observation.
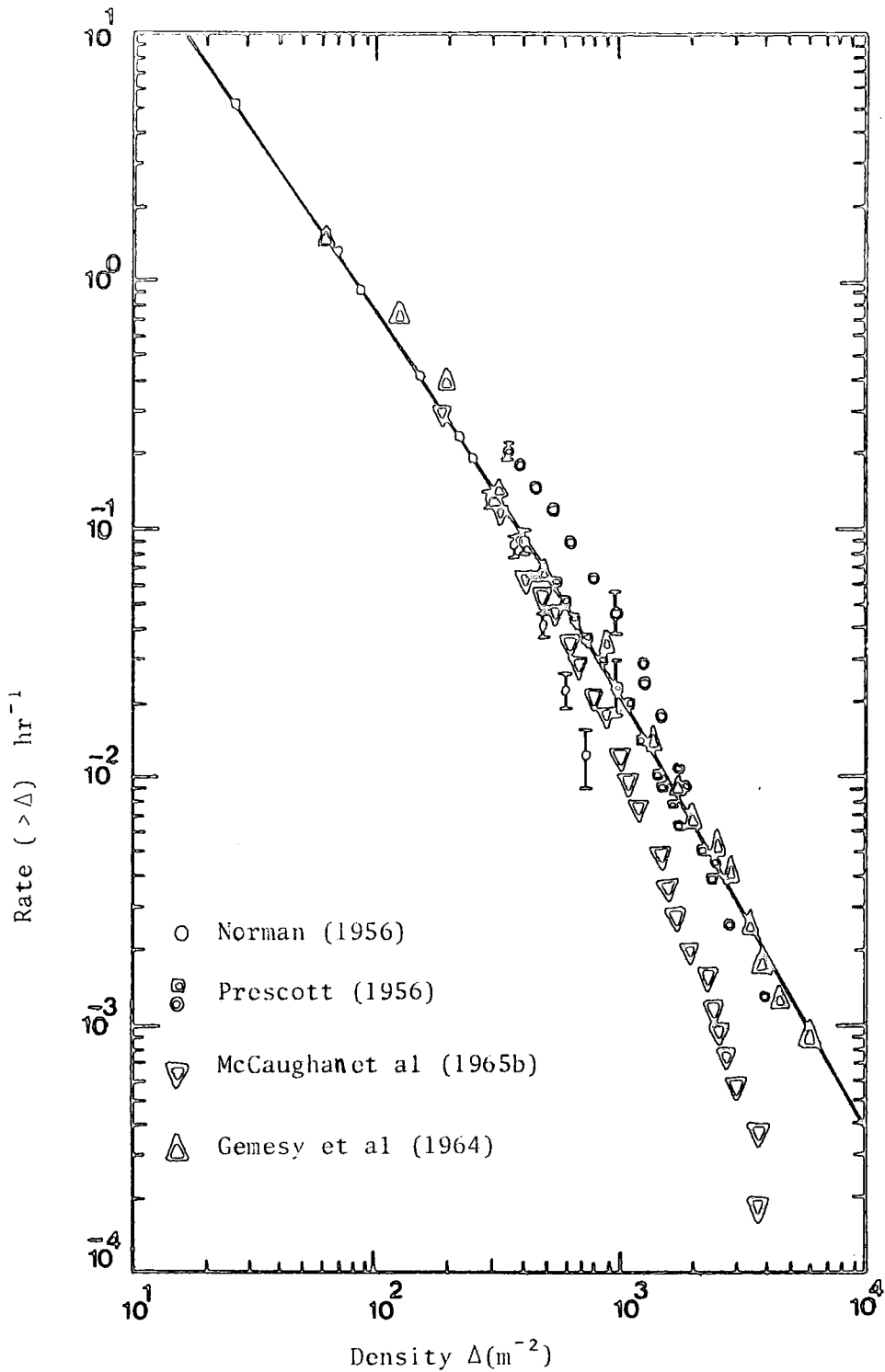
Figure 4.1 : Integral density spectra of EAS measured at sea level. The solid curve is due to Greisen (1960). The experimental observation are normalized to the solid line such that all spectra give the same rate as obtained by Greisen at their minimum observed densities.
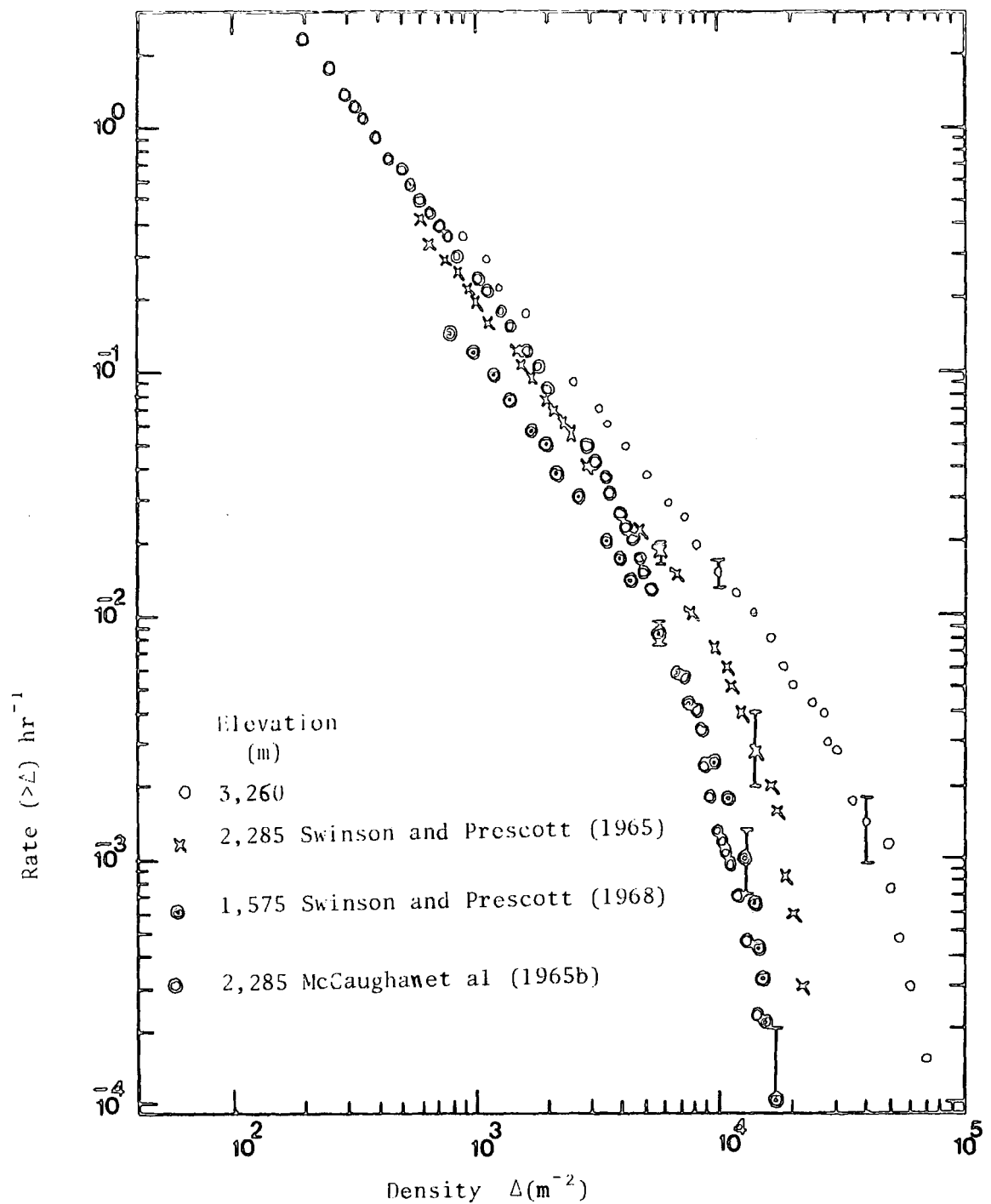
Figure 4.2 : Integral density spectra observed at mountain altitudes, with proportional counter (Swinson and Prescott) and cloud chamber (McCaughan et al). All data are normalized to the rate given by Greisen (1960) at 705 g $cm^{-2}$, assuming a 140 g $cm^{-2}$ absorption length at their minimum observed densities.

Absolute rates are assumed to be correct at 705 $gcm^{-2}$ atmospheric depth as given by Greisen; for the other altitudes they were derived from the normalised data assuming a 140 $gcm^{-2}$ absorption length for the rate at lower densities, as found in earlier experiments.

Figures 4.1 and 4.2 indicate the following -

(i)    On average, it is likely that the slope of density spectrum does not remain constant throughout the measured density spectrum $(1 - 6,000 \ m^{-2})$

(ii)   The transition region of the spectrum is rather short at sea level but the change in the slope occurs gradually at mountain altitudes.

(iii)  The transition region occurs at lower densities, using cloud chambers, than proportional counters or ionisation chambers.

(iv)   The transition region has a strong dependence on the level of observation.

In general the change in the slope of spectrum has been interpreted due to (a) a change in the characteristic of nuclear interaction or (b) as a result of a cut-off in the primary energy per nucleon spectrum.

## 4.3   INTRODUCTION TO THE PRESENT EXPERIMENT

Two scintillation counters A and B were used in the present experiment.   In brief, the purpose of the present experiment is to :

1.    Study of the response of scintillators A and B to the global cosmic ray flux and measurement of the electron density spectrum at low densities at sea level using discriminators and a two fold coincidence.

2.    Study of the correlation between the number of particles

      through scintillators A and B when events are selected

      which have an electron density greater than a threshold

      value in both A and B using the microcomputer data

      acquisition system to record the A and B densities.

3.    Measure the electron density spectrum at high densities

      at sea level using the microcomputer data acquisition

      system.

To measure and investigate the electron density spectrum

using scintillation counters A and B it is essential to know about

the design and performance of each scintillator and one needs to

measure the response of each scintillator when a single particle

passes through it at normal incidence.  These are explained in the

following sections.

## 4.4  THE PLASTIC SCINTILLATORS

The scintillation counters A and B were used in the present

experiment to measure the integral density spectrum of electrons

at sea level.  Each scintillator consisted of an NE102A phosphor

of dimensions 80 x 50 x 5 $cm^3$ viewed by two 5 cm diameter photo-

multipliers (type 53AVP) via the perspex light guides.  Their

design and performance was described in detail by Ashton et al

(1983).  To be able to easily monitor their performance when used

to measure the electron density spectrum, it is necessary that

their response to the global cosmic ray flux should yield a

distribution whose peak is well resolved from the distribution

produced by single thermal electrons leaving the photocathodes of

the photomultipliers used to view the phosphor.  Figure 4.3 shows

the design of the scintillation counter used in the present work.
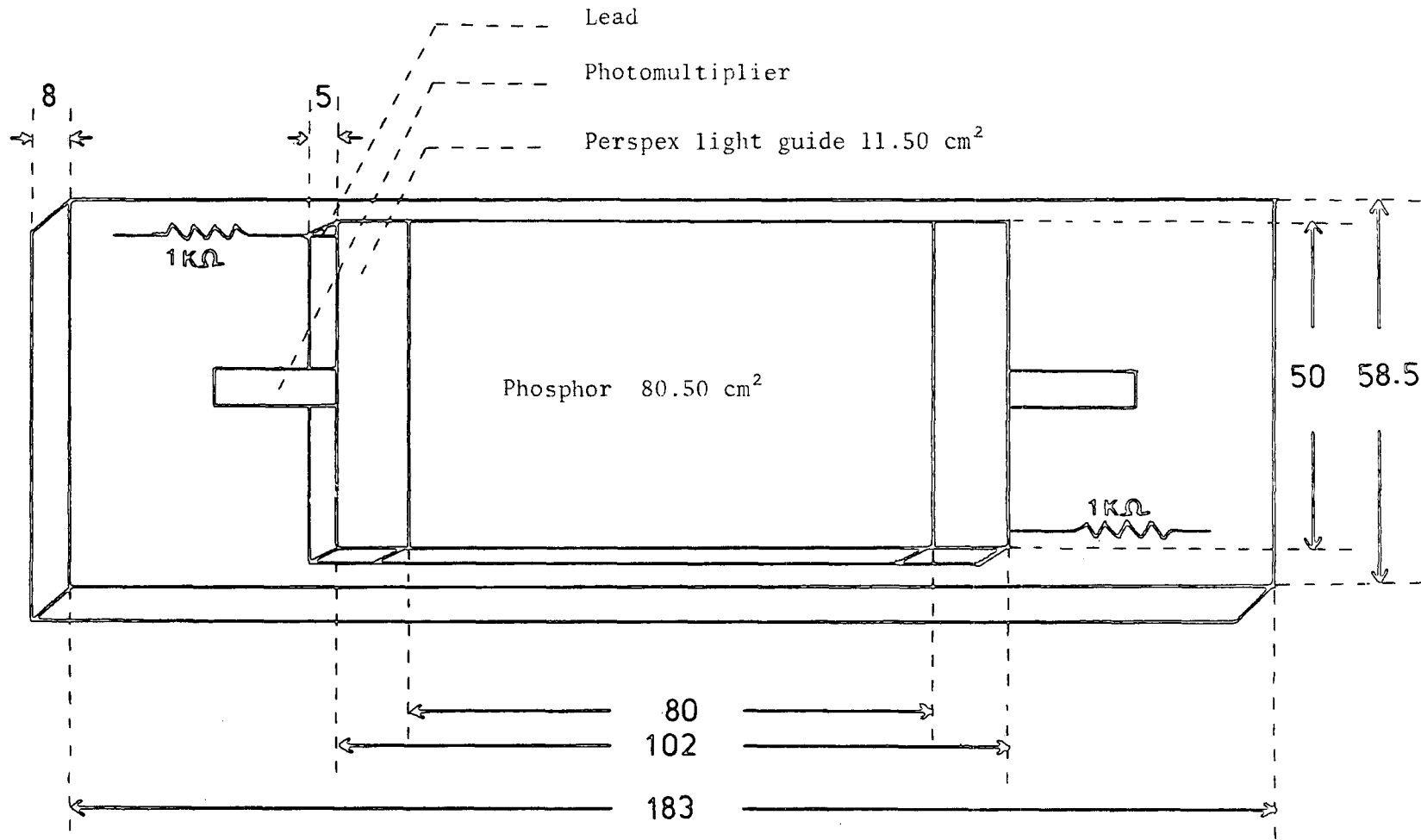
Figure 4.3 : Design of plastic scintillation counter.
All dimensions are in centimetres.

Different processes that convert the expected distribution to the observed distributions are Landau ionisation loss fluctuations that are reflected in the number of scintillation photons that arrive at the photomultiplier photocathodes, fluctuations in the number of photoelectrons produced and the non uniformity of response of the phosphor over its area.

For a perfect counter the expected most probable value of the observed distribution corresponds to particles traversing the counter at normal incidence. The effect of photon fluctuations is to broaden this distribution but the most probable value of the observed distribution is expected to correspond closely to the average pulse height produced by cosmic ray particles traversing the phosphor at normal incidence. Thus this latter quantity can be determined from the response of the detector to the global cosmic ray flux.

## 4.5 STUDY OF THE RESPONSE OF SCINTILLATORS A AND B TO THE GLOBAL COSMIC RAY FLUX USING A PULSE HEIGHT ANALYSER

To investigate the density spectrum of extensive air showers one needs to measure the response of each scintillator when single relativistic cosmic ray particles pass through it, and it is necessary that the response of the scintillator to the global cosmic ray flux should yield a distribution whose peak is well resolved from the distribution produced by single thermal electrons leaving the photocathodes of photomultipliers used to view the phosphor.

The response of the scintillators A and B to the global cosmic ray flux as observed using a pulse height analyser are shown in Figures 4.4a,b. It is seen that there is a noticeable peak due to the passage of single relativistic cosmic ray particles through each scintillator.
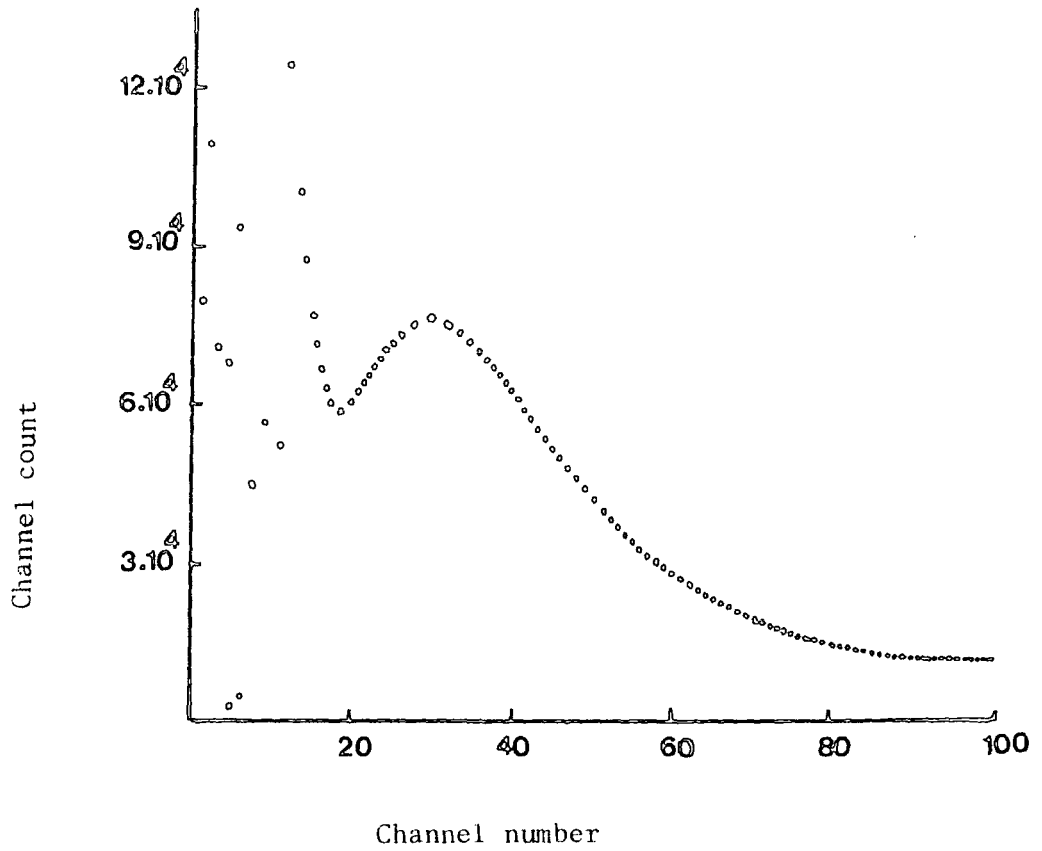
Figure 4.4a : Typical single particles cosmic ray peak
for scintillator A as displayed on the
pulse height analyser.
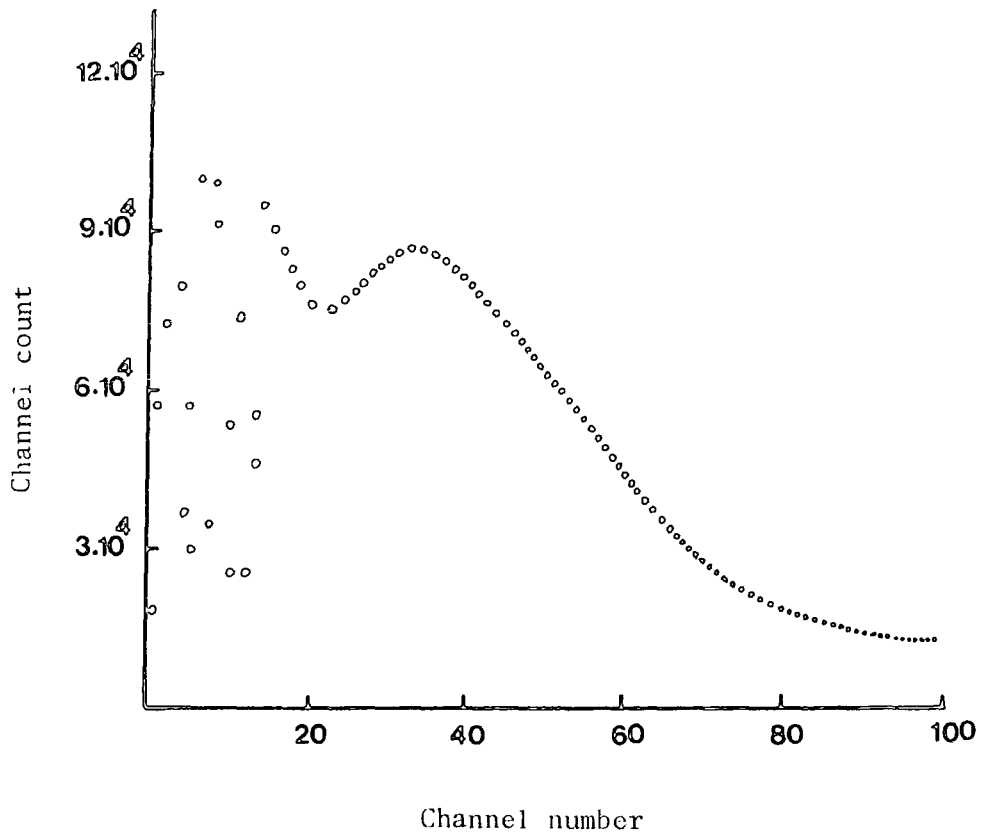
Figure 4.4b : Typical single particles cosmic
ray peak for scintillator B as displayed
on the pulse height analyser.

The pulse height analyser was calibrated to interpret the
distribution in terms of pulse height.  The calibration was done
by means of negative exponential input pulses of 1 µs width as
shown in Figure 4.5.  The solid line drawn in that figure is the
best fit through the experimental points and follows as :

$$H = (0.600 \pm 0.004)N + (2.284 \pm 0.186)$$

where H is the pulse height and N is the channel number.

## 4.6  EXPERIMENTAL ARRANGEMENT

For measurements of the density spectrum of EAS one needs a
system to identify the arrival of an EAS.  This is called a trigger
system.  In the present experiment, a region of EAS with local
electron density $>2$ $m^{-2}$ was selected by a two fold coincidence
between two plastic scintillators A and B each of area 0.4 $m^2$.
The design of the scintillators were described in section 4.4.
The centres of the scintillators were separated by 1.7 metres
in the horizontal plane.  The density of particles in the EAS sel-
ected in this way was measured using the same scintillators A and
B at the same time.  Each scintillator was calibrated by determining
the average pulse height,e,at the head unit outputs produced by
relativistic cosmic ray particles traversing the phosphor at normal
incidence.  If a pulse height, V, is produced by a shower of
particles traversing the scintillator at normal incident, the
particle density, $\Delta$, is given by $\Delta = \dfrac{V}{0.4e}$ $m^{-2}$, and the number of
particles, N, through the scintillator is given by $\dfrac{V}{e}$.

When the density, $\Delta$, measured by the plastic scintillators
exceeds a minimum value, $\Delta_0$, the pulse heights at the head unit
outputs from both scintillators A and B, both outputs almost the
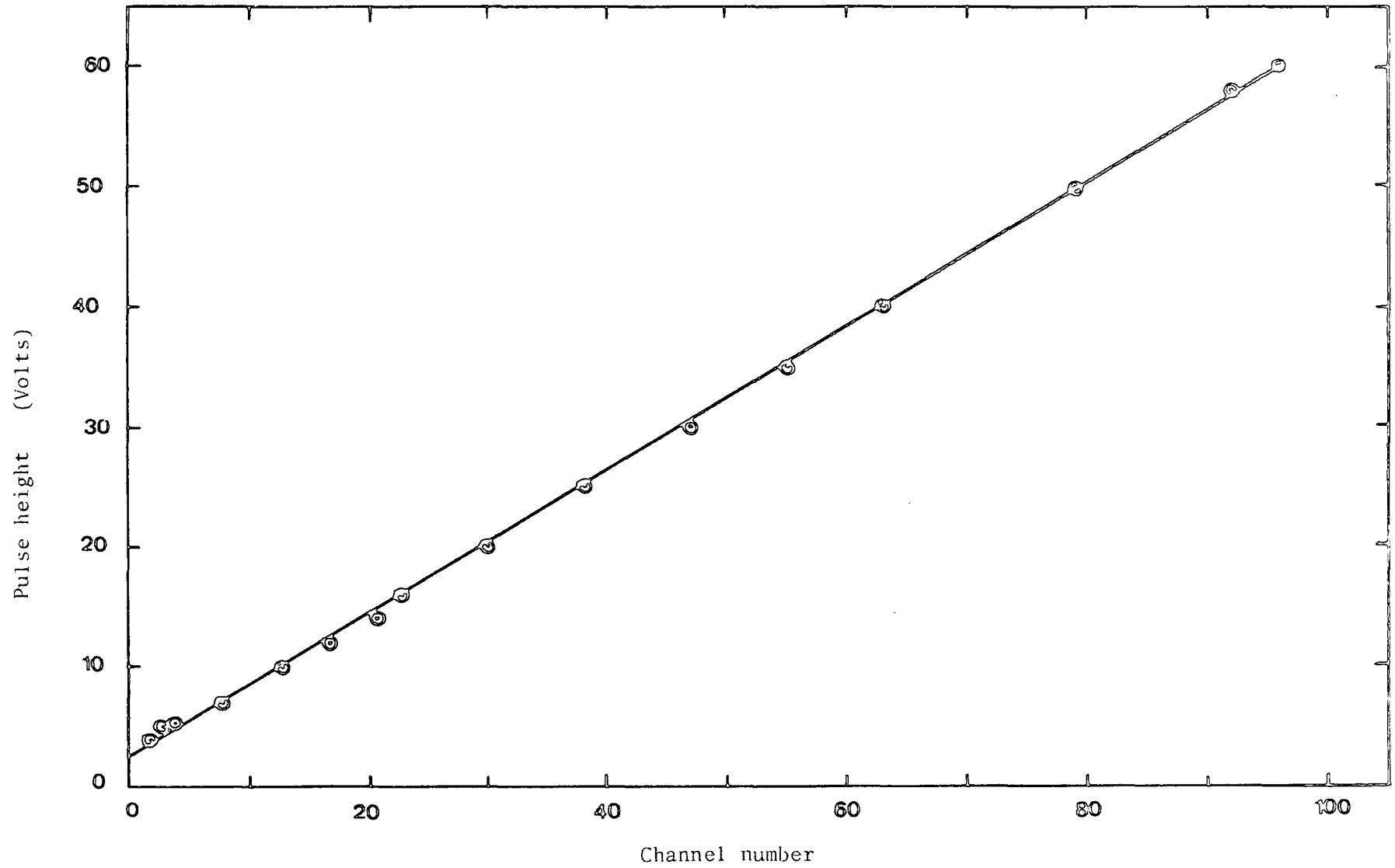
Figure 4.5 : Calibration of the pulse height analyser using 1 μs width input exponential pulses.

same, can be measured directly using channels number one and two of
the data acquisition unit respectively, after passing through two
stretcher amplifiers. The output pulse heights from both channels
were recorded on magnetic tape of the cassette drive of the
Commodore PET computer.

The triggering procedure of the data acquisition unit and
the scaler by the coincidence pulse height from the plastic
scintillators A and B were determined as follows:-
The pulse heights out of the head unit of both scintillators were
passed, first, through two amplifiers and then through two discrim-
inators. The output triggering thresholds from the discriminators
were passed through a coincidence unit, then through a fan out to
trigger the data acquisition unit and the scaler. The block
diagram of the system is shown in Figure 4.6.

The circuit diagrams for the electronics which were used in the
experiment are shown in Appendix B.


4.7    RESULTS

4.7.1  Study of the response of scintillators A and B to the global cosmic
       ray flux and measurement of the electron density spectrum at low
       densities at sea level using discriminators and a two fold coincidence

First of all, a high voltage was set on the scintillators so
that the most probable pulse height at the head unit outputs was almost
the same for both scintillators. Pulses were taken from the head
unit of each scintillator and fed through an amplifier, a discriminator
and then a scaler, and in case of coincidence measurements the pulses
from both scintillators were fed through a coincidence unit before
the scaler. Tables 4.1a,b show the basic data for the integral
spectrum for scintillators A and B from counting. The response of
both scintillators to the integral rate of cosmic ray pulses of height
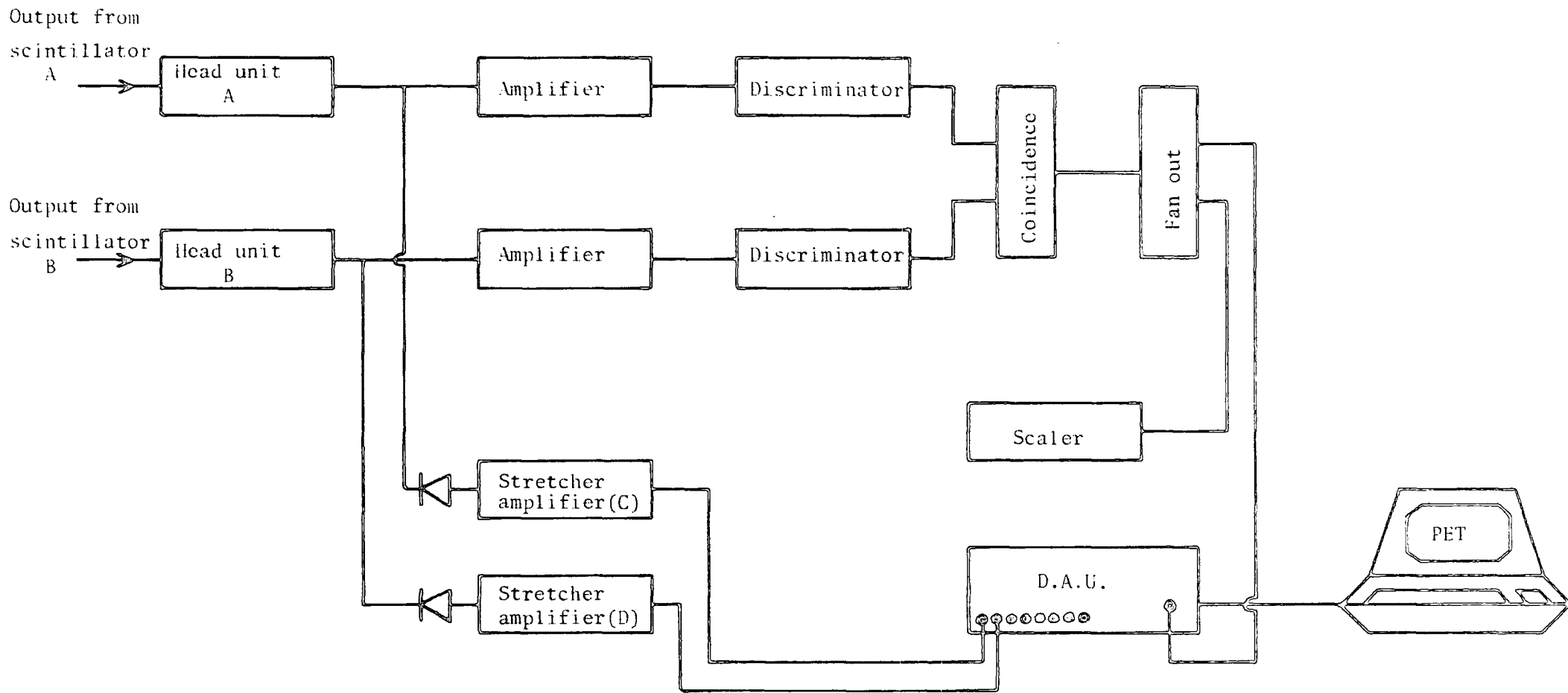
Figure 4.6 : Block diagram of the system used to measure the density
spectrum of electrons at sea level.

| Threshold (mV) | Rate of events (hr$^{-1}$) | | Density $\Delta(m^{-2})$ | |
|---|---|---|---|---|
| | A | B | A | B |
| 1 | $1.3 \times 10^{7}$ | $8.0 \times 10^{6}$ | 0.11 | 0.11 |
| 2 | $2.8 \times 10^{6}$ | $1.9 \times 10^{6}$ | 0.22 | 0.23 |
| 3 | $1.5 \times 10^{5}$ | $1.3 \times 10^{6}$ | 0.32 | 0.34 |
| 4 | $9.5 \times 10^{5}$ | $8.5 \times 10^{5}$ | 0.43 | 0.45 |
| 5 | $7.0 \times 10^{5}$ | $5.5 \times 10^{5}$ | 0.54 | 0.57 |
| 8 | $3.7 \times 10^{5}$ | $3.1 \times 10^{5}$ | 0.86 | 0.91 |
| 10 | $3.0 \times 10^{5}$ | $2.8 \times 10^{5}$ | 1.08 | 1.14 |
| 13 | $2.6 \times 10^{5}$ | $2.5 \times 10^{5}$ | 1.40 | 1.48 |
| 16 | $2.4 \times 10^{5}$ | $2.2 \times 10^{5}$ | 1.72 | 1.82 |
| 20 | $2.2 \times 10^{5}$ | $2.1 \times 10^{5}$ | 2.16 | 2.27 |
| 23 | $2.1 \times 10^{5}$ | $1.9 \times 10^{5}$ | 2.48 | 2.61 |
| 26 | $1.5 \times 10^{5}$ | $1.4 \times 10^{5}$ | 2.80 | 2.95 |
| 30 | $1.2 \times 10^{5}$ | $1.0 \times 10^{5}$ | 2.23 | 3.41 |
| 35 | $9.0 \times 10^{4}$ | $7.5 \times 10^{4}$ | 3.77 | 3.98 |
| 40 | $7.1 \times 10^{4}$ | $6.0 \times 10^{4}$ | 4.31 | 4.55 |
| 50 | $4.1 \times 10^{4}$ | $3.6 \times 10^{4}$ | 5.39 | 6.68 |
| 60 | $2.9 \times 10^{4}$ | $2.5 \times 10^{4}$ | 6.47 | 6.82 |
| 70 | $2.1 \times 10^{4}$ | $1.8 \times 10^{4}$ | 7.54 | 7.95 |
| 80 | $1.4 \times 10^{4}$ | $1.1 \times 10^{4}$ | 8.62 | 9.09 |
| 100 | $(7.5\pm0.11) \times 10^{3}$ | $(5.2\pm0.15) \times 10^{3}$ | 10.78 | 11.36 |
| 150 | $(2.6\pm0.22) \times 10^{3}$ | $(1.6\pm0.22) \times 10^{3}$ | 16.16 | 17.05 |
| 200 | $(5.8\pm1.2) \times 10^{2}$ | $(6.5\pm1.5) \times 10^{2}$ | 21.55 | 22.05 |
| 300 | $(1.5\pm0.77) \times 10^{2}$ | $(2.8\pm1.0) \times 10^{2}$ | 32.33 | 34.09 |
| 500 | $(4.5\pm2.6) \times 10$ | $(9.5\pm3.86) \times 10$ | 53.90 | 56.80 |

Table 4.1a : Table of basic data for integral spectrum for scintillators A
and B from counting with peak on 22 mV for A and 23 mV for B
as measured by using pulse height analyser.

| Single pts.of peaks at output of head unit (mV) | | Discrimination levels at output of head unit (mV) | | Density threshold Δ (m$^{-2}$) | | Run time (hr) | No. of counts | R( > Δ) (hr$^{-1}$) |
|---|---|---|---|---|---|---|---|---|
| A | B | A | B | A | B | | | |
| 26.5 | 28 | 20 | 20 | 1.88 | 1.78 | 0.45 | 457 | 1005±47 |
| 26.5 | 28 | 30 | 30 | 2.83 | 2.68 | 1.00 | 400 | 400±20 |
| 26.5 | 28 | 40 | 40 | 3.77 | 3.57 | 0.94 | 225 | 240±16 |
| 26.5 | 28 | 50 | 50 | 4.72 | 4.46 | 0.90 | 160 | 177±14 |
| 26.5 | 28 | 60 | 60 | 5.66 | 5.36 | 0.83 | 83 | 100±11 |
| 26.5 | 28 | 70 | 70 | 6.60 | 6.25 | 0.85 | 72 | 85±10 |
| 26.5 | 28 | 80 | 80 | 7.55 | 7.14 | 1.10 | 77 | 70±8 |
| 26.5 | 28 | 100 | 100 | 9.43 | 8.93 | 1.30 | 59 | 46±6 |
| 26.5 | 28 | 150 | 150 | 14.15 | 13.39 | 1.10 | 29 | 27±5 |
| 26.5 | 28 | 200 | 200 | 18.67 | 17.86 | 0.86 | 15 | 17.5±4.5 |
| 26.5 | 28 | 300 | 300 | 28.30 | 26.78 | 1.11 | 11 | 10±3.0 |
| 26.5 | 28 | 400 | 400 | 37.73 | 35.71 | 0.96 | 7 | 6±2.5 |

Table 4.1b : Table for basic data for integral density spectrum from counting.

greater than a given height (>V) versus pulse height (V) measured at the head unit output with the two fold coincidence rate are shown in Figure 4.7a. The pulse height produced by single relativistic cosmic ray particles traversing the scintillator is indicated by the arrow. The pulse height (V) was then expressed in terms of density of particles ($\Delta = \frac{V}{0.4e}$ m$^{-2}$), where each scintillator has 0.4 m$^2$ area and (e) is the average pulse height produced by single relativistic cosmic ray particles traversing the scintillator. The results for the integral density spectrum determined in this way are shown in Figure 4.7b where the result given by Greisen (1960) is also shown. As shown in this figure the single relativistic cosmic ray particles traversing the scintillator corresponding to a density of 2.5 m$^{-2}$.

Over the range $2.7 \leqslant \Delta \leqslant 36$ m$^{-2}$ the integral density spectrum from the two fold coincidence measurements which is given in Figure 4.7b has the form

$$R(\geqslant \Delta) = 2058 \ \Delta^{-(1.66 \ \pm \ 0.06)} \ hr^{-1}$$

where $\Delta$ is in terms of electrons m$^{-2}$. The results indicate that the integral electron density spectrum at sea level has a slope of -1.66 in the density range $2.7 \leqslant \Delta \leqslant 36$ m$^{-2}$.

Table 4.2 shows the basic data for the differential pulse height distribution for scintillators A and B found from differentiating the data of Table 4.1. The results of such a study are shown in Figure 4.8 which give the position of the cosmic ray peak indicated by the arrow in Figure 4.7a.
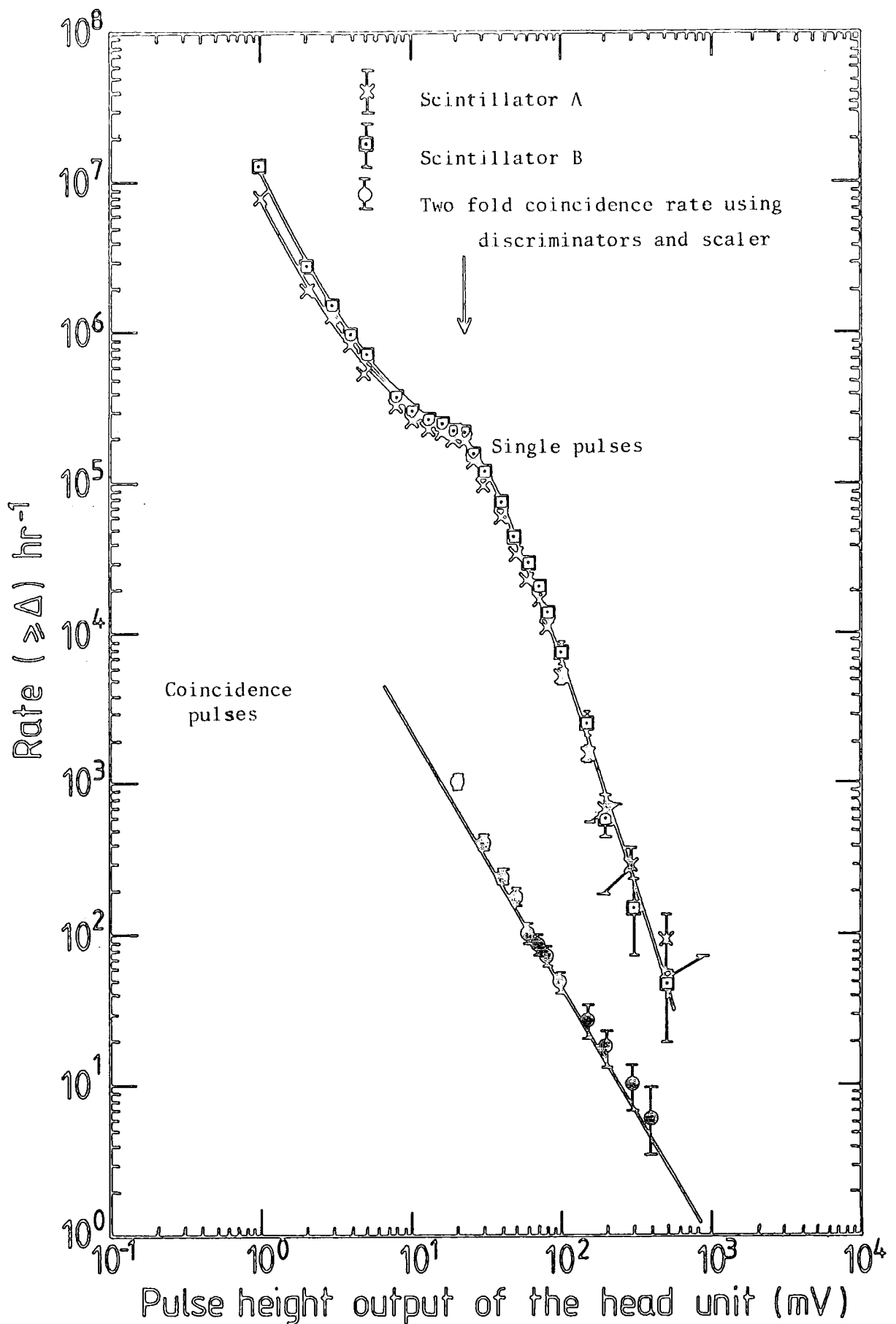
Figure 4.7a : The integral of pulses R(>V) measured at the output of the head units of scintillators A and B as a function of threshold pulse height V. Also shown is the measured coincidence rate between A and B as a function of V. The arrow is indicated to the most probable pulse height produced by single relativistic cosmic ray particles traversing their area at normal incidence. The area of both A and B are 0.4 m².
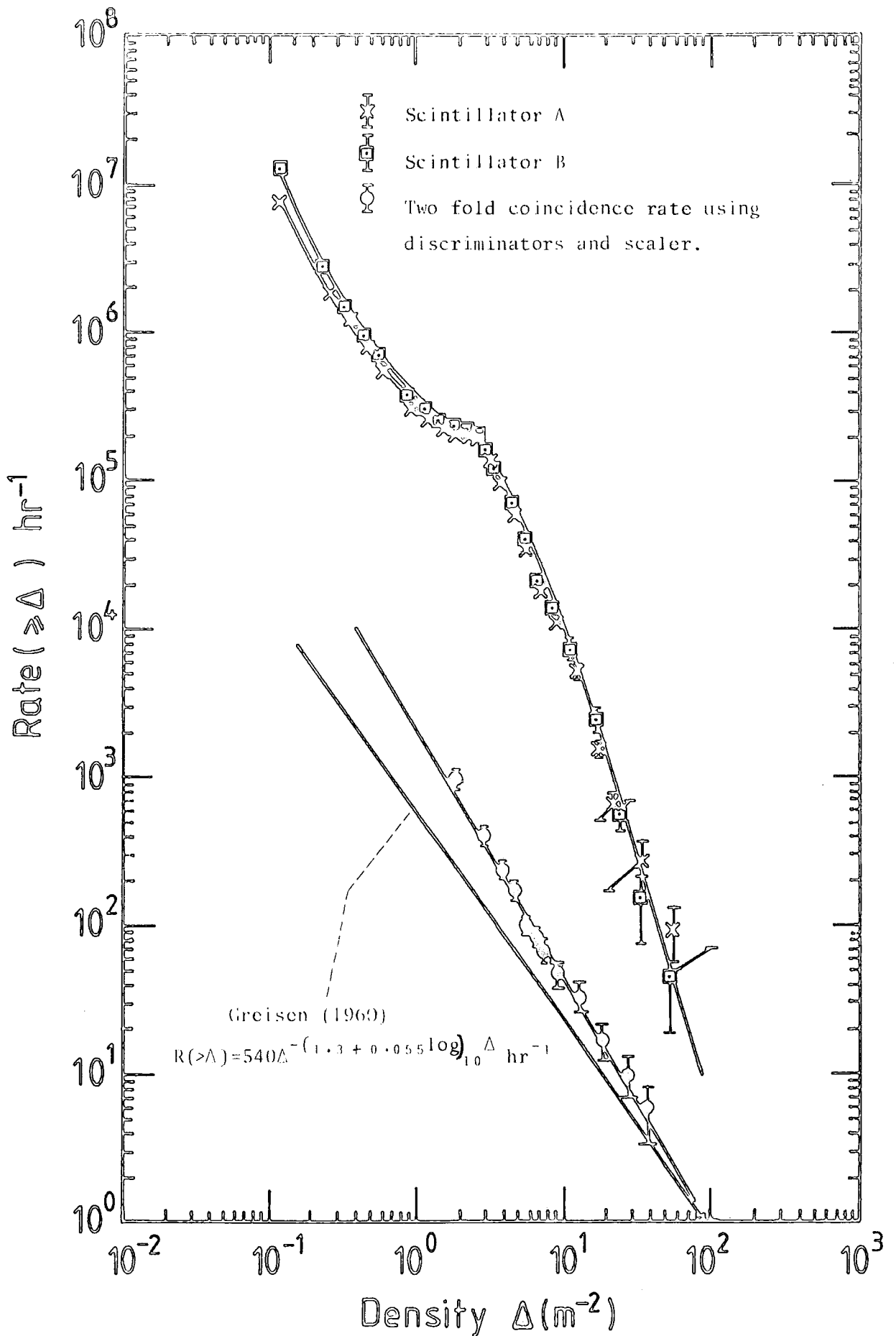
Figure 4.7b: Same as figure 4.7a except that the abscissa is plotted in terms of the apparent density of particles traversing the scintillator which has area $0.4m^2$ and the result is compared with that given by Greisen (1960). Single relativistic particles traversing the scintillator corresponding to a density of $2.5 \ m^2$.

| Threshold range (mV) $V_1 \rightarrow V_2$ | Mean of threshold range (mV) | Width $\Delta V = (V_2 - V_1)$ mV | Rate of events in threshold range $R(V_1 \rightarrow V_2)$ hr$^{-1}$ | | Differential rate at $\bar{V}$ $R(V_1 \rightarrow V_2)$ hr$^{-1}$mV$^{-1}$ | |
|---|---|---|---|---|---|---|
| | | | A | B | A | B |
| 1 - 2 | 1.5 | 1.0 | $6.1 \times 10^6$ | $1.0 \times 10^7$ | $6.1 \times 10^6$ | $1.0 \times 10^7$ |
| 2 - 3 | 2.5 | 1.0 | $1.9 \times 10^6$ | $1.3 \times 10^6$ | $1.9 \times 10^6$ | $1.3 \times 10^6$ |
| 3 - 4 | 3.5 | 1.0 | $4.5 \times 10^5$ | $5.5 \times 10^5$ | $4.5 \times 10^5$ | $5.5 \times 10^5$ |
| 4 - 5 | 4.5 | 1.0 | $3.0 \times 10^5$ | $2.5 \times 10^5$ | $3.0 \times 10^5$ | $2.5 \times 10^5$ |
| 5 - 8 | 6.5 | 3.0 | $2.4 \times 10^5$ | $3.3 \times 10^5$ | $8.0 \times 10^4$ | $1.1 \times 10^5$ |
| 8 - 10 | 9.0 | 2.0 | $1.8 \times 10^5$ | $7.0 \times 10^4$ | $1.5 \times 10^4$ | $3.5 \times 10^4$ |
| 10 - 13 | 11.5 | 3.0 | $3.0 \times 10^4$ | $3.9 \times 10^4$ | $1.0 \times 10^4$ | $1.3 \times 10^4$ |
| 13 - 16 | 14.5 | 3.0 | $3.0 \times 10^4$ | $2.0 \times 10^4$ | $1.0 \times 10^4$ | $6.6 \times 10^3$ |
| 16 - 20 | 1S.0 | 4.0 | $1.0 \times 10^4$ | $2.0 \times 10^4$ | $2.5 \times 10^3$ | $5.0 \times 10^3$ |
| 20 - 23 | 21.5 | 3.0 | $2.0 \times 10^4$ | $9.9 \times 10^3$ | $6.6 \times 10^3$ | $3.3 \times 10^3$ |
| 23 - 26 | 22.5 | 3.0 | $5.1 \times 10^4$ | $6.0 \times 10^4$ | $1.7 \times 10^4$ | $2.0 \times 10^4$ |
| 26 - 30 | 28.0 | 4.0 | $4.0 \times 10^4$ | $3.0 \times 10^4$ | $1.0 \times 10^4$ | $7.5 \times 10^3$ |
| 30 - 35 | 32.5 | 5.0 | $2.5 \times 10^4$ | $3.0 \times 10^4$ | $5.0 \times 10^3$ | $6.0 \times 10^3$ |
| 35 - 40 | 37.5 | 5.0 | $1.5 \times 10^4$ | $1.9 \times 10^4$ | $3.0 \times 10^3$ | $3.8 \times 10^3$ |
| 40 - 50 | 45.0 | 10.0 | $2.4 \times 10^4$ | $3.0 \times 10^4$ | $2.4 \times 10^3$ | $3.0 \times 10^3$ |
| 50 - 60 | 55.0 | 10.0 | $1.1 \times 10^4$ | $1.2 \times 10^4$ | $1.1 \times 10^3$ | $1.2 \times 10^3$ |
| 60 - 70 | 65.0 | 10.0 | $7.0 \times 10^3$ | $8.0 \times 10^3$ | $7.0 \times 10^2$ | $8.0 \times 10^2$ |
| 70 - 80 | 75.0 | 10.0 | $7.0 \times 10^3$ | $7.0 \times 10^3$ | $7.0 \times 10^2$ | $7.0 \times 10^2$ |
| 80 - 100 | 90.0 | 20.0 | $5.8 \times 10^3$ | $6.6 \times 10^3$ | $2.9 \times 10^2$ | $3.3 \times 10^2$ |
| 100 - 150 | 125.0 | 50.0 | $(3.6 \pm 0.05)10^3$ | $(4.9 \pm 0.25)10^3$ | $72 \pm 10$ | $98 \pm 5.0$ |
| 150 - 200 | 175.0 | 50.0 | $(9.5 \pm 2.6)10^2$ | $(2.0 \pm 0.25)10^3$ | $19 \pm 5.0$ | $40 \pm 5.0$ |
| 200 - 300 | 250.0 | 100.0 | $(3.7 \pm 1.0)10^2$ | $(4.3 \pm 1.4)10^2$ | $3.7 \pm 1.0$ | $4.3 \pm 1.4$ |
| 300 - 500 | 400.0 | 200.0 | $(1.8 \pm 1.0)10^2$ | $(1.0 \pm 0.8)10^2$ | $0.9 \pm 1.0$ | $0.5 \pm 0.8$ |

Table 4.2 : Differential pulse height distribution for scintillators A and B.
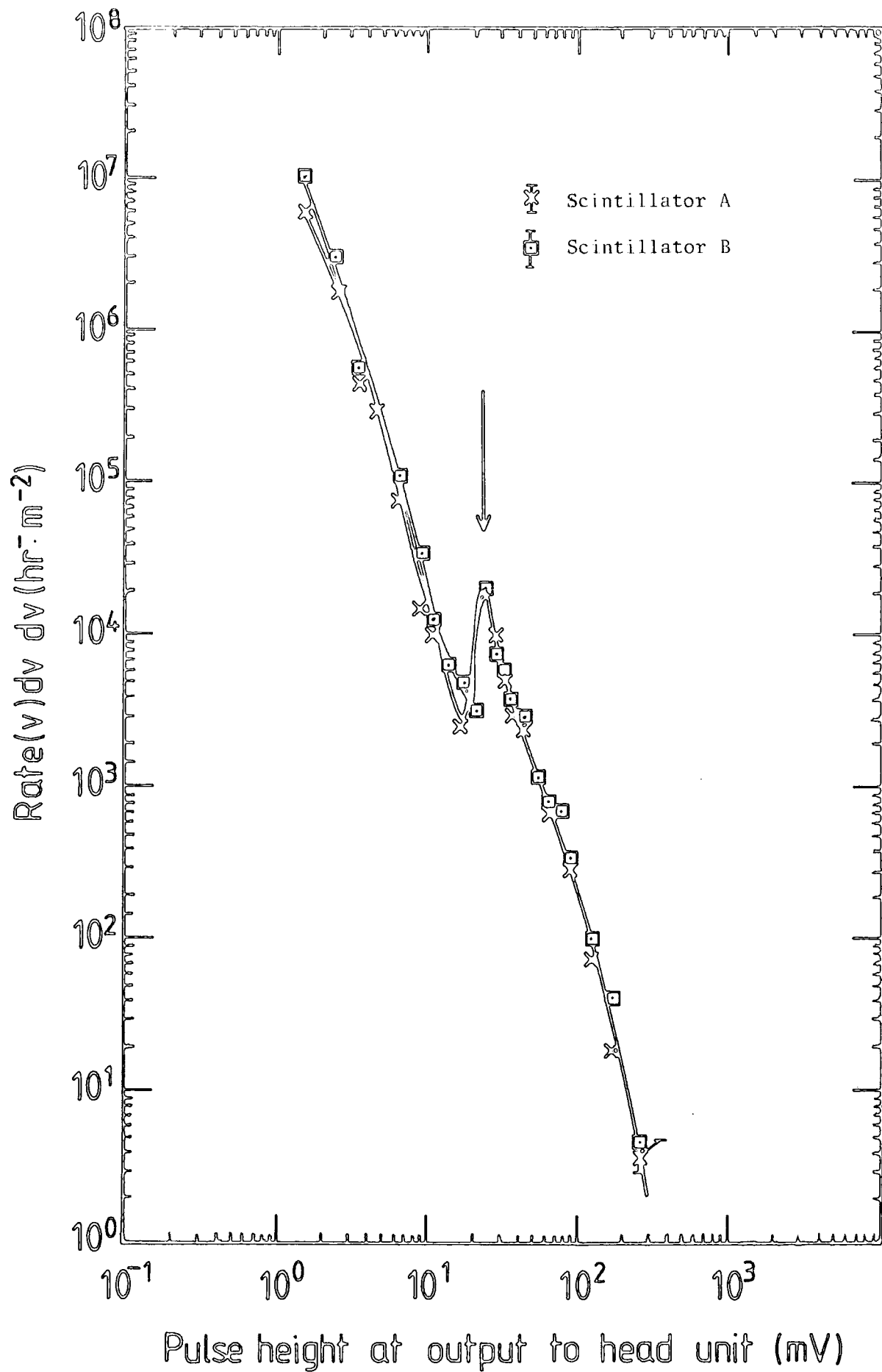
Figure 4.8 : The differential pulse height distribution as determined by differentiating the integral rate distribution determined using an amplifier, discriminator and scaler. The most probable pulse height produced by single relativistic particles traversing the scintillator is indicated by the arrow.

## 4.7.2 Study of the correlation between the detected number of particles through scintillators A and B using the microcomputer data acquisition system

The correlation between the number of particles traversing scintillators A and B has been studied using two discriminators, a two fold coincidence and the microcomputer data acquisition system. Because of the delay of 6.5 μs in the reading by the data acquisition unit (see chapter two), a stretcher amplifier was used before each channel of the data acquisition unit. Figures 4.9 a,b shows the calibration curves of the stretcher amplifiers C and D with the head units of scintillators A and B respectively using 10 μs decay time input exponential pulses. The decay time at the output of the stretcher amplifiers = 250 μs.

The pulse height (V) at the head unit output from both scintillators A and B has been measured directly on channels number one and two of the data acquisition unit respectively, after passing through two stretcher amplifiers. The output pulse heights from both channels were recorded on tape of the cassette driver of the PET. Coincidence pulses from scintillators A and B of a level set by the two discriminators, were used to trigger the data acquisition unit. Discriminators A and B were set on discrimination level $(V_{min})$ to give pulse height (V) only if the electron density is greater than a given value $\Delta_{min}$. $(V_{min.} = \Delta_{min.} 0.4e)$, where each scintillator has 0.4 m² area and (e) is the average pulse height produced by single relativistic cosmic ray particles traversing the scintillator. It is important to mention here that $(V_{min.})$ was not set on a constant value during the time of running the experiment, where it is clear from the equation $(V_{min.} = \Delta_{min.} 0.4e)$ that $(V_{min.})$ depends on (e) which was not exactly the same for both scintillators
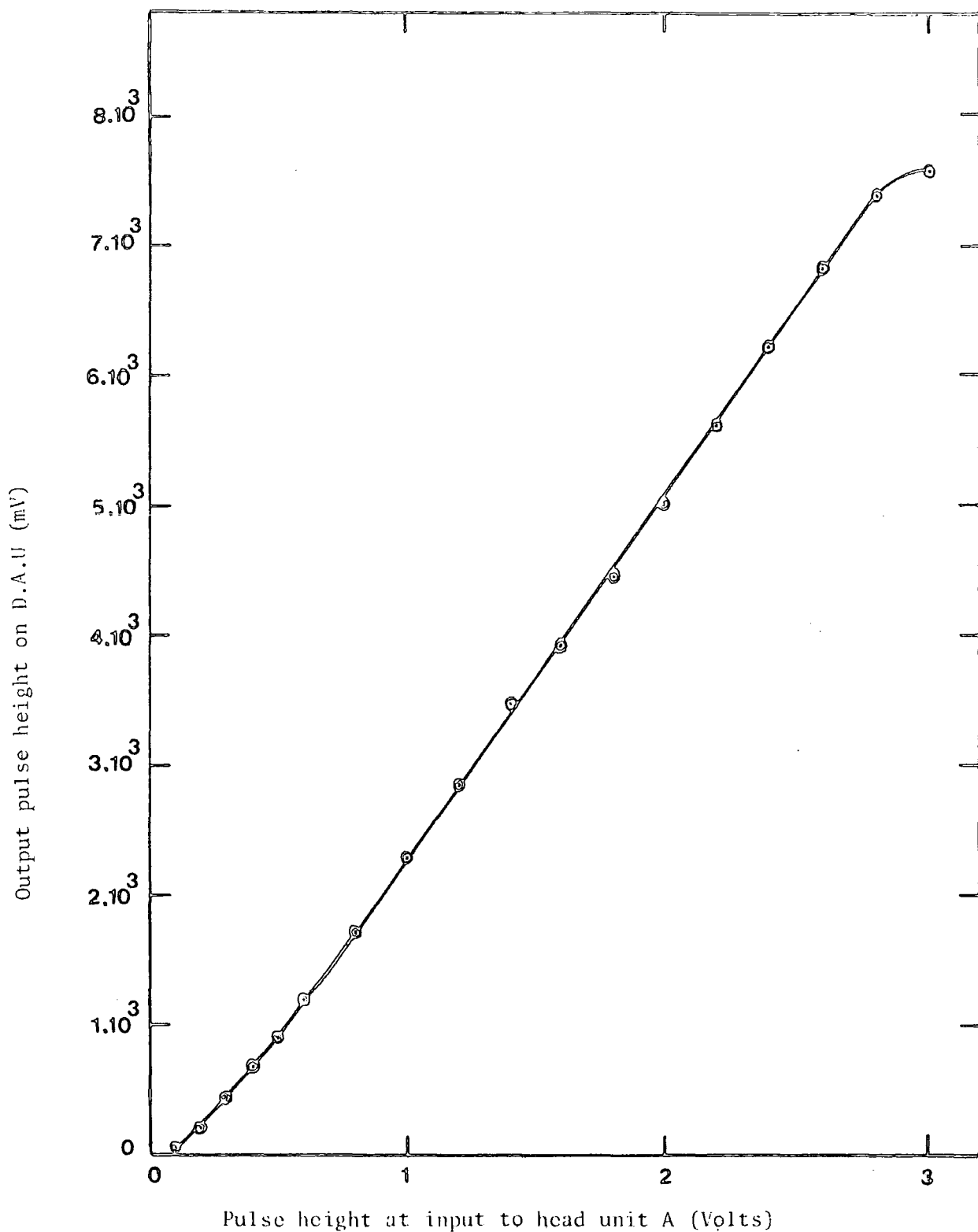
Figure 4.9a : Calibration of the stretcher amplifier (c) with the head unit of scintiallator A on channel number one of the data acquisition unit using 10 µs decay time input exponential pulses. The decay time at the output of the stretcher amplifier = 250 µs
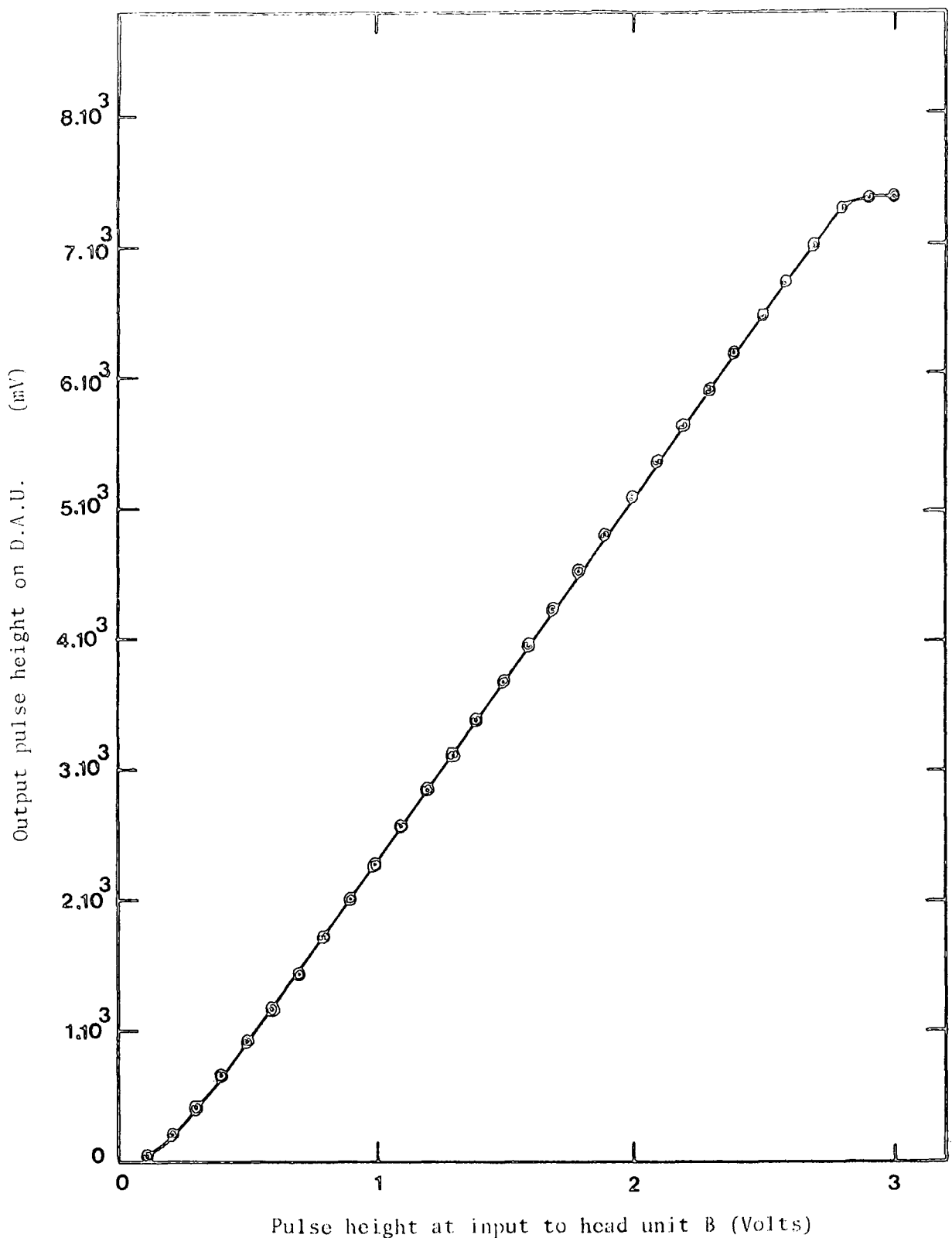
Figure 4.9b : Calibration of the stretcher amplifier (B) with the head unit of scintillator B on channel number two of the data acquisition unit using 10 µs decay time input exponential pulses. The decay time at the output of the stretcher amplifier = 250 µs.

A and B.  The experimental data were obtained in six different
runs (see table 4.3).

In 173.34 hr running time 1,496 showers were recorded.  First
of all, the data were calibrated to original cosmic ray pulse
heights using the "CALIBRATION PROGRAM" given in appendix(A) which
depended on the calibration curves (Figures 4.9a,b), then the pulse
heights (V) were converted to a number of particles (N) through
scintillators A and B (N = V/e).  It was found that the electronic
recording system is saturated if scintillator A traversed by >134
particles and it is saturated if scintillator B traversed by >134
particles.  Frequency distributions of the number of particles $N_A$
and $N_B$ through scintillators A and B respectively is shown in
Figure 4.10a for all the data.

A discrimination level at 200 mV was imposed to eliminate
drift for all data.  A number of particles (N = V/e) traversing
scintillators A and B for a 200 mV discrimination level for each
run were found and the results are shown in Table 4.4.  From that,
we see that the maximum value of the minimum number of particles
traversing each scintillator for a 200 mV discrimination level out
of six runs is 10.9 (from the result of run number 9, scintillator
A).  To combine data we had to put a cut off on each discrimination
level corresponding to 11 particles through either scintillator
as shown in Table 4.5.

Figure 4.10b shows the frequency distribution of the number
of particles $N_A$ and $N_B$ through scintillators A and B respectively,
after a cut off at a discrimination level corresponding to 11
particles through either scintillator was imposed.  Scatter plot
of the number of particles ($N_A$) through scintillator A versus the

| Run No. | Initial discrimination setting (mV) | | Sensitive time (hr) | Total number of triggers | No. of triggers with A ≥134 pts. and B≥134 pts. | No. of triggers with A≥134 pts. and B <134 pts. | No. of triggers B≥134 pts. and A< 134 pts. |
|---|---|---|---|---|---|---|---|
| | A | B | | | | | |
| 1 | 240 | 285 | 64.94 | 647 | 8 | 15 | 1 |
| 8 | 240 | 250 | 19.30 | 147 | 2 | 3 | 0 |
| 9 | 220 | 250 | 24.30 | 205 | 2 | 7 | 0 |
| 11 | 240 | 280 | 18.00 | 146 | 2 | 7 | 0 |
| 12 | 240 | 280 | 26.40 | 188 | 1 | 6 | 0 |
| 14 | 250 | 280 | 20.40 | 163 | 2 | 3 | 3 |
| Column totals | | | 173.34 | 1496 | 17 | 41 | 4 |

Table 4.3 :  Table of triggers at initial discrimination level for scintillators A and B.
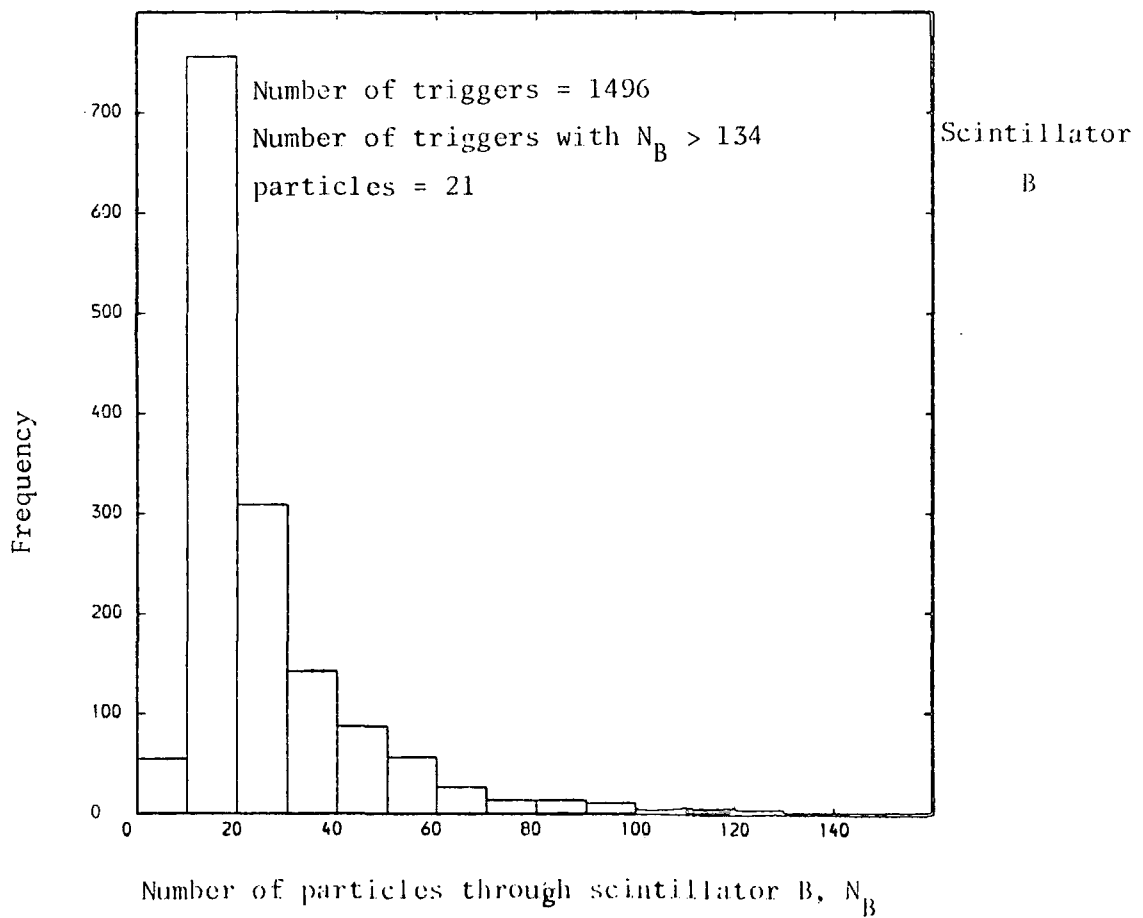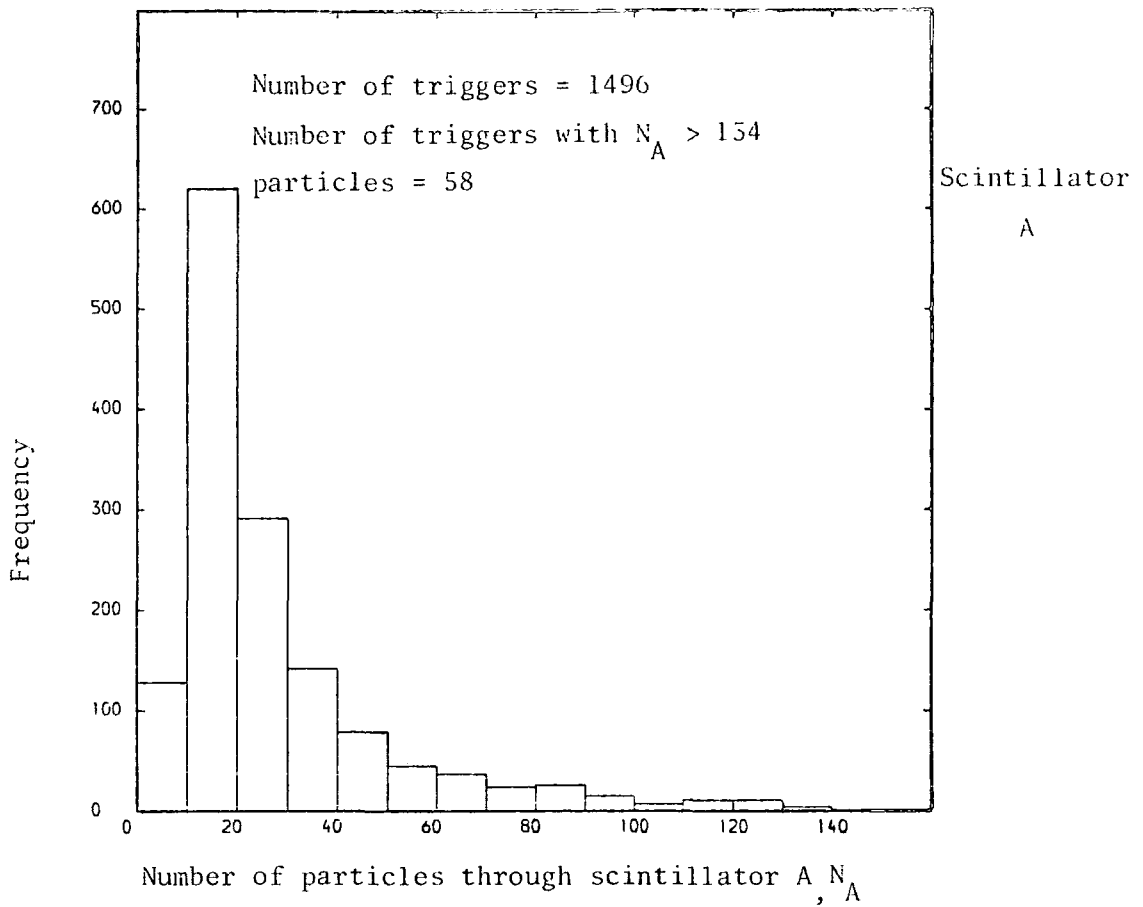
Figure 4.10a : The frequency distributions of the number of particles
through scintillators A and B for all data - no cut off.
The distributions are evaluated if $N_A$ and $N_B$ < 134 particles.

| Run No. | Average pulse height for single particles (mV) | | Imposed discriminator setting to eliminate drift. (mV) | | No. of particles traversing scintillator for a 200 mv discrimination level | | Sensitive time (hr) | Number of triggers | No. of triggers with A ≥ 134 pts. and B ≥ 134 pts. | No. of triggers with A ≥134 pts. and B <134 pts. | No. of triggers with B ≥134 pts. and A <134 pts. |
|---|---|---|---|---|---|---|---|---|---|---|---|
| | A | B | A | B | A | B | | | | | |
| 1 | 20.0 | 24.0 | 200 | 200 | 10.0 | 8.3 | 64.94 | 534 | 8 | 15 | 1 |
| 8 | 20.0 | 21.0 | 200 | 200 | 10.0 | 9.5 | 19.30 | 146 | 2 | 3 | 0 |
| 9 | 18.3 | 21.0 | 200 | 200 | 10.9 | 9.5 | 24.30 | 204 | 2 | 7 | 0 |
| 11 | 20.1 | 23.2 | 200 | 200 | 10.0 | 8.6 | 18.00 | 144 | 2 | 7 | 0 |
| 12 | 20.1 | 23.2 | 200 | 200 | 10.0 | 8.6 | 26.40 | 183 | 1 | 6 | 0 |
| 14 | 20.8 | 23.2 | 200 | 200 | 9.6 | 8.6 | 20.40 | 157 | 2 | 3 | 3 |
| Column totals | | | | | | | 173.34 | 1368 | 17 | 41 | 4 |

Table 4.4 : Table of triggers and a number of particles traversing scintillator for a 200 mV discrimination level for scintillators A and B.

| Run No. | Average pulse height for single particles (mv) | | Discrimination level corresponding to 11 pts. through scintillator | | Sensitive time (hr) | No. of triggers with ≥11 pts. through both scints.A & B ($\triangle \geqslant 27.5m^{-2}$) |
|---|---|---|---|---|---|---|
| | A | B | A | B | | |
| 1 | 20.0 | 24.0 | 220 | 264 | 64.94 | 425 |
| 8 | 20.0 | 21.0 | 220 | 231 | 19.3 | 129 |
| 9 | 18.3 | 21.0 | 201 | 231 | 24.3 | 200 |
| 11 | 20.1 | 23.2 | 221 | 255 | 18.0 | 126 |
| 12 | 20.1 | 23.2 | 221 | 255 | 26.4 | 161 |
| 14 | 20.8 | 23.2 | 228 | 255 | 20.4 | 143 |
| Column totals | | | | | 173.34 | 1184 |

Table 4.5 : Table of triggers at discrimination level corresponding to 11 particles through scintillator for scintillators A and B.
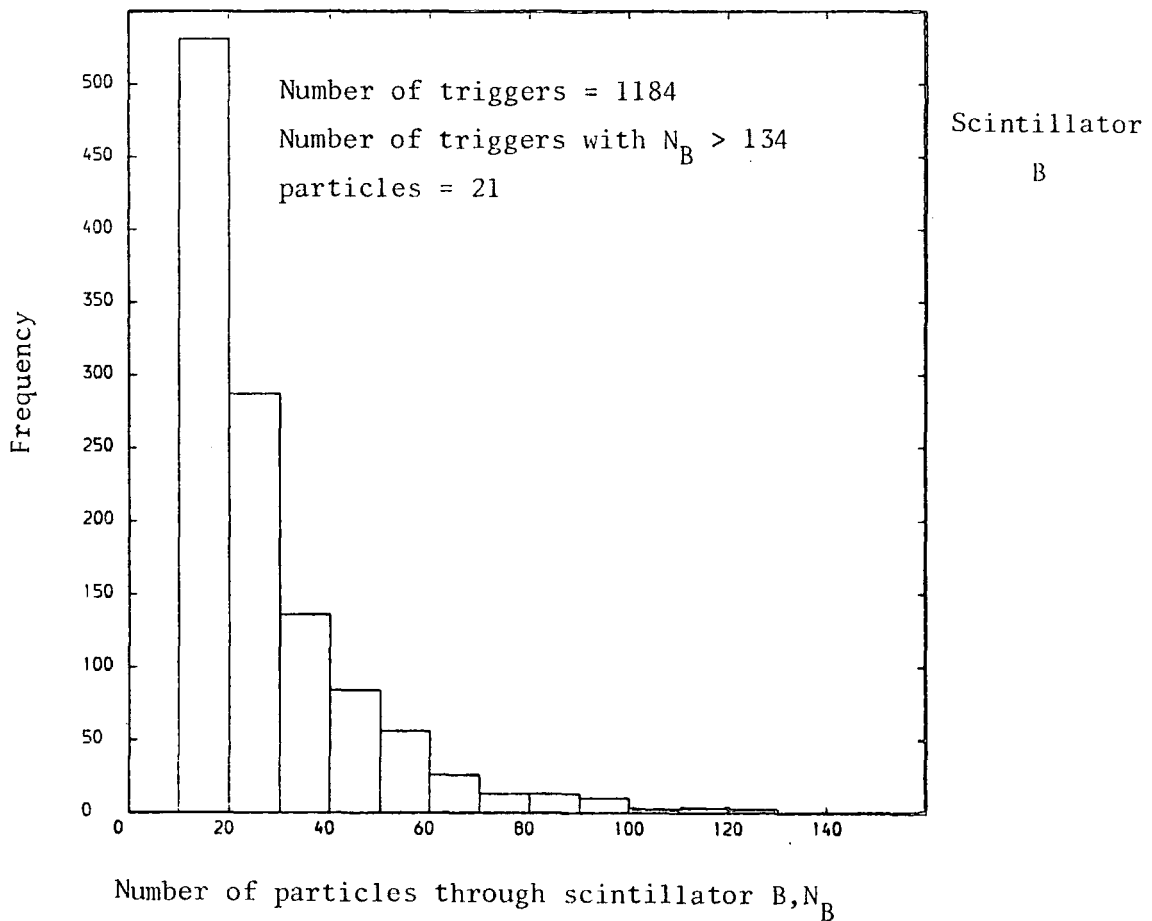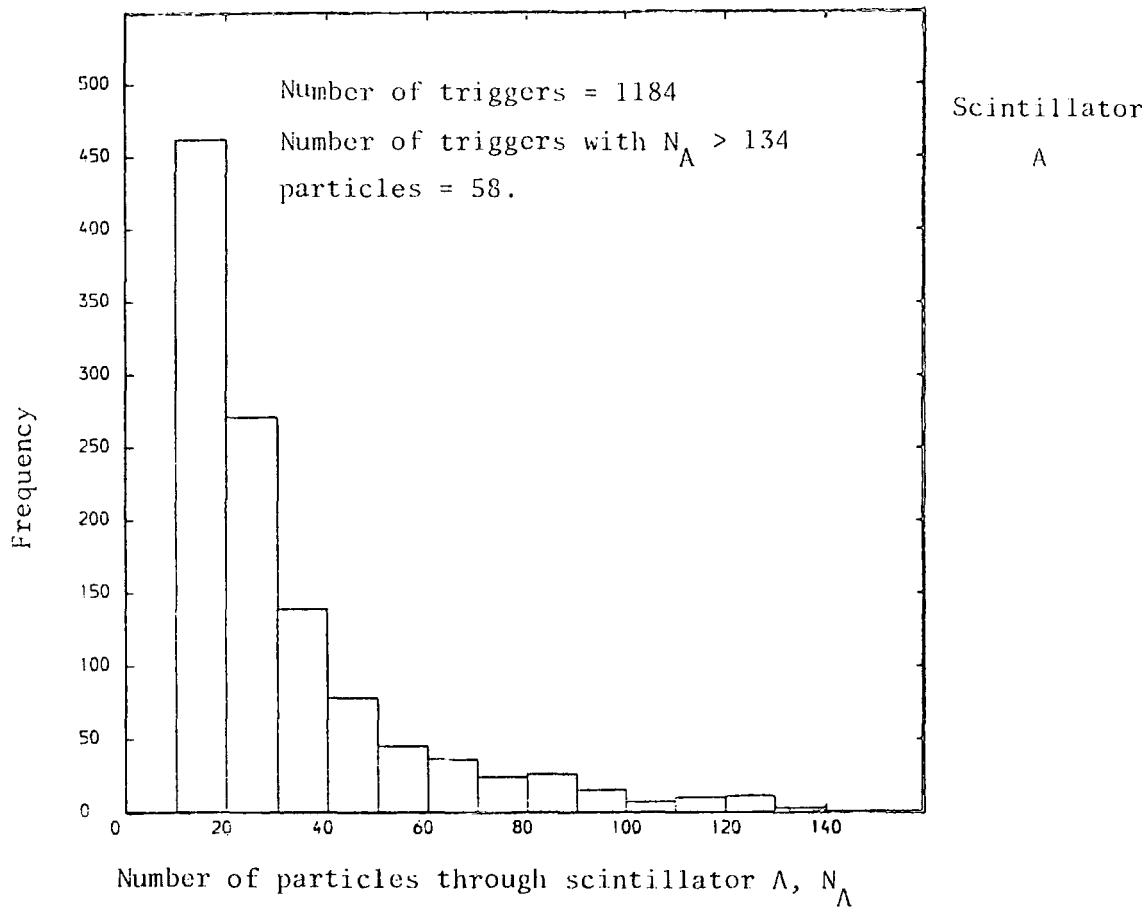
Figure 4.10b : The frequency distributions of the number of particles through scintillators A and B for data cut off at a discrimination level corresponding to 11 particles through either scintillator. The distributions are evaluated if $N_A$ and $N_B$ < 134 particles.

number of particles ($N_B$) through scintillator B for 1122 air shower triggers has also been found as shown in Figure 4.11.

The frequency distribution of the ratio of the number of particles (N) through scintillator A to that of scintillator B, $N_A/N_B$, and the number of particles through scintillator B to that of scintillator A, $N_B/N_A$, are shown in figure 4.12a. The mean values and the standard deviations of the distribution ($\sigma$) about the means are shown in that figure. Also the frequency distributions of $Log_e(N_A/N_B)$ and $Log_e(N_B/N_A)$ have been plotted and the results are shown in figure 4.12b with the mean values and the standard deviations of distributions ($\sigma$) about the means also shown. A summary of the results of all six runs are given in Table 4.6.

An extensive air shower at sea level containing a total number of (N) particles can have either a flat or sharp electron lateral distribution function. It is usual to describe the lateral distribution function of electron in terms of the Nishimura-Kamata-Greisen (NKG) function

$$\Delta(r) = N \frac{f(r/r_0)}{r_0^2}$$

$$f(\frac{r}{r_0}) = C(s) (\frac{r}{r_0})^{S-2} (\frac{r}{r_0} + 1)^{S-4.5}$$

where $r_0$ is called Moliere or scattering unit (the value of $r_0$ is 79 m at sea level), r is the perpendicular distance from the shower core, s is the age parameter and indicates the development stage of the shower and C(s) is a normalising factor such that $_0\int^{\infty} 2\pi r\Delta(r)dr = 1$, and the values of C(s) are as follows (Greisen,1960)

| s | 0.6 | 0.8 | 1.0 | 1.2 | 1.4 | 1.6 | 1.8 |
|---|---|---|---|---|---|---|---|
| C(s) | 0.22 | 0.31 | 0.40 | 0.44 | 0.43 | 0.36 | 0.25 |

Figure 4.13 shows a plot of $\Delta(r)$ versus r for N = 1.
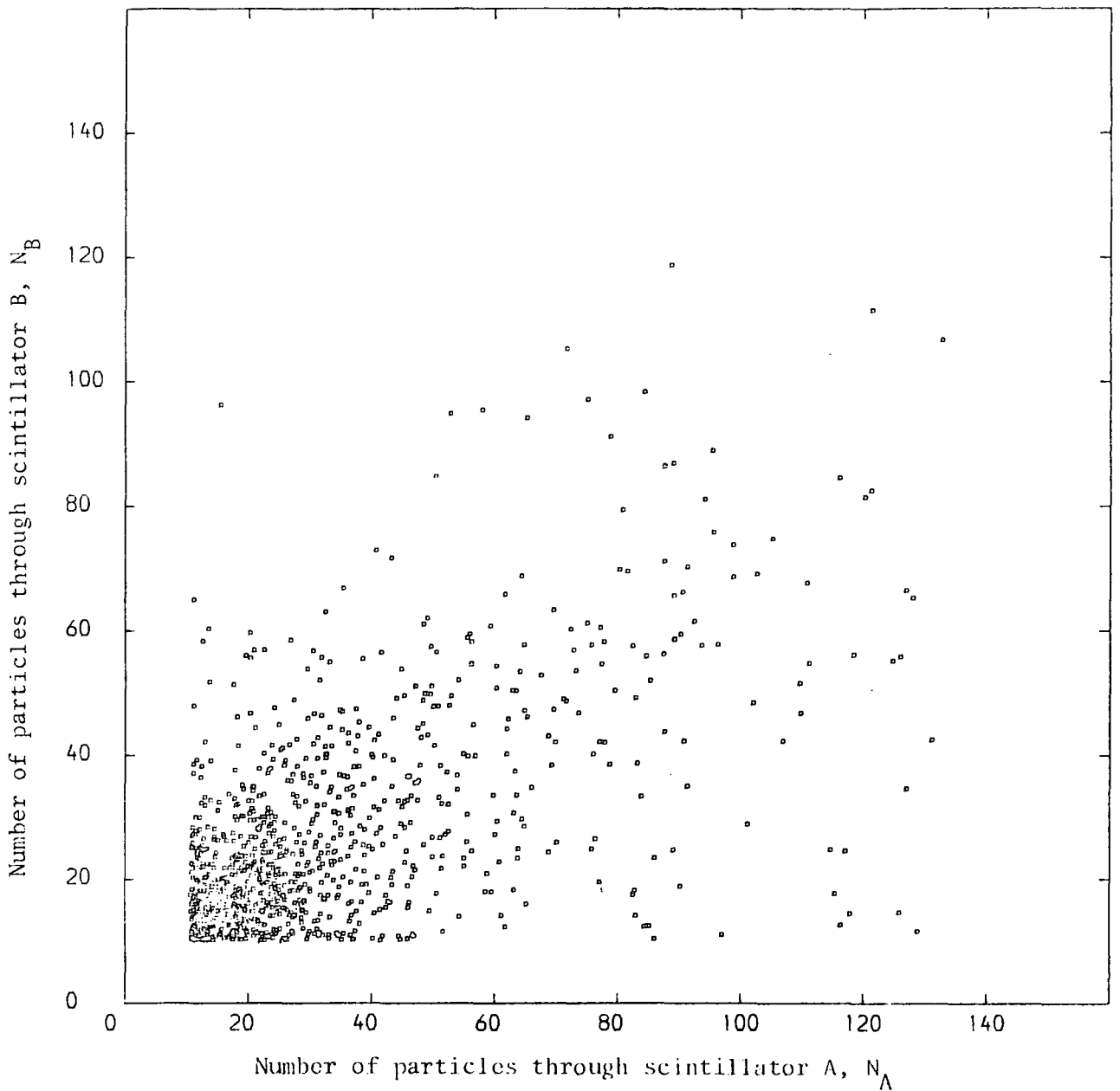
Figure 4.11 : Scatter plot of the number of particles through
scintillator A versus the number of particles through
scintillator B. The relation is evaluated if $N_A$ and
$N_B$ < 134 particles. The number of the density points = 1122.
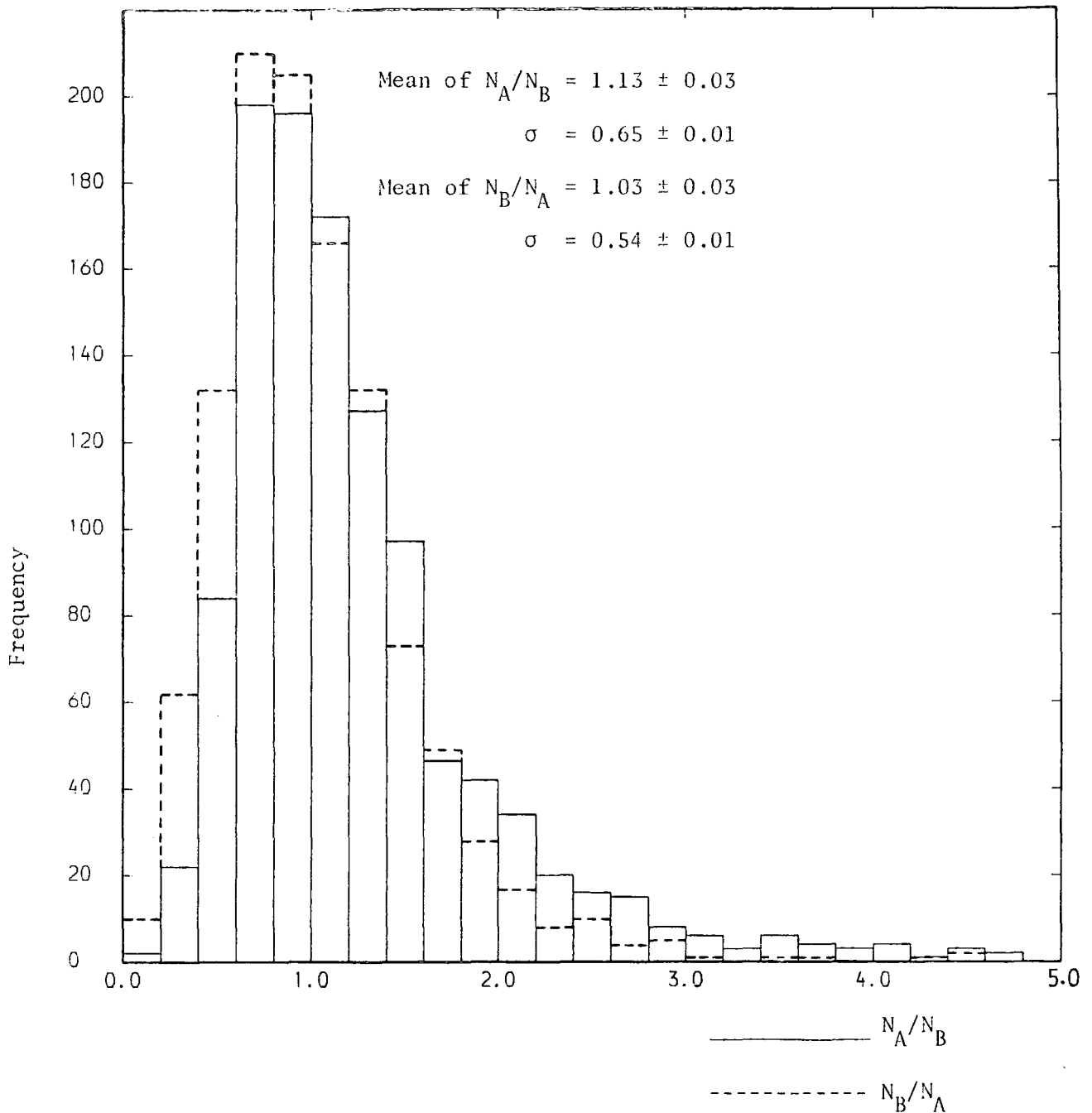
Figure 4.12a : The frequency distributions of the ratio of the number of particles through scintillator A to that of scintillator B and the number of particles through scintillator B to that of scintillator A. The ratios $N_A/N_A$ and $N_B/N_A$ are evaluated if $N_A$ and $N_B$ < 134 particles. The number of the density ratios = 1122.
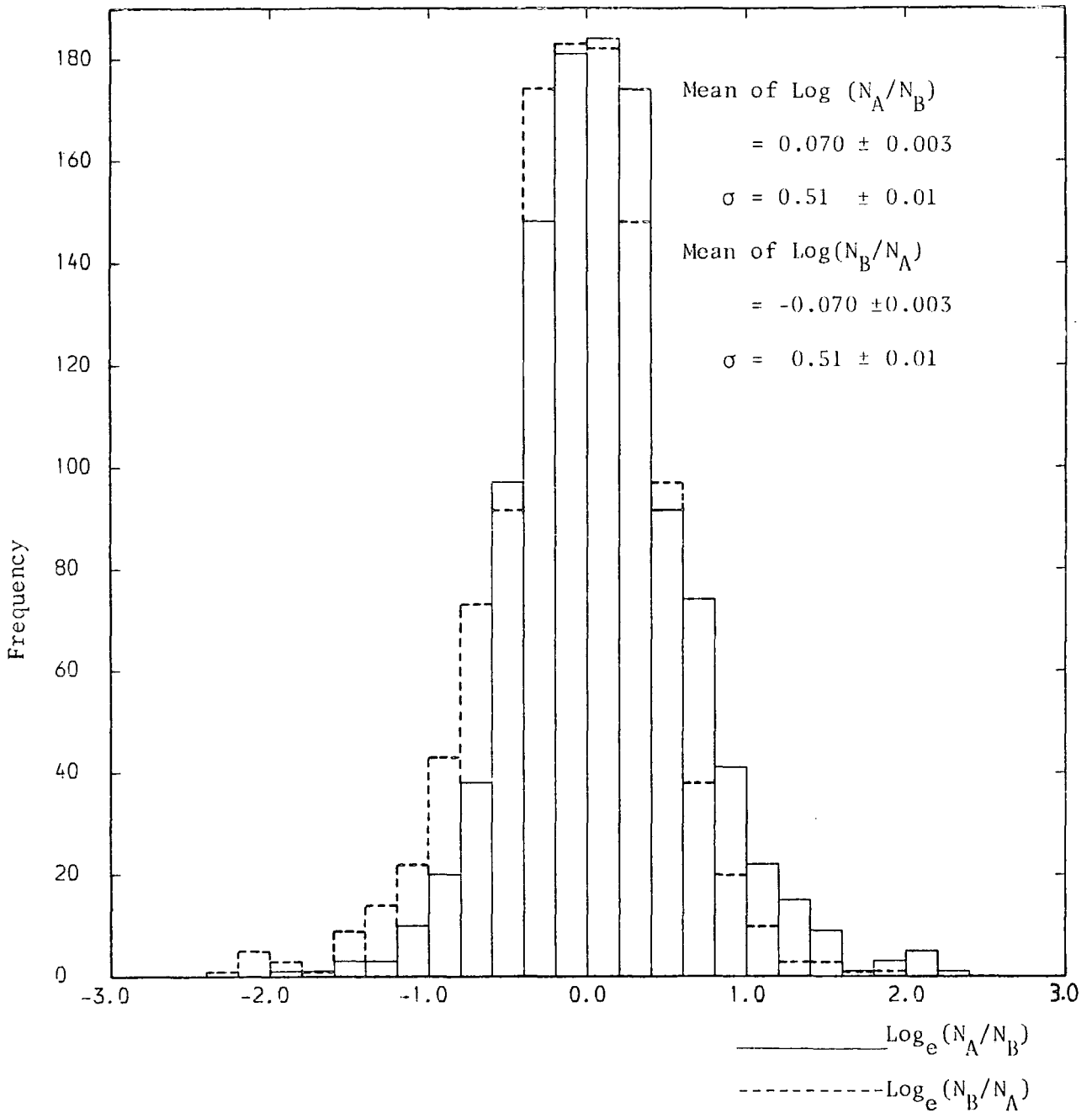
Figure 4.12b : The frequency distributions of $\log_e$ the number of particles through scintillator A to that of scintillator B and $\log_e$ the number of particles through scintillator B to that of scintillator A. The ratios $\log_e(N_A/N_B)$ and $\log_e(N_B/N_A)$ are evaluated if $N_A$ and $N_B < 134$ particles. The number of the density ratios = 1122.

| Run No. | $N_A$ | $N_B$ | $N_A/N_B$ | $N_B/N_A$ | $Log(N_A/N_B)$ | $Log(N_B/N_A)$ |
|---|---|---|---|---|---|---|
| 1 | Mean = 32.3 ±1.62 <br> σ = 22.9 ±0.81 | Mean = 26.26±1.30 <br> σ = 15.02±0.53 | Mean = 1.20±0.06 <br> σ = 0.61±0.02 | Mean = 0.98±0.05 <br> σ = 0.55±0.02 | Mean = 0.13±0.01 <br> σ = 0.29±0.01 | Mean = -0.14±0.01 <br> σ = 0.29±0.01 |
| 8 | Mean = 31.67±2.82 <br> σ = 23.30±1.47 | Mean = 29.84±2.66 <br> σ = 19.1 ±1.20 | Mean = 1.11±0.10 <br> σ = 0.71±0.06 | Mean = 1.07±0.10 <br> σ = 0.48±0.03 | Mean = 0.01±0.001 <br> σ = 0.24±0.02 | Mean = -0.013±0.001 <br> σ = 0.24±0.02 |
| 9 | Mean = 31.41±2.27 <br> σ = 23.79±1.21 | Mean = 27.24±1.97 <br> σ = 17.70±0.90 | Mean = 1.13±0.06 <br> σ = 0.70±0.04 | Mean = 1.10±0.08 <br> σ = 0.58±0.03 | Mean = 0.040±0.003 <br> σ = 0.34±0.02 | Mean = -0.040±0.003 <br> σ = 0.34±0.02 |
| 11 | Mean = 32.52±3.01 <br> σ = 23.71±1.55 | Mean = 28.85±2.67 <br> σ = 17.34±1.13 | Mean = 1.12±0.11 <br> σ = 0.61±0.04 | Mean = 1.04±0.10 <br> σ = 0.50±0.03 | Mean = 0.07±0.01 <br> σ = 0.19±0.02 | Mean = -0.07±0.01 <br> σ = 0.19±0.02 |
| 12 | Mean = 33.19±2.67 <br> σ = 25.91±1.47 | Mean = 27.32±2.19 <br> σ = 18.03±1.02 | Mean = 1.16±0.09 <br> σ = 0.67±0.04 | Mean = 0.99±0.08 <br> σ = 0.53±0.03 | Mean = 0.12±0.01 <br> σ = 0.32±0.02 | Mean = -0.13±0.01 <br> σ = 0.32±0.02 |
| 14 | Mean = 31.07±2.67 <br> σ = 23.38±2.01 | Mean = 25.07±2.16 <br> σ = 16.41±1.41 | Mean = 1.13±0.10 <br> σ = 0.74±0.05 | Mean = 1.08±0.09 <br> σ = 0.53±0.03 | Mean = 0.06±0.01 <br> σ = 0.32±0.02 | Mean = -0.040±0.003 <br> σ = 0.32±0.02 |
| All | Mean = 30.01±0.89 <br> σ = 22.07±0.47 | Mean = 27.76±0.81 <br> σ = 15.84±0.33 | Mean = 1.13±0.03 <br> σ = 0.65±0.01 | Mean = 1.03±0.03 <br> σ = 0.54±0.01 | Mean = 0.070±0.003 <br> σ = 0.51±0.01 | Mean = -0.070±0.003 <br> σ = 0.51±0.01 |

Table 4.6 : Summary of frequency distributions of the number of particles, N, through scintillators A and B.

$\Delta (r) = N \dfrac{f(r/r_o)}{r_o^2}$  where $N = 1$   $(m^{-2})$

Core distance (metres)
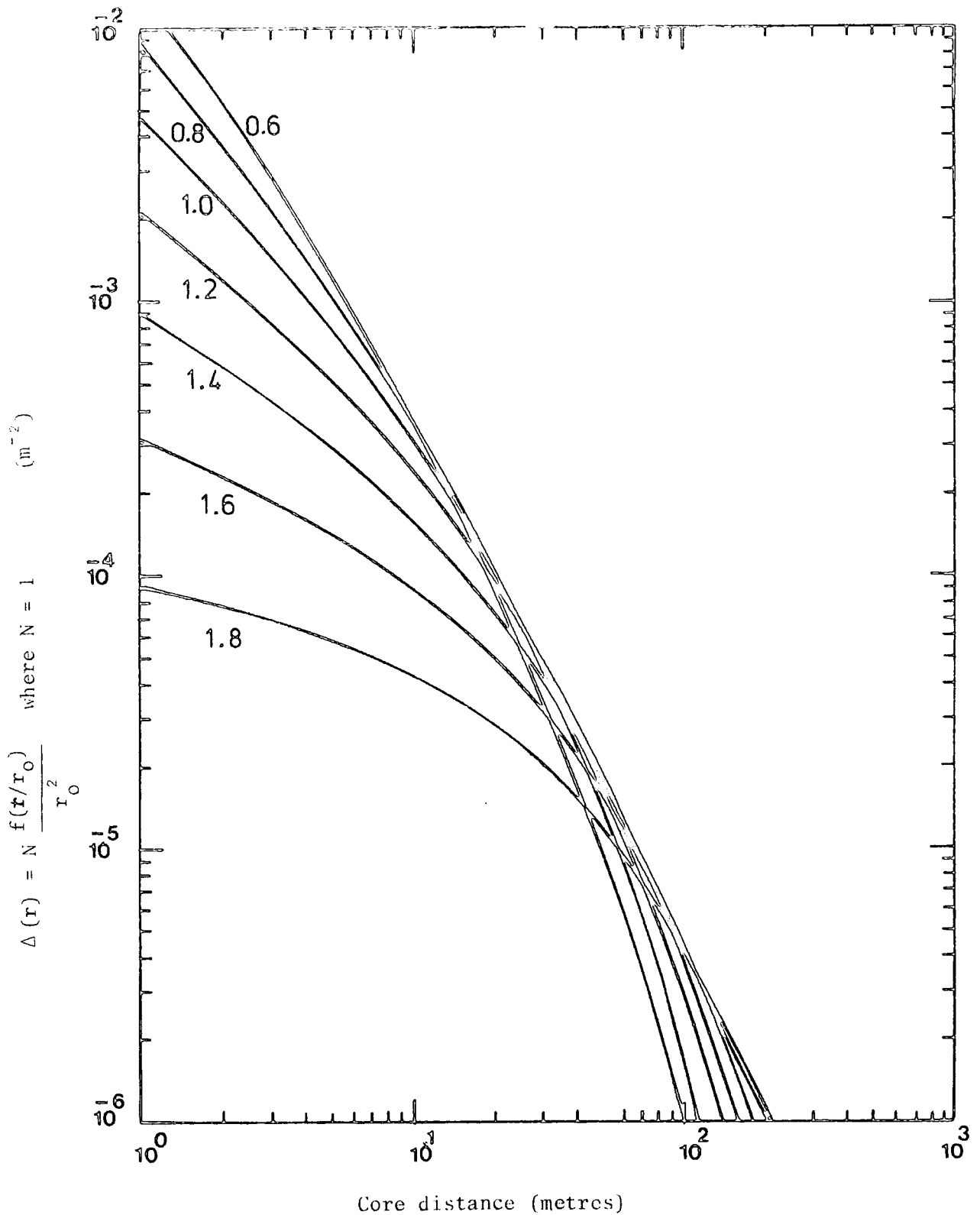
Figure 4.13 : The lateral distribution of electrons in showers of unit size in air at level ($r_o$ = 79m). The number attached to each curve is the age parameter (s) of the shower.

No attempt has been made in the present work to evaluate the expected value of the ratio of $N_A/N_B$. However the measured most probable value of close to unity is consistent with most of the showers detected falling at a core distance from scintillators A and B which is large compared to their separation (1.6 metre).

All the frequency distribution diagrams previously presented were drawn using the "FREQUENCY DISTRIBUTION PROGRAM" which is given in Appendix A.

### 4.7.3 Measurement of the electron density spectrum at sea level using the microcomputer data acquisition system

The integral density spectrum of electrons at sea level over the range $27.5 < \Delta < 335 \text{ m}^{-2}$ has been measured using two discriminators, a two fold coincidence and a microcomputer data acquisition system.

After the cut off at the discrimination level given in Table 4.5 1184 events were obtained in a sensitive time of 173.34 hours. The measurements were converted to the corresponding density spectrum ( $\Delta = \frac{V}{0.4e}$ ). Using the "INTEGRAL PROGRAM" given in appendix A the overall integral rate obtained in all six runs was found and the results are given in Table 4.7. The idea of that program is to assume a minimum density level ( $\Delta$ ) as recorded by the two recorded densities A and B or as recorded by A and B separately and count the number of events with values equal or greater than that of the required level $N(\geqslant\Delta)$. The program can also be arranged to count the number of events with values less than that of a required level $N(<\Delta)$. Because of the saturation point which happened on the stretcher amplifier reading(Figures 4.9 a,b), the maximum value of ($\Delta$) measured was $\Delta = 335 \text{ m}^{-2}$ corresponding to the maximum cosmic ray pulse height which can be measured using that graph as a calibration curve.

| Threshold density $\Delta$ ($m^{-2}$) | Taking the minimum density of the two densities recorded by A & B | | Density recorded by A only | | Density recorded by B only | | Taking the sum of all densities as recorded by A & B separately | |
|---|---|---|---|---|---|---|---|---|
| | No. of events | $R(\geq\Delta)_1$ $hr^{-1}$ | No. of events | $R(\geq\Delta)_1$ $hr^{-1}$ | No. of events | $R(\geq\Delta)_2$ $hr^{-1}$ | No. of densities | $R(\geq\Delta)_3$ $hr^{-1}$ |
| 27.5 | 1184 | 6.80 ± 0.20 | 1184 | 6.83 ± 0.20 | 1184 | 6.83 ± 0.20 | 2368 | 6.83 ± 0.20 |
| 30.0 | 1023 | 5.90 ± 0.18 | 1104 | 6.37 ± 0.19 | 1092 | 6.30 ± 0.20 | 2196 | 6.33 ± 0.19 |
| 35.0 | 804 | 4.64 ± 0.16 | 940 | 5.42 ± 0.18 | 973 | 5.61 ± 0.18 | 2032 | 5.52 ± 0.18 |
| 40.0 | 686 | 3.95 ± 0.15 | 857 | 4.94 ± 0.17 | 869 | 5.01 ± 0.18 | 1726 | 5.00 ± 0.17 |
| 45.0 | 596 | 3.44 ± 0.14 | 802 | 4.63 ± 0.16 | 748 | 4.32 ± 0.16 | 1550 | 4.47 ± 0.16 |
| 50.0 | 511 | 2.95 ± 0.13 | 722 | 4.17 ± 0.16 | 653 | 3.77 ± 0.15 | 1375 | 4.00 ± 0.15 |
| 55.0 | 432 | 2.49 ± 0.12 | 658 | 3.80 ± 0.15 | 578 | 3.33 ± 0.14 | 1236 | 3.57 ± 0.14 |
| 60.0 | 374 | 2.16 ± 0.11 | 587 | 3.39 ± 0.14 | 512 | 2.95 ± 0.13 | 1099 | 3.17 ± 0.14 |
| 70.0 | 294 | 1.70 ± 0.10 | 489 | 2.82 ± 0.13 | 403 | 2.32 ± 0.11 | 892 | 2.57 ± 0.12 |
| 80.0 | 242 | 1.40 ± 0.09 | 418 | 2.41 ± 0.12 | 332 | 1.92 ± 0.11 | 750 | 2.16 ± 0.11 |
| 90.0 | 193 | 1.11 ± 0.08 | 359 | 2.07 ± 0.11 | 271 | 1.56 ± 0.10 | 630 | 1.82 ± 0.10 |
| 100.0 | 166 | 0.96 ± 0.07 | 312 | 1.80 ± 0.10 | 230 | 1.33 ± 0.09 | 542 | 1.56 ± 0.10 |
| 120.0 | 126 | 0.73 ± 0.06 | 246 | 1.42 ± 0.09 | 160 | 0.92 ± 0.07 | 406 | 1.17 ± 0.08 |
| 140.0 | 90 | 0.52 ± 0.05 | 201 | 1.16 ± 0.08 | 117 | 0.67 ± 0.06 | 318 | 0.92 ± 0.07 |
| 160.0 | 66 | 0.38 ± 0.05 | 171 | 0.99 ± 0.08 | 77 | 0.44 ± 0.05 | 248 | 0.72 ± 0.06 |
| 180.0 | 50 | 0.29 ± 0.04 | 149 | 0.86 ± 0.07 | 59 | 0.34 ± 0.04 | 208 | 0.60 ± 0.06 |
| 200.0 | 41 | 0.24 ± 0.04 | 129 | 0.74 ± 0.07 | 51 | 0.29 ± 0.04 | 180 | 0.52 ± 0.06 |
| 220.0 | 29 | 0.20 ± 0.03 | 108 | 0.62 ± 0.06 | 39 | 0.22 ± 0.04 | 147 | 0.42 ± 0.05 |
| 240.0 | 25 | 0.17 ± 0.03 | 92 | 0.53 ± 0.06 | 33 | 0.19 ± 0.03 | 125 | 0.36 ± 0.05 |
| 260.0 | 24 | 0.15 ± 0.03 | 85 | 0.49 ± 0.05 | 28 | 0.16 ± 0.03 | 113 | 0.33 ± 0.04 |
| 280.0 | 22 | 0.13 ± 0.03 | 79 | 0.46 ± 0.05 | 25 | 0.14 ± 0.03 | 104 | 0.30 ± 0.04 |
| 300.0 | 20 | 0.12 ± 0.03 | 71 | 0.41 ± 0.05 | 23 | 0.13 ± 0.03 | 94 | 0.27 ± 0.04 |
| 335.0 | 17 | 0.10 ± 0.024 | 58 | 0.33 ± 0.04 | 21 | 0.12 ± 0.03 | 79 | 0.23 ± 0.04 |

Table 4.7 : Measurement of the integral density spectrum by using the microcomputer data acquisition system.

Taking the minimum density of the two recorded densities the integral density spectrum over the range $27.5 \leqslant \Delta \leqslant 335$ m$^{-2}$ at sea level has been measured and the result is given in Figure 4.14a compared with the results given by Greisen (1960) and Ashton et al. (1975). The measured integral spectrum has the form :

$$R( \geqslant \Delta) = 2483 \Delta^{-(1.74 \pm 0.02)} hr.^{-1}$$

where $\Delta$ is in terms of electrons m$^{-2}$. The measured slope was found to be -1.74, which is consistent with the result obtained previously using discriminators and a scaler.

The integral density spectrum over the range $2.7 \leqslant \Delta \leqslant 36$ m$^{-2}$ measured by direct counting using discriminators, the two fold coincidence plus a scaler, and that measured over the range $27.5 \leqslant \Delta \leqslant 335$ m$^{-2}$ using the microcomputer data acquisition system are shown in Figure 4.14b where the measurements are compared with the result given by Greisen (1960). The measured density spectrum has the form:
$R( \geqslant \Delta ) = 2216 \Delta^{-(1.71 \pm 0.01)} hr.^{-1}$ in the range $2.7 \leqslant \Delta \leqslant 335$ m$^{-2}$ where $\Delta$ is in terms of electrons m$^{-2}$. The measured slope was found -1.71 in that range,

Figure 4.14C shows the grand summary graph of the integral density spectrum for scintillators A and B measured separately and the integral density spectrum from coincidence measurements using discriminators plus a scaler and also that measured by using the microcomputer data acquisition system.

Greisen (1960) gives the following expression for the integral density spectrum of electrons at sea level in the range $1 < \Delta < 10^4$ m$^{-2}$

$$R( > \Delta ) = 540 \Delta^{-(1.3 + 0.055 Log_{10} \Delta)} hr.^{-1}$$
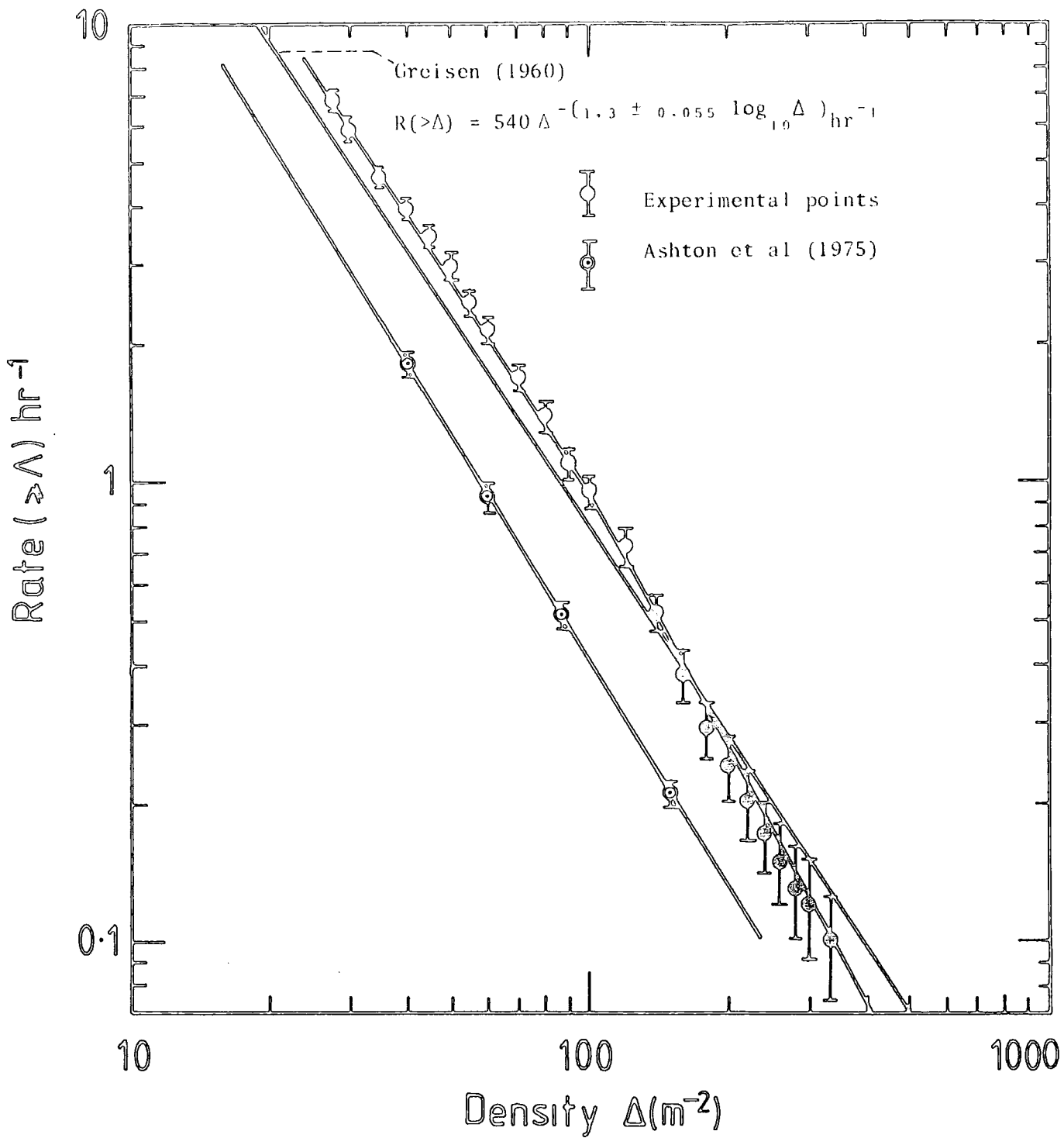
Figure 4.14a : The integral density spectrum of electrons at sea
level measured by using a microcomputer data acquisition
system compared with the results given by Greisen (1960)
and Ashton et al (1975).
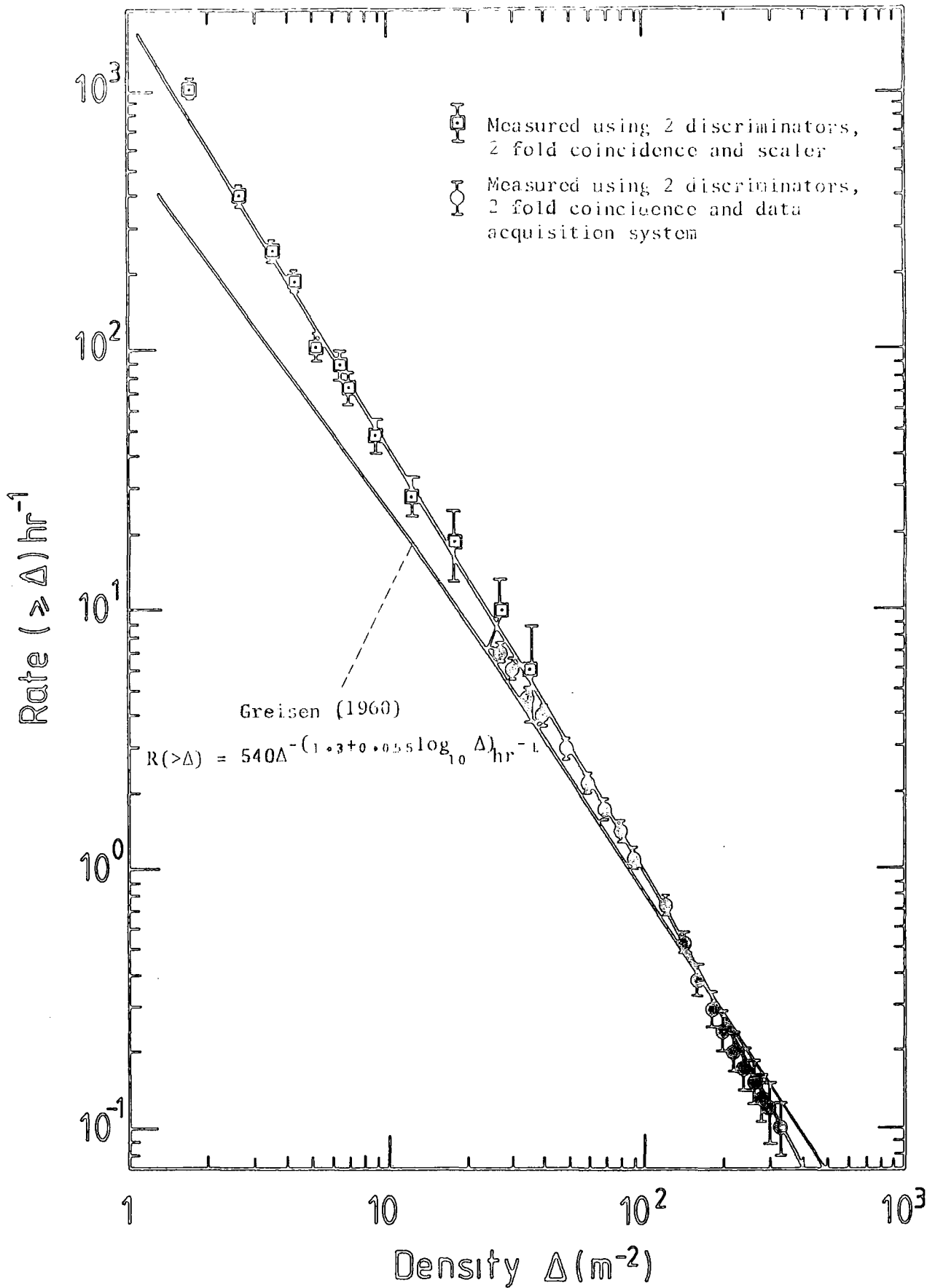
Figure 4.14b : The integral density spectrum of electrons at sea level as measured by using discriminators and scaler and by using a microcomputer data acquisition system all together compared with the result given by Greisen (1960).
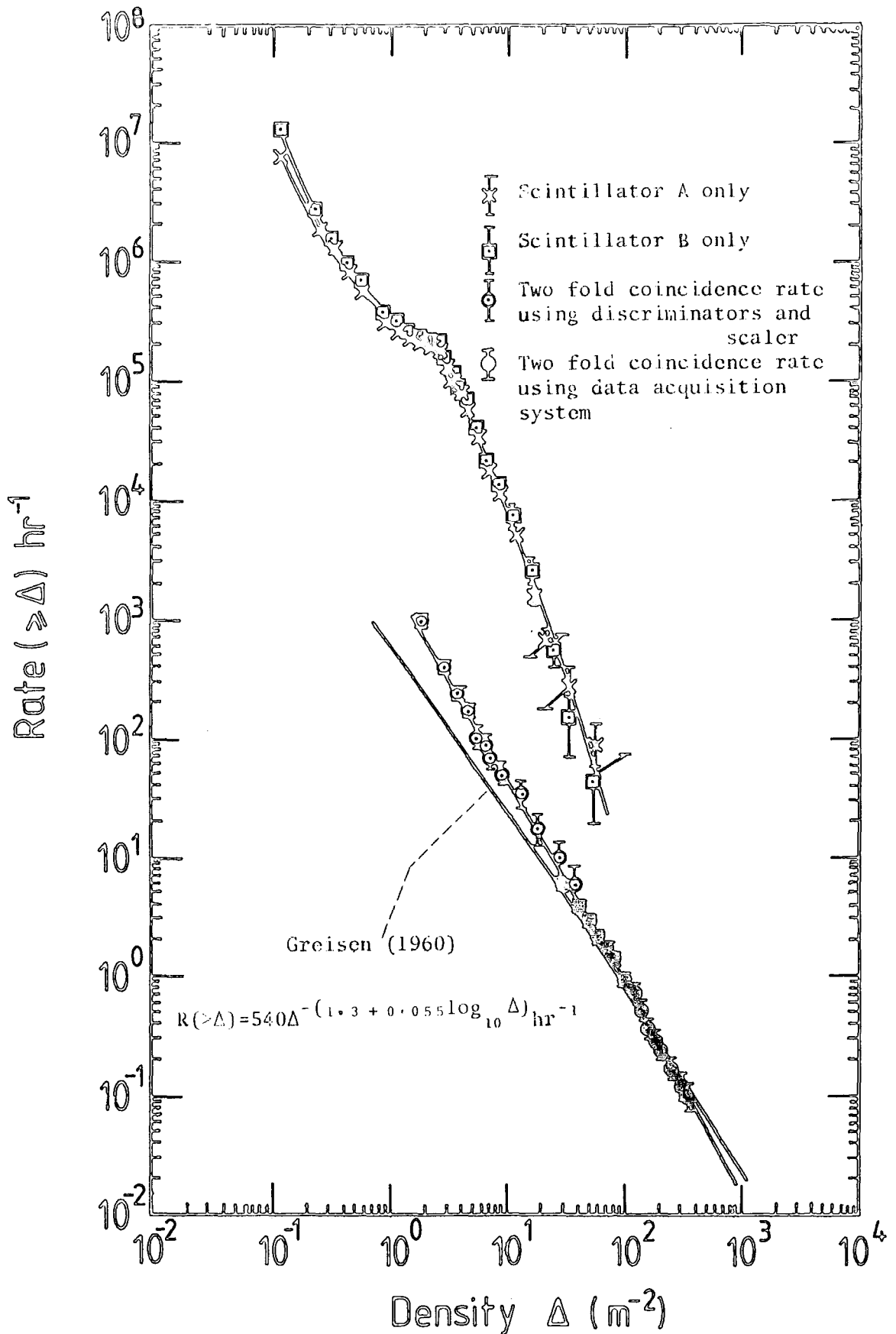
Figure 4.14c : Grand graph of the integral rate of density R(>Δ) measured
at the output of the head units of scintillators A and B as
a function of the threshold density Δ. Also shown is the
integral density spectrum of electrons at sea level measured
by using discriminators and scaler and by using a
microcomputer data acquisition system.

This suggests a gradual change in the slope of the density spectrum starting from slope $= -1.3$ at $\Delta = 1 \text{ m}^{-2}$ to slope $= -1.46$ at $\Delta = 1,000 \text{ m}^{-2}$. It can be seen that the rate observed in the present experiment at low densities is higher than the rate expected, but this is within, probably a factor of normalisation.

The integral density spectrum in the range $27.5 \leqslant \Delta \leqslant 335 \text{ m}^{-2}$ measured by taking the densities as recorded by A and B separately and by taking the minimum density of the two recorded densities are given in Figure 4.14d and are compared with the result given by Greisen (1960). Figure 4.14e shows a comparison of the measured integral density spectrum calculated by taking the sum of all densities as recorded by A and B separately and by taking the minimum density of the two recorded densities with the result given by Greisen (1960).

Measurement of $R(<\Delta)$ as distinct from $R(>\Delta)$ in the range $27.5 < \Delta < 335 \text{ m}^{-2}$ by taking the densities as recorded by A and B separately and by taking the maximum density of the two recorded densities are given in Table 4.8. The results of such a study are shown in Figure 4.15.

The experimental data of the differential density spectrum at high densities measured by using the microcomputer data acquisition system is given in Table 4.9. The data obtained by differentiating the experimental results is given in Table 4.7. Figure 4.16a shows the differential density spectrum compared with the result given by Greisen (1960). The minimum of the two recorded densities was used in the evaluation.

The differential density spectrum has the form

$$R(\Delta)d\Delta = 1590 \, \Delta^{-(2.54 \pm 0.15)} \, d\Delta \ \text{hr}^{-1} .$$
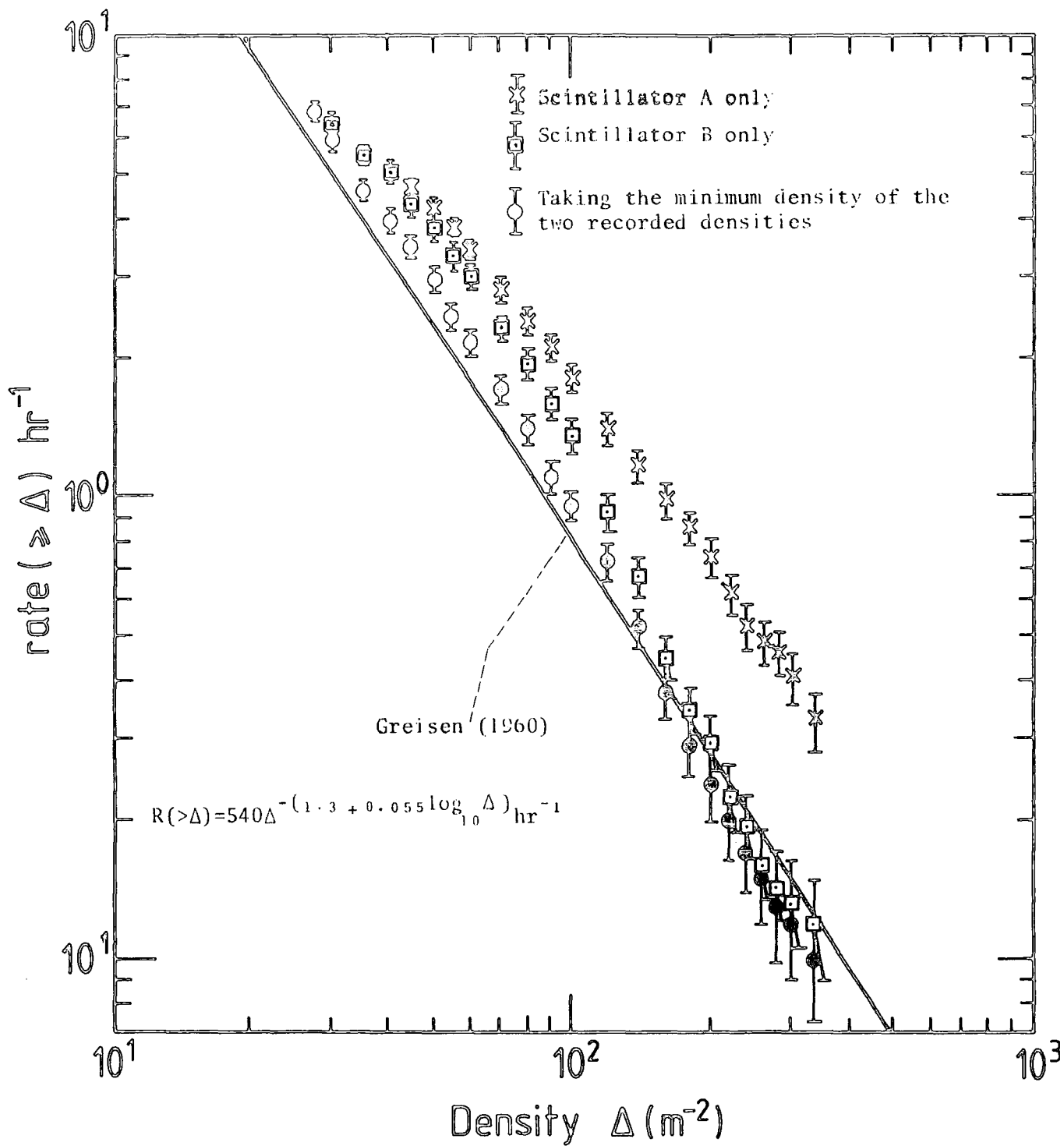
Figure 4.14d : Measurement of the integral density spectrum of electrons
at sea level by taking the densities as recorded by A and B
separately and by taking the minimum density of the two
recorded densities.
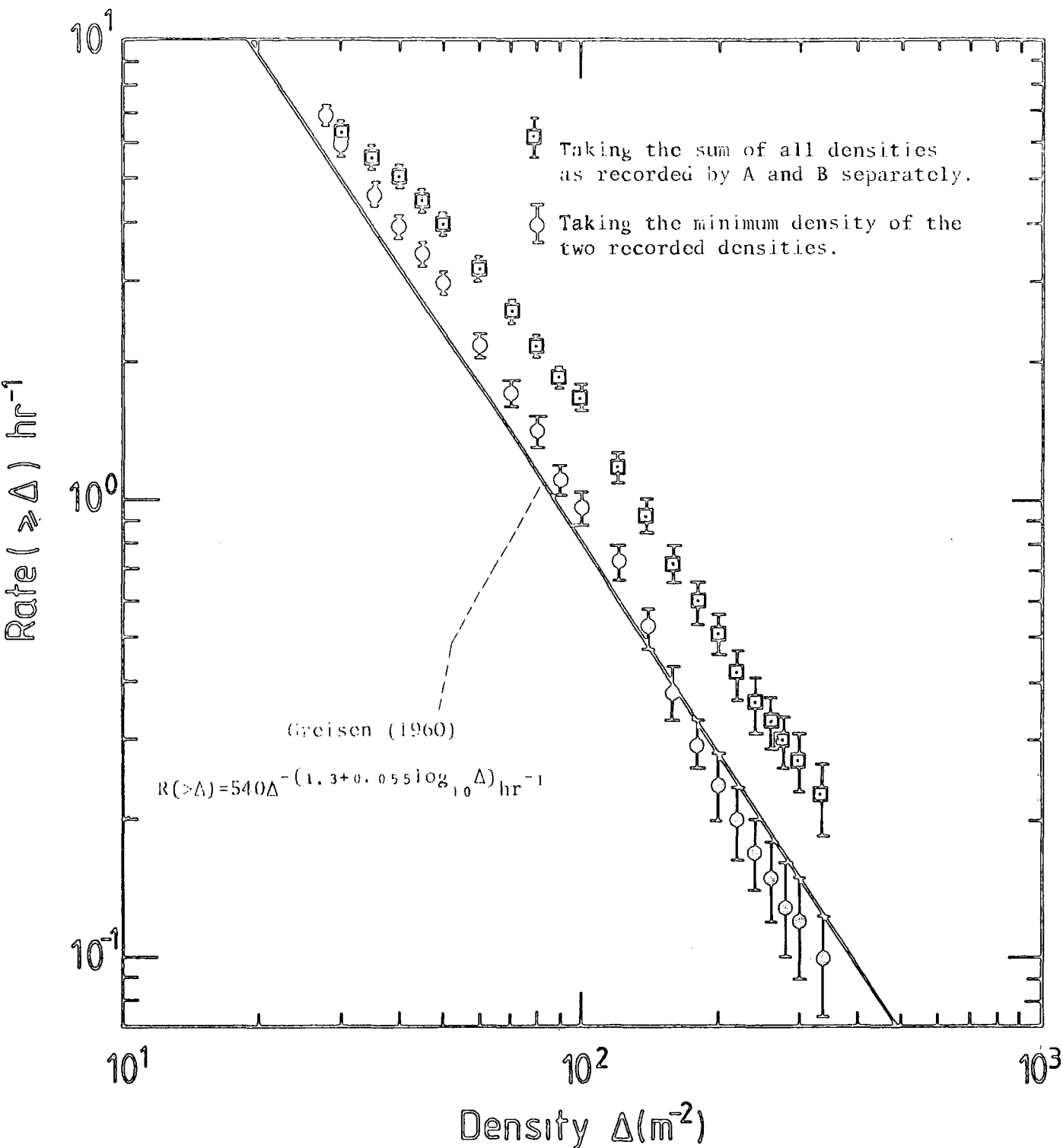
Figure 4.14e : Comparison of R(≥Δ) calculated by taking the sum of all densities as recorded by A and B separately and by taking the minimum density of the two recorded densities with the result given by Greisen (1960).

| Threshold density ($\Delta$) $m^{-2}$ | Taking the maximum density of the two recorded densities | | Density recorded by A only | | Density recorded by B only | |
|---|---|---|---|---|---|---|
| | No. of events | $R(<\underline{\Delta})$ $hr^{-1}$ | No. of events | $R(<\underline{\Delta})$ $hr^{-1}$ | No. of events | $R(<\underline{\Delta})$ $hr^{-1}$ |
| 27.5 | 0 | 0 | 0 | 0 | 0 | 0 |
| 30.0 | 11 | 0.06±0.02 | 80 | 0.46±0.05 | 92 | 0.53±0.06 |
| 35.0 | 75 | 0.43±0.05 | 244 | 1.40±0.09 | 211 | 1.22±0.08 |
| 40.0 | 144 | 0.83±0.07 | 327 | 1.89±0.10 | 315 | 1.82±0.10 |
| 45.0 | 230 | 1.33±0.08 | 382 | 2.20±0.11 | 436 | 2.52±0.12 |
| 50.0 | 320 | 1.85±0.10 | 462 | 2.67±0.12 | 531 | 3.06±0.13 |
| 55.0 | 380 | 2.19±0.11 | 526 | 3.03±0.13 | 606 | 3.50±0.14 |
| 60.0 | 459 | 2.65±0.12 | 597 | 3.44±0.14 | 672 | 3.88±0.15 |
| 70.0 | 586 | 3.38±0.14 | 695 | 3.77±0.15 | 781 | 4.51±0.16 |
| 80.0 | 676 | 3.90±0.15 | 766 | 3.95±0.15 | 852 | 4.92±0.17 |
| 90.0 | 747 | 4.31±0.16 | 825 | 4.42±0.16 | 913 | 5.27±0.17 |
| 100.0 | 808 | 4.66±0.16 | 872 | 4.76±0.17 | 954 | 5.50±0.18 |
| 120.0 | 904 | 5.22±0.17 | 938 | 5.03±0.17 | 1024 | 5.91±0.18 |
| 140.0 | 956 | 5.52±0.18 | 983 | 5.41±0.18 | 1067 | 6.16±0.19 |
| 160.0 | 1002 | 5.78±0.18 | 1013 | 5.67±0.18 | 1107 | 6.39±0.19 |
| 180.0 | 1026 | 5.92±0.18 | 1035 | 5.84±0.18 | 1125 | 6.49±0.19 |
| 200.0 | 1045 | 6.03±0.19 | 1055 | 5.97±0.19 | 1133 | 6.54±0.19 |
| 220.0 | 1066 | 6.15±0.19 | 1076 | 6.09±0.19 | 1145 | 6.61±0.20 |
| 240.0 | 1084 | 6.25±0.19 | 1092 | 6.21±0.19 | 1151 | 6.64±0.20 |
| 260.0 | 1095 | 6.32±0.19 | 1099 | 6.30±0.19 | 1156 | 6.67±0.20 |
| 280.0 | 1102 | 6.36±0.19 | 1105 | 6.34±0.19 | 1159 | 6.69±0.20 |
| 300.0 | 1110 | 6.40±0.19 | 1113 | 6.42±0.19 | 1161 | 6.70±0.20 |

Table 4.8 : Measurement of the integral density spectrum by taking the densities as recorded by A and B separately and by taking the maximum density of the two recorded densities.

Figure 4.15 : Measurement of the integral density spectrum of electrons
at sea level measured by taking the densities as recorded
by A and B separately and by taking the maximum density
of the two recorded densities.
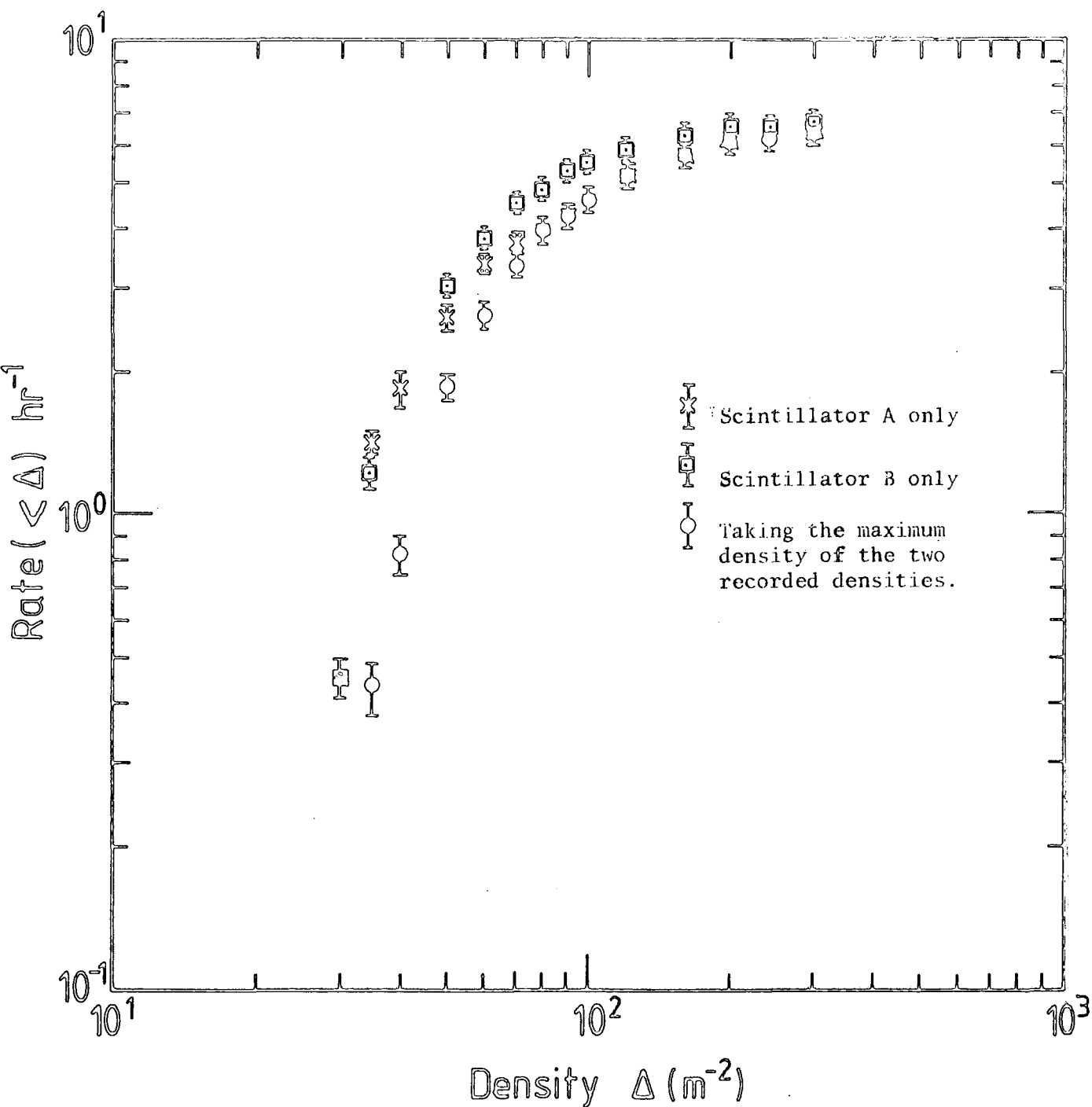
| Density range (m$^{-2}$) $\Delta_1 \to \Delta_2$ | Mean of density range (m$^{-2}$) | Width $\Delta_2 \to \Delta_1$ (m$^{-2}$) | No. of events in density range ($\Delta_1 \to \Delta_2$) | | | Rate of events in density range R($\Delta_1 \to \Delta_2$) hr$^{-1}$ | | | Differential rate at $\Delta$ R($\Delta_1 \to \Delta_2$) hr$^{-1}$m$^{-2}$ | | |
|---|---|---|---|---|---|---|---|---|---|---|---|
| | | | Taking the min.den. of the two recorded densities | Density recorded by A only | Density recorded by B only | A and B | A only | B only | A and B | A only | B only |
| 27.5-30 | 28.75 | 2.5 | 161 | 80 | 92 | $(9.3\pm0.73)10^{-1}$ | $(4.62\pm0.52)10^{-1}$ | $(5.31\pm0.55)10^{-1}$ | $(3.72\pm0.29)10^{-1}$ | $(1.85\pm0.20)10^{-1}$ | $(2.12\pm0.22)10^{-1}$ |
| 30-35 | 32.5 | 5.0 | 219 | 164 | 119 | $(12.6\pm0.90)10^{-1}$ | $(9.46\pm0.34)10^{-1}$ | $(6.87\pm0.63)10^{-1}$ | $(2.53\pm0.17)10^{-1}$ | $(1.89\pm0.15)10^{-1}$ | $(1.34\pm0.13)10^{-1}$ |
| 35-40 | 37.5 | 5.0 | 118 | 83 | 104 | $(6.8\pm0.6)10^{-1}$ | $(4.79\pm0.52)10^{-1}$ | $(6.00\pm0.59)10^{-1}$ | $(1.36\pm0.13)10^{-1}$ | $(9.60\pm1.00)10^{-2}$ | $(1.20\pm0.12)10^{-1}$ |
| 40-45 | 42.5 | 5.0 | 90 | 55 | 121 | $(5.2\pm0.55)10^{-1}$ | $(3.17\pm0.43)10^{-1}$ | $(6.98\pm0.63)10^{-1}$ | $(1.04\pm0.11)10^{-1}$ | $(6.30\pm0.90)10^{-2}$ | $(1.40\pm0.10)10^{-1}$ |
| 45-50 | 47.5 | 5.0 | 85 | 80 | 95 | $(4.9\pm0.53)10^{-1}$ | $(4.61\pm0.53)10^{-1}$ | $(5.48\pm0.56)10^{-1}$ | $(9.80\pm1.10)10^{-2}$ | $(9.20\pm1.10)10^{-2}$ | $(1.10\pm0.11)10^{-1}$ |
| 50-55 | 52.5 | 5.0 | 79 | 64 | 75 | $(4.6\pm0.51)10^{-1}$ | $(3.69\pm0.46)10^{-1}$ | $(4.33\pm0.50)10^{-1}$ | $(9.10\pm1.00)10^{-2}$ | $(7.40\pm0.90)10^{-2}$ | $(8.70\pm1.00)10^{-2}$ |
| 55-60 | 57.5 | 5.0 | 58 | 71 | 66 | $(3.3\pm0.44)10^{-1}$ | $(4.00\pm0.49)10^{-1}$ | $(3.81\pm0.47)10^{-1}$ | $(6.70\pm0.90)10^{-2}$ | $(8.20\pm1.00)10^{-2}$ | $(7.60\pm0.90)10^{-2}$ |
| 60-70 | 65.0 | 10 | 80 | 98 | 109 | $(4.6\pm0.52)10^{-1}$ | $(5.65\pm0.57)10^{-1}$ | $(6.29\pm0.60)10^{-1}$ | $(4.60\pm0.52)10^{-2}$ | $(5.65\pm0.57)10^{-2}$ | $(6.29\pm0.60)10^{-2}$ |
| 70-80 | 75.0 | 10 | 52 | 71 | 71 | $(3.0\pm0.42)10^{-1}$ | $(4.10\pm0.50)10^{-1}$ | $(4.10\pm0.50)10^{-1}$ | $(3.00\pm0.42)10^{-2}$ | $(4.10\pm0.50)10^{-2}$ | $(4.10\pm0.50)10^{-2}$ |
| 80-90 | 85.0 | 10 | 49 | 59 | 61 | $(2.8\pm0.40)10^{-1}$ | $(3.40\pm0.44)10^{-1}$ | $(3.52\pm0.45)10^{-1}$ | $(2.80\pm0.40)10^{-2}$ | $(3.40\pm0.44)10^{-2}$ | $(3.50\pm0.45)10^{-2}$ |
| 90-100 | 95.0 | 10 | 27 | 47 | 41 | $(1.60\pm0.30)10^{-1}$ | $(2.70\pm0.40)10^{-1}$ | $(2.40\pm0.40)10^{-1}$ | $(1.60\pm0.30)10^{-2}$ | $(2.70\pm0.40)10^{-2}$ | $(2.40\pm0.40)10^{-2}$ |
| 100-120 | 110 | 20 | 40 | 66 | 70 | $(2.30\pm0.36)10^{-1}$ | $(3.80\pm0.47)10^{-1}$ | $(4.00\pm0.48)10^{-1}$ | $(1.10\pm0.13)10^{-2}$ | $(2.00\pm0.18)10^{-2}$ | $(2.00\pm0.24)10^{-2}$ |
| 120-140 | 130 | 20 | 36 | 45 | 43 | $(2.10\pm0.30)10^{-1}$ | $(2.60\pm0.39)10^{-1}$ | $(2.50\pm0.38)10^{-1}$ | $(1.00\pm0.15)10^{-2}$ | $(1.28\pm0.19)10^{-2}$ | $(1.24\pm0.19)10^{-2}$ |
| 140-160 | 150 | 20 | 24 | 30 | 40 | $(1.38\pm0.28)10^{-1}$ | $(1.70\pm0.32)10^{-1}$ | $(2.30\pm0.36)10^{-1}$ | $(7.00\pm1.40)10^{-3}$ | $(8.60\pm1.60)10^{-3}$ | $(1.15\pm0.18)10^{-2}$ |
| 160-180 | 170 | 20 | 16 | 22 | 18 | $(9.20\pm2.30)10^{-2}$ | $(1.27\pm0.27)10^{-1}$ | $(1.04\pm0.24)10^{-1}$ | $(4.60\pm1.20)10^{-3}$ | $(6.00\pm1.40)10^{-3}$ | $(5.20\pm1.20)10^{-3}$ |
| 180-200 | 190 | 20 | 9 | 20 | 8 | $(5.20\pm1.70)10^{-2}$ | $(1.15\pm0.26)10^{-1}$ | $(4.60\pm1.60)10^{-2}$ | $(2.60\pm0.90)10^{-3}$ | $(5.70\pm1.30)10^{-3}$ | $(2.30\pm0.80)10^{-3}$ |
| 200-220 | 210 | 20 | 12 | 21 | 12 | $(6.90\pm2.00)10^{-2}$ | $(1.20\pm0.26)10^{-1}$ | $(9.90\pm2.00)10^{-2}$ | $(3.40\pm1.00)10^{-3}$ | $(6.00\pm1.30)10^{-3}$ | $(3.50\pm1.00)10^{-3}$ |
| 220-240 | 230 | 20 | 4 | 16 | 6 | $(2.30\pm1.00)10^{-2}$ | $(9.00\pm2.30)10^{-2}$ | $(3.46\pm1.40)10^{-2}$ | $(1.15\pm0.58)10^{-3}$ | $(4.60\pm1.15)10^{-3}$ | $(1.70\pm0.70)10^{-3}$ |
| 240-260 | 250 | 20 | 1 | 7 | 5 | $(5.70\pm6.00)10^{-3}$ | $(4.00\pm1.50)10^{-2}$ | $(2.90\pm1.30)10^{-2}$ | $(3.00\pm2.80)10^{-4}$ | $(2.00\pm0.80)10^{-3}$ | $(1.00\pm0.60)10^{-3}$ |
| 260-280 | 270 | 20 | 2 | 6 | 3 | $(1.15\pm0.80)10^{-2}$ | $(3.46\pm1.40)10^{-2}$ | $(1.70\pm1.00)10^{-2}$ | $(6.00\pm4.10)10^{-4}$ | $(2.00\pm0.70)10^{-3}$ | $(9.00\pm5.00)10^{-4}$ |
| 280-300 | 290 | 20 | 2 | 8 | 2 | $(1.15\pm0.80)10^{-2}$ | $(4.60\pm1.60)10^{-2}$ | $(1.15\pm0.80)10^{-2}$ | $(6.00\pm4.00)10^{-4}$ | $(2.30\pm0.60)10^{-3}$ | $(6.00\pm4.00)10^{-4}$ |
| 300-335 | 317.5 | 35 | 3 | 13 | 2 | $(1.70\pm0.01)10^{-2}$ | $(7.50\pm2.00)10^{-2}$ | $(1.15\pm0.80)10^{-2}$ | $(5.00\pm3.00)10^{-4}$ | $(2.00\pm0.60)10^{-3}$ | $(3.00\pm2.00)10^{-4}$ |
| > 335 | | | 17 | 58 | 21 | | | | | | |

<u>Table 4.9</u> : Measurement of the differential density spectrum by using the microcomputer data acquisition system.

Figure 4.16a : The differential density spectrum of electrons at
sea level measured by using a microcomputer data
acquisition system compared with the result given by
Greisen (1960). The minimum density of the two
recorded densities was used in the evaluation.

This result indicates that the observed differential density spectrum of EAS at sea level has a slope of -2.54 in the density range $27.5 \leqslant \Delta \leqslant 335$ m$^{-2}$.

Greisen (1960) gives the following expression for the differential density spectrum

$$R(\Delta)d\Delta = 540\Delta^{-(2.3 + 0.055 \, Log_{10}\Delta)}\{1.3 + 0.11 \, Log_{10}\Delta\} \, d\Delta \, hr^{-1}.$$

[This was found by differentiating of the form for the integral density spectrum given by Greisen (1960) which is given above]

It was found that the best fit through the experimental points in Figure 4.16a had a slope of -2.54 which is quite consistent with the result given by Greisen (1960).

Measurement of the differential density spectrum by taking the densities as recorded by A and B separately and by taking the minimum density of the two recorded densities are given in Figure 4.16b compared with the result given by Greisen (1960).

Table 4.10 gives example of some data print out from the data acquisition system in terms of pulse height (mV) which was used above to determine the density spectrum of electrons at sea level in the range $27.5 \leqslant \Delta \leqslant 335$ electrons m$^{-2}$.

## 4.8   CONCLUSION

Two scintillation counters A and B each of area 0.4 m$^2$ and 5 cm thick were used in the present experiment to measure the local electron density spectrum of extensive air shower over the range $2 < \Delta < 335$ electrons m$^{-2}$. The detailed discussions are already given in each section. Therefore, the main conclusions will be described as follows.
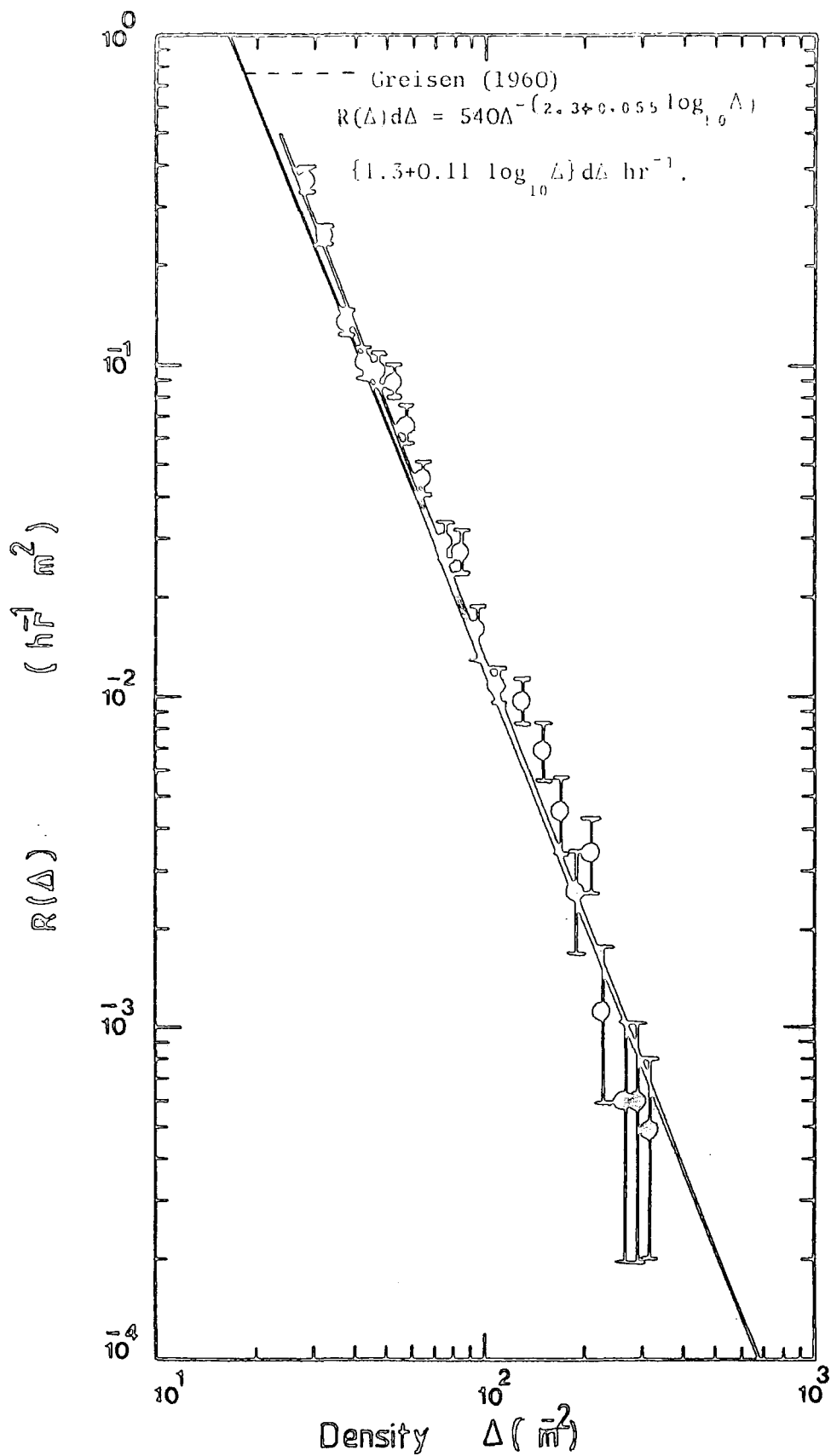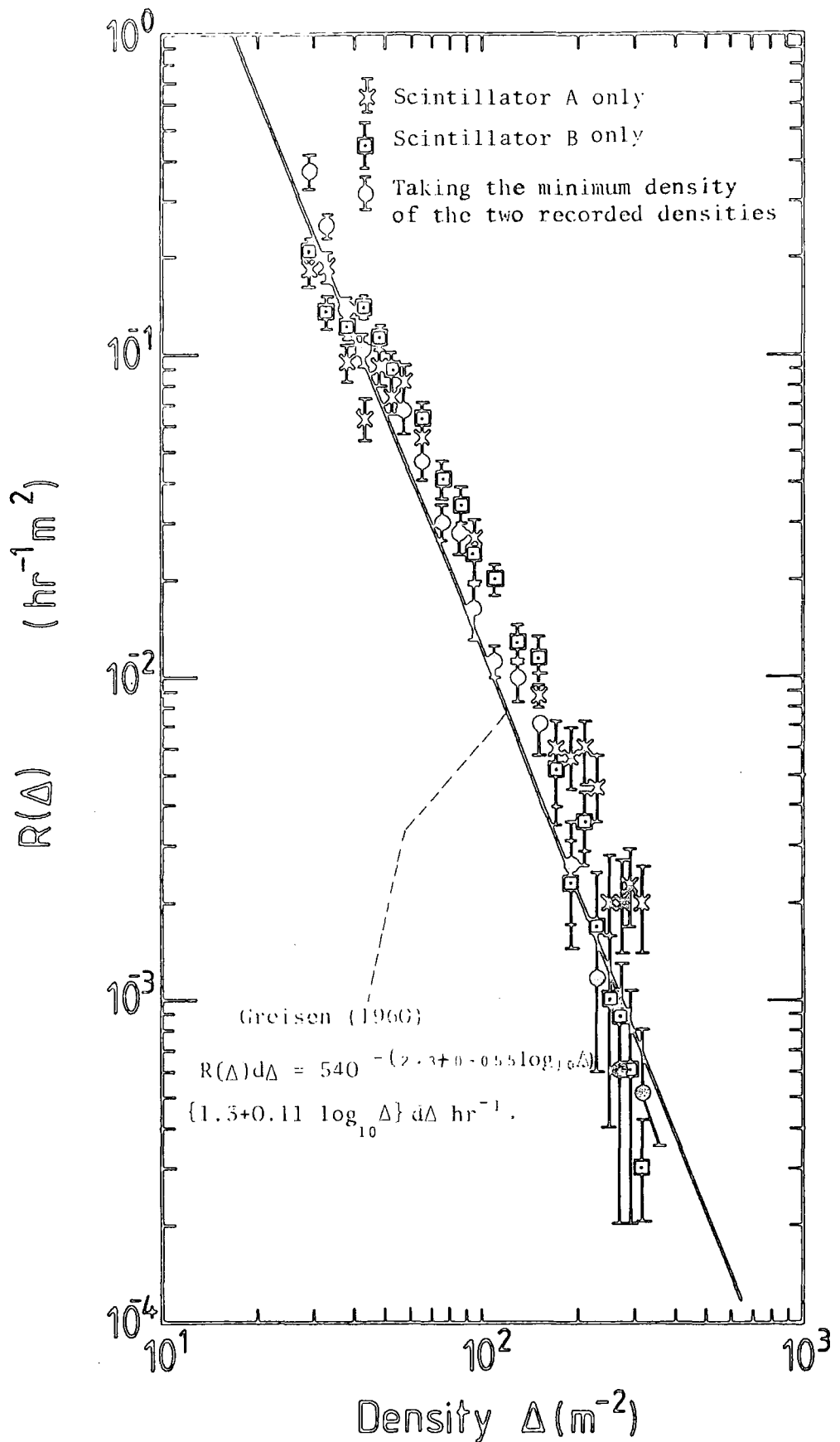
Figure 4.16b : Measurement of the differential density spectrum of electrons at sea level by using a microcomputer data acquisition system compared with the result given by Greisen (1960). The densities recorded by A and B separately and the minimum density of the two recorded densities were used in the evaluation.

| Time | Pulse height (mV) A | Pulse height (mV) B | Not used | Trigger Pulse height(mV) | Not used | Not used | Stability check | Stability check |
|---|---|---|---|---|---|---|---|---|
| 08.31.23 *8* | -560 | -605 | 0 | -3850 | 0 | 5 | 9435 | 10240 |
| 08.36.11 *8* | -1850 | -1000 | 0 | -3745 | 0 | 5 | 9440 | 10240 |
| 09.14.46 *8* | -3750 | -2445 | 0 | -3760 | 0 | 5 | 9435 | 10240 |
| 09.21.31 *8* | -505 | -395 | 10 | -3065 | 0 | 5 | 9435 | 10240 |
| 10.13.22 *8* | -3575 | -2515 | 0 | -3740 | 0 | 5 | 9435 | 10240 |
| 10.15.42 *8* | -1135 | -840 | 0 | -3815 | 0 | 5 | 9435 | 10240 |
| 10.18.14 *8* | -2205 | -1440 | 0 | -3745 | 0 | 5 | 9435 | 10240 |
| 10.34.24 *8* | -1390 | -1035 | 5 | -3745 | 0 | 5 | 9435 | 10240 |
| 10.39.37 *8* | -1040 | -2250 | 0 | -3745 | 0 | 5 | 9435 | 10240 |
| 10.40.07 *8* | -3860 | -380 | 5 | -2960 | 0 | 5 | 9435 | 10240 |
| 11.02.12 *8* | -470 | -495 | 0 | -2680 | 0 | 5 | 9435 | 10240 |
| 11.05.05 *8* | -290 | -750 | 5 | -2335 | 0 | 5 | 9435 | 10240 |
| 11.06.45 *8* | -460 | -390 | 5 | -2210 | 0 | 5 | 9435 | 10240 |
| 11.07.14 *8* | -2360 | -1345 | 0 | -3740 | 0 | 5 | 9440 | 10240 |
| 11.12.26 *8* | -810 | -950 | 0 | -3755 | 0 | 5 | 9435 | 10240 |
| 11.15.54 *8* | -250 | -705 | 0 | -2165 | 0 | 5 | 9435 | 10240 |
| 11.16.14 *8* | -2120 | -2365 | 0 | -3760 | 0 | 5 | 9440 | 10240 |
| 11.24.10 *8* | -350 | -375 | 5 | -1795 | 0 | 5 | 9430 | 10240 |
| 11.32.52 *8* | -595 | -1020 | 0 | -3620 | 0 | 5 | 9435 | 10240 |
| 11.36.27 *8* | -2700 | -2245 | 0 | -3745 | 0 | 5 | 9430 | 10240 |
| 12.04.00 *8* | -335 | -660 | 10 | -2170 | 0 | 5 | 9430 | 10240 |
| 12.17.47 *8* | -400 | -520 | 0 | -2420 | 0 | 5 | 9435 | 10240 |
| 12.23.10 *8* | -2390 | -2760 | 0 | -3750 | 0 | 5 | 9430 | 10240 |
| 12.24.23 *8* | -235 | -475 | 0 | -1740 | 0 | 5 | 9435 | 10240 |
| 12.27.55 *8* | -1620 | -2105 | 10 | -3740 | 0 | 5 | 9435 | 10240 |
| 12.37.07 *8* | -970 | -660 | 0 | -3420 | 0 | 5 | 9430 | 10240 |
| 12.39.05 *8* | -3740 | -630 | 0 | -3410 | 0 | 5 | 9430 | 10240 |
| 13.01.07 *8* | -635 | -1520 | 10 | -3840 | 0 | 5 | 9430 | 10240 |
| 13.02.14 *8* | -475 | -1765 | 0 | -2750 | 0 | 5 | 9430 | 10240 |
| 13.10.48 *8* | -340 | -535 | 5 | -2090 | 0 | 5 | 9430 | 10240 |
| 13.14.26 *8* | -325 | -1480 | 5 | -2290 | 0 | 5 | 9430 | 10240 |
| 13.23.14 *8* | -1920 | -820 | 5 | -3830 | 0 | 5 | 9430 | 10240 |
| 13.34.15 *8* | -610 | -790 | 5 | -3150 | 0 | 5 | 9430 | 10240 |
| 13.36.21 *8* | -1405 | -1605 | 0 | -3750 | 0 | 5 | 9430 | 10240 |
| 13.47.17 *8* | -7460 | -610 | 0 | -2740 | 0 | 5 | 9430 | 10240 |
| 13.53.10 *8* | -675 | -1015 | 0 | -3850 | 0 | 5 | 9430 | 10240 |
| 13.59.00 *8* | -760 | -2350 | 5 | -3760 | 0 | 5 | 9430 | 10240 |
| 14.00.05 *8* | -1965 | -1810 | 5 | -3750 | 0 | 5 | 9430 | 10240 |
| 14.03.49 *8* | -255 | -530 | 5 | -1870 | 0 | 5 | 9430 | 10240 |
| 14.06.03 *8* | -665 | -560 | 10 | -3055 | 0 | 5 | 9430 | 10240 |
| 14.09.52 *8* | -245 | -930 | 0 | -2035 | 0 | 5 | 9430 | 10240 |
| 14.19.35 *8* | -3180 | -5710 | 5 | -3745 | 0 | 5 | 9425 | 10240 |
| 14.23.12 *8* | -1370 | -2015 | 0 | -3740 | 0 | 5 | 9425 | 10240 |
| 14.24.13 *8* | -2570 | -1525 | 0 | -3745 | 0 | 5 | 9430 | 10240 |
| 14.35.03 *8* | -1295 | -660 | 0 | -3395 | 0 | 5 | 9430 | 10240 |
| 14.53.48 *8* | -825 | -580 | 0 | -3100 | 0 | 5 | 9430 | 10240 |
| 14.57.31 *8* | -280 | -475 | 5 | -1865 | 0 | 5 | 9430 | 10240 |
| 15.01.33 *8* | -225 | -525 | 5 | -1830 | 0 | 5 | 9430 | 10240 |
| 15.14.46 *8* | -4115 | -670 | 0 | -3475 | 0 | 5 | 9430 | 10240 |
| 15.19.00 *8* | -1135 | -2610 | 5 | -3740 | 0 | 5 | 9430 | 10240 |
| 15.24.36 *8* | -1860 | -1705 | 0 | -3750 | 0 | 5 | 9430 | 10240 |
| 15.41.01 *8* | -355 | -1135 | 10 | -2305 | 0 | 5 | 9430 | 10240 |
| 15.55.14 *8* | -1290 | -585 | 0 | -3085 | 0 | 5 | 9430 | 10240 |
| 16.16.27 *8* | -585 | -1375 | 0 | -3270 | 0 | 5 | 9430 | 10240 |
| 16.27.47 *8* | -430 | -665 | 0 | -2500 | 0 | 5 | 9430 | 10240 |
| 16.45.23 *8* | -4175 | -3670 | 10 | -3740 | 0 | 5 | 9430 | 10240 |

Table 4.10 : Example of some data print out from the data acquisition system in terms of pulse height (mV) out of the stretcher amplifiers for scintillators A and B.

The integral density spectrum of electrons at sea level
over the range $2.7 \leqslant \Delta \leqslant 36$ electrons $m^{-2}$ was measured by using
discriminators and a two fold coincidence circuit, and it has the
form $R(\geqslant\Delta) = 2058\Delta^{-(1.66 \pm 0.06)} hr^{-1}$. This shows that the slope
of density spectrum in that range is -1.66.

Using the microcomputer data acquisition system the integral
density spectrum over the range $27.5 \leqslant \Delta \leqslant 335\ m^{-2}$ has been
measured by taking the minimum density of the two recorded densities.
The result of the measured spectrum is described by

$$R(\geqslant\Delta) = 2483\Delta^{-(1.74 \pm 0.02)}\ hr^{-1}.$$

The value of the slope of the spectrum was found -1.74 in that range.

The integral density spectrum in the range $27.5 \leqslant \Delta \leqslant 335\ m^{-2}$
measured by taking the densities as recorded by A and B separately
and by taking the sum of all densities as recorded by A and B
separately have also been measured.

The differential density spectrum at high densities has been
measured by taking the minimum of the two recorded densities. It has
the form

$$R(\Delta)d\Delta = 1590\ \Delta^{-(2.54 \pm 0.15)}d\Delta\ hr^{-1}.$$

This indicates that the observed differential density spectrum at
sea level has a slope of -2.54 in the density range $27.5 \leqslant \Delta \leqslant 335\ m^{-2}$.
The differential density spectrum has also been measured by taking
the minimum densities as recorded by A and B separately.

# CHAPTER FIVE

## SUMMARY AND CONCLUSION

The early part of this thesis describes the calibration of a PET data acquisition system in order to make it suitable to measure the correct values of cosmic ray pulse height as generated by scintillation counters and to record the occurrence time of events. The eight channel microcomputer data acquisition system proved to be a useful instrument for the measurement of pulse heights and the occurrence time of cosmic ray showers. It is suitable for a wide range of cosmic ray experiments.

A Geiger-Müller cosmic ray telescope which consists of two layers of Geiger-Müller counters each containing six identical counters was used as a detector of cosmic rays. The vertical cosmic ray rate ($R_o$) and exponent of the angular distribution (n), and the variation of counting rate (R) with zenith angle due to geomagnetic effect, were measured using that telescope. Using a single counter in each layer the pulse heights from the counters was measured using the microcomputer data acquisition system. The mean pulse height and standard deviation of the pulse height distribution about the mean has been measured. The effect of applied voltage on the pulse height and the dependence of the standard deviation of the pulse height distribution about the mean value on the counter operating voltage have also been found.

An experiment was described to measure the local density spectrum of electrons over the range $2 < \Delta < 335$ electrons $m^{-2}$ by using a self-triggering system which consists of two scintillation counters A and B each of area $0.4$ $m^2$ and 5 cm thick.

By using discriminators and a two fold coincidence circuit, the integral density spectrum over the range $2.7 \leqslant \Delta \leqslant 36$ m$^{-2}$ was measured and it has the form $R(\geqslant \Delta) = 2058 \Delta^{-(1.66 \pm 0.06)}$hr$^{-1}$.

By using the microcomputer data acquisition system (described in chapter two), the integral density spectrum over the range $27.5 \leqslant \Delta \leqslant 335$ m$^{-2}$ was measured by taking the minimum density of the two recorded densities A and B. The result has the form $R(\geqslant \Delta) = 2483 \Delta^{-(1.74 \pm 0.02)}$ hr$^{-1}$.

The differential density spectrum of electrons at sea level over the range $27.5 \leqslant \Delta \leqslant 335$ m$^{-2}$ has been measured by using the microcomputer data acquisition system. The minimum of the two recorded densities was used in the evaluation. The differential spectrum has the form $R(\Delta)d\Delta = 1590 \Delta^{-(2.54 \pm 0.15)}d\Delta$ hr$^{-1}$ with $\Delta$ in electrons per square metre.

# APPENDIX A

## DATA COLLECTION AND PROCESSING PROGRAMS

The programs used in the collection and analysis of the data are listed in the following figures. The function of the programs are as follows:

Figure A.1  PET DATA ACQUISITION PROGRAM: This program collects data, records the pulse height and the occurrence time of it and also records it on the cassette drive of the PET and prints it on the printer.

Figure A.2  FILES READER PROGRAM : This program reads the recorded data from the cassette of the PET and prints it on the printer.

Figure A.3  CALIBRATION PROGRAM : This program calibrates the output data to its initial value before passing through the electronic system.

Figure A.4  INTEGRAL PROGRAM : This program measures the integral number of events with density values equal to or greater than a required density level $N(\geqslant\Delta)$.

Figure A.5  FREQUENCY DISTRIBUTION PROGRAM : This program calculates the frequency distribution of the data and draws the diagram for that distribution.

```
5 DIM AD%(1024)
6 DIM ZC%(8),DZ%(8),GC(8),DG(8)
7 GOTO 10500
10 DZ%(0)=0:DZ%(1)=0:DZ%(2)=0:DZ%(3)=0
11 DZ%(4)=0:DZ%(5)=0:DZ%(6)=0:DZ%(7)=0
12 ZR%=2048
20 ND(0)=1.0:ND(1)=1.0:ND(2)=1.0:ND(3)=1.0
21 ND(4)=1.0:ND(5)=1.0:ND(6)=1.0:ND(7)=1.0
22 PD(0)=1.0:PD(1)=1.0:PD(2)=1.0:PD(3)=1.0
23 PD(4)=1.0:PD(5)=1.0:PD(6)=1.0:PD(7)=1.0
29 RETURN
97 :
98 :"&&&&&&&& GET 1 CHAR &&&&&&"
99 :
100 GET £6,B$
110 IF ST AND 2 THEN GOSUB 160:GOTO 100
120 IF B$="" THEN B%=0:B$=".":GOTO 190
130 B%=ASC(B$)
140 RETURN
149 :
150 "&&&&&&&&&&&& TEST KEYBORD FOR INTERRUPT SHIFT S &&&&&&&&&"
151 :
160 GET KB$:IF KB$="" THEN RETURN
165 IF KB$()"S" THEN RETURN
170 GOSUB 40910
180 PRINT:PRINT:PRINT" SESSION INTERRUPTED FROM KEYBORD ":PRINT:PRINT:STOP
190 RETURN
197 :
198 :"&&&&&&&& GET 1 WORD &&&&&&"
199 :
200 GOSUB 100
210 W%=B%*256
220 GOSUB 100
230 W%=W%+B%
240 RETURN
241 :
245 :"&&&&&& GET 1 WORD & OVERFLO' &&&&&"
246 :
250 OV%=0:GOSUB 100:IF B%)127 THEN OV%=1:B%=B% AND 15
260 GOTO 210
297 :
298 :"&&&&&&&& PRINT HEX DIGIT &&&&&&&"
299 :
300 IF H%(10 THEN H%=H%+48:GOTO 320
310 H%=H%+55
320 PRINT CHR$(H%);
330 RETURN
397 :
398 :"&&&&&&&& PRINT HEX BYTE &&&&&&"
399 :
400 H%=B% AND 240
410 H%=H%/16
420 GOSUB 300
430 H%=B% AND 15
440 GOSUB 300
450 RETURN
497 :
498 : PRINT HEX WORD
499 :
```

```
500 B%=W%/256:GOSUB 400
510 B%=W% AND 255: GOSUB 400
520 RETURN
597 :
598 :"&&&&&& PRINT $FF,$FFFF &&&&&&"
599 :
600 PRINT " $";:GOSUB 400:RETURN
650 PRINT " $";:GOSUB 500:RETURN
999 :
1097 :
1098 :"&&&&&& GET SET OF 8 DATA FROM DACQ &&&&&"
1099 :
1100 FOR J=0 TO 7:OV%=0:GOSUB 1110:NEXT J:RETURN
1102 FOR J=0 TO 3:OV%=0:GOSUB 1110:NEXT J:RETURN
1104 FOR J=0 TO 1:OV%=0:GOSUB 1110:NEXT J:RETURN
1107 :
1108 "&&&&&&&&&GET ONE DATA FROM DACQ SUBR &&&&&&&&"
1109 :
1110 GOSUB 250: IM%=W%+ZC%(J)-ZR%
1120 IF IM%<0 THEN IM=IM%*FG(J):GOTO 1140
1130 IM=IM%*NG(J)
1140 IM%=IM+0.5:AD%(I)=-5*IM%
1150 IF OV%=0 THEN 1160
1153 IF AD%(I)<0 THEN AD%(I)=AD%(I)-20000:GOTO1160
1156 AD%(I)=AD%(I)+20000
1160 I=I+1
1170 RETURN
1197 :
1198 :"&&&&& PRINT SET OF 8 DATA ONTO PRINTER &&&&&"
1199 :
1200 IF PR=0 THEN RETURN
1205 FOR L=1 TO 8:GOSUB 1250:I=I+1:NEXT L:PRINT£4:RETURN
1210 TR%=(AD%(I)+500)/1000
1220 TR%=TR%*1000:ER%=TR%-AD%(I)
1250 IF OV%=1 THEN PRINT£4,"";
1255 AD$=STR$(AD%(I)):GP=6-LEN(AD$)
1260 FOR M=1 TO GP:PRINT£4," ";:NEXT M
1270 PRINT£4,AD$;
1275 IF OV%=1 THEN PRINT£4,"?";:RETURN
1280 PRINT£4," ";:RETURN
1299 :
1300 "&&&&&&&& PRINT ONE DAT ON CRT + OVRFLO REVERSE &&&&&&&&"
1301 :
1310 GOSUB 1360: IF OV%=1 THEN PRINT"";
1320 PRINT AD%(I),:PRINT"";:
1330 RETURN
1349 :
1350 "&&&&&&&&&STRIP OVRFLO SET FLG ON &&&&&&&&&"
1351 :
1360 IF AD%(I)>=20000 THEN OV%=1:AD%(I)=AD%(I)-20000
1370 IF AD%(I)<-20000 THEN OV%=1:AD%(I)=AD%(I)+20000
1380 RETURN
1997 :
1998 :"&&&&&& MAIN INTERACTIVE ROUTINE &&&&&"
1999 :
2000 A$="INTERACTIVE MODE":B$="***":GOSUB10000
2005 PRINT:PRINT "ENTER COMMAND LINE":PRINT
2007 CLOSE 5
2008 GOSUB 10
2010 INPUT A$
2020 GOSUB 2100
2030 PRINT:PRINT "COMMAND LINE EXECUTED":PRINT
2040 GOTO 2005
```

```
2097 :
2098 :"&&&&& SEND COMMAND & INTERPRET RETURN FROM DACQ &&&&"
2099 :
2100 OPEN 5,8
2110 PRINT£5,A$
2120 IF ST AND 128 THEN 2110
2130 CLOSE 5
2199 :
2200 OPEN 6,8,1
2210 GOSUB 100
2220 TM$=TI$
2300 IF B$="R" THEN 3000
2310 IF B$="C" THEN 4010
2320 IF B$="S" THEN 5100
2400 IF B%=114 THEN 2850
2490 IF ASC(B$)()101 THEN 2500
2495 ER=2495:ER$="ERROR RETURN FROM DACQ.UNIT":GOTO 9000
2500 ER=2500:ER$="UNEXPECTED RETURN FROMDACQ.UNIT":GOTO 9600
2599 :
2800 GOTO 2210
2850 CLOSE 6
2860 RETURN
2900 ER=2900:ER$="UNEXPECTED RETURN FROM DACQ.UNIT":GOTO 9600
2997 :
2998 :"&&&&& READ COMMAND EXECUTION &&&&&"
2999 :
3000 PRINT"READ COMMAND .. RETURN VALUES"
3010 PRINT"CHANNEL    VALUE"
3020 GOSUB 100
3030 IF ASC(B$)=116 THEN 3900
3040 IF ASC(B$)()101 THEN 3060
3050 ER=3050:GOTO 9900
3060 PRINT B$;:PRINT "            ";
3070 GOSUB 250:IF OV%=1 THEN PRINT"";
3075 GOSUB 650:PRINT"  "
3080 GOTO 3020
3900 GOTO 2800
3997 :
3998 :"&&&&& CAPT .. DOWNLOADING DATA FROM DACQ &&&&&"
3999 :
4000 "&&&&&&&&&&&& CAPT CASE &&&&&&&&&&&"
4005 :
4010 :
4020 IF NP=1 THEN PRINT:PRINT"DOWNLOADING DATA TO PET .. WAIT"
4050 TP=1:GOSUB 100:CT$=B$: IF B$="8" THEN 7010
4055 IF B$="4" THEN 7510
4060 IF B$="2" THEN 8010
4065 IF B$="1" THEN 8510
4095 ER=4095:GOTO 9920
4097 :
4098 : CAPT .. DOWNLOAD DATA
4099 :
4100 PRINT:PRINT"DOWNLOADING DATA TO PET...WAIT":PRINT
4110 I=0
4150 GOSUB 100
4160 IF B%=100 THEN GOSUB 1100:GOTO4150
4700 IF ASC(B$)=116 THEN 4900
4710 IF ASC(B$)=101 THEN ER=4710:GOTO 9900
4720 ER=4720:GOTO 9920
4900 PRINT:PRINT"DATA DOWNLOADED":PRINT:GOTO 2800
4999 :
5100 GOSUB 100:IF B%()100 THEN ER=5100:GOTO 9920
5110 I=0:GOSUB 1100
```

```
5120 GOSUB 100:IF B%=116 THEN 2800
5130 IF B%=101 THEN ER=5130:GOTO 9900
5140 ER=5140:GOTO 9900
5598 : FATAL ERROR
5599 :
7000 "&&&&&&&&&&&&& CAPT8 &&&&&&&&&&&&&"
7005 :
7010 :
7020 I=0
7030 GOSUB 100
7040 IF B%=100 THEN GOSUB 1100:GOTO 7030
7050 IF B%=116 THEN 7080
7060 IF B%=101 THEN ER=7060:GOTO 9900
7070 ER=7070:GOTO 9920
7080 IF NP=0 THEN 2800
7085 PRINT"DATA DOWNLOADED":PRINT
7110 K=I-1:J=0:OV%=0
7120 FOR I=0 TO K
7130 IF J=0 THEN GOSUB 13010
7135 GOSUB 1310
7140 IF PR=1 THEN GOSUB 1250
7145 IF CC=1 THEN GOSUB 40250
7150 OV%=0:J=J+1:IF J<>8 THEN 7170
7155 J=0:IF PR=1 THEN PRINT£4
7156 IF CC=1 THEN PRINT£10
7170 IF J=4 THEN IF CC=1 THEN PRINT£10,CHR$(11);
7175 NEXT I
7180 GOTO 2800
7500 "&&&&&&&&&&&&& CAPT4 &&&&&&&&&&&&&"
7505 :
7510 :
7520 I=0
7530 GOSUB 100
7540 IF B%=100 THEN GOSUB 1102:GOTO 7530
7550 IF B%=116 THEN 7580
7560 IF B%=101 THEN ER=7560:GOTO 9900
7570 ER=7570:GOTO 9920
7580 IF NP=0 THEN 2800
7585 PRINT"DATA DOWNLOADED":PRINT
7610 K=I-1:J=0
7620 FOR I=0 TO K
7630 IF J=0 THEN GOSUB 13010
7635 GOSUB 1310
7640 IF PR=1 THEN GOSUB 1250
7650 OV%=0:J=J+1:IF J=4 THEN J=0:IF PR=1 THEN PRINT£4
7670 NEXT I
7680 GOTO 2800
8000 "&&&&&&&&&&&&& CAPT2 &&&&&&&&&&&&&"
8005 :
8010 :
8020 I=0
8030 GOSUB 100
8040 IF B%=100 THEN GOSUB 1104:GOTO 8030
8050 IF B%=116 THEN 8080
8060 IF B%=101 THEN ER=8060:GOTO 9900
8070 ER=8070:GOTO 9920
8080 IF NP=0 THEN 2800
8085 PRINT"DATA DOWNLOADED":PRINT
8110 K=I-1:J=0
8120 FOR I=0 TO K
8130 IF J=0 THEN GOSUB 13010
8135 GOSUB 1310
8140 IF PR=1 THEN GOSUB 1250
```

```
8150 OVX=0:J=J+1:IF J=2 THEN J=0:IF PR=1 THEN PRINT£4
8170 NEXT I
8180 GOTO 2800
8499 :
8500 "&&&&&&&&&&& CAPT1 & FAST CAPT1 &&&&&"
8505 :
8510 I=0:J=0
8515 PRINT:PRINT"DOWNLOADING DATA TO PET...WAIT":PRINT
8520 GOSUB 100
8530 IF BX=100 THEN OVX=0:GOSUB 1110:GOTO 8520
8540 IF BX=116 THEN 8570
8550 IF BX=101 THEN ER=8550:GOTO 9900
8560 ER=8560:GOTO 9920
8570 PRINT"DATA DOWNLOADED":PRINT
8610 K=I-1:J=0:OVX=0
8620 FOR I=0 TO K
8630 IF J=0 THEN GOSUB 13010
8635 GOSUB 1310
8640 IF PR=1 THEN GOSUB 1250
8650 OVX=0:J=J+1:IF J=8 THEN J=0:IF PR=1 THEN PRINT£4
8670 NEXT I
8675 IF PR=1 THEN IF J()0 THEN PRINT£4
8680 GOTO 2800
8997 :
8998 :"&&&&&&& ERROR &&&&&&&&&"
8999 :
9000 PRINT:PRINT"*** ERROR ***";:PRINT ER:PRINT
9010 PRINT"      ";:PRINT ER$:PRINT"ERROR CODE:"
9020 GOSUB 100
9030 IF ASC(B$)=101 THEN 9020
9040 GOSUB 600:GOSUB 100:GOSUB 400
9050 GOSUB 100:GOSUB 600:GOSUB 100:GOSUB 600:GOSUB 100:GOSUB 600
9060 GOSUB 100:GOSUB 600:GOSUB 100:GOSUB 400
9065 GOSUB 100:GOSUB 600:GOSUB 100:GOSUB 400
9100 GOSUB 100
9110 IF ASC(B$)=116 THEN 9200
9120 ER=9120:ER$="END OF ERROR DUMP FROM DACQ.UNIT INCORRECT":GOTO 9600
9200 PRINT:PRINT:PRINT"*!*!* COMMAND LINE NOT EXECUTED *!*!*":PRINT:PRINT
9210 GOSUB 100:GOTO 2400
9597 :
9598 :"&&&&&& FATAL ERROR &&&&&"
9600 PRINT:PRINT:PRINT:PRINT"*!*!*    F A T A L  ERROR    *!*!*   ";:PRINTER
9610 PRINT:PRINT"      ";:PRINT ER$
9620 PRINT:PRINT"*!*!*! EXECUTION ABANDONNED !*!*!*"
9630 STOP
9900 ER$="ERROR RETURN FROM DACQ.UNIT":GOTO 9000
9920 ER$="UNEXPECTED RETURN FROM DACQ.UNIT... DATA INVALID":GOTO 9600
9997 :
9998 :"&&&&&& MAIN DATA COLLECTION PROGRAM &&&&&&"
9999 :
10000 PRINT "ET DATA ACQUISITION":PRINT:PRINT A$:PRINT:PRINT B$:GOSUB10050
10001 PR=0:PRINT" YOU WANT HARD COPY OF THIS SESSION?":PRINT"Y/N ?":INPUT A$
10002 IF A$="Y" THEN PR=1:OPEN 4,4,0:GOTO 10004
10003 IF A$()"N" THEN GOTO 10001
10004 :
10005 PRINT" YOU WANT COPY OF THE SESSION ON CASSETTE?"
10006 INPUT "(Y/N)?";A$:IF A$="Y" THEN GOSUB 40010:GOTO 10012
10007 IF A$()"N" THEN 10005
10012 PRINT:PRINT "ENTER SESSION IDENTIFIER"
10015 INPUT SI$
10020 PRINT:PRINT "ENTER DATE":INPUT DT$
10021 PRINT:
10022 PRINT "PLEASE CHECK TIME:    ";MID$(TI$,1,2);",";MID$(TI$,3,2);",";
```

```
10023 PRINT MID$(TI$,5,2):PRINT:PRINT"DO YOU WANT TO ALTER TIME SETTING (Y/N)?"
10024 INPUT A$:IF A$="N" THEN 10037
10026 IF A$()"Y" THEN PRINT:GOTO 10022
10030 PRINT:PRINT "ENTER CORRECT TIME (HHMMSS)"
10035 INPUT TM$:TI$=TM$
10037 GOSUB 10: GOSUB 10100: GOSUB 10200:GOSUB 10300:GOSUB 42500
10040 PRINT:PRINT"***":PRINT
10045 RETURN
10050 PRINT"EWIND PROGRAM TAPE AND REMOVE IT FROM":PRINT "CASSETTE DRIVE"
10055 PRINT:PRINT " DONE (D) ?"
10057 INPUT A$:IF A$()"D" THEN 10050
10058 RETURN
10097 :
10098 REM "&&&&&& SET ZERO &&&&&"
10099 :
10100 PRINT:PRINT"DO YOU WANT TO CALIBRATE ZERO (Y/N)?"
10110 INPUT A$
10120 IF A$="Y" THEN GOSUB 50000:RETURN
10130 IF A$()"N" THEN 10100
10150 PRINT:PRINT"DO YOU WANT TO USE DEFAULT ZERO CORRECTION (Y) OR NONE (N) ?"
10160 INPUT A$
10170 IF A$="Y" THEN FOR I=0 TO 7:ZC%(I)=DZ%(I):NEXT I:RETURN
10180 IF A$="N" THEN FOR I=0 TO 7:ZC%(I)=0:NEXT I:RETURN
10190 GOTO 10150
10197 :
10198 REM "&&&&&& SET GAIN &&&&&"
10199 :
10200 :
10210 PRINT:PRINT "DO YOU WANT TO CALIBRATE GAIN (Y/N)?":INPUT A$
10220 IF A$="Y" THEN GOSUB 50500:RETURN
10230 IF A$()"N" THEN 10210
10240 PRINT:PRINT "DO YOU WANT TO USE DEFAULT GAIN"
10245 PRINT "CORRECTION (Y) OR NONE (N) ?"
10250 INPUT A$
10260 IF A$="Y" THEN FOR J=0 TO 7:NG(J)=ND(J):PG(J)=PD(J):NEXT J:RETURN
10270 IF A$="N" THEN FOR J=0 TO 7:NG(J)=1.0:PG(J)=1.0:NEXT J:RETURN
10280 GOTO 10240
10290 :
10297 :
10298 REM "&&&&&& PRINT SETTINGS"
10299 :
10300 IF PR=0 THEN GOTO 10400
10305 FOR I=0 TO 3:PRINT£4:NEXT I
10310 FOR I=0 TO 70:PRINT£4,"*";:NEXT I:PRINT£4
10315 FOR I=0 TO 70:PRINT£4,"*";:NEXT I:PRINT£4:PRINT£4
10320 PRINT£4,SI$:PRINT£4:PRINT£4,DT$:PRINT£4
10325 FOR I=0 TO 70:PRINT£4,"*";:NEXT I:PRINT£4:
10390 :
10399 :
10400 IF PR=0 THEN RETURN
10413 PRINT£4,"*":PRINT£4,"***":PRINT£4,"*"
10414 PRINT£4,"ZERO OFFSET CORRECTION VALUES FOR THIS SESSION ARE:"
10416 FOR I=0 TO 3:PRINT£4,ZC%(I),:NEXT I:PRINT£4
10418 FOR I=4 TO 7:PRINT£4,ZC%(I),:NEXT I:PRINT£4
10422 PRINT£4,"*":PRINT£4,"***":PRINT£4,"*"
10424 PRINT£4,"NEGATIVE GAIN CORRECTION VALUES FOR THIS SESSION ARE:"
10426 FOR I=0 TO 3:PRINT£4,NG(I),:NEXT I:PRINT£4
10428 FOR I=4 TO 7:PRINT£4,NG(I),:NEXT I:PRINT£4
10432 PRINT£4,"*":PRINT£4,"***":PRINT£4,"*"
10434 PRINT£4,"POSITIVE GAIN CORRECTION VALUES FOR THIS SESSION ARE:"
10436 FOR I=0 TO 3:PRINT£4,PG(I),:NEXT I:PRINT£4
10438 FOR I=4 TO 7:PRINT£4,PG(I),:NEXT I:PRINT£4
10440 PRINT£4,"*":PRINT£4,"***":PRINT£4,"*"
```

```
10442 FOR I=0 TO 70:PRINT£4,"*";:NEXT I
10444 FOR I=0 TO 3:PRINT£4
10445 RETURN
10497 :
10498 REM "&&&&&& MAIN PROGRAM LOOP &&&&&"
10499 :
10500 A$="#**":B$="**":GOSUB 10000
10510 NP=1
10515 A$="INIT;TRG EXTDH":GOSUB 2100
10517 A$="CAPT8 1":GOSUB 2100:GOTO 10517
10520 A$="INIT;TRG TMR2;TMR 50R5":GOSUB 2100
10525 A$="CAPT8 1"
10530 GOSUB 2100:GOTO 10530
10995 :::
10996 ::
10997 :"&&&&&& MAIN PROGRAM SOUBROUTINES &&&&&"
10998 :"&&&&&&& PRINT ONE LINE .. TIME AND SET OF 8 &&&&&&"
10999 :
11010 IF NP=0 THEN RETURN
11012 FOR I=0 TO 7:IF ABS(AD%(I))>19999 THEN OV%=1
11014 NEXT I
11015 PRINT
11016 IF OV%=1 THEN IF PR=1 THEN PRINT£4,"";
11017 IF OV%=1 THEN PRINT"";
11020 :
11025 PRINT MID$(TM$,1,2);:PRINT".";
11030 IF PR=1 THEN PRINT£4,MID$(TM$,1,2);:PRINT£4,".";
11040 PRINT MID$(TM$,3,2);:PRINT".";
11050 IF PR=1 THEN PRINT£4,MID$(TM$,3,2);:PRINT£4,".";
11060 PRINT MID$(TM$,5,2);:PRINT
11070 IF PR=1 THEN PRINT£4,MID$(TM$,5,2);:PRINT£4,"   ";
11080 FOR I=0 TO 3:PRINT AD%(I),:NEXT I
11090 FOR I=4 TO 7:PRINT AD%(I),:NEXT I:PRINT
11100 I=0:GOSUB 1200
11120 RETURN
13000 "&&&&&&&&&&&PRINT TIME OR JUST SPACES &&&&&&&&&"
13001 :
13010 IF TP=1 THEN GOSUB 13110:TP=0:RETURN
13020 IF PR=1 THEN PRINT£4,"                ";
13030 PRINT:RETURN
13099 :
13100 "&&&&&&&&&&&PRINT TIME & CAPTURE TYPE SUBR &&&&&&&&&&&&"
13101 :
13110 :
13130 PRINT MID$(TM$,1,2);:PRINT".";
13132 PRINT MID$(TM$,3,2);:PRINT".";
13134 PRINT MID$(TM$,5,2);:PRINT "    *";CT$;"*"
13140 IF PR=0 THEN 13160
13150 PRINT£4,MID$(TM$,1,2);:PRINT£4,".";
13152 PRINT£4,MID$(TM$,3,2);:PRINT£4,".";
13154 PRINT£4,MID$(TM$,5,2);:PRINT£4," *";CT$;"*   ";
13160 IF CC=0 THEN RETURN
13170 PRINT£10,CHR$(11);
13172 PRINT£10,MID$(TM$,1,2);:PRINT£10,".";
13174 PRINT£10,MID$(TM$,3,2);:PRINT£10,".";
13176 PRINT£10,MID$(TM$,5,2);:PRINT£10," *";CT$;"*   ";
13178 PRINT£10,CHR$(11);
13190 RETURN
18999 :
19000 CLOSE 4
20000 OPEN 4,4,0
20010 GOTO 11010
30000 CLOSE 6
```

```
40000 "&&&&&&&&&&& CASSETTE SUPPORT &&&&&&&&"
40001 :
40010 :
40020 PRINT:PRINT:PRINT "LOAD DATA CASSETE TO CASSETE DRIVE":PRINT
40022 PRINT "REWIND TAPE TO BEGINNING &"
40023 PRINT "CHECK THAT CASSETTE STOPPED ON":PRINT "CLEAR LEADER":PRINT
40024 PRINT"CHECK THAT NO KEY IS PRESSED DOWN"
40026 PRINT"DONE (D) ?"
40028 GET KB$:IF KB$()"D" THEN 40028
40029 PRINT
40050 CC=1:PRINT"TER NAME OF THE CASSETTE FILE":PRINT"    8 CHARACTERS MAX."
40060 INPUT A$:TN$=LEFT$(A$,8)
40070 TN$=LEFT$(A$,8)
40110 OPEN 10,1,1,TN$
40120 RETURN
40198 :"&&&&& PRINT SET OF 8 DATA ONTO PRINTER &&&&&"
40199 :
40200 IF CC=0 THEN RETURN
40205 FOR L=1 TO 4:GOSUB 40250:I=I+1:NEXT L:PRINT£10,CHR$(11);:PRINT£10:RETURN
40207 FOR L=1 TO 4:GOSUB 40250:I=I+1:NEXT L:PRINT£10:RETURN
40210 TR%=(AD%(I)+500)/1000
40220 TR%=TR%*1000:ER%=TR%-AD%(I)
40250 IF OV%=1 THEN PRINT£10,"";
40255 AD$=STR$(AD%(I)):GP=6-LEN(AD$)
40260 FOR M=1 TO GP:PRINT£10," ";:NEXT M
40270 PRINT£10,AD$;
40275 IF OV%=1 THEN PRINT£10,"?";:RETURN
40280 PRINT£10," ";:RETURN
40299 :
40900 "&&&&&&&&& CLOSE CASSETTE FILE &&&&&&&"
40901 :
40910 CLOSE 10
40920 RETURN
42000 :
42001 GOTO 42005
42002 :
42003 "&&&&&&&&&&&&&&& PRINT DATA FROM TAPE &&&&&&&&"
42004 :
42005 PRINT"":PRINT"DATA FROM TAPE TO PRINTER":PRINT:PRINT:
42110 PRINT" ENTER NAME OF THE FILE TO PRINT":INPUT NF$
42115 PRINT:PRINT:PRINT"REWIND THE TAPE & PRESS ANY KEY"
42120 GET A$:IF A$="" THEN 42120
42125 OPEN 10,1,0,NF$:OPEN 4,4:PRINT£4:PRINT£4
42130 GET£10,A$:IF ST()0 THEN 42230
42135 IF HC=1 THEN IF A$()CHR$(11) THEN PRINT£4,A$;
42140 IF A$=CHR$(11) THEN PRINT:GOTO 42130
42145 PRINT A$;
42160 GOTO 42130
42210 OPEN 10,1,0,NF$:OPEN 4,4:PRINT£4:PRINT£4
42220 GET£10,A$:IF ST=0 THEN PRINT£4,A$;:GOTO 42220
42230 IF (ST) AND 4 THEN PRINT"SHORT BLOCK ERROR":GOTO 42450
42240 IF (ST) AND 8 THEN PRINT"LONG BLOCK ERROR":GOTO 42450
42250 IF (ST) AND 16 THEN PRINT"READ ERROR ":GOTO 42450
42260 IF (ST) AND 32 THEN PRINT"CHECKSUM ERROR":GOTO 42450
42270 IF (ST) AND 64 THEN PRINT:PRINT "END OF FILE ENCOUNTERED":GOTO 42410
42280 IF (ST) AND 128 THEN PRINT "UNEXPECTED END OF TAPE ENCOUNTERED":STOP
42410 PRINT£4:PRINT£4:PRINT£4,"END OF FILE ";NF$:PRINT£4:PRINT£4
42420 END
42497 :
42498 REM "&&&&& PRINT SETTINGS"
42499 :
42500 IF CC=0 THEN GOTO 42600
42505 FOR I=0 TO 3:PRINT£10:NEXT I
```

```
42510 FOR I=0 TO 70:PRINT£10,"*";:NEXT I:PRINT£10
42515 FOR I=0 TO 70:PRINT£10,"*";:NEXT I:PRINT£10:PRINT£10
42520 PRINT£10,SI$:PRINT£10:PRINT£10,DT$:PRINT£10
42525 FOR I=0 TO 70:PRINT£10,"*";:NEXT I:PRINT£10
42590 :
42599 :
42600 IF CC=0 THEN RETURN
42613 PRINT£10,"*":PRINT£10,"***":PRINT£10,"*"
42614 PRINT£10,"ZERO OFFSET CORRECTION VALUES FOR THIS SESSION ARE:"
42616 FOR I=0 TO 3:PRINT£10,ZC%(I),CHR$(11);:NEXT I:PRINT£10
42618 FOR I=4 TO 7:PRINT£10,ZC%(I),:NEXT I:PRINT£10
42622 PRINT£10,"*":PRINT£10,"***":PRINT£10,"*"
42624 PRINT£10,"NEGATIVE GAIN CORRECTION VALUES FOR THIS SESSION ARE:"
42626 FOR I=0 TO 3:PRINT£10,NG(I),:NEXT I:PRINT£10
42628 FOR I=4 TO 7:PRINT£10,NG(I),:NEXT I:PRINT£10
42632 PRINT£10,"*":PRINT£10,"***":PRINT£10,"*"
42634 PRINT£10,"POSITIVE GAIN CORRECTION VALUES FOR THIS SESSION ARE:"
42636 FOR I=0 TO 3:PRINT£10,PG(I),:NEXT I:PRINT£10
42638 FOR I=4 TO 7:PRINT£10,PG(I),:NEXT I:PRINT£10
42640 PRINT£10,"*":PRINT£10,"***":PRINT£10,"*"
42642 FOR I=0 TO 70:PRINT£10,"*";:NEXT I
42644 FOR I=0 TO 3:PRINT£10
42645 RETURN
42697 :
49997 :
49998 "&&&&&& ZERO COMPENSATION SUBROUTINE &&&&&&"
49999 :
50000 PRINT:PRINT"CONNECT ALL INPUTS TO GROUND &"
50011 PRINT " PRESS .D. TO SAVE READING AS":PRINT " NEW ZERO CORRECTION":PRINT
50105 PRINT":PRINT" DONE (D) ?                "
50111 :
50112 FOR I=0 TO 7:ZC%(I)=0:NEXT I
50113 FOR I=0 TO 7:PG(I)=1.0:NG(I)=1.0:NEXT I
50114 :
50120 GOSUB 50200
50130 FOR I=0 TO 7:IM=WK%(I)/15:ZC%(I)=IM+0.5:NEXT I
50140 RETURN
50197 :
50198 "&&&&&& GAIN CALIBRATION SUBR &&&&&&"
50199 :
50200 A$="INIT;TRG INTR":GOSUB 2100
50210 A$="CAPT8 1":NP=0:GOSUB 2100:GOSUB50400
50300 GET KB$:IF KB$="" THEN 50340
50310 IF KB$="D" THEN 50350
50340 PRINT":GOTO 50210
50341 :
50342 :
50350 FOR I=0 TO 7:WK%(I)=0:NEXT I
50355 :
50360 FOR N=0 TO 2
50365 I=0:A$="CAPT8 1":NP=0:GOSUB 2100
50370 FOR I=0 TO 7:GOSUB 1360:WK%(I)=WK%(I)+AD%(I):NEXT I
50375 PRINT"";N:PRINT:GOSUB 50400:NEXT N
50380 RETURN
50400 :
50405 PRINT "                                      ":PRINT "
50410 FOR I=0 TO 3:PRINT AD%(I),:NEXT I:PRINT
50415 PRINT "                                      ":PRINT "
50420 FOR I=4 TO 7:PRINT AD%(I),:NEXT I:PRINT
50425 RETURN
50430 :
50497 :
50498 "&&&&&& GAIN CALIBRATION &&&&&&"
```

```
50499 :
50500 PRINT "*":PRINT "***":PRINT "*"
50510 PRINT "CONNECT ALL INPUTS TO POSITIVE VOLTAGE"
50512 PRINT" (IN THE REGION OF 9.5V)
50520 PRINT
50560 PRINT "PRESS .D. WHEN DONE":PRINT"DONE (D) ?":PRINT
50565 FOR I=0 TO 7:PG(I)=1:NEXT I
50570 GOSUB 50210
50580 GOSUB 50610
50585 FOR I=0 TO 7:IM=WK%(I)/3:PG(I)=GM/IM:NEXT I
50590 GOTO 50700
50597 :
50598 "&&&&&& GET TRUE VOLTAGE SUBROUTINE &&&&&"
50599 :
50600 :
50601 :
50610 PRINT"*":PRINT"***":PRINT"*"
50620 PRINT "ENTER INPUT VOLTAGE TO 5MILIVOLT"
50625 PRINT "PRECISION (E.G. 10.005)"
50630 INPUT A$:GM=VAL(A$)
50640 PRINT A$;: PRINT "MV  OK (Y/N)?":INPUT A$
50660 IF A$()"Y"THEN 50500
50670 IF GM=0 THEN PRINT"ZERO IS UNACCEPTABLE ..CANNOT CALIBRATE":PRINT"???"
50680 RETURN
50690 :
50700 PRINT"*":PRINT"***":PRINT"*"
50710 PRINT"NOW REVERSE POLARITY OF THE INPUT VOLTAGE"
50730 PRINT"DONE (D) ?"
50740 GOSUB 50210
50750 GOSUB 50610
50751 :
50752 IF GM(0 THEN 50760
50754 PRINT"!*! INPUT VOLTAGE MUST BE NEGATIVE !*!"
50756 PRINT"!*! ENTER AS -9500 !*!":PRINT
50758 GOTO 50700
50759 :
50760 FOR I=0 TO 7:IM=WK%(I)/3:NG(I)=GM/IM.NEXT I
50770 RETURN
59997 :
59998 :
59999 :
60000 A$="INIT:TRG TMR2":GOSUB 2100
60005 A$="TMR 3OR5":GOSUB 2100
60010 A$="CAPT8 1":NF=1
60020 PRINT"+":GOSUB 2100:PRINT"£":GOTO 60020
```

Figure A.2   :   "FILES READER PROGRAM"

```
1 PRINT""
2 INPUT"DO YOU WANT A HARD COPY (Y/N)";X$
3 PRINT:PRINT: PRINT" PRESS P TO PAUSE THE DATA READING"
4 IF X$ ="Y" THEN HC =1: IF X$ = "N" THEN HC =0
5 IF X$ () "Y" THEN IF X$()"N" THEN 3
6 PRINT " " :PRINT "DATA FROM TAPE":PRINT:PRINT
10 PRINT" ENTER NAME OF THE FILE ":INPUT NF$
15 PRINT:PRINT:PRINT"REWIND THE TAPE & PRESS ANY KEY"
20 GET A$ : IF A$ ="" THEN 20
25 OPEN 10,1,0,NF$ :OPEN 4,4:IF HC=1 THEN PRINT£4
26 IF HC=1 THEN PRINT£4,"*************************************";
27 IF HC =1 THEN PRINT£4,"**************************************"
28 IF HC=1 THEN PRINT£4,"FILE NAME IS (";NF$;")"
30 GET£10, A$
32 IF STATUS AND 64 THEN 210
35 IF HC =1 THEN IF A$ () CHR$(11) THEN PRINT£4,A$;
40 IF A$ = CHR$(11) THEN PRINT : GOTO 30
45 PRINT A$;
50 GET S$: IF S$="P" THEN GOSUB 350
60 GOTO 30
110 OPEN 10,1,0,NF$: OPEN 4,4:PRINT£4
120 GET£10,A$: IF ST = 0 THEN PRINT£4,A$;:GOTO 120
210 IF HC =1 THEN PRINT£4
211 IF HC=1 THEN PRINT£4," END OF FILE  ";NF$:IF HC=1 THEN PRINT£4
212 PRINT  : PRINT  " END OF FILE  ";NF$:PRINT  :PRINT
300 END
350 PRINT" PRESS C TO CONTENUE";
355 GET S$:IF S$()"C" THEN 355
360 PRINT"                    ";
361 PRINT"                    ";
365 PRINT"                         ";:RETURN
```

Figure A.3

```
 >      1     CCCCCCCCCCCCCCCCCCCCCCCCCCCCCCCCCC
 >      2     CCCCC                        CCCCC
 >      3     CCCCC  CALIBRATION PROGRAM   CCCCC
 >      4     CCCCC                        CCCCC
 >      5     CCCCCCCCCCCCCCCCCCCCCCCCCCCCCCCCCC
 >      6            DIMENSION X(15),Y(15)
 >      7            X(1)=40.0
 >      8            Y(1)=25.0
 >      9            X(2)=70.0
 >     10            Y(2)=30.0
 >     11            X(3)=80.0
 >     12            Y(3)=35.0
 >     13            X(4)=100.0
 >     14            Y(4)=45.0
 >     15            X(5)=120.0
 >     16            Y(5)=60.0
 >     17            X(6)=150.0
 >     18            Y(6)=105.0
 >     19            X(7)=200.0
 >     20            Y(7)=190.0
 >     21            X(8)=250.0
 >     22            Y(8)=295.0
 >     23            X(9)=300.0
 >     24            Y(9)=435.0
 >     25            X(10)=350.0
 >     26            Y(10)=500.0
 >     27     CCCCCCCCCCCCCCCCCCCCCCCCCCCCCCCCCC
 >     28       50   READ (5,100) A,B
 >     29      100   FORMAT(2F10.2)
 >     30     CCC    A   CCC
 >     31            IF(A .EQ. 9999.9) GOTO 400
 >     32            IF(A .GT. 7345.) GOTO 110
 >     33            IF(A .LT. 232) GOTO 50
 >     34            IF(A .GE. 500. ) GOTO 120
 >     35            DO 160 J=1,10
 >     36            IF(A .EQ. Y(J)) GOTO 130
 >     37            IF(A .GT. Y(J) .AND. A .LT. Y(J+1)) GOTO 140
 >     38      160   CONTINUE
 >     39      110   AC= 10000.0
 >     40            GOTO 200
 >     41      120   AC=(A+486.39)/2.7826
 >     42            GOTO 200
 >     43      130   AC=X(J)
 >     44            GOTO 200
 >     45      140   S=(Y(J)-Y(J+1))/(X(J)-X(J+1))
 >     46            YO=Y(J)-S*X(J)
 >     47            AC=(A-YO)/S
 >     48      200   CONTINUE
 >     49     CCC    B    CCC
 >     50            IF (B .GT. 7345.) GOTO 210
 >     51            IF(B .LT. 334.2) GOTO 50
 >     52            IF (B .GE. 500. ) GOTO 220
 >     53            DO 260 J=1,10
 >     54            IF (B .EQ. Y(J) ) GOTO 230
 >     55            IF (B .GT. Y(J) .AND. B .LT. Y(J+1)) GOTO 240
 >     56      260   CONTINUE
 >     57      210   BC=10000.0
 >     58            GOTO 300
 >     59      220   BC=(B+486.39)/ 2.7826
 >     60            GOTO 300
```

```
>      61      230    BC = X(J)
>      62             GOTO 300
>      63      240    S=(Y(J)-Y(J+1))  /  (X(J)-X(J+1))
>      64             YO=Y(J)  -  S*X(J)
>      65             BC=(B-YO)/S
>      66      300    CONTINUE
>      67      CCCCCCCCCCCCCCCCCCCCCCCCC
>      68             WRITE(6,100) AC,BC
>      69      CCCCCCCCCCCCCCCCCCCCCCCCCCC
>      70      CCC    PN=NUMBER OF PARTICLES
>      71             PNA= AC/20.8
>      72             PNB= BC/23.2
>      73             WRITE(7,100)PNA,PNB
>      74
>      75             GOTO 50
>      76      400    STOP
>      77             END
#End of file
#
```

Figure A.4

```
>    1         CCCCCCCCCCCCCCCCCCCCCCCCCCCCCC
>    2         CCCCC                     CCCCC
>    3         CCCCC   INTEGRAL PROGRAM CCCCC
>    4         CCCCC                     CCCCC
>    5         CCCCCCCCCCCCCCCCCCCCCCCCCCCCCC
>    6               DIMENSION DELTA(40)
>    7               DIMENSION A(1500) ,B(1500)
>    8               DELTA(1)=20.0
>    9               DELTA(2)=27.5
>   10               DELTA(3)=30.0
>   11               DELTA(4)=35.0
>   12               DELTA(5)=40.0
>   13               DELTA(6)=45.0
>   14               DELTA(7)=50.0
>   15               DELTA(8)=55.0
>   16               DELTA(9)=60.0
>   17               DELTA(10)=65.0
>   18               DELTA(11)=70.0
>   19               DELTA(12)=75.0
>   20               DELTA(13)=80.0
>   21               DELTA(14)=85.0
>   22               DELTA(15)=90.0
>   23               DELTA(16)=95.0
>   24               DELTA(17)=100.0
>   25               DELTA(18)=110.0
>   26               DELTA(19)=120.0
>   27               DELTA(20)=130.0
>   28               DELTA(21)=140.0
>   29               DELTA(22)=150.0
>   30               DELTA(23)=160.0
>   31               DELTA(24)=170.0
>   32               DELTA(25)=180.0
>   33               DELTA(26)=190.0
>   34               DELTA(27)=200.0
>   35               DELTA(28)=220.0
>   36               DELTA(29)=240.0
>   37               DELTA(30)=260.0
>   38               DELTA(31)=280.0
>   39               DELTA(32)=300.0
>   40               DELTA(33)=320.0
>   41               DELTA(34)=340.0
>   42         CCCCCCCCCCCCCCCCCCCCCCCCCCCCCCCCCC
>   43               I=1
>   44      50      READ(5,75)A(I),B(I)
>   45      75      FORMAT(2F10.2)
>   46               IF(A(I) .EQ. 9999.9) GOTO 80
>   47               I=I+1
>   48               GOTO 50
>   49      80      N=I-1
>   50         CCCCCCCCCCCCCCCCCCCCCCCCCCCCCCCCCC
>   51               KSUM=0
>   52               WRITE(6,99)
>   53      99      FORMAT(25HDELTA   COUNTS .GE. DELTA)
>   54         CCCCCCCCCCCCCCCCCCCCCCCCCCCCCCCCCC
>   55         CC                                CC
>   56               DO 200 I=1,34
>   57               AMIN = 0.4 * DELTA(I)
>   58               BMIN = 0.4 * DELTA(I)
>   59               DO 100 J=1,N
>   60         CC
```

```
>     61              IF(A(J) .LT. AMIN) GOTO 100
>     62              IF(B(J) .LT. BMIN) GOTO 100
>     63       CC
>     64              KSUM=KSUM+1
>     65       CC
>     66        100   CONTINUE
>     67       cccccccccccccccccccccccccccccccccccccc
>     68        500   CONTINUE
>     69              WRITE (6,77)DELTA(I),KSUM
>     70        77    FORMAT(F5.1,3X,I4)
>     71       cccccccccccccccccccccccccccccccccccccc
>     72              KSUM=0
>     73        200   CONTINUE
>     74       cccccccccccccccccccccccccccccccccccccc
>     75              STOP
>     76              END
#End of file
#
```

Figure A.5

```
>    1      CCCCCCCCCCCCCCCCCCCCCCCCCCCCCCCCCCCCCCCCCC
>    2      CCCCC                                 CCCCC
>    3      CCCCC   FREQUENCY DISTRIBUTION PROGRAM   CCCCC
>    4      CCCCC                                 CCCCC
>    5      CCCCCCCCCCCCCCCCCCCCCCCCCCCCCCCCCCCCCCCCCC
>    6              DIMENSION F(60)
>    7              DO 20 I=1,60
>    8      20    F(I)=0.0
>    9      CCCCCC  SET THESE TO SUIT DATA
>   10              FMAX=200.0
>   11              PEAK=20.0
>   12              AMIN=0.0
>   13              N=30
>   14              AMAX=3000.0
>   15              W= (AMAX - AMIN) / N
>   16      CCCCCCCCCCCCCCCCCCCCCCCCCCCCCCCCCC
>   17              KSAT=0
>   18              BIG=0.0
>   19              KSUM=0
>   20      CCCCCCCCCCCCCCCCCCCCCCCCCCCCCCCCCC
>   21      75    READ(5,100)X
>   22      CCCCC  FORMAT MUST BE SUITABLE TO DATA FILE
>   23      100   FORMAT(F10.2)
>   24      CCCCC  9999.9 For the end of the file
>   25      CCCCC  10000. For the over saturation pulse heigh
>   26              IF(X .EQ. 9999.9) GOTO 300
>   27              IF(X .EQ. 10000.) KSAT=KSAT+1
>   28              IF(X .EQ. 10000.) GOTO 75
>   29              IF(X .GT. AMAX) BIG=BIG+1.
>   30              IF(X .GT. AMAX)  GOTO 75
>   31              IF(X .EQ. AMAX) F(N)=F(N)+1
>   32              IF(X .EQ. AMAX) GOTO 75
>   33              I = ( X - AMIN ) / W  + 1
>   34              F(I)= F(I)+ 1
>   35              KSUM=KSUM + 1
>   36              GOTO 75
>   37      CCCCCCCCCCCCCCCCCCCCCCCCCCC
>   38      300   CONTINUE
>   39      CCCCCCCCCCCCCCCCCCCCCCCCCCC
>   40              WRITE (6,310)
>   41      310   FORMAT(25H INTERVAL          FREQUENCY)
>   42              DO 350 I=1,N
>   43              JC = (I-1)*W
>   44              JD=JC+W
>   45              WRITE (6,340)JC,JD,F(I)
>   46      340   FORMAT(I5,2X,I5,4X,F5.0)
>   47      350   CONTINUE
>   48              WRITE(6,380)KSUM
>   49      380   FORMAT(6H TOTAL,I4)
>   50              WRITE(6,390)KSAT
>   51      390   FORMAT(17H OVER SATURATION=,I3)
>   52              WRITE(6,392)BIG
>   53      392   FORMAT(18H GREATER THAN MAX=,F4.0)
>   54      CCCCCCCCCCCCCCC  CCCCC CCCCCCCCCCCCCCCCCCCCCCCCCCCCCC
>   55              CALL PAPER(1)
>   56              CALL PSPACE(.1969,.9843,.3037,.9343)
>   57              CALL MAP(0.0,AMAX,0.0,BMAX)
>   58              CALL BORDER
>   59              CALL SCALES
>   60              CALL HISTGM(0.0,0.0,W,F,1,N)
```

```
>    61              BBC=-(FMAX/15.)
>    62              DO 10 JH=1,5
>    63              BAA=AMAX/6*JH
>    64              CALL PLOTNC(BAA,4*BBC,30)
>    65              CALL PLOTNC(BAA,8*BBC,30)
>    66              CALL CTRMAG(10)
>    67              RRR=(AMAX/6)*JH/ PEAK
>    68              CALL PLOTNF(BAA,4.3*BBC,RRR,2)
>    69              CALL PLOTNF(BAA,8.3*BBC,RRR/.4,2)
>    70              CALL CTRMAG(20)
>    71      10      CONTINUE
>    72              CALL PLOTCS(AMAX/10.,4*BBC/4.,'PULSE HEIGHT AT OUTPUT',22)
>    73              CALL PLOTCS(AMAX*.9,BBC,'( V)',4)
>    74              CALL PLOTCS(AMAX/10.,5*BBC,'IN NUMBER OF PARTICLES',22)
>    75              CALL PLOTCS(AMAX/9.,9*BBC,'DENSITY',7)
>    76              CALL CTRSET (2)
>    77              CALL PLOTNC (AMAX*.85,9*BBC,23)
>    78              CALL PLOTNC (AMAX*.925,BBC,23)
>    79              CALL CTRSET (1)
>    80              CALL CTRMAG(15)
>    81              CALL PLOTNI(AMAX*.89,8.7*BBC,-2)
>    82              CALL CTRMAG(20)
>    83              CALL CTRORI(1.0)
>    84              CALL PLOTCS(-AMAX*.1,FMAX*.3,'FREQUENCY',9)
>    85              CALL GRNPEN
>    86              CALL GRATIC
>    87              CALL GREND
>    88      CCCCCCCCCCCCCCCCCCCCCCCCCCCCCCCCCCCCCCCCCCCCCCCCCCCCCCCCCCC
>    89              STOP
>    90              END
#End of file
#
```

# APPENDIX B

## ELECTRONICS

Circuit diagrams for the electronics units used for the experiments described are shown in this appendix. Unless otherwise stated all values of resistance are quoted in $K\Omega(10^3\Omega)$, all values of capacitance are quoted in $\mu F(10^{-6}F)$, and all transistors used were of the type OC171.
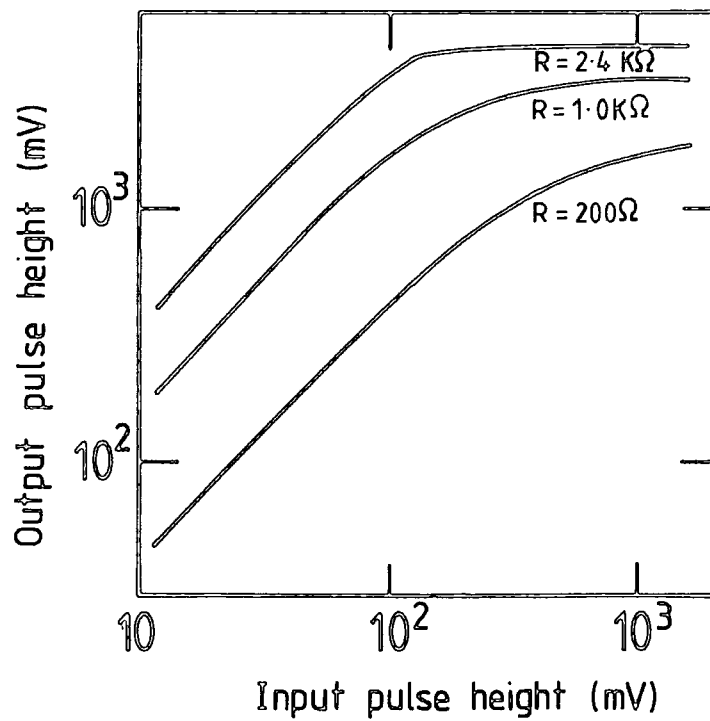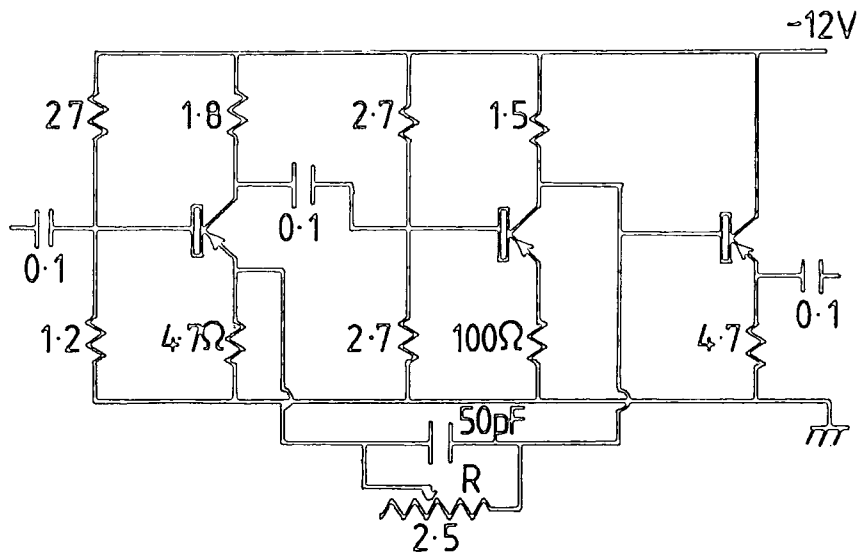
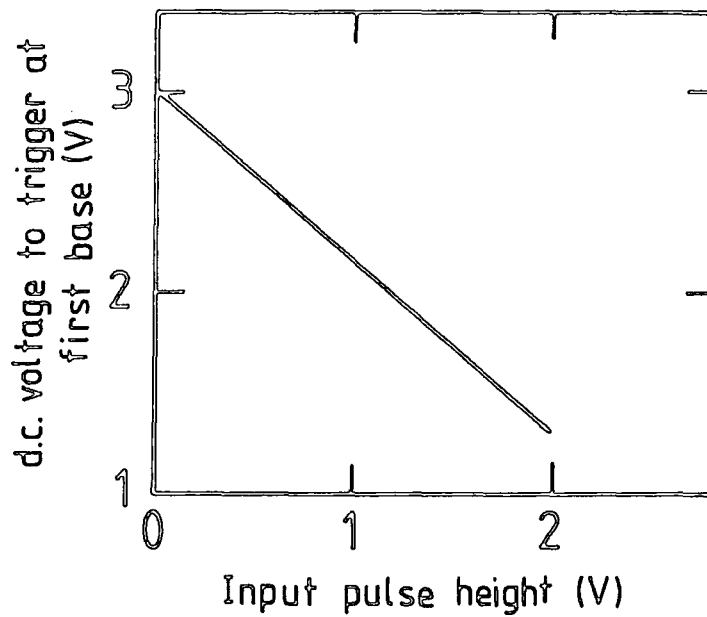Figure B.1 : The voltage amplifier and its characteristics for various values of feedback resistance, R.
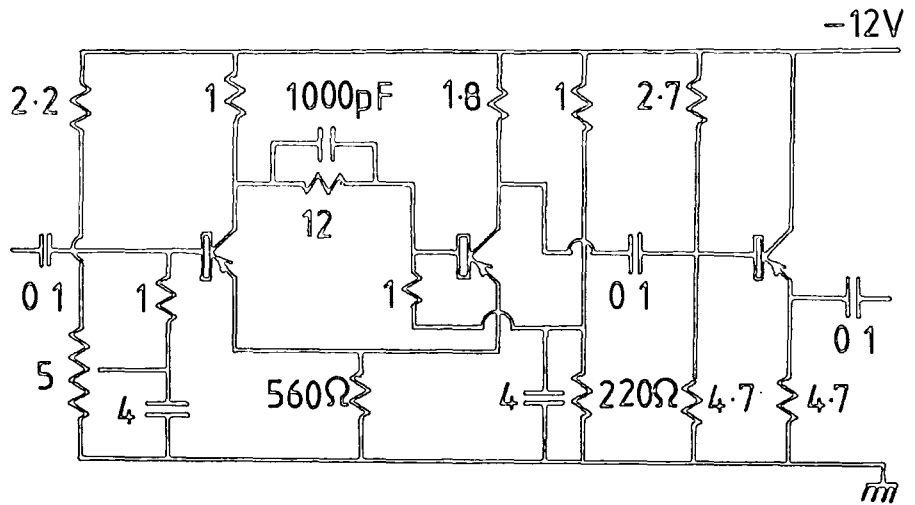
Figure B.2 : The discriminator circuit and its relationship
between the d.c. level on the first transistor
and the minimum input pulse height required to
trigger the circuit.
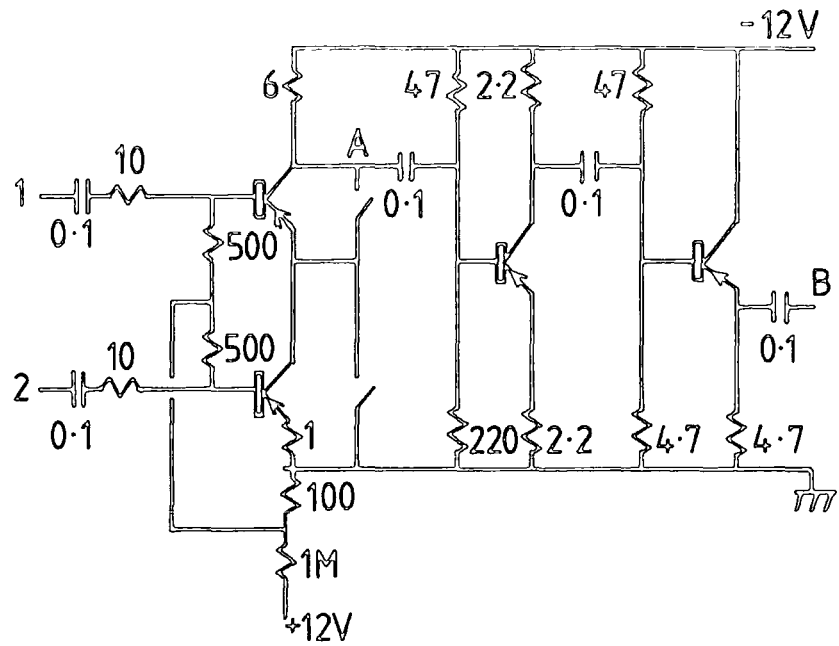
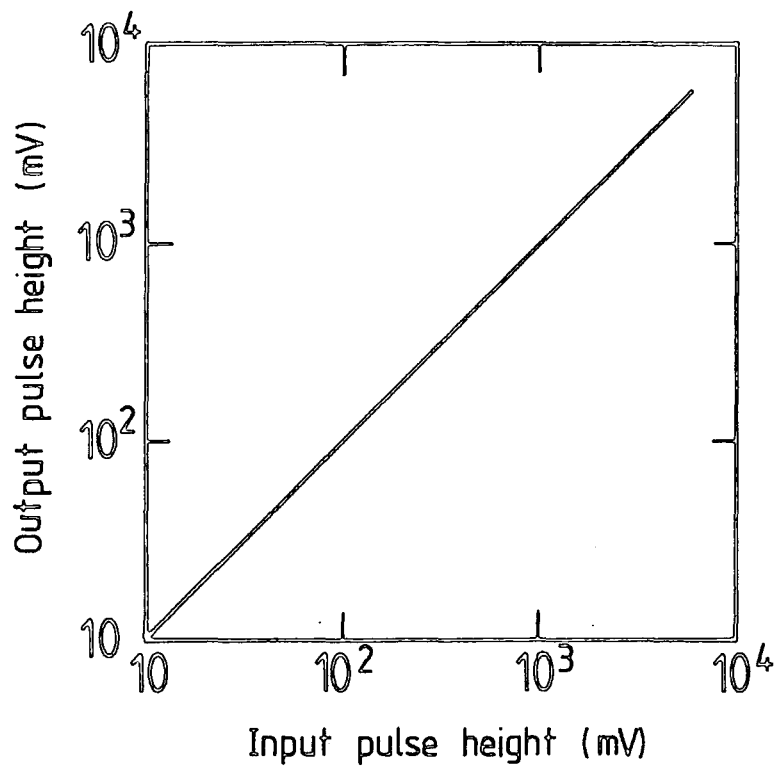| | Input from Discrimination | Output at A | | Output at B | | |
|---|---|---|---|---|---|---|
| | | 1 fold | 2 fold | 1 fold | 2 fold | pulse width |
| Channel 1 | −5V | ÷0·15V | ÷5·4V | −0·05V | −4·1V | 1μs |
| Channel 2 | −5V | ÷0·02 | | −0·04 | | 1μs |

Figure B.3 : A two fold coincidence unit.
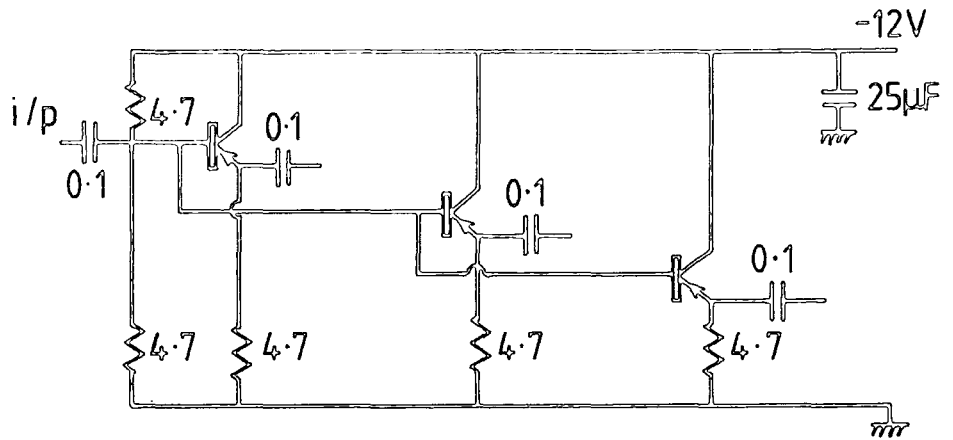
Figure B.4 : The fan out and its input-output characteristics.

-12 VOLT

V INPUT

0.1μF

1MΩ

1MΩ

1KΩ

10μF

V OUTPUT

GAIN ≈ 0.98

Output pulse height (Volts)
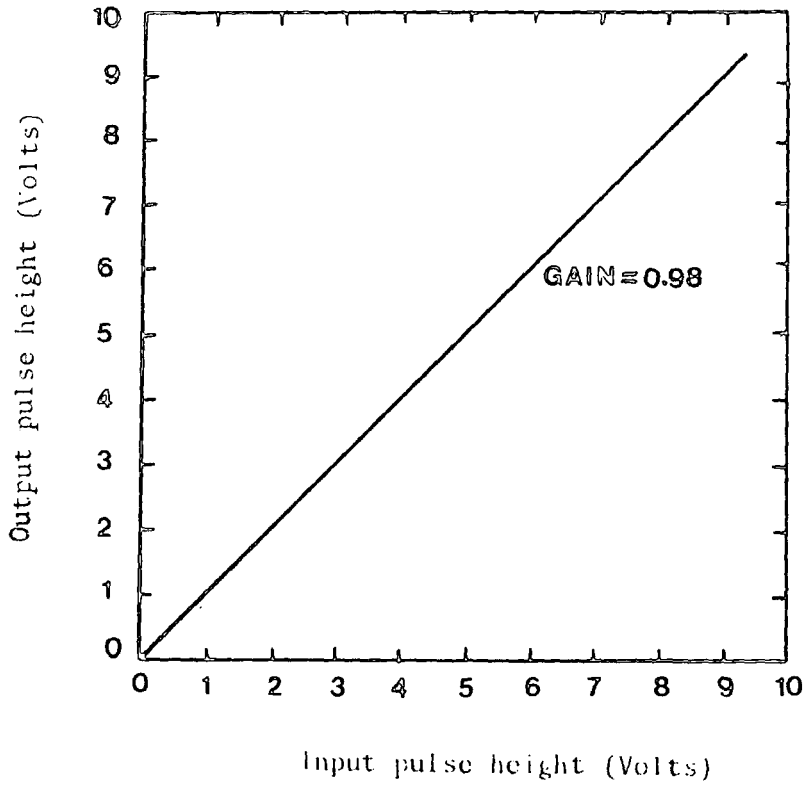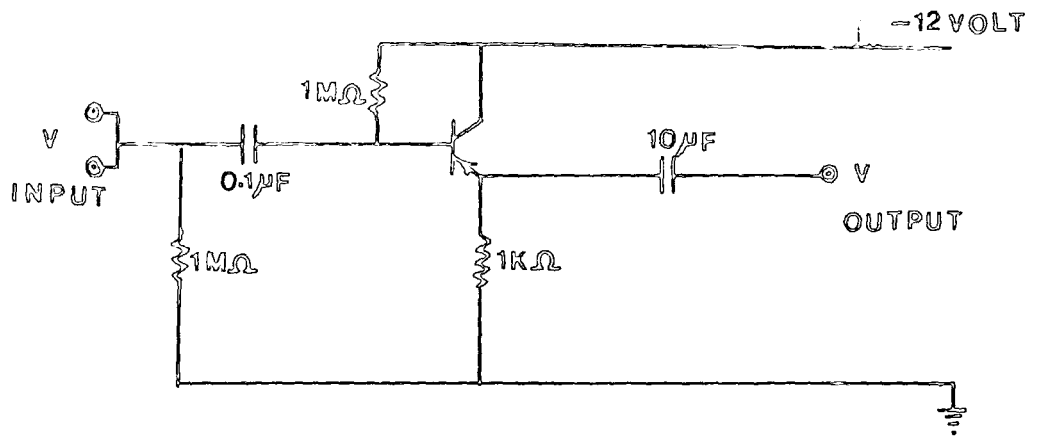
Input pulse height (Volts)

Figure B.5 : Circuit diagram and response of head unit.

# REFERENCES

(PICCR = Proceedings of the International Conference of Cosmic Rays)

Allkofer, O.C., Dau, W.D. and Jokisch, H. (1970b), Proc. 16th.
    Interamerican Seminar on Cosmic Rays (La Paz : Univeridal
    Mayor De San Andres), 6, 1930.

Anderson, C.D. (1932), Science, 76, 238.

Ashton, F. et al (1965), PICCR, London, 2, 1079.

Ashton, F. et al (1973), PICCR, Denver, 4, 2489.

Ashton, F. et al (1973), Cosmic Rays at Ground Level, Ed. Wolfendale,
    A.W., (Inst.Phys.)

Ashton, F. et al (1975), PICCR, Munich, 8, 2719.

Ashton, F. et al (1975), PICCR, Munich, 8, 2831.

Ashton, F. et al (1977), PICCR, Plovdiv, 12, 172.

Ashton, F. et al (1979) PICCR, Kyoto, 13, 238.

Ashton, F. et al (1983), 18th. ICRC, Bangalore, India, 8, 149.

Auger, P., et al (1939), Rev. Mod. Phys., 11, 288.

Aurela, A.M. and Wolfendale, A.W. (1967), Ann. Acad. Sci. Fenn. A6, 226.

Ayre, C.A. et al (1971a), J. Phys. A : Gen. Phys. 4, L89.
Bell, M.C. (1974), Ph.D. Thesis, Durham University.
Blatt, J. (1949) Phys. Rev., 10, 75, 1584.

Blockh, Y.L., Dorman, L.I., and Kaminer, N.S. (1959), Proc. IUPAP
    Cosmic Ray Conf. Moscow, 4, 155.

Clay, J., et al (1927), Proc. Roy, Acad, Amsterdam, 30, 115.

Cocconi, G., and Cocconi Tongiorgi, V. (1949), Phys. Ref.,
    7, 75, 1058.

Cocconi, G. (1961), Handbuch der Physik, XLVI/I, 215.

Crookes, J.N. and Rastin, B. (1971a), Proc. 12th. Int. Conf. on
    Cosmic Rays, Tasmania, 4, 1325.
Edge, D.M., et al (1973), J. Phys. 6A, 1612.
Euler, H. and Heisenberg, W. (1938), Ergeb. d. exakt. Naturwiss, 17,1.

Froman, D.K. and Stearn, J.C. (1938), Can. J. Research, A16, 29.

Galbraith, W. (1958), Extensive Air Showers, Butterworths Pub. Ltd.
Grigorov, N.L., et al (1970), Sov. J. Nucl. Phys., 11, 588.
Daudin, J. (1945), Ann. de Phys., 20, 563.
Deutschmann, M. (1948), Naphthalene Counters for Beta and Gamma
Rays, Nucleonics, 2, 58.
Dorman, L.J. (1959), Cosmic Ray Variations, Moscow, Section
VII, ICM Programme (CP), No. 1

Gemesy, J., et al (1964), PICCR, Jaipur, 4, 180.

Ginzburg, V.L. and Syrovatskii, S.I. (1964), "The Original of
　　　　　Cosmic Rays" Pergamon Press, New York.

Greisen, K. (1942), Phys. Rev., 61, 212.

Greisen, K. and Nereson, N. (1942), Phys. Rev., 62, 316.

Greisen, K. (1943), Phys. Rev., 63, 323.

Greisen, K. (1956), Prog. Cosmic Ray Physics, North Holland, 3, 1.

Greisen, K. (1960), Ann. Rev. Nucl.Sci., 10, 63.

Greisen, K. (1965), PICCR, London, 2, 609.

Greisen, K. (1966), Phys. Rev. Lett., 16, 748.

Hayakawa, S. (1969), "Cosmic Ray Physics" published by
　　　　　Wiley - Int. Science.

Hess, V.F. (1912), Physik, Z., 13, 1084.

Hillas, A.M. (1972), Cosmic Rays.

Hillas, A.M. (1975), Phys. Rep., 20C, 61.

~~Hiss, V.F. (1912), Physik, Z., 13, 1084.~~

Johnson, T.H. (1933), Phys. Rev., 43, 834.

Juliusson, et al. (1972), Phys. Rev. Lett., 29, 445.

Julliusson, E. (1975), PICCR, Munich, 8, 2689.

Kalmykov, N.N., Fomin, Yu, A. and Khristiansen, G.B. (1973),
　　　　　PICCR, Denver, 4, 2633.

Karakula, S., et al. (1974), J. Phys., A, 1, 437.

Katsumata, I. (1964), J. Phys. Soc., Japan, 6, 19, 800.

Kempa, J., et al (1974), J. Phys., A, 7, 1213.

Khristiansen, G.B., Kulikov, G.V. and Solov'eva, V.I. (1974),
　　　　　S.J. Nucl.Phys. 19, 162.

Khristiansen, G.B. (1977), PICCR, Plovdiv, 8, 145.

King, J. (1970), Ph.D. Thesis, Durham University.

Kolhorster, W., Matthes, I. and Weber, E. (1938),
　　　　　Naturwiss, 26, 576.

Kraybill, H. (1949), Phys. Rev. 76, 1092.

Lapp, R. and Andrews, H. (1972), Nuclear Radiation Physics.

Lemaitre, G. and Vallarta, M.S. (1933), Phys. Rev., 43, 87.

Mathews, T. (1963), Phil. Mag., 8, 387.

McCaughan, J.B.J., et al (1965b), PICCR, London, 2, 720.

Meyer, P., et al (1974), Phys. Today, 27, 23.

Norman, R.J. (1955), Aus. J. Phys., 8, 419.

Norman, R.J. (1956), Proc. Phys. Soc., 69, A, 804.

Parvaresh, A. (1975), Ph.D. Thesis, Durham University.

Peters, B. (1960), Proc. IUPAP Cosmic Ray Conf., Mosco, 3, 157.

Prescott, J.R. (1956), Proc. Phys. Soc., 69, A, 870.

Rose, M.E. and Ramsey, W.E. (1941), Phys. Rev., 59, 616.

Rossi, B. (1948), Rev. Mod. Phys. 20, 537.

Ryan, M.J., et al. (1972), Phys. Rev. Lett., 28, 985.

Stever, G.H. (1942), Phys. Rev., 61, 38.

Störmer, C. (1932), Ergebnisse der Kosmischen Physik, I, 1.

Strong, A.W. (1974), J. Phys., A, 7, 1489.

Swinson, D.B. and Prescott, J.R. (1965), PICCR, London, 2, 721.

Swinson, D.B. and Prescott, J.R. (1968), Cana. J. Phys., 46, 5292.

Vernov, S.N. et al (1970), Acta Phys. Hung., 29, Suppl., 3, 429.

Webber, W.R. and Quenby, J.J. (1959), Phil.Mag., 4, 654.

Wolfendale, A.W. (1963), Cosmic Rays.

Wolfendale, A.W. (1973), Cosmic rays at ground level.